2012

Ammonia Production at Ambient Temperature and Pressure: An Electrochemical and Biological Approach

Timothy Michael Paschkewitz
University of Iowa

AMMONIA PRODUCTION AT AMBIENT TEMPERATURE AND PRESSURE: AN ELECTROCHEMICAL AND BIOLOGICAL APPROACH

by

Timothy Michael Paschkewitz

An Abstract

Of a thesis submitted in partial fulfillment
of the requirements for the Doctor of
Philosophy degree in Chemistry
in the Graduate College of
The University of Iowa

May 2012

Thesis Supervisor: Associate Professor Johna Leddy

ABSTRACT

The majority of power generated worldwide is from combustion of fossil fuels. The sustainability and environmental impacts of this non renewable process are severe. Alternative fuels and power generation systems are needed, however, to cope with increasing energy demands. Ammonia shows promise for use in power generation, however it is costly to produce and very few methods of using it as a fuel are developed. To address the need for alternative methods of ammonia synthesis, this research designed and tested a bioelectrochemical device that generates NH_3 through electrode induced enzyme catalysis. The ammonia generating device consists of an electrode modified with a polymer that contains whole cell *Anabaena variabilis*, a photosynthetic cyanobacterium. *A. variabilis* contains nitrogenase and nitrate/nitrite reductase, catalysts for the production of ammonia. In this system, the electrode supplies driving force and generates a reductive microenvironment near cells to facilitate enzymatic production of NH_3 at ambient temperatures and pressures.

Farm animal wastes contain significant amounts of NO_2^- and NO_3^-, which can leech into groundwater sources and contaminate them. The system described here recycles NO_2^- and NO_3^- to NH_4^+ by the nitrate/nitrite reductase enzyme. Unlike nitrogen fixation by the nitrogenase enzyme whose substrate is atmospheric N_2, the substrates for nitrate/nitrite reductase are NO_2^- and NO_3^-. The ammonia produced by this system shows great potential as a crop fertilizer.

While the substrates and enzymatic basis for ammonia production by nitrogenase and nitrate/nitrite reductase are very different, there is utility in the comparison

of commercially produced ammonia by the Haber Bosch synthesis and by the bioelectrocatalytic device described here. In one day, the Haber Bosch process produces 1800 tons of NH_3 at an energetic cost of \$500/ton. Per ton of ammonia, the Haber Bosch process consumes 28 GJ of energy. The bioelectrocatalytic device produces 1 ton of NH_3 for \$10/ton, consuming only 0.04 GJ energy, which can be obtained by sunlight via installation of a photovoltaic device. Thus, the system presented here demonstrates ammonia production with significant impact to the economy.

NH_3 production by the bioelectrocatalytic is dependent upon *A. var.* cell density and electrode polarization. The faradaic current response from cyclic voltammetry is linearly related to cell density and ammonia production. Without electrode polarization, immobilized *A. var.* do not produce ammonia above the basal level of 2.8 ± 0.4 μM. Ten minutes after cycled potential is applied across the electrode, average ammonia output increases to 22 ± 8 μM depending on the mediator and substrate chemicals present. Ammonia is produced by this system at 25 °C and 1 atm. The electrochemical basis for enhanced NH_3 by immobilized cyanobacteria is complex with multiple levels of feedback.

Abstract Approved: _____
Thesis Supervisor

_____
Title and Department

_____
Date

AMMONIA PRODUCTION AT AMBIENT TEMPERATURE AND PRESSURE: AN ELECTROCHEMICAL AND BIOLOGICAL APPROACH

by

Timothy Michael Paschkewitz

A thesis submitted in partial fulfillment
of the requirements for the Doctor of
Philosophy degree in Chemistry
in the Graduate College of
The University of Iowa

May 2012

Thesis Supervisor: Associate Professor Johna Leddy

Graduate College
The University of Iowa
Iowa City, Iowa

CERTIFICATE OF APPROVAL

PH.D. THESIS

This is to certify that the Ph.D. thesis of

Timothy Michael Paschkewitz

has been approved by the Examining Committee for the thesis requirement for the Doctor of Philosophy degree in Chemistry at the May 2012 graduation.

Thesis Committee:

Johna Leddy, Thesis Supervisor

Ned Bowden

Lei M. Geng

Amnon Kohen

Tonya Peeples

To my father, Michael Andrew Paschkewitz.

ACKNOWLEDGMENTS

Without supportive friends, family, peers, and advisors, completing this body of work would not likely have been possible. I sincerely thank my advisor, Professor Johna Leddy for her caring support, advice, encouragement and guidance. It was truly a privilege to work with such an accomplished scientist. I wish to thank present and past students of the Leddy lab with whom I worked, Murat Unlu, Stephanie Schmidt, Heung Chan Lee, Chester Duda, Garett Lee, Perry Motsegood, Jessica Jewett, Krysti Knoche, Sarah Cyrus, and Emily Mrugacz for all their support. I also thank Michael Ivanov and David Rotsch for helpful conversations, support, and guidance along the way. For financial assistance, I acknowledge the the Iowa Energy Center.

While this page cannot accommodate the list of persons for whom I wish to acknowledge, I have the space to name a few. For endless love and support throughout this long journey, I thank Nana, Mom, Heidi, Dave, Sarah, and Andy. I acknowledge all my Wisconsin friends, too numerous to name, but certainly, you know who you are. Lastly, but not least significantly, I thank Michael Combs for putting up with me and being there when my stress levels would drive away just about anyone. You've been with me through the best and worst parts of this process for the last couple years. Only bigger and better things can come next. Thank you, everyone.

TABLE OF CONTENTS

LIST OF TABLES

Table

LIST OF FIGURES

Figure

CHAPTER 1

INTRODUCTION

Energy, measured in Joules (J), is the ability to do physical work. Energy is also a commodity in commerce and serves as the fundamental currency of the planet. Power is the rate of energy transfer measured in Watts (J/s). Systems that allow energy harvest and power generation are often made by processing a material to obtain stored energy. Materials that contain stored energy are fuels. Fuels are available on earth in many different forms; many are chemical. All living organisms depend upon adequate availability of energy and sufficient rates of energy transformation, power. There are several technologies and strategies currently used to harvest energy. These technologies are as follows: large turbine blades convert wind energy to electricity; solar powered semiconductor photovoltaic devices generate electricity from sunlight; fuels obtained from plant matter, called biomass, are burned to release energy; and hot water and steam heated by geothermal energy from below the earth's surface heats buildings and generates electricity.

Combustion of hydrocarbon rich fuels serves as the means of power generation worldwide despite severe environmental consequences and the broader impacts of overusing hydrocarbon based energy supplies. Hydrocarbon rich energy sources such as crude oil, natural gas, and coal, are in limited supply. These are often called fossil fuels because their presence on earth goes back to decayed organic plant and animal materials. Greenhouse gas emissions arise from fossil fuel combustion. These include CO_2, CH_4, N_2O, NO_x, and SO_2, which contribute to depletion of the ozone layer, acid rain, and diminished air quality [1]. Further, overuse of hydrocarbon

based fuels has a direct effect on the world's economy, because it costs more to produce less as demand for power continues to rise and the supply of energy rich fuels continues to decrease. Lastly, most combustion processes are irreversible and therefore not renewable as the products of hydrocarbon combustion are primarily polluting chemical waste. While energy is of concern to humankind, lower organisms and plants adapted and already depend upon a renewable source of energy, the sun.

Living organisms depend on an external source of energy to grow and function. Many plants and some bacteria obtain energy directly from the sunlight through a process called photosynthesis. Photosynthesis is the light driven reduction of CO_2 into biomass energy [2]. Plant life is the largest source of agricultural foodstuffs. Plant life obtains its energy in a clean and renewable manner. Plant energy utilization schemes can serve as a model for alternative strategies of energy production for humankind.

Energy supply, demand, production, and consumption are important topics. Reducing our dependence upon limited carbon based fuels requires new energy technologies and applications. Additional methods to use renewable fuels must be developed to meet an increasing energy needs [3].

1.1 Renewable Energy Outlook

The British thermal unit (Btu) is the unit of energy used in the U.S. There are 1,055 J in 1 Btu. The U.S. Department of Energy reports that renewable energy capacity installed both worldwide and in the United States has nearly tripled between 1949 and 2009, rising from about 32 quadrillion Btu to 95 quadrillion Btu

for all sources of energy. Of the 94.6 quadrillion Btu, the majority were supplied by carbon based petroleum (35.3%), natural gas (23.4%), coal (19.7%), and nuclear sources (8.3%). Thus, only 7.7% of U.S. energy consumption comes from renewable sources [4]. Renewable energy sources are regenerable and can be sustained indefinitely. Carbon based fossil fuels are not renewable and will eventually be exhausted. The most commonly utilized renewable energy resources are biomass (wood and wood waste, municipal solid waste, landfill gas, and biofuels such as ethanol), hydropower, geothermal, wind, and solar sources [1, 3, 5]. Renewable energy technologies have the potential to strengthen our national energy security, improve environmental quality, and contribute to a strong energy economy [4]. Because implementation of renewable energy technologies is generally more expensive than historically used nonrenewable sources, renewable energy is less commonly used. An additional complexity is that renewable sources such as wind, solar, and hydroelectric are subject to environmental variations such as cloud cover, night, drought, and stagnant air. Under such environmental conditions, renewable sources are not always available for energy production.

A significant amount of research focuses on alternative fuels that provide hydrogen. Hydrogen is the simplest and most abundant element in the universe; however, hydrogen is rarely found alone in nature. Hydrogen is present in compounds such as water (H_2O), hydrocarbons that include natural gas and methane, CH_4, and almost all other organic matter. Efficient release of hydrogen from these compounds is the largest impediment to widespread implementation. Currently, steam reforming of CH_4 accounts for about 95% of the hydrogen produced in the United States [4].

Hydrogen burns well in energy devices, has a wide range of flammability, and has a large heat of combustion per unit mass. The combustion of H_2 releases only water, however processing CH_4 to harvest the hydrogen contributes to greenhouse gas emission, because energy for processing is typically generated by combustion of fossil fuels. Hydrogen is extremely flammable and combustible and is therefore dangerous to handle, store, transport, and use. Thus, H_2 as an alterative energy source is limited despite the high energy content of hydrogen [1, 6, 7].

With energy consumption projected to increase at a rate of 1.3 % annually until 2025, sustainable and environmentally friendly fuels, methods to synthesize and obtain such fuel, and devices to use these fuels are now imperative research vectors [5]. Well developed systems that operate on alternative and renewable fuels will lessen the dependence on carbon based fuel sources. One fuel worthy of development is anhydrous ammonia [8].

1.2 Ammonia as a Fuel

Structurally, ammonia is a central nitrogen atom bonded to three peripheral hydrogen atoms. Ammonia (NH_3) is widely used in plastics, explosives, and crop fertilizers. Crops grow with NH_3 supplementation as plants uptake ammonia to synthesize amino acids essential to living cells. Nitrogen is the nutrient element that most frequently limits growth of green plants. Typically, the limitation arises as nitrogen is lost from the soil. The regular removal of nitrogen containing crop residues that is common in modern farming practices depletes soil of nitrogen. Addition of N, called "fixed" or reduced nitrogen, to soil in the form of NH_3

replenishes lost nitrogen [9]. A less commonly known use of ammonia is as a fuel. It can be used in internal combustion engines with minimal modification to a traditional engine, directly in ammonia fuel cells, and as a hydrogen source in hydrogen fuel cells [10–14]. Ammonia as a fuel is not a newly discovered technology. Ammonia was first used as a fuel in Belgium during 1943 to power a bus fleet during World War II [8].

Ammonia shares similar alternative fuel benefits with hydrogen. Advantageous properties of ammonia fuel are as follows: 1) no greenhouse gases upon combustion, only N_2 and H_2O as products;

$$4NH_3 + 3O_2 \rightleftharpoons 2N_2 + 6H_2O \tag{1}$$

2) renewable resource, synthesized commercially from a hydrogen source and atmospheric N_2; 3) flexibility, as ammonia can be produced from any primary energy source [12]; 4) storage, as anhydrous ammonia is liquid at moderate pressure, whereas hydrogen requires cryogenic temperatures to condense the gas to liquid; 5) transportation and delivery, as significant systems and existing infrastructure are already in place for industry and farming applications of ammonia; 6) domestic, as the U.S. is a significant producer of NH_3, thus dependence on imported fuel is negligible; and 7) existing technologies, as the scientific community is actively developing new systems to utilize ammonia as a fuel [13, 14]. The energy density of ammonia as a fuel exceeds that of hydrogen, whose technological use and development currently far exceeds that of ammonia. Table 1 compares some common liquid fuels.

Table 1. Comparison of the energy density of common fuels.

Fuel	**Energy density (MJ/L) as liquid fuel**
H_2	8.5
CH_3OH	15.8
NH_3	17.2
CH_4	20.9
CH_3CH_2OH	24.3
Gasoline	31.2
Diesel	31.4

Note: The energy density is reported as MJ/L for liquid fuels. The energy value does not consider any external energy input necessary to store or use as a liquid, such as high pressure. These data were obtained from various sources available on the U.S. Department of Energy website.

Ammonia as a fuel faces challenges that are largely of economic and energetic costs. Despite the promise of ammonia, the fuel is currently produced through the Haber Bosch synthesis, an energetically costly and environmentally taxing process. Additionally, Haber Bosch synthesis requires a source of H_2, commonly obtained by steam reforming CH_4 [15]. The steam reformation of CH_4 to produce H_2 puts into question the renewable and non polluting nature of ammonia as a fuel.

1.3 Haber Bosch Synthesis

Fritz Haber successfully developed a process for direct combination of nitrogen and hydrogen to produce ammonia in 1909. Carl Bosch, a chemist working for BASF, successfully scaled up Haber's process to industrial scale NH_3 production. Prior to their combined efforts, ammonia was difficult to produce on an industrial scale. The success of the commercial NH_3 process has contributed to sustaining approximately one third of the Earth's population through increased access to crop

fertilization [16]. In 2009, the world production of ammonia was 1.3×10^{14} g [17] and more than 90% of ammonia production worldwide uses the Haber Bosch synthesis process [18].

The Haber Bosch chemical synthesis of ammonia uses iron oxide as a catalyst and other oxide promoters (K_2O, Al_2O, and CaO) to react N_2 and H_2 in the gas phase. Overall, the net reaction is thermodynamically exothermic.

$$N_{2(g)} + 3H_{2(g)} \rightleftharpoons 2NH_{3(g)} \qquad \Delta H^\circ = -92 \text{ kJ} \tag{2}$$

The Haber Bosch synthesis mechanism includes dissociation of N_2 to atomic nitrogen using on iron oxides (Fe_3O_4 and Fe_2O_3) catalyst and formation of NH_3 by reaction with oxidized H_2, as follows [19, 20] (where the subscripts g = gas and ad = adsorbed):

$$H_{2(\text{g})} \rightleftharpoons 2H_{(\text{ad})} \tag{3}$$

$$N_{2(\text{g})} \rightleftharpoons N_{2(\text{ad})} \rightleftharpoons 2N_{(\text{ad})} \tag{4}$$

$$N_{(\text{s})} + H_{(\text{ad})} \rightleftharpoons NH_{(\text{ad})} \tag{5}$$

$$NH_{(\text{ad})} + H_{(\text{ad})} \rightleftharpoons NH_{2(\text{ad})} \tag{6}$$

$$NH_{2(\text{ad})} + H_{(\text{ad})} \rightleftharpoons NH_{3(\text{ad})} \tag{7}$$

$$NH_{3(\text{ad})} \rightleftharpoons NH_{3(\text{g})} \tag{8}$$

A temperature increase would increase the sluggish kinetics of the exothermic reaction (Reaction 2). An increase in temperature would also shift the reaction to favor the reactants and reduce NH_3 produced. Fe_3O_4 and Fe_2O_3 catalyst in Haber Bosch process requires high temperatures between 400-600 °C for efficient

catalysis. Ammonia production can be entropically enhanced with elevated gas pressure between 200 and 400 atm as there are 4 moles of gas reactant for every 2 moles of gas product; however, increasing the pressure of a system has significant economic costs as pressure is an expensive commodity. Therefore, in consideration of the challenging thermodynamic and kinetic limitations of the system, cost and energy efficient reduction of N_2 to NH_3 requires a fine balance between elevated temperature and pressure. Additionally, the process requires H_2, which is not readily available as a reagent. Steam reforming methane, the most commonly used method to obtain hydrogen, produces H_2 required in step 3. Steam reforming CH_4 releases ozone layer depleting CO_2 as a by product. Alternatively, it is possible to supply hydrogen renewably by the electrolysis of water $\left(2H_2O_{(l)} \rightleftharpoons 2H_{2(g)} + O_{2(g)}\right)$, however steam reforming CH_4 is less costly with current industrial technology.

Despite the costs of production, the Haber Bosch synthesis is highly efficient. To date, there has not been development of other ammonia syntheses that approach the Haber Bosch 8 15% conversion rates [21, 22]. Therefore, despite the high energetic cost and environmental tax of Haber Bosch produced ammonia, it remains the most used synthetic method for ammonia production. Richard Shrock recently stated, "Even though the huge and highly successful Haber Bosch process is unlikely to be displaced readily by a new process, even if efficient and inexpensive, it must be kept in mind that >1% of the energy consumed by humans is consumed by the Haber Bosch process" [15]. Shrock's statement sets expectations for those researching ammonia syntheses: do not try to compete with the Haber Bosch synthesis but instead, focus on development of methods of ammonia synthesis that are less costly,

both financially and environmentally, more sustainable, and cleaner.

Inclusion of the energetic, environmental, and resource costs of commercial production of NH_3 in the cost analysis of Haber Bosch synthesis of anhydrous ammonia does not conclude that ammonia is an economically viable alternative fuel, despite its excellent properties as a fuel. The expected energetic output as compared to the energetic input is not favorable. The economic cost of ammonia synthesis is high, due in part to the very strong triple bond between the nitrogen atoms that must be broken for effective synthesis. Similar chemical processes that require only atmospheric temperature and pressure are achieved by numerous bacteria. In contrast to the commercial process of making NH_3, biological processes offer an interesting model of low energy and renewable ammonia synthesis.

1.4 Biological Production of Ammonia

There are at least two significant biological methods of producing ammonia; nitrogen fixation by the nitrogenase enzyme and nitrate/nitrite reductase catalysis of NO_2^- and NO_3^-. *In vivo*, these enzyme depend upon other biochemical pathways for the recycling of redox cofactors, generation of substrates, and low potential electron carrier cycling. Together, the enzyme and dependent chemical processes are the reaction centers within the cell (Figure 1). All of these reaction centers involve electron transfer.

The reaction centers illustrated in Figure 1 represent the most probable and important pathways and chemicals in the electrochemically induced production of ammonia from immobilized cyanobacteria. These reaction centers are: Nitrogenase,

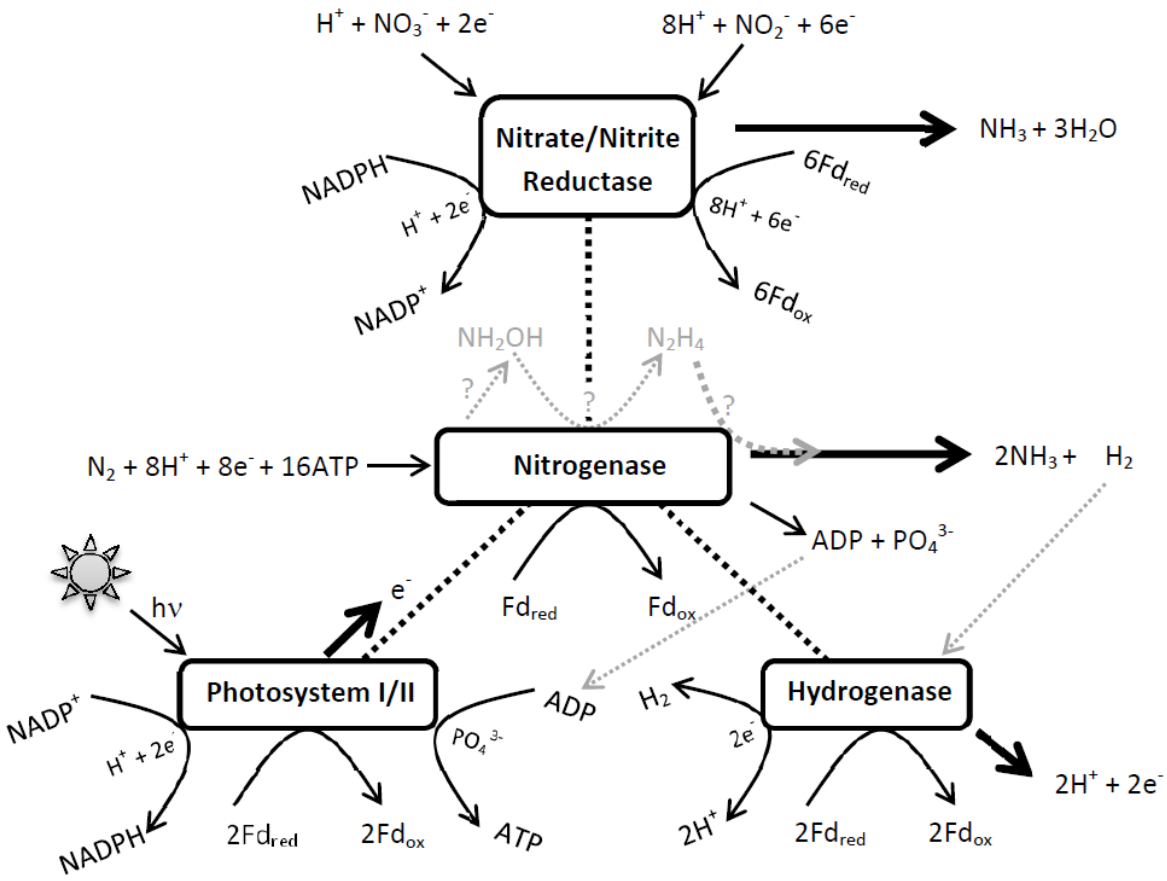

Figure 1. Illustration of the interrelated reaction centers in *Anabaena variabilis*. Nitrogenase is one target enzyme for its ability to generate NH_3 from N_2. Peripheral reaction centers have shared mediators, co-factors, reactants, and products. Major reaction centers are shown in boxes and are Photosystem I/II, Hydrogenase, Nitrogenase, and Nitrate/Nitrite Reductase. Solid black lines represent known pathways and reactions. Gray lines and text are possible reactions and chemicals, not necessarily known paths or species.

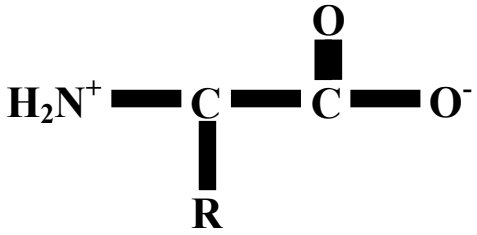

Figure 2. The chemical structure of the amino acid backbone. One end is ammonium terminated and the other is carboxylic acid terminated. Cellular synthesis of essential amino acids depends on the availability of ammonium for amino acid synthesis. Specifically in *Anabaena variabilis*, the end product of ammonium is glutamine synthetase, the enzyme that produces glutamine. R changes depending on the noncyclic amino acid. For glutamine, R = $CH_2-CH_2-CONH_2$.

Hydrogenase, Nitrate/Nitrite Reductase, and Photosystem I/II. Each of these reaction centers have specific roles in the biochemistry of *Anabaena variabilis* and as shown, they share many levels of simultaneous feedback. Here, these reaction center specifics are studied for their role in producing ammonia

Plants and photosynthetic organisms depend upon a fixed source of nitrogen for growth and development. The most readily and easily used form of fixed nitrogen is the ammonium ion, NH_4^+. Ammonium is an essential component in the amino acid backbone shown in Figure 2. When the availability of free NH_4^+ in the local environment is low, organisms rely on their own biological processes to produce NH_4^+. Their production of NH_4^+ by enzymes contained within the cell cytosol (the liquid found inside cells where most chemical reactions take place) depend on a sufficient supply of substrate. Many organisms utilize atmospheric N_2, a very stable but abundant compound.

About 80% of earth's atmosphere is N_2, a stable and inert gas. Plants must

assimilate significant amounts of nitrogen for amino acid and nucleotide biosynthesis, as shown in Figure 2. Despite the renewable supply of N_2, it is not usable by plants due to its chemical stability. Thus, the unreactive nature of N_2 requires strategies to reduce N_2 to more reactive nitrogen species for further incorporation into biochemical pathways. In general, fixation of nitrogen is the reduction of triple bonded dintrogen, N_2, to other stable nitrogen containing species such as N_2O, NO_3^-, NO_2^-, and NH_4^+ [19, 23–25]. Biological nitrogen fixation (BNF), the evolutionary response of many organisms to obtain nitrogen from the environment, reduces atmospheric N_2 to NH_3/NH_4^+. Nitrogen fixing organisms produce an estimated 1.80×10^{14} tons of ammonia annually worldwide [15, 26]. A vast majority of the ammonia produced never leaves the ecosystem and is consumed as it is produced; therefore, the total mass produced by biological sources is difficult to estimate.

Although nitrogen fixation involves a number of oxidation reduction reactions that occur sequentially, the net reaction for the complete conversion in an acidic environment is:

$$N_2 + 8H^+ + 6e \rightleftharpoons 2NH_4^+ \qquad E^{\circ\prime}_{pH=7} = 0.034 \text{ V} \tag{9}$$

Organisms evolved to fix nitrogen in a cascading reaction sequence that is eloquent and complex. Many research hours and dollars spent on constructing an inorganic mimic to biological nitrogen fixation have not yet achieved the success of the biological system [27, 28]. Biological organisms catalyze the reduction of atmospheric nitrogen, a kinetically challenging task, by an enzyme catalyst called nitrogenase.

Here, the main objective is generation of ammonia at an electrode modified with ammonia producing cells or their ammonia producing enzymes. Either cells or enzymes would be held at the electrode with a benign polymer matrix. The electrode is to serve as a component in the redox sequence, either directly or by means of a mediator.

Nitrogenase was an enzyme of interest for this research because the enzyme reduces N_2 and produces NH_3 as a product and the fundamental goal of this research was to generate ammonia at ambient temperature and pressure for use as a fuel. Another major enzymatic pathway for cyanobacterial production of ammonia is the nitrate/nitrite reductase enzyme. Unlike nitrogenase, nitrate/nitrite reductase catalyzes the formation of NH_4^+ from already reduced (or fixed) sources of nitrogen, NO_2^- and NO_3^-. The ammonia produced by nitrate/nitrite reductase is not as well studied but significant to the work described here. Both nitrogenase and nitrate/nitrite reductase enzymes have been considered in this research. Nitrogenase was the primary enzyme of interest as it has been the target of many studies and its feedstock of ubiquitous N_2 and sunlight were very attractive from a renewable energy perspective. Less is known and reported about the nitrate/nitrite reductase enzyme, however electrochemically, there are more reaction possibilities with nitrates and nitrites. Further, there are high concentrations of NO_2^- and NO_3^- in livestock wastes. These wastes can contaminate groundwater sources and contribute to hazardous runoff into fresh water systems near farming operations. Therefore, there is considerable interest in ammonia production by the nitrate/nitrite reductase enzyme for waste remediation and ammonia production purposes. Experiments conducted

early in this research sought to correlate observed electrochemical phenomena with known nitrogenase biochemistry and kinetics as related to ammonia production. Some data provide evidence of electrode nitrogenase interactions but much data did not correlate well. Data from experiments conducted with cells whose nitrogenase synthesis had been suppressed suggested that an alternative enzyme and biochemical pathway results in unique voltammetry and increased ammonia production. It is important to note that both pathways are biologically capable of producing ammonia, but at an electrode surface, nitrate/nitrite reductase produced ammonia agrees more consistently with data obtained and observations made.

1.4.1 Reaction Center Chemicals of Interest

The focus of this research is NH_4^+ production at an electrode surface modified with cells that contain ammonia producing enzymes. A critical question was whether electrode enzyme interactions are accomplished by direct electron transfer between electrode and enzyme. There are two significant considerations about such a question: 1) enzymes are buried within cells where the cell membrane is at least 10 nm thick, a distance greater than can be easily traversed by electron tunneling during a charge transfer reaction; and 2) electron transfer through a hydrophobic membrane without known electron channels has not been reported and is difficult to justify without appropriate electrostatic compensation While direct electron transfer case is more straightforward and easier to model and verify experimentally, it is not the only possible method by which electron transfer reactions occur. Indirect electron transfer depends on a mediating chemical species that either cycles electrons to and

from the electrode and cell, or a chemical species that transfers electrons to the cytosol that elicits a more reductive environment within the cell. Many chemicals can passively diffuse across the cell membrane while others pass through a cellular energy gated channel. Because known spatial, temporal, and physical barriers exist that challenge the likelihood of direct electron transfer between electrode and enzymes, indirect electron transfer will be considered here. Known *in vivo* mediators and cofactors (redox recycling agents) for several enzymes within cyanobacteria are: ATP (required by nitrogenase, produced by photosystem I), $NADP^+$/NADPH (required in redox recycling in Nitrate/Nitrite Reductase, photosystem I), and ferredoxins, which are low potential reductant used by all reaction centers in Figure 1. These mediators and cofactors are discussed in the following sections.

1.4.1.1 Adenosine Triphosphate

Adenosine triphosphate, ATP, is a biological energy source. As in Figure 3, the electrochemistry of the adenine base is reported as similar to ATP, a molecule containing the adenine moiety [29]. At macro electrode cyclic voltammetry (as in this research), only a single peak has been detected (step III to IV in Figure 3), however two other steps have been observed at microelectrodes under fast scan CV. Thus, step III is the kinetically slow step in the reaction sequence. In the reaction, I, II, and III for adenosine refer to the structures in Figure 3. ATP participates in respiratory reactions in Photosystem I and II, becoming hydrolyzed to adenosine diphosphate (ADP) and possibly again to adenosine monophosphate (AMP). The hydrolysis shift reactions for each step are analogous to the electron and proton

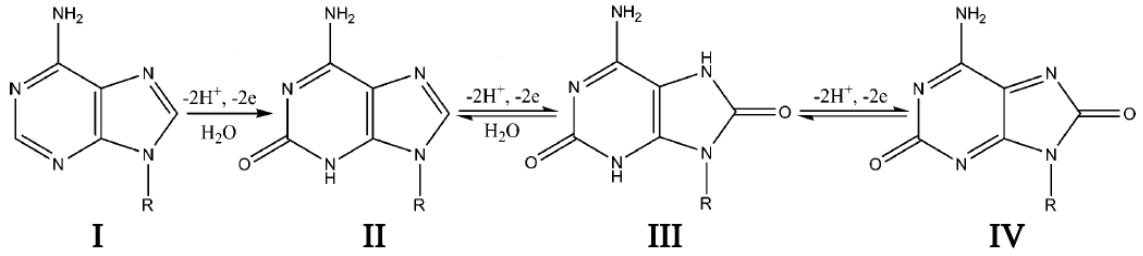

Figure 3. The stepwise reductions of the adenosine molecule, the backbone of ATP. R = a ribose unit, the moiety that undergoes phosphorylation and dephosphorylation (addition and removal of a phosphate group) in biochemical pathways. Steps III to IV most closely resemble the oxidation of ATP to ADP.

transfer steps of adenine, the active moiety of ATP, ADP, and AMP (Figure 3). Thus, ATP to ADP hydrolysis is not an electron transfer reaction. Known adenine electrochemical reactions are useful comparisons for ATP hydrolysis.

Nitrogenase, for example, requires binding to the Mg salt of ATP to undergo a conformational change of the Fe protein during the reduction of N_2 to NH_3. Thus, without sufficient ATP available, NH_3 production by Nitrogenase is not expected. When ATP is dephosphorylated to ADP during the Nitrogenase reaction, it must be removed (diffuse away or itself be recycled) else become inhibitory to Nitrogenase. Based upon data for the adenine molecule, the reduction potential for steps I III in Figure 3 are 0.958 V vs. SCE or more positive. Thus, free ATP or ADP near the electrode surface may be electrolyzed. It is unlikely ATP and ADP diffuse from within the cell, however the nature of voltammetric perturbation can elicit these events that would be sensed electrochemically.

1.4.1.2 Nicotinamide Adenine Dinucleotide Phosphate

The ubiquitous nature of nicotinamide adenine dinucleotide phosphate (NADPH) in the reaction center in Figure 1 is clear. NADPH is one of the most important electron donors in many organisms. NADPH/$NADP^+$ shares a close redox recycling relationship with ferredoxins. *In vivo*, NADPH is directly involved in photosystem I/II and nitrate/nitrite reductase enzyme and indirectly involved in nitrogenase by the recycling of ATP to ADP (Figure 1). The redox reaction of the NADPH/$NADP^+$ system is

$$NADP^+ + H^+ + 2e \rightarrow NADPH \qquad E^{o'}_{pH=7} = -0.565 \text{ V vs. SCE} \qquad (10)$$

In aqueous solutions, the solvent limit at a glassy carbon electrode nears 1.0 V vs. SCE. Thus, faradaic current arising from direct electron transfer between electrode and $NADP^+$ or NADPH will overlap with the capacitive current of water and not be sufficiently resolved for direct electrochemical analysis. Extensive, but contradictory, data regarding the electrochemical reversibilitiy of reaction 10 that results in biochemically active species is difficult, but possible [30].

1.4.1.3 Ferredoxins

Ferredoxins are small iron sulfur proteins that receive electrons from photosystem I and transfers the electrons to various reductases. Ferredoxins are also ubiquitous in cyanobacteria freely diffusible within cells. Ferredoxins act as biological capacitors, that accept and discharge electrons as part of several enzymatic pathways (Figure 1). Components of the nitrogenase proteins are structurally similar to ferredoxin

in that both contain Fe-S linkages. In the Nitrogenase proteins, the Fe-S linkages are in the cysteine residues of the terminal end of the enzyme proteins. Generally, ferredoxins are one electron transfer reagents that alter the oxidation state of an Fe atom (between +2/+3). Ferredoxins are electroactive and exist within the cell as both freely mobile and membrane bound reductants within cells. This low potential electron donor matches well with the low redox potentials of nitrogenase enzyme proteins. The redox reaction of ferredoxins are represented as [25]:

$$Fd\left(Fe^{3+}\right) + e \rightleftharpoons Fd\left(Fe^{2+}\right) \qquad E^{\circ'}_{pH=7} = -0.596 \text{ V vs. SCE} \qquad (11)$$

1.4.2 Ammonia Production by Biological Nitrogen Fixation (Nitrogenase)

Biological reduction of atmospheric N_2 is achieved by the nitrogenase enzyme. To meet the challenge of dinitrogen fixation, a kinetically challenging task, the nitrogenase enzyme has multiple redox centers. The nitrogenase complex consists of two sets of metalloproteins, the Fe and FeMo proteins. The Fe protein, dinitrogenase reductase (DiN), is two 64 kDa $[Fe_4S_4]^{2+/1+}$ α_2 dimers and the FeMo protein, dinitrogenase (DiNR), is a $[Fe_8S_7]$P cluster and a 230 kDa [Mo:Fe_7S_9]:homocitrate $\alpha_2\beta_2$ tetramer (Figure 4) [9, 23–25, 27, 31–34]. N_2 is the substrate for nitrogenase and the primary product of nitrogenase catalysis is NH_4^+ as shown in Figure 5. Figure 4 illustration *a* shows the protein crystal structure of the nitrogenase enzyme and illustration *b* shows the reaction chemistry of the nitrogenase enzyme. The protein crystal structure shows the three distinct proteins that are nitrogenase; Fe protein, MoFe protein, and the second Fe protein. The figure shows the binding

of ATP (bound nucelotide), the Fe-S based P cluster, and the FeMo cofactor species intercalated into the protein residues. In image *b*, the reaction chemistry of nitrogenase is diagrammed. The basic steps are outlined and include ATP to ADP hydrolysis, electron transfer, complex formation, and complex dissociation.

Briefly, the overall reaction by nitrogenase is:

$$N_2 + 8H^+ + 8e + 16ATP \rightleftharpoons 2NH_3 + H_2 + 16ADP + 16P_i \tag{12}$$

There is not a singular reduction potential that can be reported for Reaction 12 due to multiple processes that are electron transfer dependent. Overall, the required potential for essential steps have been reported in the range of -350 to -450 mV vs. NHE. [33, 35, 36] Generally, the reported redox potentials for the nitrogenase reaction refer to the electron donors such as ferredoxin [37, 38]. From Reaction 12 and shown in Figure 5, dinitrogen is reduced to ammonia with protons, electrons, and adenosine triphosphate (ATP). ATP is the biological unit of currency for energy transfer in living cells. Energy is stored in the phosphate group $\left(PO_4^{3-}\right)$ bonds and is reversibly transferred upon phosphorylation and desphosphorylation, the addition and removal of a phosphate group. Biologically, 16 moles of ATP is a high energy requirement. Reversible energy transfer with ATP/ADP is mediated by other chemical species and driven by photosynthesis. Thus, sunlight and a source of CO_2 are the initial energetic inputs Cells obtain N_2 from the atmosphere (Figure 5). The nitrogenase enzyme reduces N_2 at ambient temperature and pressure.

Nitrogenase requires N_2, a low potential reductant, and a source of energy, namely ATP, to catalyze the reduction of nitrogen. Nitrogenase requires a continuous

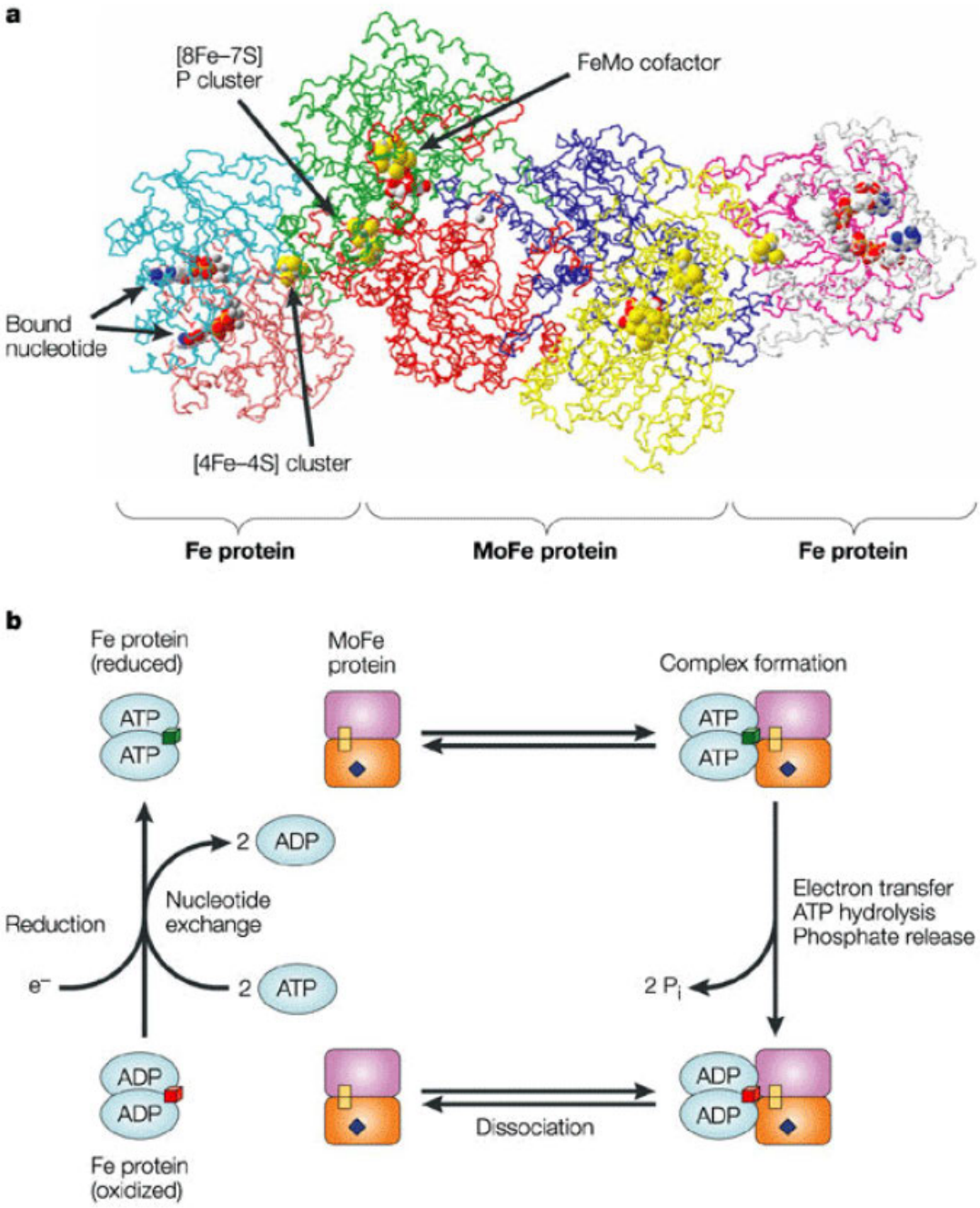

Figure 4. Structure and reaction pathway for the nitrogenase enzyme. a) Protein structure of the nitrogenase enzyme showing the Fe protein, FeMo protein, and Fe protein. b) Diagram of the reaction pathway and involved species for the fixation of N_2. Image reprinted from [31].

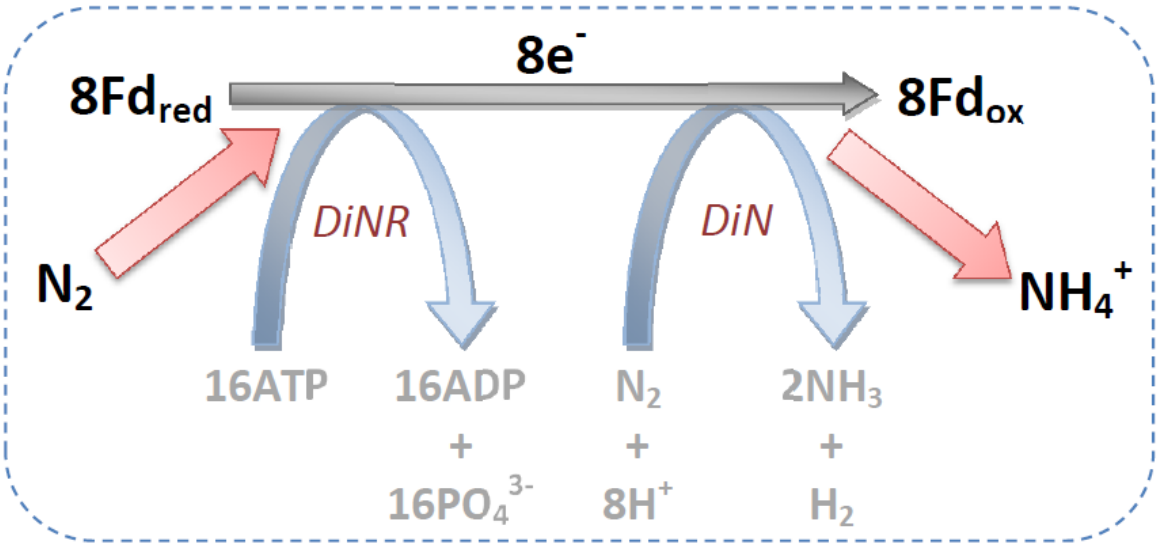

Figure 5. Schematic representation of the nitrogenase enzyme. The enzyme substrate is N_2. There are several components to the enzyme. Dinitrogenase reductase (DiNR) reduces ATP with a subsequent conformational change of the Fe protein in the enzyme. Eight electrons are obtained from reduced ferredoxins (Fd) and transfer to the dinitrogenase enzyme (DiN) that contains the FeMo protein. At this point in the enzyme, electrons from Fd, H^+, and N_2 substrate are catalyzed to 2 NH_3 and H_2.

supply of ATP during nitrogen fixation and shows a high rate of ATP utilization. The electron carrier in the nitrogenase system is ferredoxin. The free energy for reduction of N_2 by ferredoxins is negative, but additional energy required for fixation arises from ATP hydrolysis. Nitrogenase is synthesized by cells in response to ammonia starvation. Such ammonia starvation triggers nif genes to transcribe nitrogenase protein synthesis. Due to the high cellular energetic tax to fix nitrogen, other enzyme pathways can also produce ammonia. Such is the case when a fixed source of nitrogen is available to the cell. High fixed nitrogen represses nitrogenase synthesis. Common environmental sources of fixed nitrogen are nitrates and nitrites.

1.4.3 Ammonia Production by Enzymatic Conversion of Fixed Nitrogen Sources (Nitrate/Nitrite Reductase Enzyme)

This research initially focused on nitrogenase mediated NH_4^+ production. This was achieved by removing all ammonia from the cell culture medium. Nitrogen starvation in *Anabaena variabilis* elicits a genetic response to synthesize nitrogenase within heterocysts to fix nitrogen to ammonia. Thus, under starvation conditions, nitrogenase produced ammonia is the primary source of any ammonia measured. Nitrate and nitrite are also substrates for another enzyme found in cyanobacteria, the nitrate/nitrite reductase enzyme.

The nitrate/nitrite reductase complex consists of two components, ferredoxin nitrite reductase (NiR) and nitrate reductase (NR) (Figure 6). NiR is a monomeric protein of approximately 63 kDa in size. NiR contains a single $[4Fe-4S]$ cluster and a single heme like prosthetic group that serves as the active site to achieve

reduction of nitrogen. NR is a Mo centered homo dimer protein with two identical subunits joined by the molybdenum cofactor (MoC, molecular weight 100 - 114 kDa) [39–41]. The reduction of NO_3^- by nitrate/nitrite reductase is a two step process. First, nitrate/nitrite reductase catalyzes the reduction of NO_3^- to NO_2^-. This occurs in the cytosol and requires reductant in the form of NADPH. The second step of the nitrate/nitrite reductase, dependent on ferredoxins as electron carriers, is reduction of NO_2^- to NH_4^+.

Addition of NO_3^- and NO_2^- to the electrolyte impacts NH_3 production and the faradaic response due to voltammetric perturbation. As shown in Figure 6, the electrochemical reactions of interest in nitrate/nitrite reductase are

$$NO_3^- + 2H^+ + 2e \rightleftharpoons NO_2^- + H_2O \qquad E^{\circ\prime}_{pH=7} = 0.18 \text{ V vs. SCE} \quad (13)$$

$$NO_2^- + 8H^+ + 6e \rightleftharpoons NH_4^+ \qquad E^{\circ\prime}_{pH=7} = 0.071 \text{ V vs. SCE} \quad (14)$$

The formal potentials stated for Reactions 13 and 14 are thermodynamic values. The nitrate/nitrite reductase reactions are significantly dependent on pH and the H^+/e ratio. Further, Chapter 4 will discuss the complexity of the electrochemical reaction possibilities for nitrates and nitrites. Chapter 4 discusses how the redox potentials to drive these reactions are closely related and difficult to distinguish. The likelihood of disproportionation reactions is large, which complicates exact identification of the stepwise ammonia generation. The intermediates in denitrification are NO and N_2O. Denitrification is a dissilmilatory route for the reduction of NO_2^- and NO_3^- in prokaryotic organisms like *Anabaena variabilis* [41]. The end product of denitrification is N_2. Denitrification is a catalytic process dependent upon enzymes.

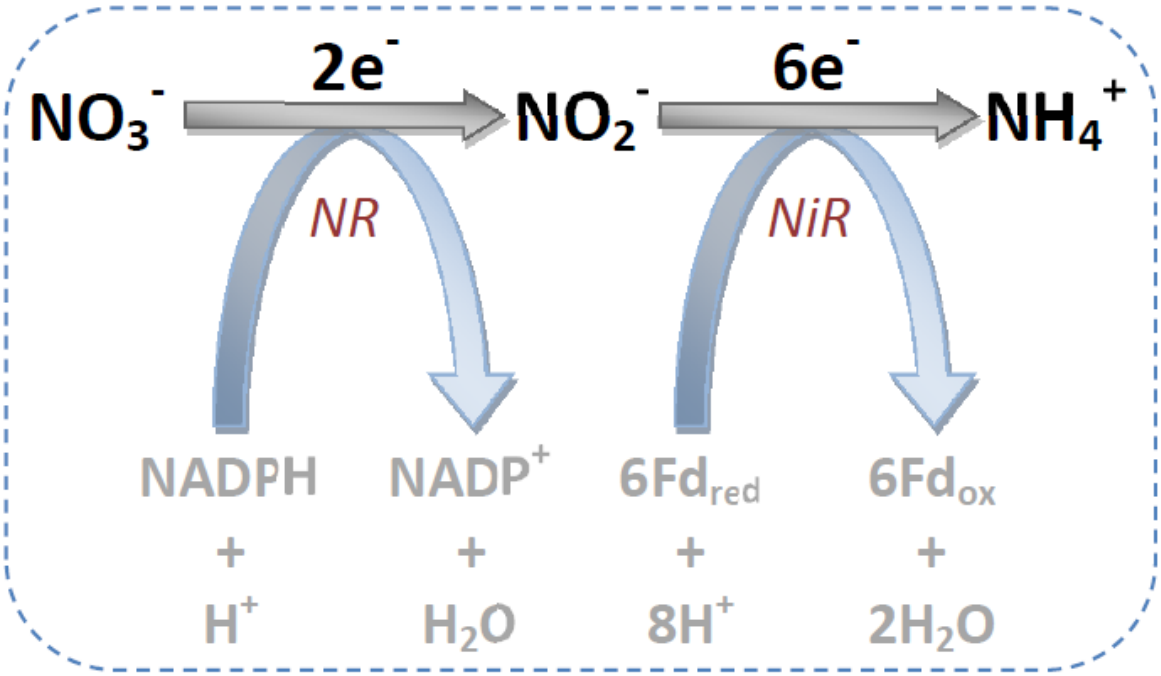

Figure 6. Representation of the nitrate/nitrite reductase enzyme. The enzyme substrates are are NO_3^- and NO_2^-. Reduction of NO_3^- first yields NO_2^- followed by subsequent reduction of NO_2^- to NH_4^+. The reduction of NO_3^- (NR = nitrate reductase) is NADPH dependent whereas the reduction of NO_2^- (NiR = nitrite reductase) is a ferredoxin dependent reaction.

It is not of interest for this research other than to recognize possible intermediate products like NO and N_2O, which are also substrates for the denitrification pathway. Nitrate and nitrite reactions provide an amazing economy of the energetics involved in the cyanobacteria electrode production of NH_3.

1.4.4 Nitrogenase and Nitrate/Nitrite Reductase Relationship

Scientists who study the biological nitrogen cycle have considered the impact of nitrate/nitrite reductase. Nitrate assimilation is a general term to describe the

enzymatic bacterial conversion of NO_3^- to NH_4^+. In the denitrification pathway, the roles of NO_3^- and NO_2^- are considered for the formation of N_2, the substrate for nitrogen fixation. Thus, in the absence of ammonia, nitrate/nitrite reductase produces ammonia from NO_3^- or NO_2^-. If both enzymes are present and active, perhaps when nitrogenase synthesis has not yet been repressed but has low activity, some NO_2^- can divert to the denitrification path for eventual N_2 formation and fixation. [41–43]

Both nitrogenase and nitrate/nitrite reductase produce ammonia as a product. Nitrogenase requires gaseous N_2 as a substrate whereas nitrate/nitrite reductase depends on reduced nitrogen in the NO_2^- or NO_3^- form as a substrate. Nitrogenase is an ATP dependent reaction. Biochemically, respiration through photosystem I recycles ADP to ATP in a ferredoxins and NADPH dependent manner. Further, it is known that ATP binding to the Fe protein of nitrogenase is the rate limiting step. Nitrate/nitrite reductase does not depend on reducing equivalents provided by the dephosphorylation or ATP to ADP, which simplifies the mechanism. Nitrogenase produced H_2 as a byproduct, but nitrate/nitrite reductase does not. Both nitrogenase and nitrate/nitrite reductase depend on the reducing power of NADPH. NADPH electrolysis is a ubiquitous electron transfer reaction in living organisms. The relationship between nitrogenase and nitrate/nitrite reductase presents a complex system with multiple levels of shared substrates, cofactors, and mediators. Decoupling the exclusive contribution to total ammonia production by each enzyme is not the goal of this research. Rather, the goal is to capitalize on either or both enzyme contributions to sustained and increased production of

ammonia.

1.5 Research Goals

Ammonia as a fuel shows promise but is limited by the production costs. The research presented here focuses on developing a system to gain electrochemical influence over biological production of ammonia, whether by nitrogen fixation from atmospheric N_2 (nitrogenase) or catalytic reduction of reduced nitrogen species (nitrate/nitrite reductase). With solar radiation as the primary source of energy to drive the production of ammonia, appropriate system design will efficiently produce sustained concentrations of NH_4^+ at ambient temperature and pressure. Photosynthetic cyanobacteria are the source of the ammonia producing enzymes nitrogenase and nitrate/nitrite reductase. Nitrogenase and nitrate/nitrite reductase are present in many photosynthetic microorganisms and are abundantly available, renewable, ecologically benign, and environmentally adaptive. Photosynthetic cyanobacteria produce ammonia by reduction of N_2 (nitrogen fixation) or reduction of NO_3^- and NO_2^- (nitrate assimilation) biological nitrogen fixation.

This research exploits nitrogenase and nitrate/nitrite reductase enzymes by incorporation of the enzymes into an electrochemical system for the sustained ammonia production. Specifically, cyanobacterial nitrogenase and nitrate/nitrite reductase enzymes will be immobilized in a modified Nafion® polymer film attached to an electrode This investigation is undertaken in a multistep process that draws from a variety of scientific domains that include electroanalytical, biological, and physical chemistry. The essential components of this research include culture of

photosynthetic cyanobacteria that contain at least two ammonia producing enzymes (Chapter 2); immobilization of the cells containing enzyme in an immobilization polymer on an electrode (Chapters 2, 3); characterization of cells and enzymes electrochemically (Chapter 3); evaluation of the ammonia production efficiency of the electrode immobilized cells (Chapter 5); and development of the mechanistic model framework to describe the observed ammonia production (Chapter 5).

CHAPTER 2

EXPERIMENTAL BACKGROUND AND DESIGN

An alternative method for ammonia production that is not dependent upon high temperatures and pressures and a fossil fuel based source of hydrogen would make ammonia a more financially and environmentally promising fuel. Biological nitrogen fixation and other cyanobacterial enzyme processes achieve ammonia production under ambient conditions with sunlight as its primary energy source. Each known ammonia producing enzyme within cyanobacteria depends on low potential electron carriers to diffuse to the enzyme and increase the reductive potential within the cell. Reactions involved in the biocatalytic conversion of nitrogen sources to ammonia require low potential driving forces to accomplish efficient conversion. The need for low potential electron transfer presents an electrochemically interesting system to study. Many currently investigate cell and enzyme immobilization to electrode surfaces for enhancing electrocatalysis [44–51]. Free living photosynthetic cyanobacteria produce ammonia along existing biosynthetic pathways in their natural habitat. The complex electrochemical system driving the reduction of nitrogen to ammonia via nitrogenase, for example, is only partially understood from an electrochemical approach of study [27, 35, 38, 52–59]. Electrochemical interrogation of ammonia producing enzymes with cyclic voltammetry and subsequent modeling assists in a broader understanding of the cell, enzyme, and electrode interactions. While these biological systems tend to be very complex, electrochemical analysis of enzyme|electrode reactions provides a framework for understanding increased

ammonia production by immobilized cells.

As the goal for this research is to produce ammonia at ambient temperature and pressure, organisms already capable of achieving this on a small scale were selected as to exploit the ability of cells to drive the kinetically challenging and energy intensive process of producing ammonia. In general, the ammonia produced by these cells is destined for amino acid synthesis for organism growth and nutrition. A system that intercepts or diverts the flow of ammonia produced enzymatically has significant implications. This research attempts to construct a multiple domain architecture to support the ammonia producing mechanism of cyanobacteria without the requirement of significant energy input. The research also extends further into the system by building a foundation for the correlation of electrochemical data with ammonia production data and a resultant kinetic model framework.

2.1 Cyanobacteria

Cyanobacteria, commonly referred to as blue green algae, is a phylum of bacteria that obtain their energy through carbon sequestration via photosynthesis. The ability of cyanobacteria to perform oxygenic photosynthesis is thought to have converted the early reducing atmosphere of Earth into an oxidizing environment, which dramatically changed the composition of life forms on Earth by stimulating biodiversity and leading to the near extinction of oxygen intolerant organisms. Cyanobacteria are a ubiquitous genera of organism found in almost every possible environment, from oceans to fresh water to bare rock and soil. Cyanobacteria are easy to culture in a laboratory and are available commercially from the American

Type Culture Collection (ATCC). Ammonia producing cyanobacterial strains have several key characteristics that warrant study from an energy perspective. Cyanobacteria depend upon sunlight for energy (a renewable source), produces ammonia (alternative fuel and essential fertilizer), fix carbon (releases O_2 as a product), and grows as a self contained ecosystem with 2 - 8 % conversion efficiencies [1, 7, 23–25, 60, 61]. Biotechnological development of energy systems have often focused on algae for biomass or H_2 production, but few have focused on using algae for NH_3 production. *Anabaena variabilis* is a strain of photosynthetic cyanobacteria that contains enzymes that produce NH_3 at ambient temperatures and pressures.

2.1.1 *Anabaena variabilis*

Anabaena variabilis (ATCC #29314) is a hearty strain of filamentous heterocystic cyanobacteria that have been studied and investigated since their discovery and genetic sequencing in the early 1980's. A great deal has been reported about culturing cyanobacteria and immobilizing live cells for the purpose of NH_3 and H_2 production [38, 62–69]. The *A. var.* strain was primarily selected because it produced some of the highest NH_3 output relative to other strains of cyanobacteria. Further, *A. var.* is a commonly found strain of cyanobacteria that does not have extreme environmental conditions for survival and growth.

Anabaena variabilis cells grow as long chains of connected cells called filaments (Figure 7). The two most significant cell types within a filament are vegetative cells and heterocysts. The vegetative cells, labeled V in Figures 7 and 8 comprise 80-85 % of *A. var.* cellular density. The vegetative cells contain photosystem I

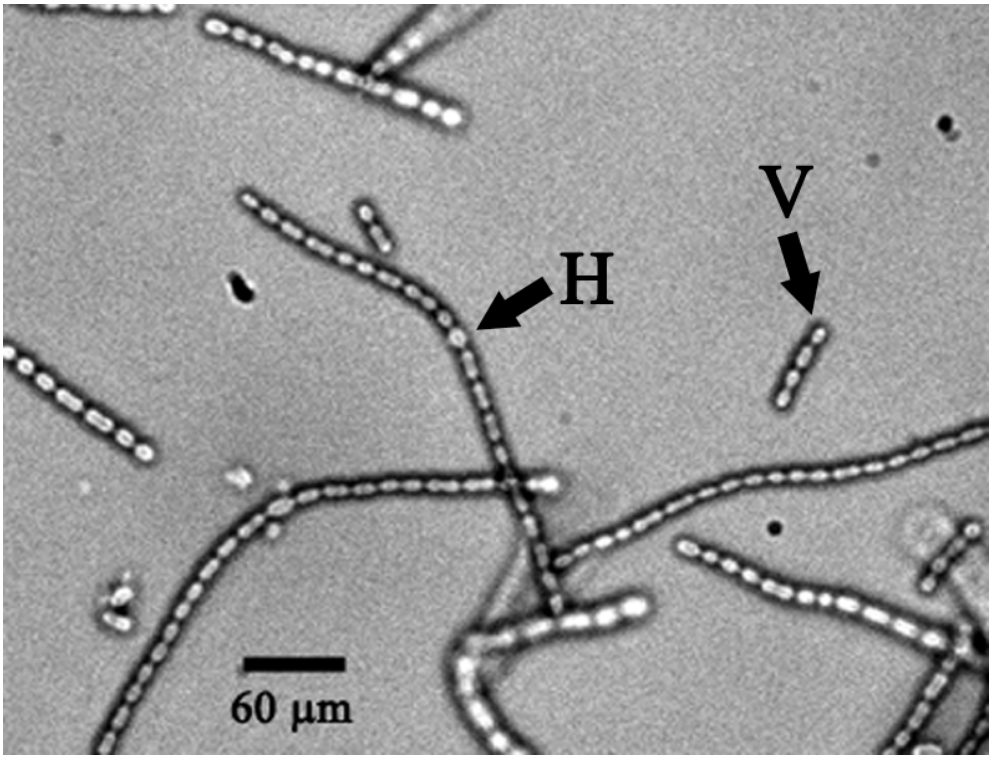

Figure 7. 50× brightfield image of *Anabaena variabilis* SA-1. 5 μL of cell suspension was applied to a new glass slide, covered with a coverslip, and imaged on an inverted microscope. Two significant cell types are highlighted, vegetative cells (V) and heterocysts (H). Scale bar indicates 60 μm.

and II, the active sites of cellular respiration and carbon fixation. Additionally, the vegetative cells contain many enzymes within the cytosol. The enzyme of interest located in vegetative cells is nitrate/nitrite reductase. The cell membranes are multilayered structures approximately 1 μm in diameter. The vegetative cells fuse into long filaments, typically 20-30 cells in length. The membrane is a typical phospholipid bilayer with additional cellular layers interspersed. The membrane contains numerous channels for the passage of species into and out of the cell. Some of these channels are actively controlled. An active channel requires cellular energy, such as adenosine triphosphate (ATP), to bind to the channel and thereby allow entrance or exit of chemical species from the cytosol. Passive channels are typically ion selective and allow for the passive diffusion of ions into the cytosol. Uncharged species can freely diffuse through the membrane as well, thus enzyme substrates like NO_3^- and NO_2^- and N_2 and products like NH_4^+ are able to enter and exit the cell. At an approximate 10 % spacing density, heterocysts are found in *A. var.* grown without a fixed source of nitrogen; thus, one in ten cells in a *Anabaena variabilis* filament is a nitrogenase containing heterocyst.

Under fixed nitrogen starvation conditions, nitrogen fixation (nif) genes encode for the formation of heterocysts, the evolutionary response to an organism's limited fixed nitrogen availability. Heterocysts have thickened (2 μm) diameter cell membranes and are relatively impermeable to O_2. Nitrogenase is strictly located in the heterocysts. Due to protection offered by the heterocysts, nitrogenase is protected from its most common inhibitor, O_2, which irreversibly binds to nitrogenase. Heterocysts, labeled *H* in Figures 7 and 8 are easily distinguished visually due to

their larger size and lack of color resulting from the absence of photosystem I/II. To achieve nitrogen fixation, nitrogenase requires ATP, which is the end product of the respiratory electron transport chain in the vegetative cell chloroplasts. Heterocysts and vegetative cells are connected by a thin channel that allows shuttling of products and reactants from one cell type to another. Heterocysts can be isolated and exhibit high enzyme activity for short periods of time if not supplemented with an ATP recycling system, normally provided by the vegetative cells.

Ammonia produced by *A. var.* is the primary substrate for the enzyme glutamine synthetase; therefore, nearly all NH_4^+ produced enzymatically never exits the cytosol. *A.var.* have been genetically mutated to be nitrogenase derepressed [70–74]. The process of mutagenesis is described elsewhere in full detail [73]. Briefly, the procedure to generate *Anabaena variabilis* SA-1 was accomplished by ethyl methanesulfonate (EMS) mutagenesis. EMS is a mutagenic organic compound that produces random nucleotide substitutions in genetic sequences. After screening resultant mutants, the SA-1 strain was isolated and subcultured, producing only nitrogenase derepressed progeny. The method is fully described by Spiller, *et. al* [73].

The mutant strain SA-1 is used in this research because enzymatic production of NH_4^+ is blocked at the assimilation step of glutamine synthetase, the primary route for intercellularly produced NH_4^+. NH_4^+ itself is a mediator of nitrogenase synthesis and nitrate/nitrite reductase activity. In wild type cells, sufficient NH_4^+ in medium repress enzymatic production of NH_4^+ due to decreased synthesis of nitrogenase enzyme. Genetic manipulation has generated several strains of *A. var.*

The SA-1 strain shows derepression which is the activation of the genes responsible for ammonia producing enzyme synthesis, that are otherwise repressed by NH_4^+. Further, the SA-1 *A. var.* mutant produces nitrogenase and nitrate/nitrite reductase in the presence of NH_4^+ and excretes the NH_4^+ synthesized into the external medium [75–77]. For these reasons, *A. var.* SA-1 is the ideal strain for sustained NH_3 production by the nitrogenase and nitrate/nitrite reductase.

2.2 Cell Culture

Two strains of *Anabaena variabilis* were cultured in this research. The commercial strain (ATCC #29413) was purchased from the American Type Culture Collection and the SA-1 genetic mutant strain was graciously received from K.T. Shanmugam (The University of Florida), were inoculated in June, 2009 [70, 71, 73, 77]. The cell cultures were grown in 250 mL baffled glass flasks that contain approximately 200 mL of media. BG-11_0 freshwater algae media was prepared in the lab following the recipe used by many involved in cyanobacteria research [11, 66, 78] (Appendix A). BG-11_0 does not contain NH_4^+, NO_2^-, or NO_3^- so as promote nitrogenase synthesis. The flasks were grown autotrophically at 32 °C in a thermostated water jacketed incubator on an orbital shaker (New Brunswick) at 125 RPM. The incubator was fitted with two broad spectrum (400-700 nm) fluorescent lamps that illuminates the culture flasks at a Photosynthetic Photon Flux Density (PPFD) of 31.8 ± 1.6 μE m^{-2} s^{-1}, where one Einstein (E) is a unit defined as one mole (6.022×10^{23}) of photons (LI 190 Quantum Sensor; Li-Cor) [79]. PPFD is a measure of Photosynthetically Active Radiation (PAR). See Appendix A for further details

of the PAR and PPFD. The interior of the incubator is kept at a 0.05 % CO_2 atmosphere. Cell media was refreshed at least every two weeks (Appendix A). Cells in excess were subjected to DMSO pretreatment and frozen 80 °F in cryovials.

2.2.1 Monitoring Culture

Several variables are important in monitoring the health, viability, structure, and function of a cyanobacterial culture. A major indicator of health is color. As *Anabaena variabilis* are photosynthetic, they appear bright green in color. Degradation of the cell or a decline in the health of the culture is primarily observed by a either a yellowing or bleaching of the cell culture media. Several analytical methods were employed to follow the growth, density, and health of the cultures that include digital imaging, chlorophyll a assays, and total protein assays.

Cultures of *A. var.* were monitored visually with an inverted microscope (Olympus IX-71). Brightfield phase contrast 50× and 100× images were captured with a CCD camera at 1.45 M effective pixels (Olympus DP-70). Figure 8 show digital images of representative *A. var.* SA-1 cells. Regular visual inspection during the initial inoculation phase of the culture closely monitored the health, growth, and physiological features of the cells. These were compared to literature reports for this culture.

2.2.2 Density Assays

Cell density at an electrode surface is an important value to for quantitative assessments. Cell density is the link between ammonia production and

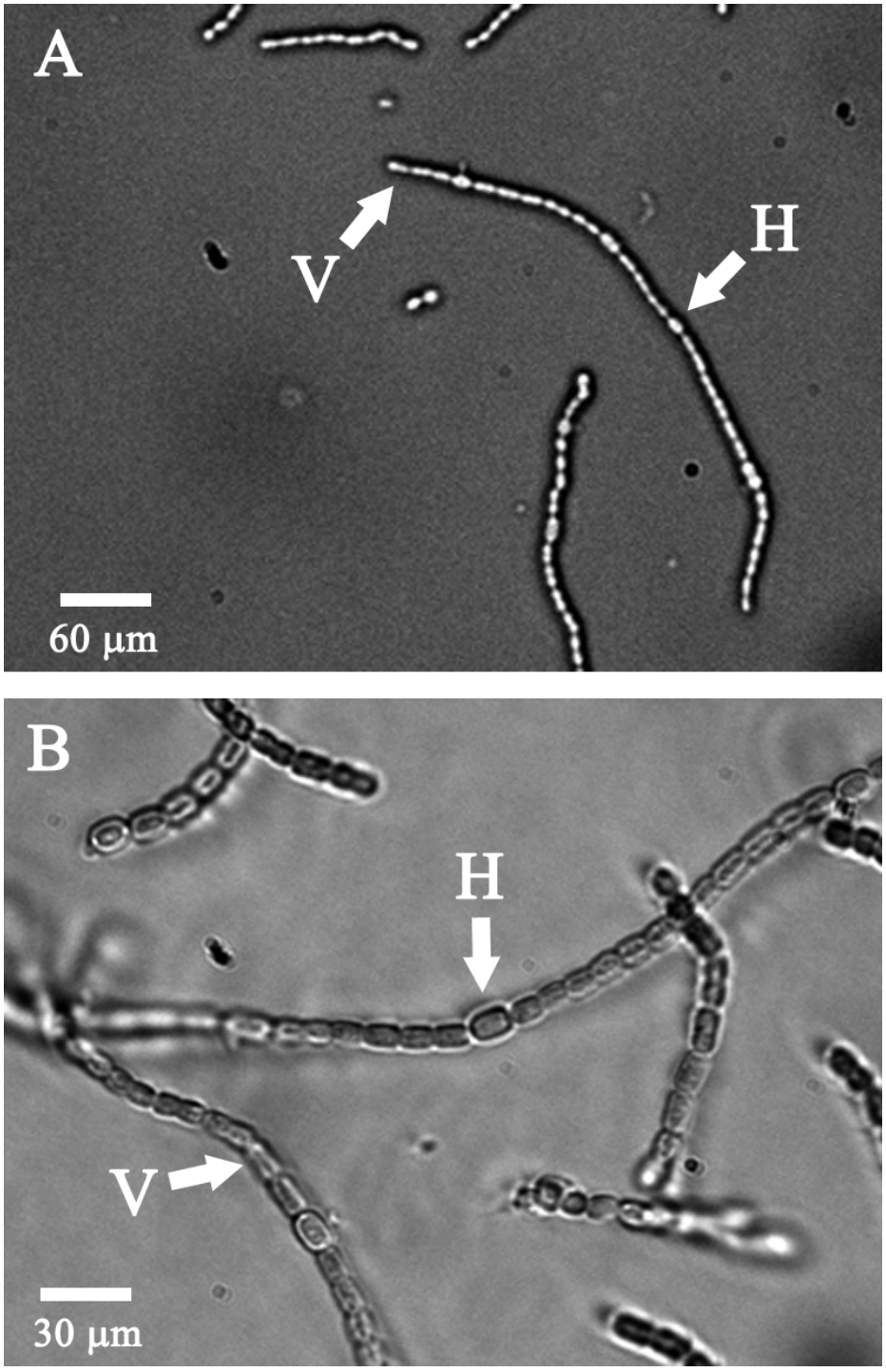

Figure 8. Brightfield images of *Anabaena variabilis* SA-1 captured at 50× and 100× magnification. 5 μL of cell suspension was applied to a new glass slide, covered with a coverslip, and imaged on an inverted microscope. A) 50× magnification of cell filaments, scale bar 60 μm; B) 100× magnification of cell filaments, scale bar 30 μm. Two significant cell types are highlighted, vegetative cells (**V**) and heterocysts (**H**).

electrochemical signals. Catalytic production of ammonia is proportional to the amount of enzyme present. Thus, for a fixed concentration of enzyme per cell, total cell density is a reasonable estimate and measure by which to normalize ammonia output data. This research used two methods by which to estimate cell density in a suspension, total chlorophyll a extraction and total protein measurements.

2.2.2.1 Chlorophyll a Assay

Algae research data relate total chlorophyll a concentration to nearly all measured parameters. Chlorophyll a is the major pigment found in oxygen tolerant photosynthetic organisms. Chlorophyll a is a porphyrin ring with a long hydrocarbon tail. The tail interacts with the hydrophobic thylakoid membranes to hold its position within the cell. Solar radiation incident to a cell surface excites electrons in the porphyrin ring and transfers them into the electron transport chain. The reaction centers photosystem I and II contain chlorophyll a molecules and are only located within vegetative *Anabaena variabilis* cells. A calibration between chlorophyll a concentration and cell density is difficult to construct because cells contain various concentrations of chlorophyll a depending on the growth cycle stage and environment where the cells are grown. Thus, while [chlorophyll a] is not a direct measure of cell density, it is a manner by which to relate analytical measurements such as ammonia output to the photosynthetic activity of a culture sample.

Chlorophyll a has a peak of maximum absorption at 565 nm. By the method of Mackinney [80], chlorophyll a is extracted from the cells in 100 % methanol whose

absorbance is measured at 565 nm in a UV-Vis spectrometer (Ocean Optics 4000). A 250 mL culture flask is well mixed. 1.5 mL sample of cell suspension is placed into a microcentrifuge tube and centrifuged at 4,400× for 5 minutes (Eppendorf 5260). The media is decanted and replaced with 1.5 mL 100 % methanol. After mixing for 5 minutes by vortexing, the methanol extracts chlorophyll a from the cells in a dark container to minimize light oxidation of the pigment. Cells and cellular debris are centrifuged from the methanol solution at 4,400× for 5 minutes. The resultant chlorophyll a solution in methanol is placed into a 1 cm cuvette. The absorbance at 750 nm, if any, results from interfering pigments such as chlorophyll b. Absorbance at 750 nm is subtracted from absorbance at 565 nm. By the Beer Lambert law,

$$A = \epsilon bc \tag{15}$$

where A = absorbance in arbitrary units, ϵ = the molar extinction coefficient for chlorophyll a in units of mL μg^{-1}, b = the path length of the cell in cm, and c = concentration of the analyte in μg mL^{-1}. In 100 % methanol, $\epsilon_{chlorophyll\ a} = 12.7$ mL μg^{-1}. All absorbance measurements reported have the background methanol absorbance subtracted. The density of chlorophyll is useful to normalize data obtained from the system, such as ammonia concentration per unit of cells immobilized, which is proportional to the density of chlorophyll a extracted.

2.2.2.2 Total Protein Assay

Another method to estimate the density of *A. var.* is to measure the total protein in a sample. The Coomassie (Bradford) Assay is a colorimetric method for total

protein quantitation. The method used in this research is a modification of the Bradford method [81, 82]. A Coomassie Plus (Bradford) Assay Kit was purchased from Thermo Scientific. This kit supplies a coomassie reagent that results in significantly less protein to protein variation than is observed with traditionally used Bradford reagents.

When the coomassie dye binds to protein in an acidic solution, an immediate shift in absorption maximum occurs from 465 nm to 595 nm with a simultaneous color change from a clear brown to a brilliant clear blue. The absorbance at 595 nm is measured with a UV-Vis spectrometer (Ocean Optics 4000) and correlated to a calibration completed with bovine serum albumin (BSA) as the standard protein. The working range of the Coomassie Plus Assay is 100-1500 μg mL^{-1} of protein. This range sufficiently covers the density of cells immobilized to electrode surfaces in this research.

The process of binding the coomassie dye to protein residues is the same for both the standard (BSA) and *A. var. s*uspensions. In 1.5 mL microcentrifuge tubes, 50 μL of sample containing protein is added to 1.5 mL of Coomassie Plus Reagent and thoroughly mixed by vortexing for 2 minutes. The tube is incubated at room temperature for 10 minutes for more consistent results. The UV-Vis spectrum of the blank (BG-11$_0$ media) was obtained and stored for subtraction. Absorbance was measured, in quadruplicate, for nine BSA standards. The BSA standard were prepared from commercially obtained BSA (2 mg/mL). Figure 9 is the representative calibration curve for the BSA standards. Vertical error bars represent $\pm$ 1σ from the mean of 4 samples. Total protein measurements from solutions of

different cell density are analyzed in the same manner. Protein concentration is measured versus the calibration shown in Figure 9.

2.3 Cell Immobilization

Modification of electrodes with enzymes is not a new idea. The literature has examples of hydrogen fuel cells in which the catalytic breakdown of H_2 is achieved with enzymatic machinery instead of expensive metal catalysts on the anode surface [49]. Minteer and her group have provided a wealth of information and methods for immobilizing enzymes in polymer layers on electrodes and exploiting enzymes to catalyze electrochemical reactions and drive biofuel cells [83]. Most often, enzymes are more stable and more effective when immobilized in a matrix than in their natural state [48].

Others have immobilized enzymes in modified Nafion layers on electrodes and demonstrated effective enzyme catalysis of appropriate substrates.[83] The Nafion matrix provides enhanced stability and lifetime of the enzyme and enhances enzyme reactivity. Where such systems are stable and efficient, product output is low. An ideal immobilization polymer should provide structural support and allow for ready diffusion of species to and from the cells and active enzyme sites. With some modification, Nafion is an ideal physical support polymer.

2.3.1 Nafion

Nafion is a highly acidic ion exchange polymer, sharing the same polymeric fluorocarbon backbone as Teflon®. The molecular structure of the hydrogen form

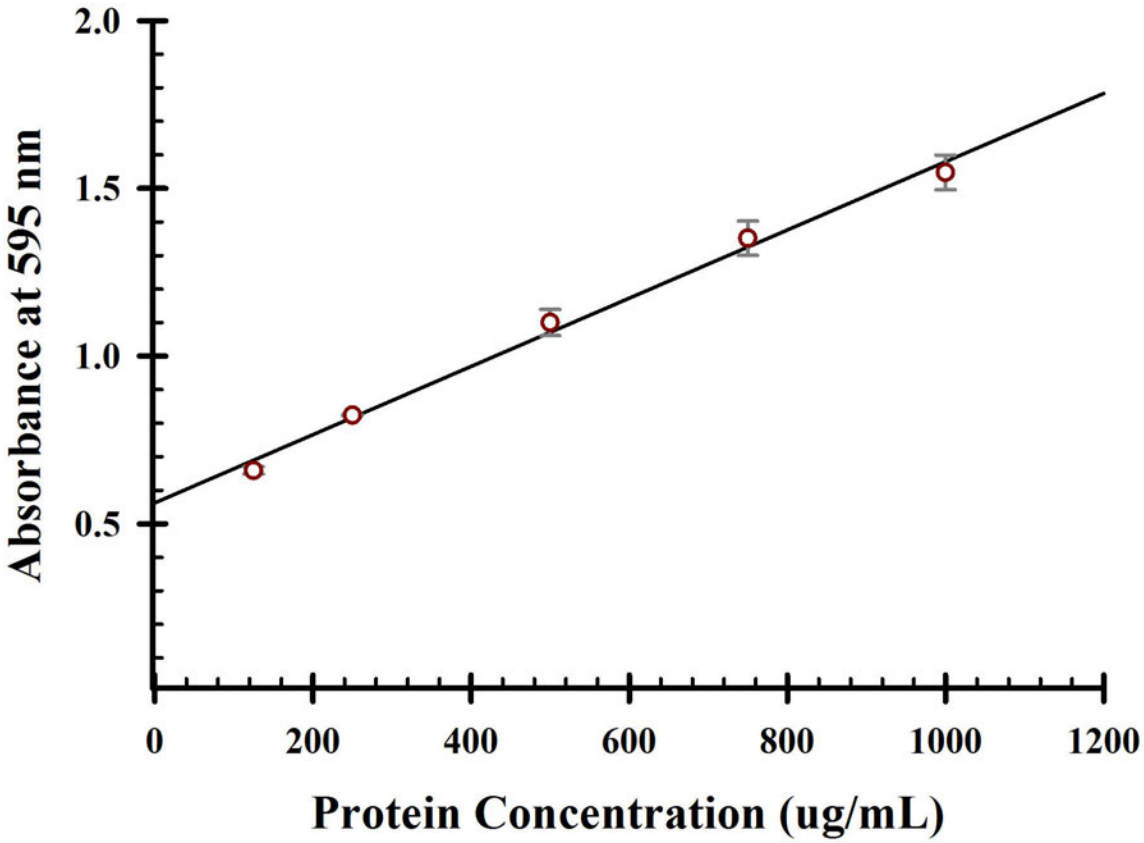

Figure 9. Total protein calibration plot by the Bradford method. Absorbance at 595 nm was measured from concentrations of bovine serum albumin (BSA) standards. The linear range (125 - 1000 $\mu g/mL$ BSA) results in the following regression: $y = 0.06x + 0.001$, $R^2 = 0.98$. Vertical error bars are ± 1 σ for each concentration of BSA tested, $n = 4$.

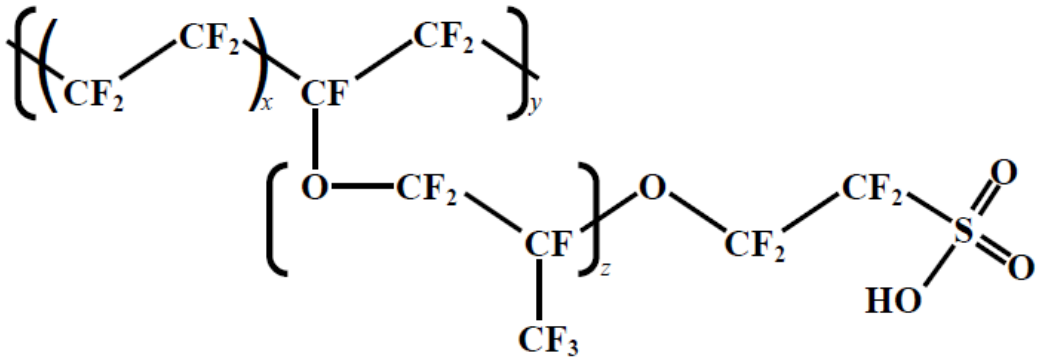

Figure 10. Chemical structure of Nafion ion exchange polymer. Nafion has a tetrafluoroethylene (Teflon like) backbone (x) with an additional fluoropolymer (y) and end terminated with perfluorovinyl ether groups (z) and a sulfonic acid site.

Nafion is shown, where the sulfonic acid ($R'SO_3^-$) site is neutralized by a proton (Figure 10),where z is usually 1; $5 \leq x \leq 7$. Commercial preparations of Nafion 1100 EW are available as suspensions in lower aliphatic alcohols and water (5% w/w; Sigma Aldrich). Hydrated Nafion film structure is modeled as a cluster|network, similar to an inverted micelle structure [84]. Figure 11 shows a diagram of the micellar structure of hydrated Nafion polymer.

Because the ion selective nature and acidity of Nafion create an inhospitable environment for living cells, the polymer structure is modified. In modified Nafion, the proton is replaced with an organic alkyl ammonium cation, R_4N^+. Introduction of R_4N^+ alters the properties of Nafion to reduce its corrosive nature and allow transport of anions into the matrix [85]. This exchange of proton for R_4N^+ provides a matrix that supports and stabilizes the enzymes to provide long term enzyme stability and catalytic efficiency [48, 49, 85, 86]. Modified Nafion will be used to stabilize the nitrogenase in a matrix where reactants can be introduced to the

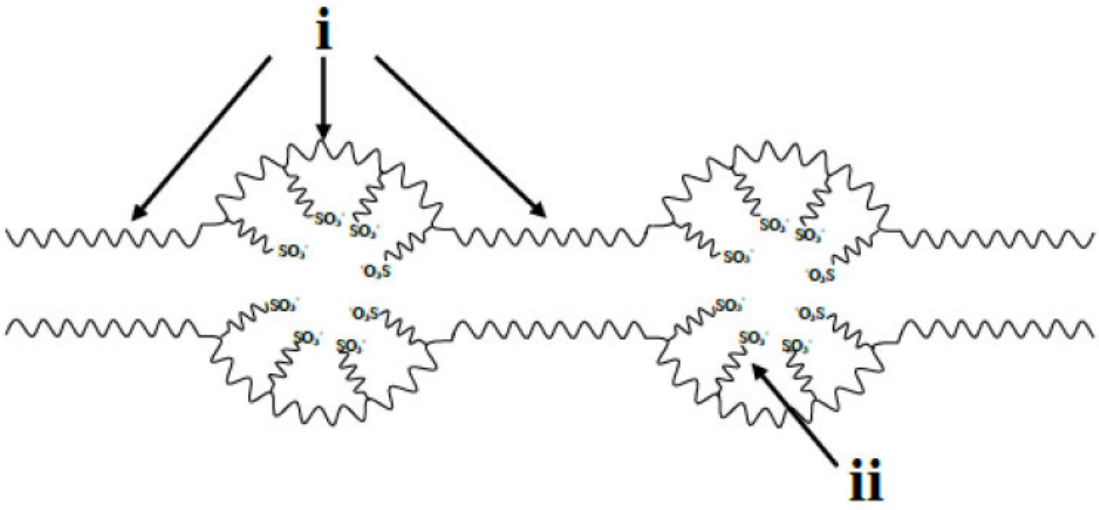

Figure 11. Drawing of the micellar structure of Nafion. The copolymerization of the tetrafluoroethylene backbone (i) and sulfonic acid terminated perfluorovinyl ether polymer (ii) creates a micellar structure with pore diameters of 4 nm and intermicellar pores of of 1 nm. The drawing is not to scale. Drawing created by Garett Lee, The University of Iowa.

enzyme and products can be removed. Modified Nafion also serves to bind the cells to the electrode surface for more efficient electrochemical processing.

2.3.2 Trimethyloctadecyl Ammonium Bromide Modified Nafion

The approximate diameter of single *Anabaena variabilis* vary between 5 μm and 10 μm depending on cell type and chain length. Based on work by Minteer et. al. [48, 49, 85–89], Nafion was modified with trimethyloctadecyl ammonium (TMODA) bromide (Sigma Aldrich) (Figure 12). The long hydrocarbon tail of the alkyl ammonium bromide significantly increases the Nafion pore diameter by increasing hydrophobicity, reduces acidity, and nearly eliminates ion selectivity as compared

Figure 12. Chemical structure of octadecyltrimethylammonium (TMODA) bromide. TMODA is a long chain alkyl ammonium cation. It is reacted with Nafion to increase the hydrophobic regions of Nafion micellar pores, thus altering mass transport through the film and creating a structurally robust and protective microenvironment for cyanobacteria immobilization.

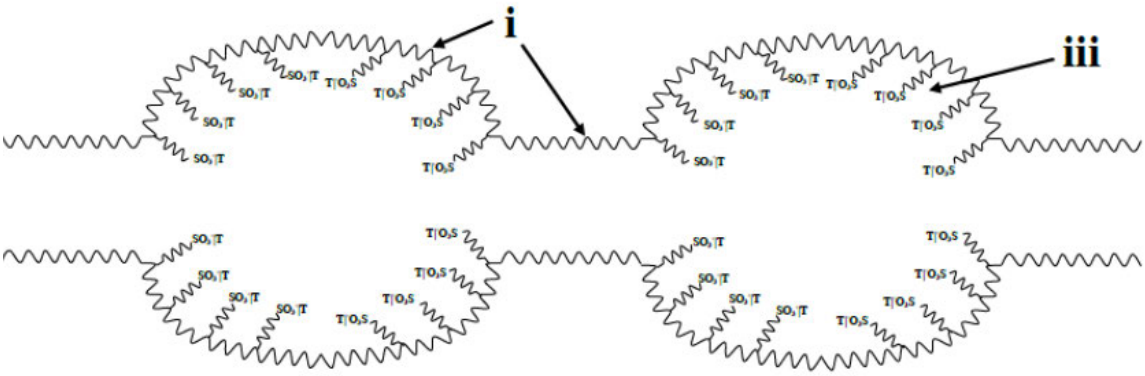

Figure 13. Drawing of the micellar structure of octadecyltrimethylammonium (TMODA) bromide modified Nafion. The tetrafluoroethylene backbone (i) and cation exchanged TMODA terminated perfluorovinyl ether polymer (iii) creates micellar pores of significantly increased diameter. The drawing is not to scale. Drawing created by Garett Lee, The University of Iowa.

to Nafion (Figure 13). The pores/micelles created create an ideal environment for structural support of biomolecules and cells.

5 mL of TMODA Nafion suspension was prepared by mixing a 20 % molar excess of TMODA salt (0.092 g; Sigma Aldrich) with 5 mL of 5 % 1100 EW Nafion suspension (Ion Power) and vortex mixed for 10-15 minutes. The resultant solution was poured into a weighing dish and dried in a $CaCO_3$ (Drierite) desiccator overnight. Distilled and deionized water (18.1 MΩ; Millipore) is added to the

weighing dish in excess and allowed to soak overnight to remove the bromide salt side products formed during the exchange. The water with bromide salt waste is decanted and the resultant polymer is rinsed several times with distilled and deionized water and again dried in a desiccator overnight. The resultant TMODA Nafion film is suspended in 70 % alcohols and water (63.4 % v/v ethanol, 3.2 % v/v methanol, 3.4 % v/v isopropanol, 30 % v/v water; Decon Labs). Significant agitation is necessary to solubilize the solid TMODA Nafion. Mixing the solid and alcohols in a 15 mL culture tube and adding glass beads facilitates mixing when rotator mixed for 8 hours. Prior to use, the polymer suspension is vortexed for 1-2 minutes.

2.3.3 Film Casting

Cell suspensions are freely miscible with TMODA Nafion suspensions. Film suspensions are prepared as follows. The desired volume and estimated density of *Anabaena variabilis* SA-1 cell suspension is obtained from an incubated sample. The cell suspension is vortexed for 5 minutes to break up cellular clusters and to reduce filament length. The resultant cell suspension is centrifuged at 3500× for 3.5 minutes. The remaining spent media is decanted. Distilled and deionized water is added in excess to the resultant cell pellet and vortexed again for 1-2 minutes. This process is repeated two times to fully remove extracellular chemical components and cell debris. Background electrolyte (0.1 M Na_2SO_4) of the same volume originally withdrawn from the culture flask is added to the culture tube that contains washed cells and vortexed for 1-2 minutes to thoroughly mix the suspension. The desired

volume of cell suspension is mixed with well vortexed TMODA Nafion suspension to create the casting suspension.

To modify the electrodes, the desired volume of cells:TMODA Nafion are pipetted onto the surface of freshly cleaned and polished glassy carbon electrodes (Pine Research Instrumentation, 0.46 cm^2 or ALS, 0.20 cm^2). Care is taken to ensure an even layer of suspension is applied to the entire working surface of the electrode by use of the pipet tip. The resulting films are 10 μm thick and of fairly uniform dispersion. Once the solvent used to deliver the TMODA Nafion suspension has evaporated and the film is air dried (about 15 minutes), the electrodes are immersed in electrolyte solution. For all experiments, three types of electrodes are analyzed simultaneously (Figure 14). As shown in Figure 14, an unmodified (Bare) electrode (A), TMODA Nafion electrode (B), and X:TMODA Nafion electrode (C) where X = the volume ratio of cell suspension used preparation of the casting solution are used simultaneously in every experiment. The electrodes in Figure 14 are the large diameter Pine Research Instrumentation electrodes, while those in Figure 15 are the 5 mm diameter glassy carbon electrodes from ALS Japan. As shown in Figures 14 and 15, TMODA Nafion is a waxy polymer whose film is more heterogeneous than of Nafion alone. Homogeneity of the film can be improved by gentle mixing on the electrode surface during solvent evaporation after casting. Image B in Figures 14 and 15 shows the tendency of TMODA Nafion films to aggregate into islands of polymer. This phenomenon is minimized by pipet agitation as described. Immobilized cells can be observed visually as a distinct green polymer, whose intensity depends on the density of cells incorporated into the film. This research

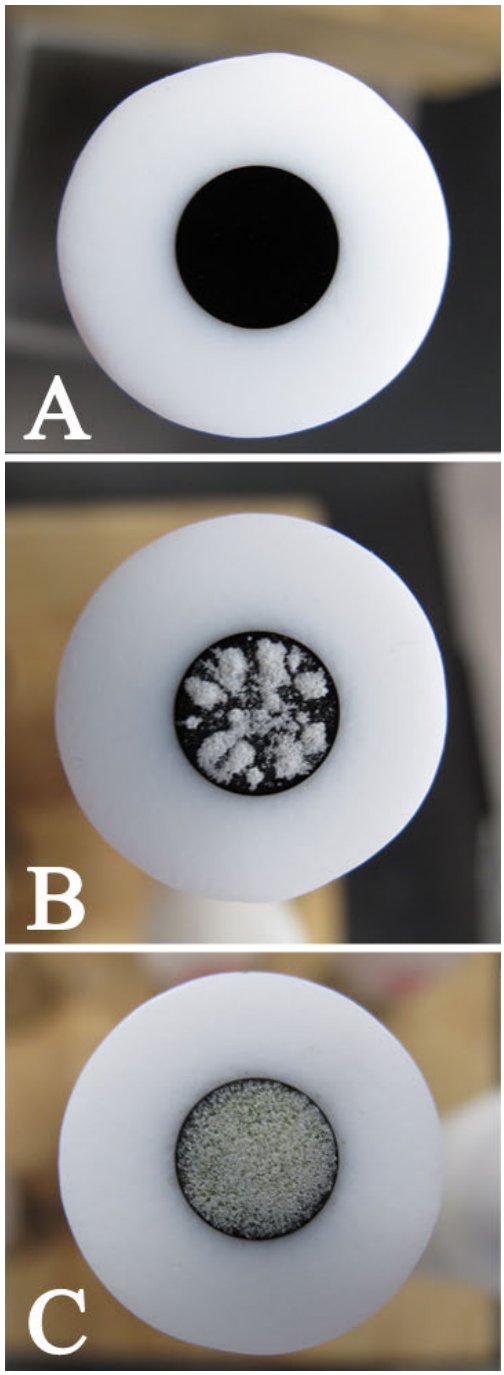

Figure 14. Modification of glassy carbon electrode surfaces (A = 0.460 cm^2; Pine Research Instrumentation, Inc.). *A*) Unmodified (bare) electrode; *B*) with a 12-15 μm thick layer of TMODA-Nafion; and *C*) with a 12-15 μm thick layer of 1:1 (v/v) *Anabaena variabilis* SA-1 suspension : TMODA-Nafion.

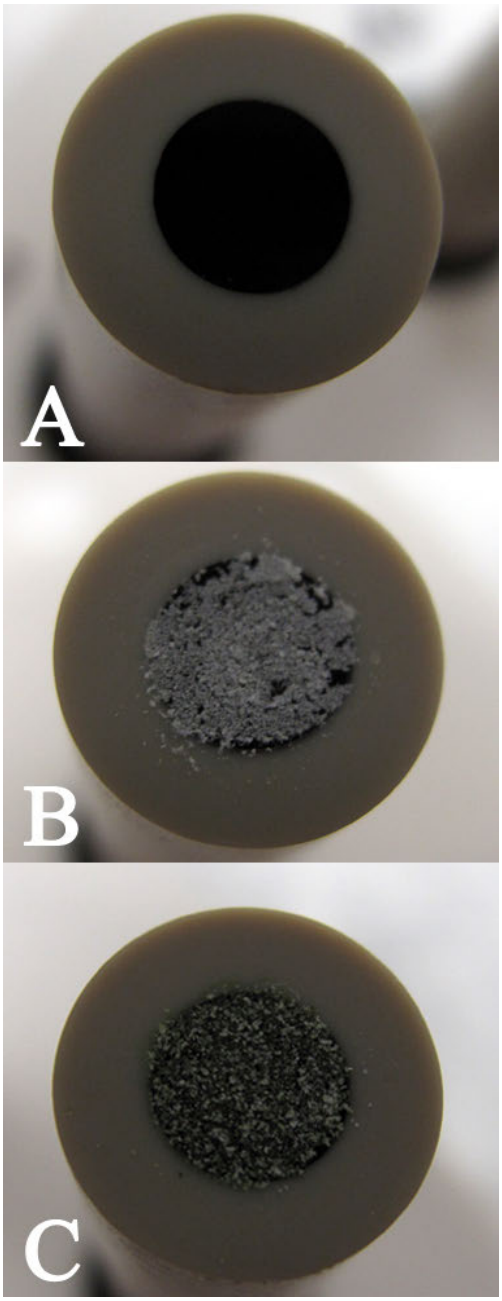

Figure 15. Modification of glassy carbon electrode surfaces (A = 0.20 cm^2; ALS Japan). *A*) Unmodified (bare) electrode; *B*) with a 12-15 μm thick layer of TMODA–Nafion; and *C*) with a 12-15 μm thick layer of 1:1 (v/v) *Anabaena variabilis* SA-1 suspension : TMODA-Nafion.

employed two types of working electrodes. Glassy carbon electrodes shrouded in Teflon with an electroactive area of 0.456 cm^2 (Pine Research Instrumentation, Inc.) give a total current spread of approximately $\pm 50\ \mu A$ whereas those glassy carbon electrodes shrouded in PEEK polymer with an electroactive area of 0.196 cm^2 (ALS, distributed by BAS Instruments) give a total current spread of approximately $\pm$ 10 μA. Most data are not reported as current density, thus a note is made regarding the electrode used. The electrodes give the same voltammetric morphologies, however the larger electrodes are more prone to solution leakage that resulted in false currents.

2.4 Electroanalytical Methods

The ability to produce sustained levels of ammonia by immobilized *Anabaena variabilis* immobilized to a glassy carbon electrode depends upon voltammetric perturbation. A potential gradient can be established at a solution electrode interface by a variety of methods and techniques.

2.4.1 Cyclic Voltammetry

Cyclic voltammetry is a useful technique in electrochemistry for studying chemical processes that involve electron transfer reactions. The technique is similar to other voltammetric procedures in that the current generated at an electrode surface is measured as a function of a scanned electrode potential. The distinguishing characteristic of cyclic voltammetry is that the potential is scanned in both the forward and reverse directions. Effectively, this allows the analyst to investigate

both forward and reverse redox (electron transfer) reactions. For example, the potential can be scanned in a forward direction to carry out a reaction. Reversing the potential scan now allows the products produced in the forward reaction to react themselves. In this way, the mechanisms of electrode reactions can be studied.

The resulting current in a cyclic voltammogram can be used for quantitation. The peak current is described by the solution to Fick's I and II Laws with appropriate boundary conditions [90]

$$i_p = 0.4463 \left(\frac{F^3}{RT}\right)^{1/2} n^{3/2} A D_o^{1/2} C_O^* \upsilon^{1/2} \tag{16}$$

Cyclic voltammetry (CV) is a voltammetric analytical technique for studying electroactive chemical species. Many scientific disciplines use CV due to its versatility and general ease of measurement. In cyclic voltammetry, the potential at the working electrode, here GC|TMODA Nafion + enzyme (cells), is swept linearly from a potential where no faradaic (electron transfer at the electrode) current flows to a potential where the direction of the potential sweep is reversed; the sweep is continued, often back to the initial potential. In some cases, the potential cycles between the initial and switching potential multiple times.

In the Equation 16 i_p, is the peak current in amperes (A), n is the electron stoichiometry, A is the electrode area (cm^2), D_O is the diffusion coefficient ($cm^2\ s^{-1}$), C^* is the concentration (mol cm^{-3}), and υ is the scan rate (V s^{-1}). Equation 16 is appropriate at a large flat electrode when the electron transfer rate is fast compared to the mass transport rate. Alteration of the electrode surface with TMODA results in current responses that deviate from equation 16. In practice, a calibration curve

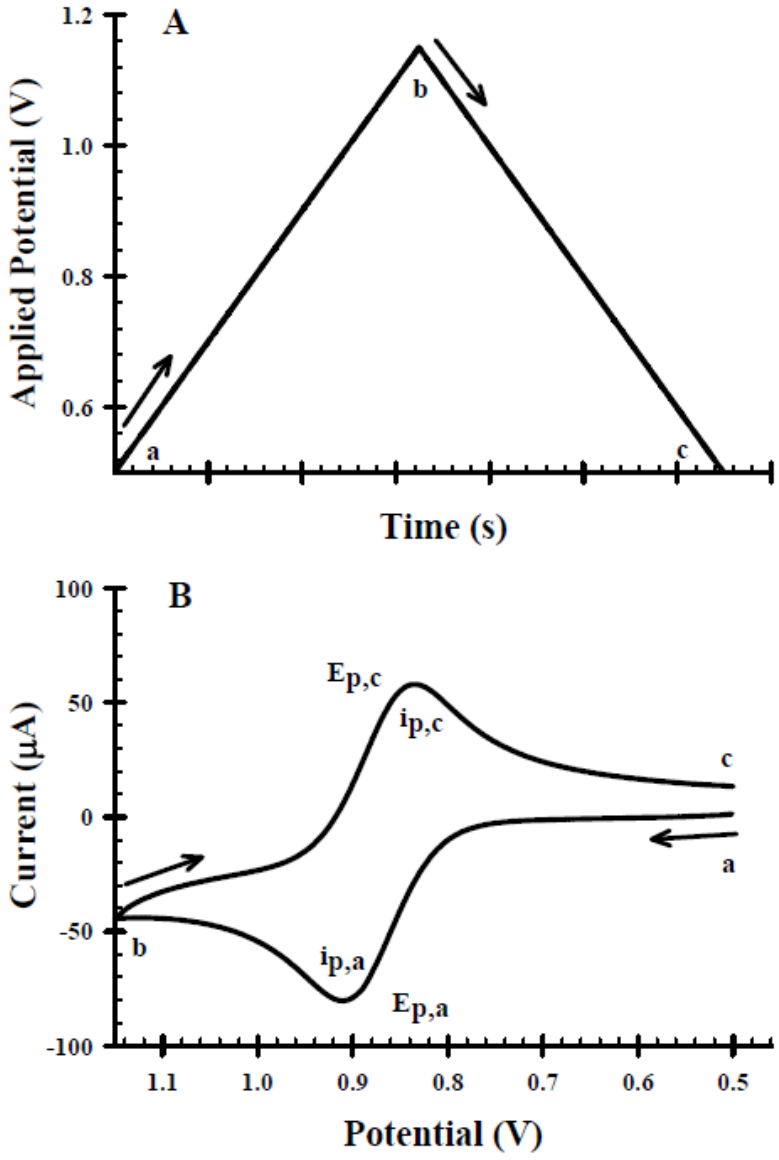

Figure 16. Illustration of the cyclic voltammetry (CV) electroanalytical method. *A*) A wave generator sweeps potential linearly from an intial potential (a) where no reaction occurs to a switching potential (b). Polarity is then reversed and the potential is swept linearly vs. time back to a final potential (c), often the same potential as the initial potential. *B*) A cyclic voltammogram. Current is measured as a function of the potential sweep rate. (a, b, c) correspond to the same labeled points in diagram*A*. Current is negliglble initially at point (a). As potential nears the standard potential for the redox couple in solution, faradaic currents rise, eventually reaching the cathodic mass transport limit $i_{p,a}$. As the potential sweep continues, the current response decays until potential is switched at (b). The same process occurs for the oxidation, but now the reductive current is measured. The mass transport limit is reached at $i_{p,c}$. As potential linearly sweeps back to the final potential, faradaic current decays to near the original value (c) . The current peaks at $i_{p,a}$ and $i_{p,c}$ arise at the peak potential, $E_{p,a}$ and $E_{p,c}$, respectively.

is generated between i_p and concentration, employing a set of standard solutions. In the use of cyclic voltammetry for quantitative analyses, two considerations are important. First, a baseline must be established on the voltammogram. This usually involves an extrapolation of the baseline current. A second important consideration is the subtraction of any current due to the supporting electrolyte. Failure to subtract the background current can lead to a systematic error in a subsequent prediction of concentration.

The experimental parameters in cyclic voltammetry are the potential range scanned, the scan rate, and the type of working electrode. The potential range is dependent upon the electrochemical properties of the species being studied and the working electrode material. Each type of working electrode (Pt, Au, C, etc.) possesses a different working potential range. The presence of electrochemical reactions involving the electrode determines the operating range of each. The scan rate selected depends on the information desired. For reaction studies, the use of a fast scan rate may lead to missed information. For example, a slow scan rate may allow time for a species produced in a chemical reaction to accumulate to the level required for its subsequent oxidation or reduction to be observed.

2.4.2 Three Electrode Cell

The electrochemical methodology uses a three electrode system that includes a saturated calomel reference electrode (SCE) and a glassy carbon electrode modified with either heterocysts or whole cells supported in TMODA Nafion. The third electrode is a high surface area counter electrode. In cyclic voltammetry, the

potential at the working electrode, here GC|TMODA Nafion + whole cells, is swept linear from a potential where no faradaic (electron transfer at the electrode) current flows to a potential where the direction of the potential sweep is reversed; the sweep is continued, often back to the initial potential. In some cases, the potential cycles between the initial and switching potential multiple times.

2.4.3 Experimental Parameters

The bioelectrocatalytic device generates ammonia at *Anabaena variabilis* modified electrodes. Electrodes are modified with a modified ion exchange polymer, TMODA Nafion, that contains the cells. To modify the electrodes, octadecyltrimethylammonium bromide modified Nafion (1100 EW) (TMODA Nafion) is mixed with cell/heterocysts (SA-1 strain) suspensions and cast onto glassy carbon (GC) electrodes (0.5 cm^2). The resulting films are approximately 10 μm thick and of fairly uniform dispersion. Once the solvent used to deliver the TMODA Nafion suspension evaporates and the film is air dried (about 15 minutes), the electrodes are immersed in test electrolyte solution. The electrolyte used is 100 mM Na_2SO_4 to provide ionic conductivity. The electrodes are evaluated by cyclic voltammetry (CV). By varying CV scan rates, faradaic (electrolysis) currents are analyzed and compiled to build a kinetic model of electron transfer within the system. In all cases, controls are run with two unmodified (bare) electrodes, two electrodes modified with only TMODA Nafion, and at least 4 cell modified electrodes. This simultaneous electrode measurements allows discrimination between matrix effects and cellular/enzyme activity. In the laboratory, the electrode is connected

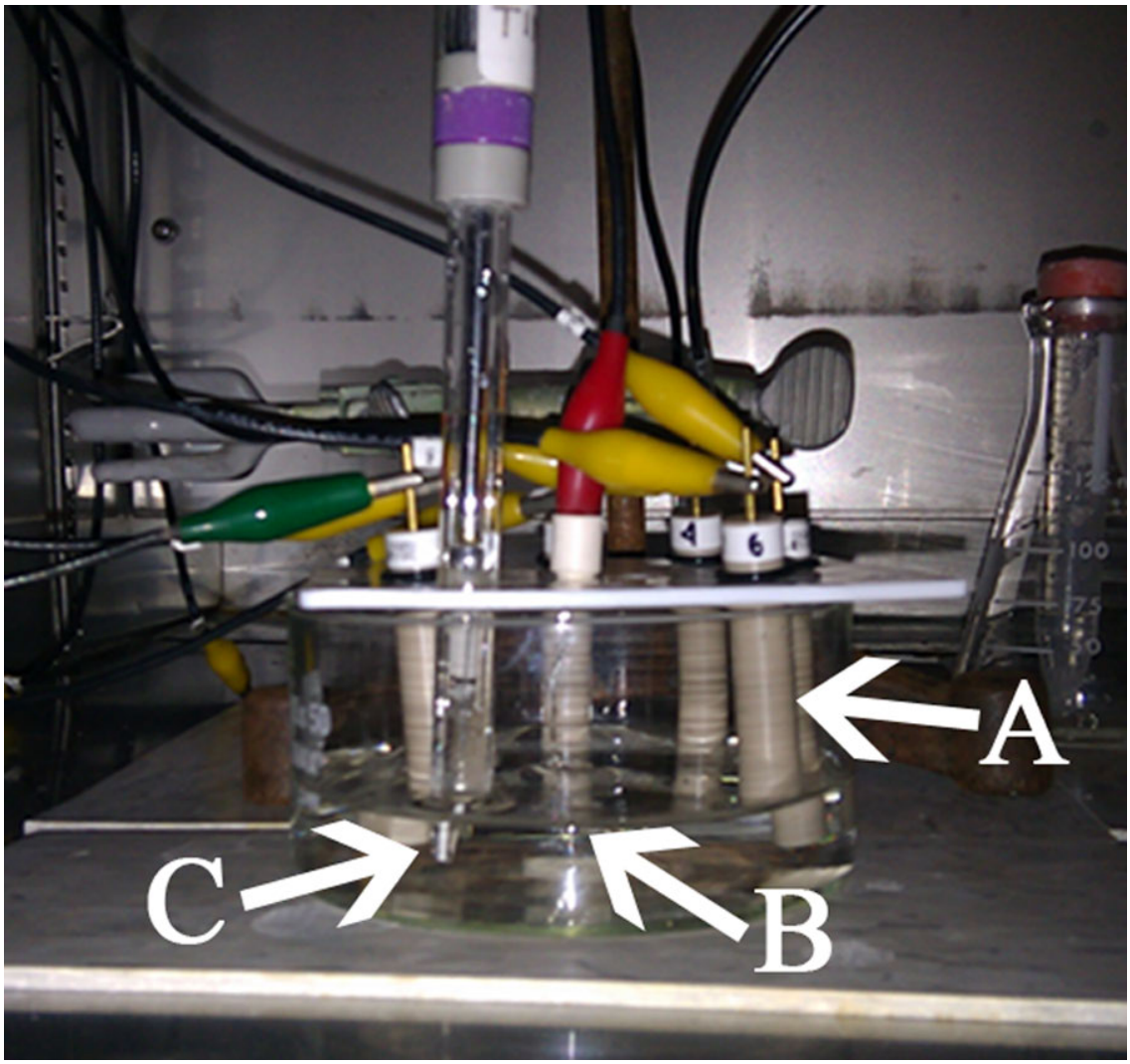

Figure 17. Photograph of the three electrode cell used in this research. *A*) 8 mm diameter glassy carbon working electrodes (8 simultaneously; 2 bare, 2 TMODA-Nafion, and 4 cell modified electrodes). *B*) Pt mesh high surface area counter electrode. C) SCE reference electrode.

to a potentiostat. The potentiostat controls the potential drop between the cell immobilized working electrode and the reference electrode where no current flows. The counter electrode passes current sufficient to balance the current measured at the working electrode. The potentiostat used is an 8-channel potentiostat 1030A (CH Instruments). Up to eight working electrodes share a common counter and reference electrode. Each channel independently records current vs. potential for cyclic voltammetry sweeps. The instrument does not provide iR compensation.

2.4.4 Quantification of Ammonia Production

Low level detection and quantification of ammonia can be a challenging analytical task.. Ammonia detection is of significant interest as it is commonly studied due to the toxic effects exerted on plant and animal life when found in high concentrations as, for example, resulting from runoff. The oceanography and limnology fields of study rely upon an indophenol reaction at high pH with colorimetric detection [91]. While the method is fast and selective, its lower limit of quantitation is high relative to the small amounts of NH_3 produced by immobilized cyanobacteria.

In water, ammonia exists simultaneously as free un-ionized gaseous ammonia (NH_3) and as the ionized ammonium ion (NH_4^+). The ratio of NH_3 to NH_4^+ that exists in water depend strongly on pH and to a lesser degree, temperature. Given that the pK_a of NH_3 is 9.24, at 25 °C, aqueous samples of ammonia are nearly all NH_4^+, equally NH_3 and NH_4^+, and all NH_3 at pH 7.3, 9.3, and 11.3, respectively. Thus, the local pH near the site of ammonia release by cyanobacteria have a significant effect on the form and physical state of ammonia.

The acid base nature of ammonia can be harnessed and coupled to a pH probe for sensitive and fast detection and quantitation. Ammonia can be measured directly by an ion selective electrode (ISE). As shown in Figure 18, dissolved NH_3 is gaseous and passes through the hydrophobic polytetrafluoroethylene (PTFE) membrane of the ammonia ISE. To ensure all ammonia present exists as the gaseous form, the sample is spiked with 1 % (v/v) 10 ± 0.5 M NaOH, that converts all NH_4^+ to NH_3 as given by the equilibrium

$$NH_3 + H_2O \rightleftharpoons NH_4^+ + OH^- \tag{17}$$

The pH change of the electrolyte solution on the other side of the membrane (0.083 ±0.005 M NH_4Cl) caused by the diffused NH_3 (g) is sensed by the inner body of the ammonia electrode, which is a common pH electrode. The pH change is relative to the amount of dissolved NH_3 present and can be measured with a pH or ion meter. The dissolved ammonia present in a sample diffuses through the membrane until the partial pressure of ammonia has reach equilibrium on either side of the ammonia. In any sample the partial pressure of ammonia is proportional to its concentration. Ammonia diffusing through the membrane dissolves into the electrode filling solution and, to a small extent, reacts reversibly with water. As shown in equation 17, the base equilibrium constant expression is given by

$$K_b = \frac{\left[NH_4^+\right][OH^-]}{[NH_3]} \tag{18}$$

The concentration of ammonium chloride in the thin layer between the PTFE membrane and glass membrane pH electrode body is sufficiently high so the

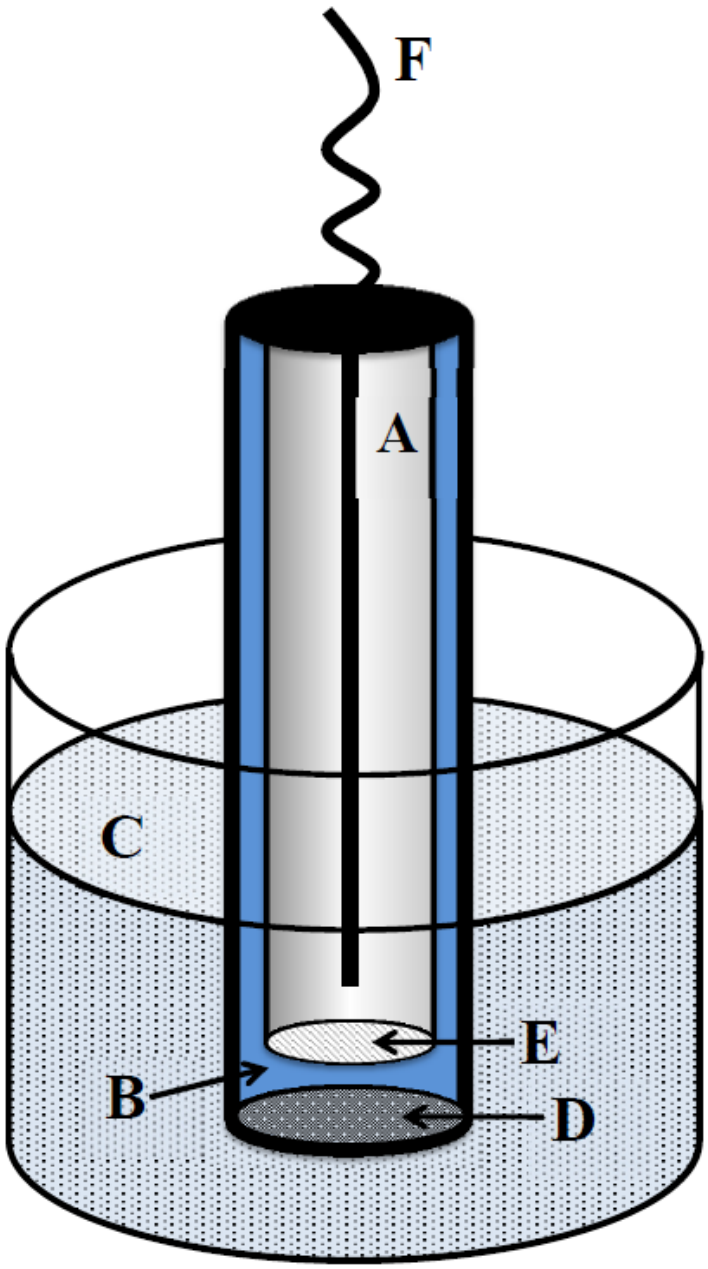

Figure 18. Diagram of the ammonia ion selective electrode components. A pH electrode *A*) in direct contact with a fixed concentration solution of NH_4Cl *B*) senses a change in pH that results from diffusion of gaseous NH_3 (from solution *C*) across a gas permeable PTFE membrane *D*) is in equilibrium with a fixed concentration of NH_4^+ in the solution surrounding the pH electrode through the pH electrode glass membrane *E*). The electrode connects directly to a pH/volt meter through a BNC connector *F*).

concentration of NH_4^+approaches unity,

$$\left[OH^-\right] = \left[NH_3\right] \frac{K_b}{\left[NH_4^+\right]} \tag{19}$$

The potential of the sensing element with respect to the internal reference element is described by the Nernst equation,

$$E = E^{\circ'} - S \log \left[OH^-\right] \tag{20}$$

where E = measured electrode potential (mV), $E^{0'}$ = reference potential (mV), and S = the electrode slope as determined from calibration (-59 mV/decade). Thus, since $[OH^-] \propto [NH_3]$ as shown in equation 19, electrode response to ammonia is also Nernstian

$$E = E^{\circ'} - S \log \left[NH_3\right] \tag{21}$$

Measurement of NH_3 with the ion selective electrode is fast, requires minimal setup and sample preparation, and is regularly calibrated. Daily calibration is necessary for low level ammonia detection, < 70 μM. Calibrations were performed with commercially purchased ammonia standards (0.01 ppm, 0.1 ppm, 1 ppm, 10 ppm, and 100 ppm; Aqua Solutions). The concentration detection range of the electrode is between 5 $\times 10^{-7}$ M and 1 M (0.01 and 17,000 ppm NH_3). Between analyses, the electrode is stored in a solution of 1 ppm NH_3 standard containing 1 % alkaline reagent (10 M NaOH).

To calibrate the ion selective electrode, 15 mL of standard is placed into a 20 mL scintillation vial with a magnetic stir bar. 150 μL of 10 M NaOH is added to the stirring analyte. The ISE is cleaned with four successive washes in distilled and

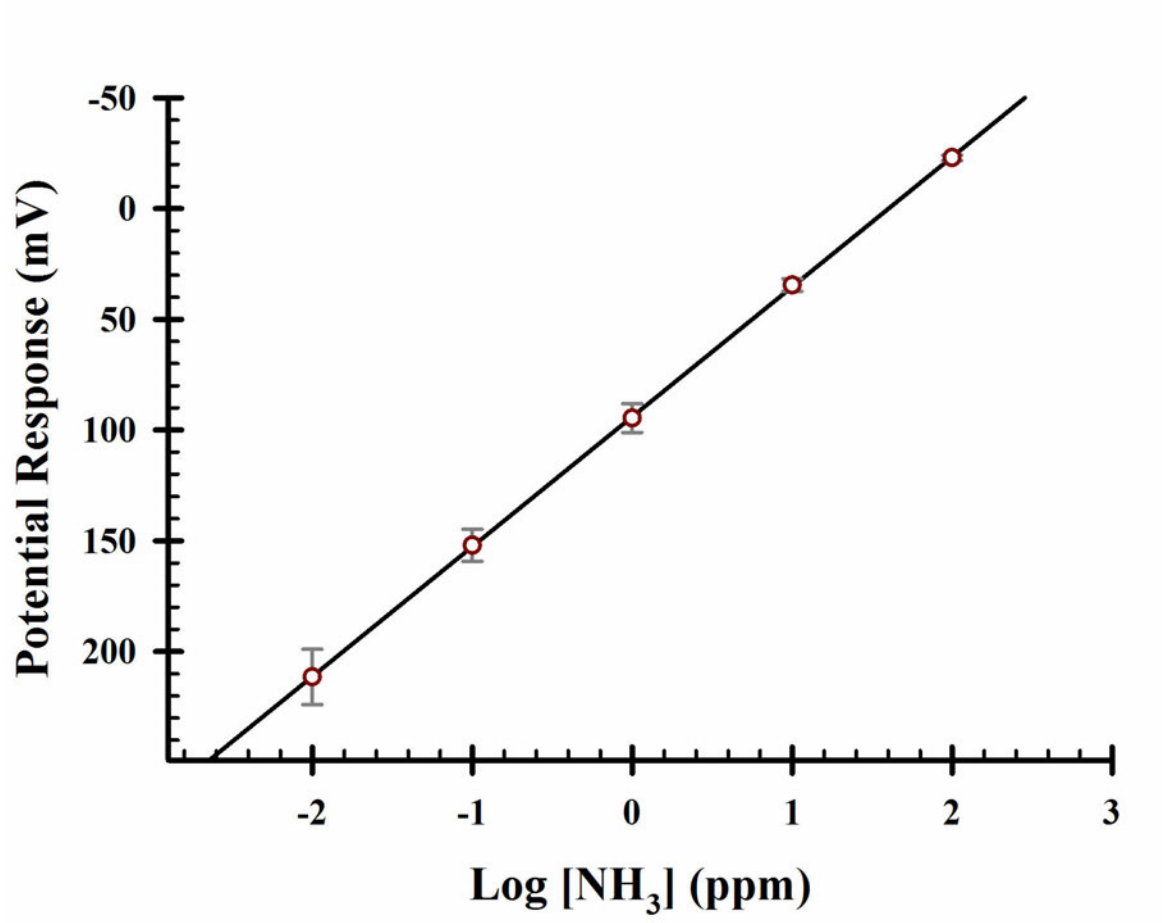

Figure 19. Calibration plot of the ammonia ion selective electrode. Linear regression results in $y = -(58.8 \pm 1.1)\,x + 94.4 \pm 1.6$, $R^2 = 0.99$. Vertical error bars are $\pm\ 1\sigma$ calculated for $n = 6$ separate calibrations for each commercial standard purchased (0.01 to 100 ppm NH_3 as N). As expected, the error increases as concentration of NH_3 decreases due primarily to ammonia absorption from the air.

deionized water. The ISE is placed into the test solution and the vial is covered with Parafilm to minimize NH_3 losses. Within 1 3 minutes (more time for lower concentrations of NH_3), the resultant potential is recorded. A plot of potential response vs. log $[NH_3]$ yields a linear curve with an expected $m = -59$ mV. at 25 °C. Figure 19 shows the calibration of the NH_3 ISE for 6 trials. The error bars show $\pm$ 1σ for each NH_3 standard potential measurement. Slight fluctuations in lab temperature are the major contributing factor to error. Further, at the lower limit of detection, equilibration between analyte and inner NH_4Cl solution takes longer time and is more subject to drift thus the error is more significant at lower $[NH_3]$, as observed by the larger relative error at low concentrations of NH_3.

2.5 Bioelectrocatalytic Device Design

The bioelectrocatalytic device is simple in design. The most important element is the working electrode whose surface has been modified with *Anabaena variabilis* SA-1 cells immobilized in TMODA Nafion. A basic diagram showing the anticipated reactions at the working electrode are shown in Figure 20. The glassy carbon electrode with a thin (10 ± 1 μm thickness as estimated by calculation) film of TMODA that contain cyanobacteria is fully immersed into a conductive background electrolyte solution. Enzyme substrate diffuses through solution to the TMODA Nafion|solution interface. TMODA Nafion is not a selective polymer and solution equilibrates fully into the membrane after ~5 minutes of soaking.

2.5.1 Experimental Setup

This research investigates NH_3 generation from cyanobacterial enzymes immobilized in a modified Nafion polymer film and attached to an electrode (Figure 20). This will be undertaken in a multistep process that draws from a variety of scientific domains. The essential steps are grow the enzyme; isolate the enzyme; embed the enzyme in an ion exchange polymer on an electrode; evaluate the efficiency of the electrode bound enzyme to convert N_2 to ammonia and model the kinetics; and use the model to optimize the system for ammonia production.

Figure 21 illustrates the biological to electrochemical interface and involved reactions. Vegetative and heterocyst cells of *A. variabilis* are in close contact with the electrode. The heterocyst contains the nitrogenase enzyme. The vegetative cell contains nitrate/nitrite reductase enzyme and photosystem I and II. Both cell types contain the NADPH Ferredoxin oxioreductase enzyme that catalyzes the redox of the $NADP^+$/NADPH and oxidized ferredoxin/reduced ferredoxin reactions. Solid arrows represent biochemical reactions. The double headed arrow show transport of molecules. The transport may be passive by diffusion or active by gated channels. The diagram highlights the complexity of the system. Accordingly, data obtained capture several levels of interrelated mechanisms.

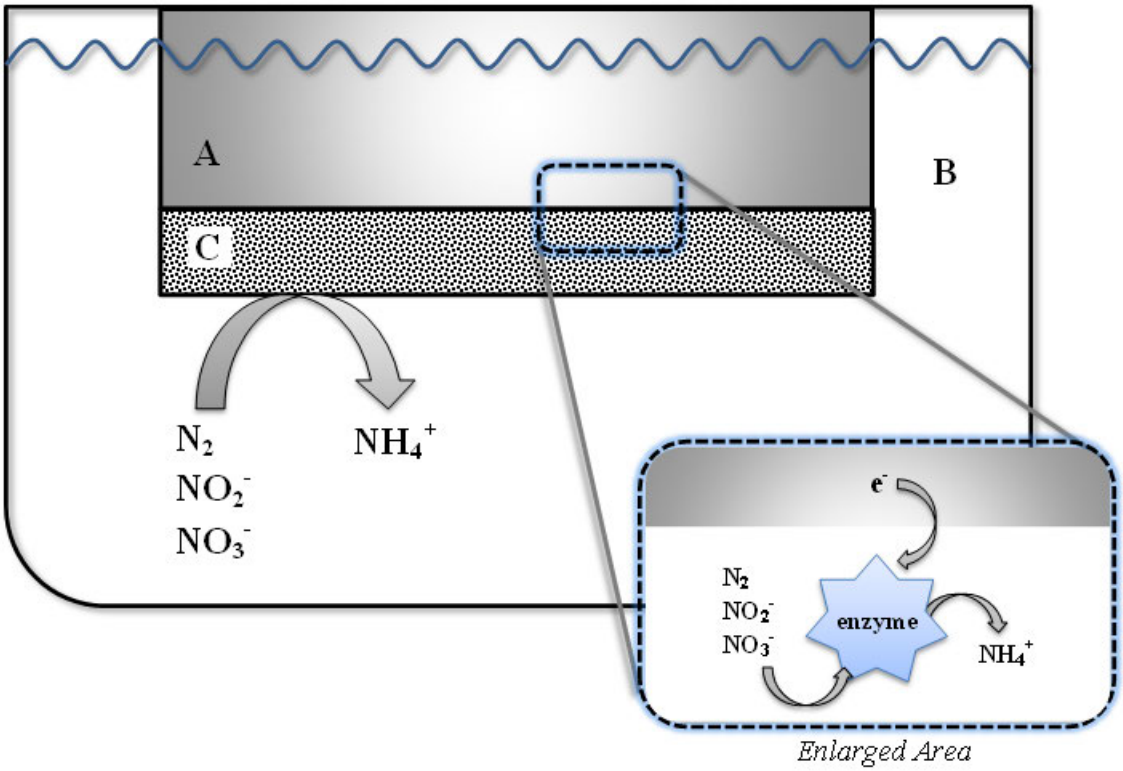

Figure 20. Schematic of the bioelectrocatalytic device for ammonia production. At a glassy carbon electrode (A), ammonia producing cyanobacteria are immobilized in a modified Nafion film (C). The test solution (B) contains enzyme substrates. Interaction of these substrates with enzymes (N_2 for nitrogenase; NO_2^- and NO_3^- for nitrate-nitrite reductase) under voltammetric perturbation supplies electrons as shown in the enlarged image) to release NH_4^+ into the external media.

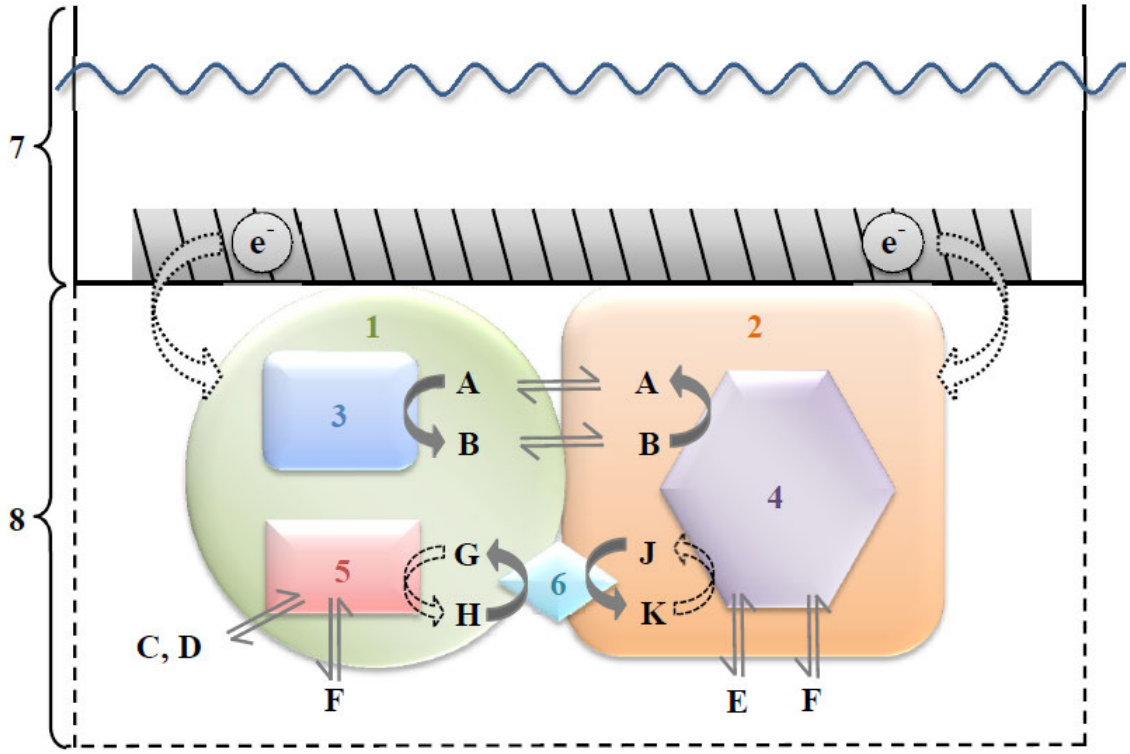

Figure 21. Illustration of the most important biochemical and electrochemical processes present in the system at cell immobilized electrodes. Major components of the system are: 1) Vegetative cell of *Anabaena variabilis*; 2) Heterocyst cell of *Anabaena variabilis*; 3) Photosystem I and II; 4) Nitrogenase; 5) Nitrate/Nitrite Reductase; 6) Ferredoxin-NADP$^+$ oxioreductase; 7) Glassy carbon working electrode submerged in 0.1 M Na_2SO_4; and 8) TMODA-Nafion polymer film containing cells. Chemicals are as follows: *A*) Adenosine diphosphate (ADP); *B*) Adenosine triphosphate (ATP); *C*) NO_3^- ion, substrate for 5; *D*) NO_2^- ion, substrate for 5; *E*) N_2, substrate for 4; *F*) NH_4^+, ammonium produced; *G*) reduced Nicotinamide adenine phosphate (NADPH); *H*) Oxidized nicotinamide adenine phosphate (NADP$^+$) *K*) Reduced ferredoxin, Fe(*II*) complex; and *J*) Oxidized ferredoxin, Fe(*III*) complex.

CHAPTER 3

AMMONIA GENERATION BY ELECTRODE IMMOBILIZED *ANABAENA VARIABILIS*

3.1 Background

Ammonia is a chemical compound of significant demand that is energetically and environmentally taxing to synthesize. H_2, most commonly obtained by thermal processing of CH_4, reacts with atmospheric N_2 over a bed of catalysts and promoters in reaction vessels held at high temperature and pressure to produce NH_4^+. Similarly, cyanobacteria contain enzymes that catalyze the reduction of N_2, NO_2^-, and NO_3^- to NH_4^+ but at ambient temperature and pressure. Two enzymes of significant interest are nitrogenase and nitrate/nitrite reductase. *Anabaena variabilis*, a common photosynthetic cyanobacteria, produce some of the highest amounts of NH_4^+ of prokaryotes. [11, 53, 63, 64, 78, 92, 93]

NH_4^+ production by cyanobacteria is highly regulated with multiple levels of biochemical feedback. Sufficient concentrations of NH_4^+ in the external medium of the cells represses nitrogenase synthesis, thus biologically, sustained production and release of NH_4^+ by *A. var.* is not observed. Nitrogenase derepressed genetic mutants of *A. var,* the SA-1 strain, release NH_4^+ externally. Despite the presence of NH_4^+ or other reduced forms of nitrogen like NO_2^- and NO_3^-, the *A. var.* SA-1 mutant continues to produce NH_4^+ by nitrogenase and nitrate/nitrite reductase enzymes. [70, 71, 73, 74]

Many of the biochemical reactions necessary to reduce nitrogen sources to ammonia are electron transfer reactions. Electrical potential affects charge transfer reactions and the thermodynamics of physical and biological systems. Immobilization of enzymes at an electrode surface increases biocatalytic capacity, stabilized enzyme activities, and provides an environment where continuous enzymatic turnover is highly likely [48, 49, 83]. Electroanalytical study of enzymes in fuel cells [49, 61, 83, 94], protein films on electrodes [50, 85, 95, 96], and of biological mediators [29, 50, 96–98] promote the approach to whole cell ammonia production at ambient temperature and pressure. Thus, immobilization of *A. var.* within a polymer at a glassy carbon surface presents an interesting system to study.

This interdisciplinary research describes a system that capitalizes on well studied cyanobacterial enzyme pathways nitrogenase and nitrate/nitrite reductase. These enzyme exhibit high rates of catalytic activity in vivo and are dependent upon a network of redox reactions. Use of isolated pure enzymes significantly reduces the complexity of analysis required to decouple simultaneous biological and electrochemical processes. While certain enzyme lifetimes have been extended by entrapment in a polymer at an electrode surface [44–48, 99, 100], additional considerations arise that complicates the use of isolated enzymes. If the enzyme depends on ATP, as does nitrogenase for example, then an ATP/ADP recycling system must be added to the system and regularly replenished. In the case of phototrophic cyanobacteria, purified and isolated enzymes do not have access to cellular respiration products as the cellular components necessary to achieve respiration are absent from enzyme isolates. Wastes and cellular byproducts must

be removed, especially those that mediate enzyme activity. Many enzymes such as nitrogenase are very sensitive to even low concentrations of O_2. To prevent irreversible binding and deactivation of enzymes due to O_2, special construction and removal of O_2 from the system must ensue. Thus, while more complicated, introducing enzymes and studying their activity within whole living cells avoids many concerns resulting from isolation.

Electrochemical interrogation of whole cell systems has several advantages over systems where specific cellular enzymes, components, or species are isolated as follows: 1) Self sustaining - all necessary components to sustain the organisms; 2) viability, structure, and function are present. Energy generation by sunlight (photosynthesis), cellular energy and recycling (ATP), growth (protein synthesis), and necessary mediators and cofactors are present in their natural state; 3) renewable - growth of the cells depends upon adequate sunlight and organic carbon sources (i.e., glucose and fructose), which are essentially in infinite supply; 4) technology is built and designed around an already self contained, efficient system.; 5) sample preparation is significantly simplified; and 6) species already adapted to oxygenic environments can be studied in ambient conditions. Whole cell analysis also presents several challenges as follows: 1) extremely complex multilayer enzyme systems that share feedback chemicals and pathways; 2) selectivity - it is difficult to target specific components when all are present and functional; and 3) Access to target of interest - components like the cell membrane present a physical and electrochemical barrier to direct study. Despite the challenges, this research uses whole cells. As correlations and models are built from electrochemical data, the models can be transferred to

Table 2. Listing of chemical substrates and corresponding enzyme considered in this research.

Substrate	**Enzyme**
N_2	nitrogenase
NO_2^-	nitrate/nitrite reductase
NO_3^-	nitrate/nitrite reductase
O_2	nitrogenase

Note: Whereas O_2 is not a desirable substrate, it irreversibly binds to nitrogenase and is considered in this work.

other research and emerging technologies. Without the need to prepare, isolate, separate, and alter an already functional system, the work here studies the intact system *in vivo*. This supports exploitation of an already functional and efficient system that has not yet ever been synthetically reproduced. Enzymes and required substrates for ammonia generation by *Anabaena variabilis* in this research are summarized in Table 2.

3.2 Experimental

Unless noted otherwise, experimental setup shared the characteristics as described in this section. In general, at least two of each electrode were analyzed simultaneously in electrochemical experiments. Whenever available, data are reported with statistics.

3.2.1 Cyclic Voltammetric Analysis of System

CV uses a three electrode system that includes a saturated calomel reference electrode (SCE) and a glassy carbon electrode modified with whole cells supported

in TMODA Nafion. The third electrode is a high surface area platinum counter electrode. By varying CV scan rates, faradaic (electrolysis) currents are analyzed and compiled to build a kinetic model of electron transfer within the system. In all cases, controls are run with an unmodified (bare) electrode, an electrode modified with only TMODA Nafion, and at least 4 cell modified electrodes. This simultaneous electrode measurements allows discrimination between matrix effects and cellular/enzyme activity. The six working electrodes are connected to a multi channel potentiostat (CH Instruments 1030A) and share a common reference and counter electrode.. The potentiostat controls the potential drop between the cell immobilized working electrode and the reference electrode.

Working electrodes are coated with a modified ion exchange polymer, TMODA Nafion, that contains the cells. To modify the electrodes, octadecyltrimethylammonium (TMODA) modified Nafion (1100 EW) is mixed with cell/heterocysts (SA-1 strain) suspensions and cast onto glassy carbon electrodes (0.5 cm^2) The resulting films are approximately 10 μm thick and of fairly uniform dispersion. Once the solvent used to deliver the TMODA Nafion suspension evaporates and the film is air dried (about 15 minutes), the electrodes are immersed in 15 mL electrolyte solution. The electrolyte used is 100 mM Na_2SO_4 to provide ionic conductivity. The electrodes are evaluated by cyclic voltammetry (CV). Cyclic voltammetry is conducted at the scan rates as follows (in order): 100, 75, 50, 25, 50, 75, 100 mV/s. This manner of voltammetric perturbation exposes cells to about 10 minutes of voltammetric perturbation. Following CV, the electrodes are removed and electrolyte analyzed for produced ammonia.

3.2.2 Ammonia Quantification Method

NH_3 production from this bioelectrocatalytic device is following with an ammonia ion selective electrode (Thermo Fisher). Dissolved NH_3 is gaseous and passes through the hydrophobic membrane of the ammonia ion selective electrode (ISE). The pH change of the electrolyte solution on the other side of the membrane caused by the diffused gas is sensed by the inner body of the ammonia electrode which is a pH electrode. The pH change is relative to the amount of dissolved NH_3 present and is measured with a pH capable of voltage readings. The lower limit of quantitation with the ammonia ISE is 0.5 μM NH_3. The response time to concentrations of $NH_3 \leq 1$ μM is significantly higher as the pH change across the membranes requires longer equilibration time. To ensure ammonia measured was above the lower limit of quantitation, six working electrodes were analyzed in a single 15 mL vial of Na_2SO_4.

Following cyclic voltammetric analysis, the solution was collected for ammonia analysis. To the 15 mL solution sample,1 % (v/v) 10 $\pm$ 0.5 M NaOH (150 μL) is added to raise the pH to near 14, thus converting all protonated NH_4^+ to gaseous NH_3 ($pK_a = 9.3$). Under constant stirring, the ISE is place into the solution and the vial is covered with Parafilm to minimize loss of gaseous NH_3. The potential is measured. A calibration of NH_4^+ standard resulted in a linear equation of $y = -(58.8 \pm 1.1)\,x + (94.4 \pm 1.6)$ with a correlational coefficient of $R^2 = 0.99$. Ammonia concentrations in the sample were calculated from this calibration equation.

3.2.3 Chlorophyll a Assay

By the method of Mackinney [80], chlorophyll a is extracted from the cells in methanol whose absorbance is measured at 565 nm in a UV-Vis spectrometer (Ocean Optics 4000). Absorbance at 750 nm can arise from the extraction of other pigments like carotenoids and chlorophyll b; thus, the absorbance at 750 nm is subtracted from the absorbance at 565 nm.. Briefly, a 1.5 mL sample of cell suspension is placed into a micro centrifuge tube and centrifuged at 4,400× for 5 minutes (Eppendorf 5260). The media is decanted and replaced with 1.5 mL methanol (HPLC grade; Sigma). Following a 5 minute mixing by vortexing, the methanol extracts chlorophyll a from the cells in a dark container to minimize light oxidation of the pigment. Cells and cellular debris are centrifuged from the methanol solution at 4,400x for 5 minutes. The resultant chlorophyll a solution in methanol is placed into a 1 cm cuvette. Chlorophyll a concentration is calculated from the Beer Lambert law, $A = \epsilon bc$ for $\epsilon = 12.7$ mL μg^{-1}, $b = 1$ cm, and $A =$ absorbance in arbitrary units. All absorbance measurements reported have the background methanol absorbance subtracted. The concentration of chlorophyll a is used to relate ammonia produced to cell density. The relationship is an arbitrary comparison, but because chlorophyll a concentration correlates to some K vegetative cell density, and nitrate/nitrite reductase is located within vegetative cells, normalization of ammonia output to chlorophyll a density is representative of ammonia output per unit enzyme. When statistics are reported, they represent $\overline{x} \pm 1\sigma$ for $n = 4$ samples of cell suspension.

3.2.4 Total Protein Assay

Total protein was assayed by the Bradford method [81, 82]. Commercially available Coomassie Assay kit was purchased (Sigma). A calibration plot was constructed against bovine serum albumin (BSA). The linear response range for the calibration is 100-1500 μg/mL total protein. In 1.5 mL microcentrifuge tubes, 50 μL of sample containing protein is added to 1.5 mL of Coomassie Plus Reagent and thoroughly mixed by vortexing for 2 minutes. The tube is incubated at room temperature for 10 minutes for more consistent results. The UV-Vis spectrum of the blank (BG-11_0 media) was obtained and stored for subtraction. Absorbance was measured, in quadruplicate, for nine BSA standards. The BSA standard were prepared from commercially obtained BSA (2 mg/mL). Figure 9 is the representative calibration curve for the BSA standards. Vertical error bars represent $\pm$ 1σ from the mean of 4 samples. Total protein measurements from suspensions of *A. var.* were measured in the same manner and compared to the BSA calibration. Total protein quantifies protein contribution from both vegetative and heterocyst cells. Nitrate/nitrate reductase is found within vegetative cells while nitrogenase is located in heterocysts. Thus, the total protein normalization factor is useful when the ammonia output is from both nitrogenase and nitrate/nitrite reductase.

3.3 Results

For every CV experiment, six electrodes are prepared for the electrochemical cells. 100 mM Na_2SO_4 is the electrolyte and provides sufficient ionic conductivity.

By varying cyclic voltammetric scan rates, faradaic (electrolysis) currents can be analyzed within established kinetic models. In all cases, controls are run. For statistical redundancy, at least two of each type electrode are run simultaneously: two unmodified glassy carbon electrodes, two GC electrodes with only TMODA Nafion films, and two electrodes with TMODA Nafion:cells (whole cells or cell wall ruptured cells). This allows discrimination between matrix effects and enzyme activity.

In cyclic voltammetry, electron flux to the electrode surface is measured as current. Redox active species in solution diffuse to the electrode surface, undergo electron transfer, and diffuse away. If the electron transfer is reversible and chemical reactions are not apparent, what is oxidized on the forward sweep is reduced on the reverse sweep, typically at a separation of 60 mV/n electrons transferred. The flux of electrons during these electrolysis steps are limited by diffusion, concentration, and kinetics. Thus, a current signal may appear as a distinct peak or a sigmoidal wave. The working potential range for *Anabaena variabilis* immobilized to glassy carbon is between 0.9 V and 0.5 V vs SCE. This potential range is adequate to study nitrogenase, nitrate/nitrite reductase, and the mediating chemical reactions corresponding to the enzyme process as their reported redox potentials fall within this range vs. SCE [35,37,56,96,98,101–104]. Solvent electrolysis arises at potentials greater than 0.9 V and O_2 reduction currents arise at potentials more negative than 0.5 V. Increasing current at either limit interfere with measurement of intended faradaic processes. Whether CV initiated with an oxidative or reductive sweep first had no significant effect in the observed current responses. Data are more

reproducible when CVs are initiated at 0.8 V and scanned reductively to 0.5 V, then cycled back to +1.1 V.

Data will be presented and discussed from the most prominent studies conducted in this research. When appropriate, data are statistically vetted. Modification of electrodes with polymer films carries an inherent error in thickness, distribution, and flux characteristics due to variability in temperature, humidity, and heterogeneity of casting suspensions. Depending on the extent of potential window electrolysis, the current scale in reported CV data has been adjusted accordingly.

3.3.1 Initial Voltammetric Response and Ammonia Output

The presence of whole *Anabaena variabilis* near the electrode surface provides a unique electrochemical response when studied with CV (Figure 22). In these experiments, faradaic current peaks/plateaus arise only when cells are immobilized to an electrode. Faradaic current waves arise at 0.65 V (oxidation) and 0.3 V (reduction) for the electrode where cells are present. A 1:1 (v/v) cell suspension : TMODA Nafion suspension was used to cast an approximately 10 μm thick film on the electrode. The faradaic waves are of higher current than both the responses at bare and TMODA Nafion electrodes. The current signals that appear in Figure 22 are not indicative of a reversible electrolysis of a single species. Data suggest at least two distinct electron transfer reactions occur under cycled voltammetric perturbation. The waves are separated by approximately 300 mV. At more positive potentials, electrolysis of H_2O begins to overlap with the oxidative current signal as

shown by the increasing negative current at potentials > 0.9 V. Data presented in Figure 22 are representative of the typical voltammetric response initially obtained by the bioelectrocatalytic device. The large oxidative capacitive current response observed for the cell modified electrode is due to an irregular film. A film that is less homogenous across the electrode alters the background electrolyte electrolysis current, indicated by the large negative current of the cell modified electrode. In future experiments, films were prepared simultaneously to eliminate this artifact. Neither a bare electrode nor TMODA Nafion electrode (Figure 22) show faradaic current responses, which indicates no electron transfer reactions arise at these electrodes. These data suggest faradaic currents arise due to electron transfer reactions between the electrode and species only available when cells are present. These data do not identify the species involved nor whether they are reactions with species accessible on the surface of the cells, or species capable of diffusing into and out of the cell membrane.

Further evidence the waves observed at cell modified electrodes (Figure 22) are related to the presence of *A. var.* is shown in Figure 23). Four different ratios of cell:TMODA Nafion casting suspensions were used to vary the density of cells near the electrode surface. 2:1 (v/v), 1:1 (v/v), 0.5:1 (v/v), and 0.25:1 (v/v) cell suspension:TMODA Nafion casting suspensions were used to modified electrodes (Table 3). The sigmoidal like faradaic wave current was measured at 0.62 V for each electrode response in Figure 23. Chlorophyll a and total protein measurements were made on each suspension of cells. The chlorophyll a and total protein measurements were correlated to the measured oxidative current (Table 3).

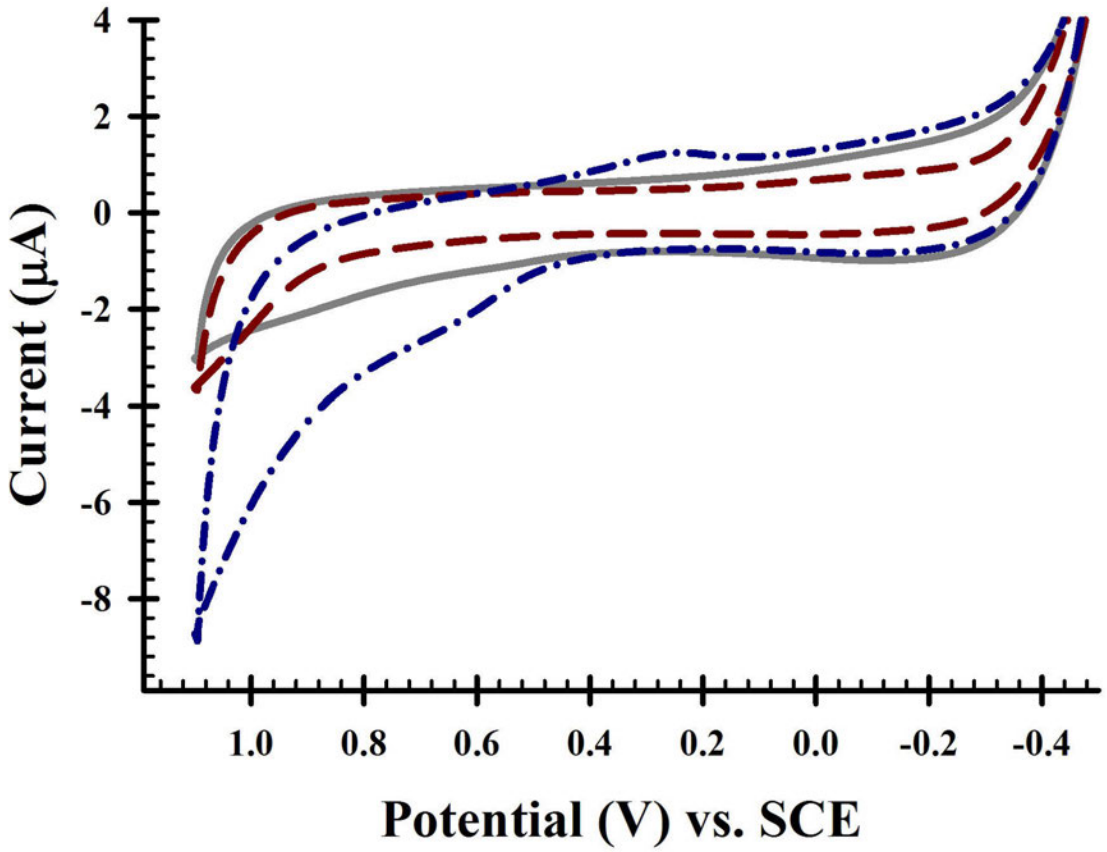

Figure 22. Cyclic voltammogram in 100 mM Na_2SO_4 that shows the current response of the electrodes in the bioelectrocatalytic device. The electrodes are the 0.196 cm^2 ALS glassy carbon. Overlay shows the voltammetric waves indicating a faradaic process occurs when cells are immobilized to an electrode. CV was performed at 75 mV/s in an ambient electrochemical cell. Comparison of Bare (— —), TMODA Nafion (—), and 1:1 TMODA:Cells (– · –) electrode responses.

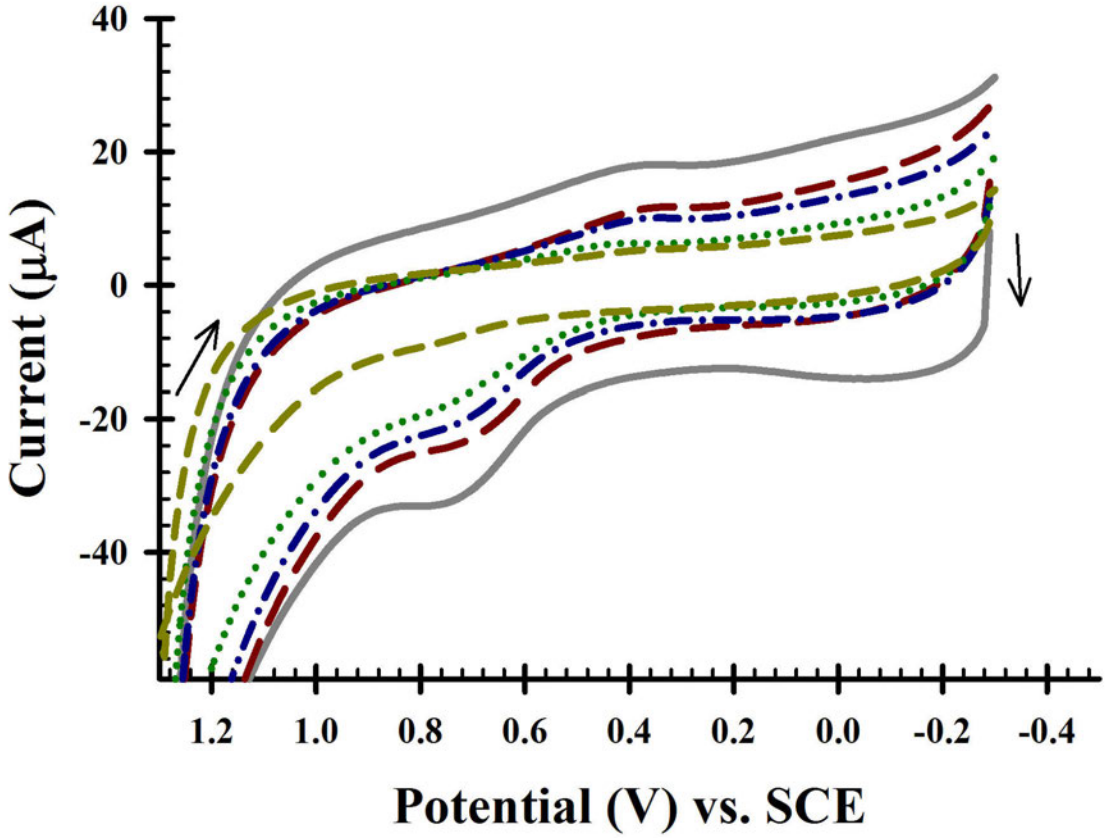

Figure 23. Overlay of cyclic voltammograms, each with a different density loading of *Anabaena variabilis* cells. The casting ratios are represented as volume cell suspension : volume TMODA Nafion. The ratios shown include 2:1 (—), 1:1 (— —), 0.50:1 (— ·),0.25:1 (· · ·), and bare (– –). The axes were adjusted to highlight the morphological features of the CV overlay, excluding data from the plot. The data excluded are background solvent electrolysis current, unimportant to the experiment.

Table 3. Total protein, Chlorophyll a density, and reverse wave current measurements in different *Anabaena variabilis* SA-1 cell suspension:TMODA Nafion suspension (v/v) ratios.

Cell : TMODA Casting Ratio (v/v)	**Total Protein** ($\mu g/m$L)	**[Chl a]** ($\mu g/m$L)	**Wave Current** (μA)
0.25:1	141.9 ± 15.1	0.97 ± 0.1	11.2 ± 0.9
0.5:1	426.5 ± 20.1	1.94 ± 0.11	13.3 ± 1.1
1:1	621.3 ± 14.8	3.88 ± 0.16	15.4 ± 0.7
2:1	827.5 ± 17.4	7.76 ± 0.20	19.6 ± 0.6

Note: Total protein was measured with the Bradford method against a BSA calibration and the error reported is from that calibration. Chlorophyll a absorbance was measured from methanolic extracts [80] and is reported as $\overline{x} \pm 1\sigma$ for $n = 5$ extraction assays. Wave currents reported as $\overline{x} \pm 1\sigma$ for $n = 4$ electrodes and two 100 mV/s cyclic voltammograms.

Total casting solution volume was 10 μL. These data suggest a direct correlation between electrochemical signal and cell density. There exists a linear agreement between wave current and chlorophyll a content ($y = 1.2x + 10.6,\ \mathrm{R}^2 = 0.99$) and total protein ($y = 0.1x + 8.9,\ \mathrm{R}^2 = 0.94$). The y intercept is expected to be zero for both correlations, however they both result in a similar value between 8 and 10 $\mu g/m$L.

This semi quantitative analysis resulted from initial observations of the electrochemical behavior of the system. Attempts to quantify ammonia production were not successful due to the poor lower limit of detection of the ISE available during the time of these experiments. These initial observations about the behavior of *A. var.* immobilized to an electrode reveal a correlation between faradaic current response and the density of cells present on the electrode

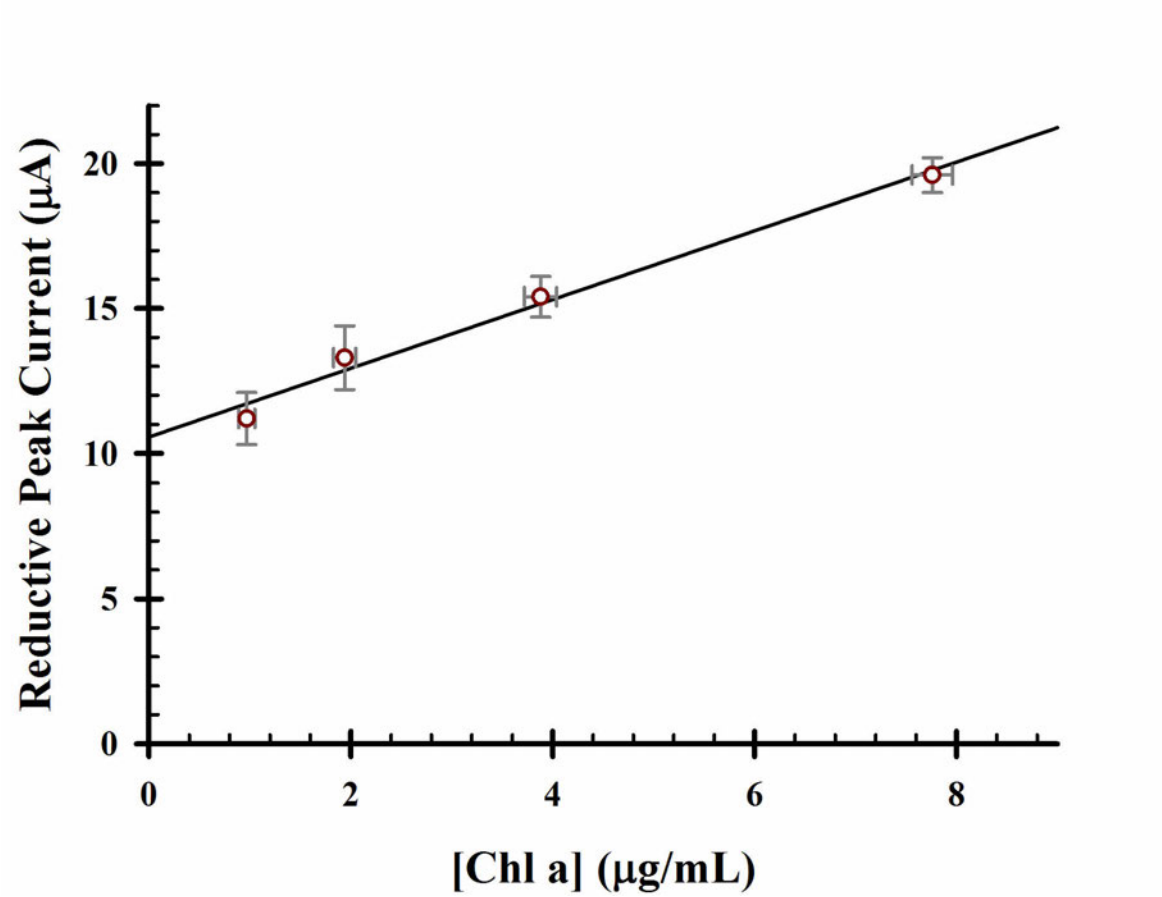

Figure 24. Relationship between oxidative peak current and chlorophyll a concentration. The data for this plot are from Table 3. The current error bars represent the $\pm 1\sigma$ for $n = 4$ electrodes and the [Chl a] error bars represent $\pm 1\sigma$ for $n = 5$ extraction assays. Chlrophyll extracted in methanol as in [80]. The linear equation is $y = 1.2x + 10.6$, $R^2 = 0.99$.

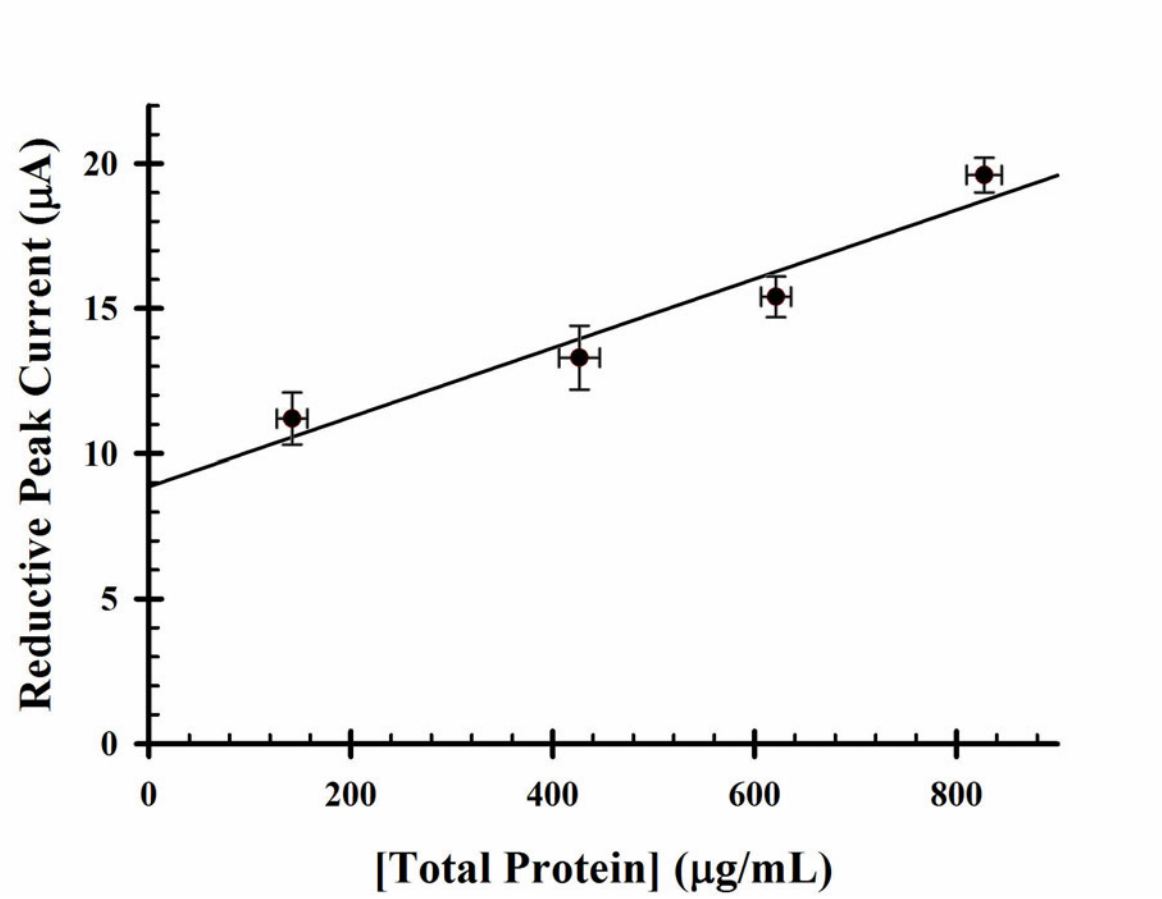

Figure 25. Relationship between oxidative peak current and total protein concentration. The data for this plot are from Table 3. The current error bars represent the $\pm 1\sigma$ for $n = 4$ electrodes and the [total protein] error bars represent $\pm$ the error in calibration. Total protein measured spectroscopically as in [81]. The linear equation is $y = 0.1x + 8.9$, $R^2 = 0.94$.

3.3.2 Cofactor, Chemical, and Substrate Effects

Although the faradaic currents observed from the CV analysis are consistent with a direct proportionality with *A. var.* density, they do not describe the specific chemical reactions. NH_4^+ is not electroactive in the potential limits used in this research. Catalytic reduction or oxidation shifts observed electrochemical potentials. Several chemical species were introduced to the background electrolyte and their effects on voltammetry observed. Either directly or indirectly, NH_4^+ (as NH_4OH or NH_4Cl), nicotinamide adenine dinucleotide phosphate ($NADPH/NADP^+$), ferredoxins, and adenosine triphosphate (ATP) are each involved in the enzymatic production of ammonia from *A. var* (Figure 1). Addition of these species to the background electrolyte followed by voltammetric analysis provides data to delineate the chemical basis for faradaic response generated between cells and the electrode.

3.3.2.1 Ammonia

Ammonia is the desired product in this system. The simplest case would be direct electrochemical assessment of ammonia production. NH_4OH was added to the background electrolyte for two reasons: 1) as a standard addition to probe whether or not the faradaic currents observed in Figures 22 and 23 are representative of an ammonia electron transfer reaction and 2) as a means to repress nitrogenase and nitrate/nitrite reductase synthesis when the concentration of NH_4^+ in the external media is sufficiently high Repression is the blocking of gene expression. This repression has been shown to be rapid and not nif gene dependent for short periods

of NH_4^+ abundance [64, 76, 79, 92]. Current enhancement and peak potential shifts of peaks as a direct result of ammonia addition would suggest electron transfer reactions arise due to reactions between the electrode and either the cell or enzyme contained within the cell.

Initial control cyclic voltammograms were obtained in the common background electrolyte (0.1 M Na_2SO_4) at several scan rates. These cyclic voltammograms were compared to those run in background electrolyte with the addition of NH_4OH to 1 mM. The small addition of NH_4OH alters the pH of the test solution by approximately 3 pH units (test solution pH $\sim$ 7, pH of 1 mM $NH_4OH \sim 10$), which then shifts potential axis by 0.059 V/ΔpH= 0.02 V. Thus, aside from a small shift of the potential axis, differences between voltammograms from control and NH_4^+ additions are noted.

From an overlay of voltammograms from the controls in Figure 26, a forward oxidative wave at 0.65 V and a reverse reductive wave at 0.3 V was observed but only when cells are present. This is as was observed in Figure 22. These faradaic waves are discernible above bare and TMODA Nafion electrode responses.

After the addition of NH_4OH to 1 mM, the electrodes equilibrated in solution for 5 minutes prior to voltammetric analysis. An overlay of the voltammograms resulting from the ammonia containing electrolyte does not show faradaic current responses for any electrode (Figure 27). These data suggest NH_4OH suppressed the waves observed at the 1:1 TMODA:Cells electrode. The notable differences between data in Figures 26 and 27 are that NH_4OH addition elicited higher background charging and solvent electrolysis as shown by the higher oxidative currents $>$ 1 V,

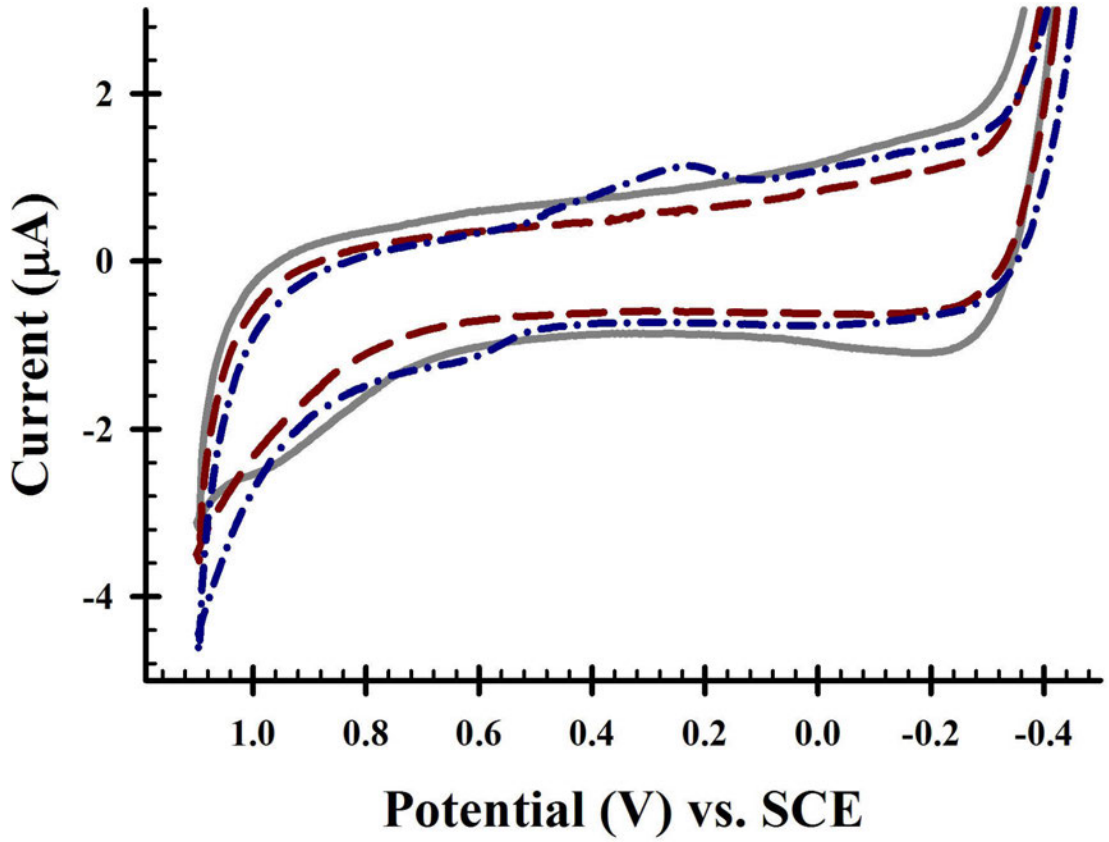

Figure 26. Cyclic voltammogram overlay that compares the typical bare, TMODA Nafion and 1:1 Cells:TMODA Nafion electrode response. Glassy Carbon working electrodes, Pt mesh counter electrode, SCE reference electrode at 50 mV/s. Comparison of Bare (— —), TMODA Nafion (—), and 1:1 TMODA:Cells (– · –) electrode responses.

a slight negative shift in potential in the same background region, and absence of any current peaks or sigmoids. Both capacitance and oxidative current are less than observed without the addition of NH_4OH. The lack of difference between bare and TMODA Nafion electrode responses in control (Figure 26) and 1 mM NH_4OH (Figure 27) and absence of faradaic waves from the cell modified electrode suggest NH_4^+ participates in a cellular based reaction. NH_4^+ can diffuse into *Anabaena variabilis* passively through the cell membrane. Rapid repression of ammonia producing enzymes in response to NH_4^+ is a genetically linked process that can occur on the time scale of a minute. The duration of total voltammetric perturbation for a series of replicates at several scan rates is between 7 and 10 minutes, long enough to inhibit NH_4^+ production by *A. var.* enzymes. From the data, the faradaic waves observed at cell modified electrodes are consistent with electrochemical manifestation of ammonia producing enzyme activity. Data from the cell density study (Table **??**) are consistent with this observation because with a higher density of cells and thereby higher concentration of *A. var.* enzymes, peak current increase linearly.

The same electrodes used to obtain data in Figures 26 and 27 were gently rinsed with 0.1 M Na_2SO_4 and returned to the electrochemical cell with 0.1 M Na_2SO_4. After the electrodes equilibrated in freshly prepared 0.1 M Na_2SO_4 for 5 minutes, cyclic voltammograms were obtained in the same manner as above. See Figure 28 . The voltammetric waves near 0.65 V and 0.3 V appeared again at the cell modified electrodes. Temporary suppression of nitrogenase and nitrate/nitrite reductase enzymes with increased NH_4^+ in the external media explain this observation. The reductive wave appears $\sim$100 mV more positive than initially observed (Figure

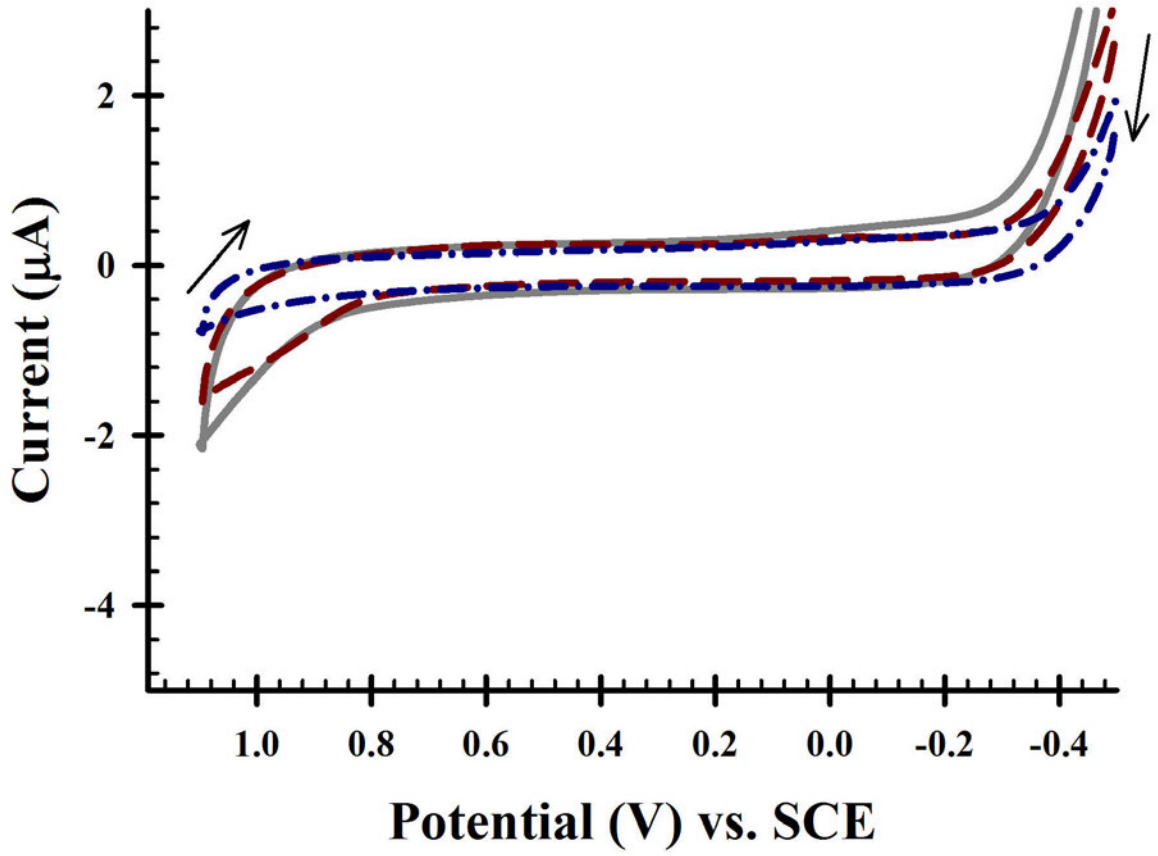

Figure 27. Cyclic voltammogram overlay of bare, TMODA Nafion, and 1:1 (v/v) cells:TMODA Nafion electrodes in 1 mM NH_4OH. Glassy Carbon working electrodes, Pt mesh counter electrode, SCE reference electrode at 50 mV/s. Comparison of Bare (— —), TMODA Nafion (—), and 1:1 TMODA:Cells (– · –) electrode responses.

26), but the oxidative wave remains at 0.6 V. The shift in the reductive wave as the oxidative wave potential does not change is consistent with the reduction and oxidation waves associated with distinct rather than a common chemical reaction. The TMODA Nafion electrode departs from background current near 0.65 V that was not observed previously. The reason for this is not known. Sensitization of channels to NH_4^+ on the time scale of these experiments likely manifests itself voltammetrically

3.3.2.2 Nicotinamide Adenine Dinucleotide Phosphate

The ubiquitous nature of nicotinamide adenine dinucleotide phosphate ($NADPH/NADP^+$) in cyanobacteria can not be ignored. NADPH is the most important electron shuttle in cyanobacteria [43, 102]. The $NADP^+$/NADPH couple shares a close redox recycling relationship with ferredoxins. This includes ferredoxins bound to enzyme protein residues and as a freely mobile molecule. *In vivo*, NADPH is directly involved in photosystem I and II and nitrate/nitrite reductase in the conversion of NO_2^- to NH_3 and indirectly involved in nitrogenase through ATP to ADP recycling (See Figure 1).

The pH dependent redox reaction of the NADP/NADPH system is

$$NADP^+ + H^+ + 2e \rightleftharpoons NADPH \qquad E^{\circ'}_{pH=7} = -0.565 \text{ V vs. SCE} \qquad (22)$$

Much has been reported on the electrochemical recycling of $NADP^+$, yet the direct electrolysis of the $NADP^+$/NADPH couple at a bare electrode [30] is not reported. Synthetic recycling of $NADP^+$ at an electrodes requires enzyme and mediators [30].

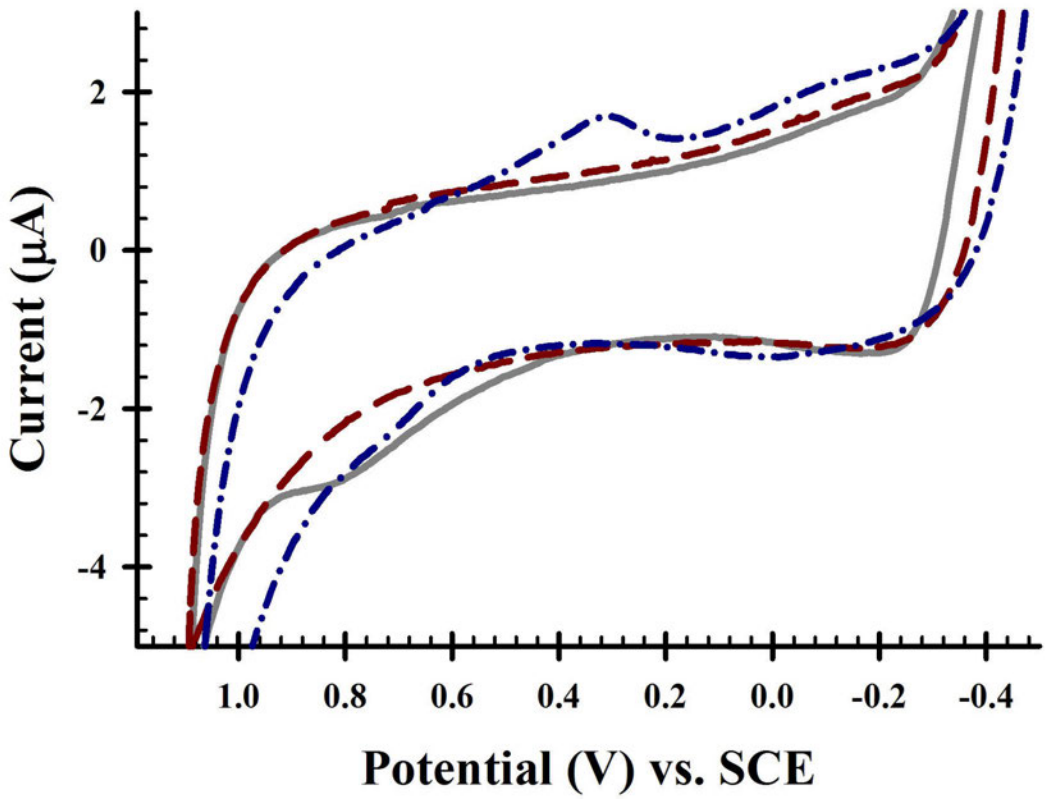

Figure 28. Cyclic voltammogram in freshly prepared 100 mM Na_2SO_4, that followed previous analysis of same electrodes in a 1 mM NH_4OH solution. Glassy Carbon working electrodes, Pt mesh counter electrode, SCE reference electrode at 50 mV/s. Comparison of Bare (— —), TMODA Nafion (—), and 1:1 TMODA:Cells (– · –) electrode responses. The axes were adjusted to highlight the morphological features of the CV overlay, excluding data from the plot. The data excluded are background solvent electrolysis current.

No direct electrolysis of $NADP^+$/NADPH is observed here.

An overlay of cyclic voltammograms with and without 1 mM NADPH is shown in Figure 29. Note, with these experiments and all cyclic voltammetry that follows, the potential sweep parameters were changed. Due to background charging currents at positive potential, cyclic voltammetric sweeps were initiated at 0.8 V and then swept reductively to -0.5 V and reversed back to 1.1 V. Thus, the current response has a discontinuity at more positive potential. As expected, the oxidation of NADPH shows no activity or current signal at a bare or TMODA Nafion electrode. When cells are present, however, NADPH causes an enhancement in the reductive wave at ∼0.1 V. Data are consistent the species or process that gives rise here to the current signal at 0.1 V are the same as observed more typically at 0.3 V (Figures 22, 23, and 26). The appearance of this peak at more negative potentials mar arise from differences in pH and buffering capacity of the $NADP^+$/NADPH redox couple. Because many enzymes and reaction centers within the cell depend upon NADPH as a reductant and electron carrier, it is challenging to identify the mechanism and kinetic basis for the current enhancement observed at 0.1 V.

Ammonia concentration measurements in these NADPH addition experiments were made and normalized to the concentration of chlorophyll a (Table 4). Normalization of ammonia data to chlorophyll a density is an indirect relation to amount of enzyme present on the electrode surface, because chlorophyll a density $\propto K \cdot [\text{enzyme}]$. K was not determined. The ammonia was measured for the entire 15 mL volume of background electrolyte, thus it would include any contribution of

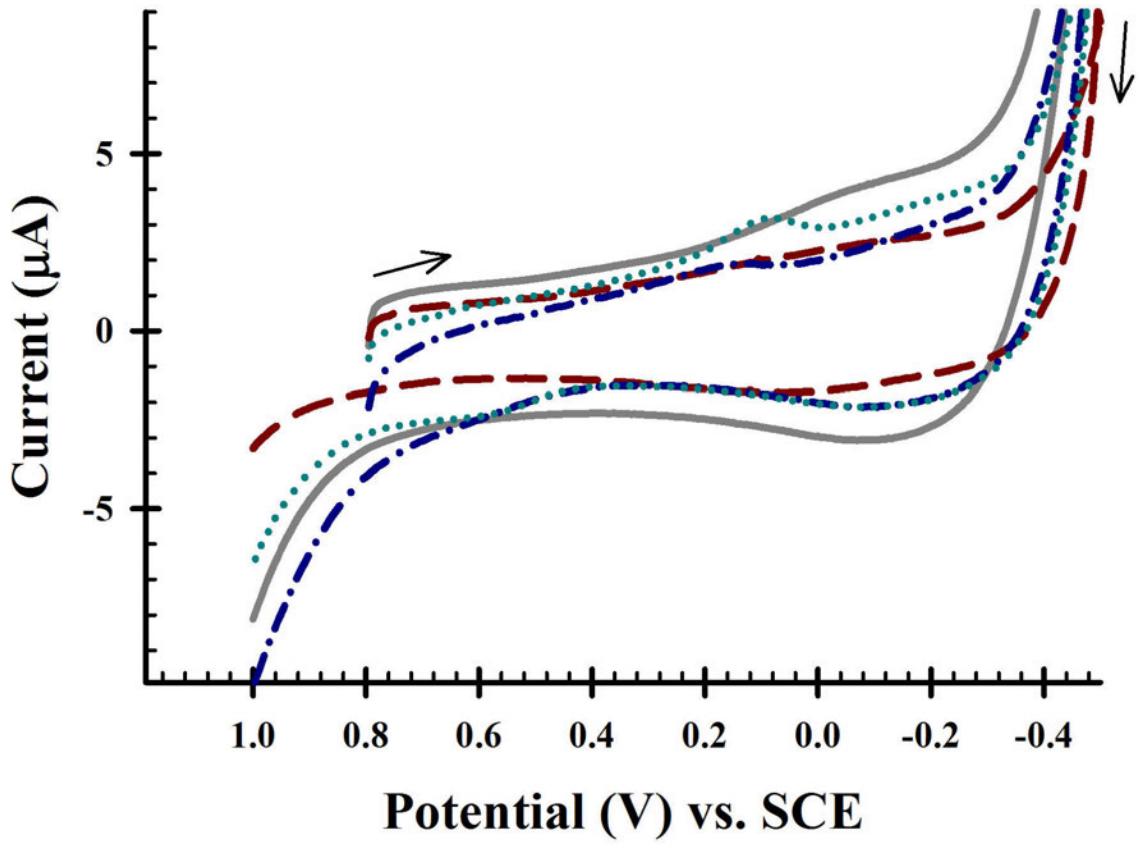

Figure 29. Overlay of cyclic voltammetric responses after the addition of sufficient NADPH to the background electrolyte. Cyclic voltammogram overlay of Bare (——), TMODA-Nafion (— —), and 1:1 Cells:TMODA-Nafion (· · ·) electrodes in 0.1 M Na_2SO_4 and NADPH added for a final concentration of 1 mM. For comparison, a 1:1 Cells:TMODA-Nafion (— ·) in 0.1 M Na_2SO_4 without NADPH is overlayed. Pt mesh counter electrode, SCE reference electrode, 100 mV/s.

Table 4. Values of NH_3 concentration, Chl a density, and reductive peak current obtained after voltammetric perturbation of the system when NADPH is added to the electrolyte.

Cell : TMODA Casting Ratio (v/v)	**Total Protein** ($\mu g/m$L)	**[Chl a]** ($\mu g/m$L)	**Wave Current** (μA)
0.25:1	141.9 ± 15.1	0.97 ± 0.1	11.2 ± 0.9
0.5:1	426.5 ± 20.1	1.94 ± 0.11	13.3 ± 1.1
1:1	621.3 ± 14.8	3.88 ± 0.16	15.4 ± 0.7
2:1	827.5 ± 17.4	7.76 ± 0.20	19.6 ± 0.6

Note: Ammonia concentration, reported as $\overline{x} \pm 1\sigma$ for $n = 4$ electrodes, is measured by ISE and normalized to chlorophyll a concentration. Total cell volume is 15 mL. Total film casting volume is 10 μL. Chlorophyll a absorbance determined spectrophotometrically after extraction from cell suspension in methanol [80] and reported as $\overline{x} \pm 1\sigma$ for $n = 3$ extraction assays. Peak current is for the forward (reductive) peak (Figure 29) as measured from the leading baseline.

NH_3 from the bare and TMODA Nafion electrodes. Based on known biochemistry of ammonia production, the NH_3 reported in Table 4 is likely an enzyme product. These data are consistent with the known importance of NADPH for the production of ammonia by immobilized cells. The correlation between ammonia production and observed electrochemical current signals can not be calculated directly from these data due to the uncertainty of mechanistic interaction between NADPH and the cells, but more NH_3 is produced and reductive peak current increases on addition of NADPH.

The initial polarity of the sweep and potential sweep limits were changed beginning with this experiment. The potential waveform initiates at 0.8 V, sweeps negative (reductively) to 0.5 V, and cycles back to 1.1 V. This change to the experimental protocol was made for the two reasons. First, in CV, it is ideal to initiate the potential where no faradaic reaction occurs. Previous parameters

measured current immediately following the quiet time of the instruments. Starting closer to zero current aids in establishing a baseline current not related to faradaic processes. Second, peak current data for the reductive process are more pronounced against background.

The forward (reductive) peak current doubled from 0.45 μA in 0.1 M Na_2SO_4 background to 0.9 μA after the addition of NADPH to 1 mM. Because the faradaic waves are absent at bare and TMODA Nafion electrodes, the increase in peak current does not correlate to direct reduction of $NADP^+$ reduction reaction (Reaction 22). Current increase is consistent with a chemical or kinetic step between the immobilized *A. var.* and electrode. These observations do not discriminate between a cell surface reaction and a catalytic enzyme reaction. The reverse oxidative wave, while enhanced after the addition of NADPH to 1 mM, is not easily measured from a complex baseline.

Significantly increased NH_3 was measured in the external media after cyclic voltammetric assessment as shown in Table 4. Normalized by chlorophyll a density in the parent cell suspension, the measured NH_3 increased tenfold after the addition of NADPH to 1 mM. While difficult to explain mechanistically, certainly it is well documented that NADPH has a significant role in electron transfer reactions for ammonia producing enzymes nitrogenase and nitrate/nitrite reductase. If the concentration of NADPH increases, so do NH_3 concentration and peak current for the reduction here.

3.3.2.3 Ferredoxins

Ferredoxins are small iron sulfur proteins that receive electrons from photosystem I and transfers the electrons to various reductases. Ferredoxins are ubiquitous in cyanobacteria and mobile so as to exchange electrons with various oxidants in the system [43, 105–108]. Ferredoxins act as biological capacitors, accepting and discharging electrons as part of several enzymatic pathways. As shown in Figure 1, ferredoxins are involved in all the reaction centers considered in this research. Generally, ferredoxins are modeled as one electron transfer reagents that alter the oxidation state of an Fe atom (between +2/+3) or as a delocalized electron. The nature of ferredoxins suggests they are electroactive and freely mobile within the cells. The redox reaction of ferredoxins are represented as [25, 104, 109, 110]:

$$Fd\left(Fe^{3+}\right) + e \rightleftharpoons Fd\left(Fe^{2+}\right) \qquad E^{\circ\prime}_{pH=7} = -0.671 \text{ V vs. SCE} \qquad (23)$$

Spinach ferredoxins (Sigma Aldrich) were added to 15 mL of 0.1 M Na_2SO_4 to a final concentration of 0.01 mg/mL. Ferredoxins are not easily quantifiable in typical units such as molarity due to the mixture of Fe_2 S_2 and Fe_4 S_4 types isolated from spinach. Ferredoxin has a significant effect on the electrochemical peak currents of cell modified electrodes as compared to a bare and TMODA Nafion electrodes where no significant effect is observed (Figure 30). Addition of ferredoxins to 0.01 mg/mL to the background electrolyte increases the reductive faradaic peak current observed at 0.3 V from 0.38 μA to 1.4 μA at cell modified electrodes but shows no effect at bare or TMODA Nafion electrodes. In response to the addition of ferredoxins the reverse oxidative faradaic wave at 0.6 V exhibits increased current but to a lesser

Table 5. Values of NH_3 concentration, Chl a density, and reductive peak current at 1:1 (v/v) cells:TMODA Nafion modified electrodes after voltammetric perturbation of the system when ferredoxins are added to the background electrolyte.

Solution	**[NH_3]** (μM)	**[Chl a]** ($\mu g/mL$)	**NH_3 Density** (μmol $NH_3/\mu g$ Chl a)	**Peak Current** (μA)
0.1 M Na_2SO_4	2.9 ± 0.6	3.9 ± 0.5	1.1 ± 0.2	0.38
0.01 mg/mL Fd	3.4 ± 1.1	4.0 ± 0.3	1.3 ± 0.3	1.4

Note: Ammonia concentration, measured by ISE, is normalized to chlorophyll a concentration and reported as $\overline{x} \pm 1\sigma$ for $n = 4$ electrodes and two 100 mV/s sweeps. Total cell volume is 15 mL. Total film casting volume is 10 μL. Chlorophyll a absorbance determined spectrophotometrically after extraction from cell suspension in methanol [80] and reported as $\overline{x} \pm 1\sigma$ for $n = 3$ extraction assays. Peak current is for the forward (reductive) peak (Figure 30), as measured from the leading baseline.

degree. As was observed for NADPH additions (Figures 29 and data in Table 4), ferredoxins addition does not affect the current response at bare and TMODA Nafion electrodes, but increases current for both faradaic waves (Figure 30). These data consistent with an electron transfer step between ferredoxins and cells (or enzymes contained within) requires an applied potential.

Despite the increased current, the ferredoxins addition did not significantly increase the NH_3 resulting in the external media. Normalized to chlorophyll a concentration, the NH_3 densities are similar for both the control and ferredoxins addition experiments. Basal ammonia production by immobilized *A. var.* in 0.1 M Na_2SO_4 after 10 minutes of cycled voltammetric perturbation was statistically the same as the ammonia production in 0.01 mg/mL ferredoxins (Table 5). Thus, ferredoxins do not impact NH_3 production directly but do impact the peak current at 0.3 V.

Overall, the data from these experiments are consistent with an electrochemical response by *A. var.* to increased ferredoxins in the external electrolyte, but alone

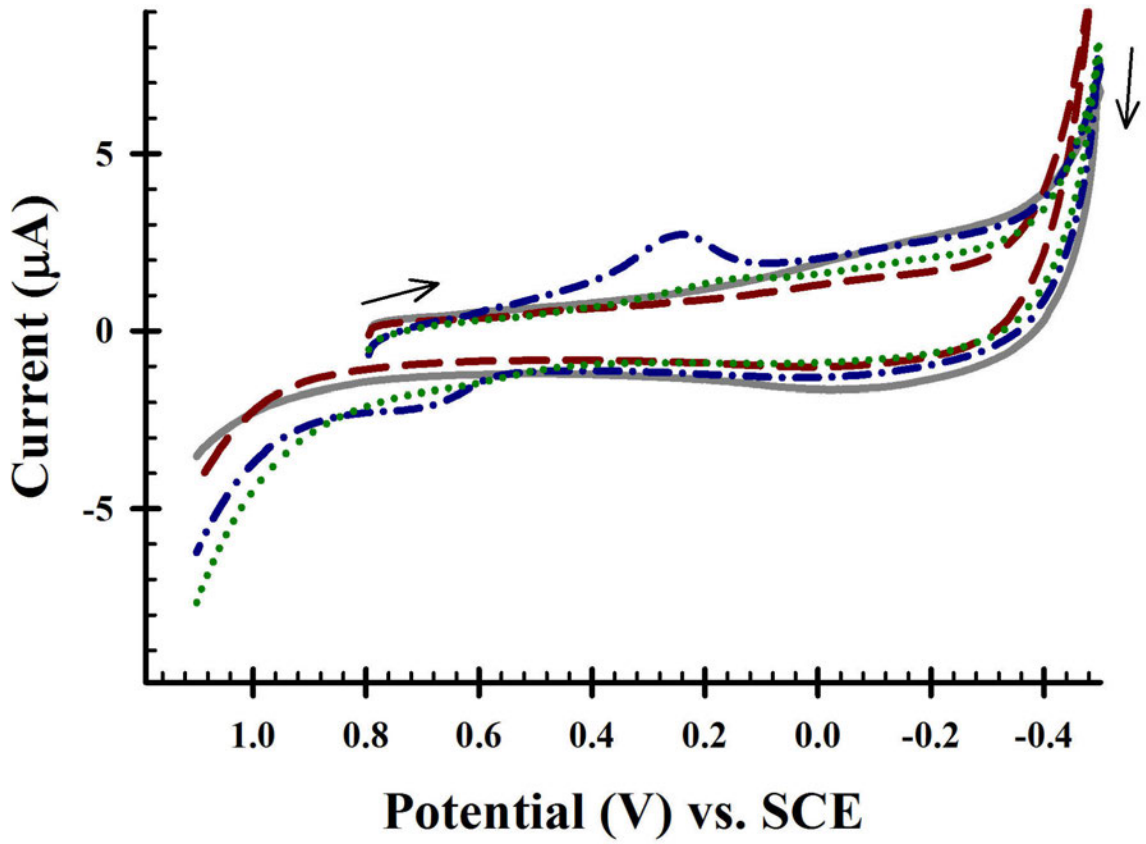

Figure 30. Effect of adding ferredoxins to the background electrolyte during cyclic voltammetry. Cyclic voltammogram overlay of Bare (——), TMODA-Nafion (— —), and 1:1 Cells:TMODA-Nafion (— ·) electrodes in 0.1 M Na_2SO_4 with 0.1 mg/mL ferredoxin added. For comparison, a 1:1 Cells:TMODA-Nafion (···) in 0.1 M Na_2SO_4 without ferredoxin is overlayed. Pt mesh counter electrode, SCE reference electrode, 75 mV/s.

it does not elicit increased NH_3 production. It appears the cells can catalyze the irreversible reduction of ferredoxins from $Fd(Fe^{3+})$ to $Fd(Fe^{2+})$ (Reaction 23), but the reduced ferredoxin does not interact with nitrogenase or nitrate/nitrite reductase on the time scale of the experiment to facilitate increased NH_3 production. Even at slow scan rates (10 mV/s) the same effects were observed.

3.3.2.4 Comparison of NADPH, ATP, and Ferredoxins Additions

As shown in Figure 1, NADPH and ferredoxins are found concomitantly in enzyme pathways that produce NH_3. Both NADPH and ferredoxin interactions with immobilized *Anabaena variabilis* have been studied electrochemically (Figures 30 and 29). Both species elicit significant changes in the observed reduction wave near 0.1 to 0.3 V at cell modified electrodes. Nitrogenase requires binding of adenosine triphosphate (ATP) for catalytic conversion of N_2 to NH_3. ATP recycling depends on low potential reductants such as ferredoxins and $NADP^+$ as shown for the pertinent reactions of photosystem I and II (Figure 1). In this experiment, the collective contribution NADPH, ferredoxins, and ATP present in background media to ammonia production and voltammetric character of immobilized cells is evaluated.

After electrodes were modified with *A. var.*, NADPH, ATP, or ferredoxins were added to 0.1 M Na_2SO_4 and analyzed by cyclic voltammetry. Each chemical was added to background electrolyte independently. Following cyclic voltammetric analysis, the background electrolyte was refreshed at which time the next species was added. The effects of NADPH to 1 mM, ATP to 1 mM, and ferredoxins to 0.01 mg/mL added to 0.1 M Na_2SO_4 were investigated. Figure 31 shows the bare

electrode cyclic voltammogram response for each solution. With the exception of the NADPH, the addition of the biochemicals had no effect. The voltammograms in Figure 31 show only current arising from the solvent background. A small faradaic peak appears at 0.1 after introducing NADPH to the solution as observed previously (Figure 29). Direct reduction of $NADP^+$ at an unmodified surface has not been previously reported and requires either an enzyme or coenzyme to catalyze the reduction to $NADP^+$ [111, 112]. The wave is not consistent with the reduction potential of $NADP^+|NADPH$, $E^{\circ'}_{pH=7} = 0.565$ V vs. SCE. In a later experiment, the wave near 0 V also appears immediately following addition of NADPH The wave arises from a solution based impurity. Figure 32 overlay the responses of the TMODA Nafion modified electrode. The response in 0.1 M Na_2SO_4 is overlaid with the responses after the addition of 1 mM NADPH, 0.01 mg/mL ferredoxins, and 1 mM ATP. Similarly to the bare electrode response, the cyclic voltammograms reveal only background charging currents. No faradaic current signals are observed. The unexpected broad wave at after NADPH addition at a bare electrode (Figure 31) is absent at TMODA Nafion. From the bare and TMODA Nafion modified electrode responses, the additions of the cofactor and mediating chemicals do not themselves elicit significant responses.

Figure 33 compares the 1:1 (v/v) cells:TMODA Nafion modified electrode responses to additions of NADPH to 1 mM, ferredoxins to 0.01 mg/mL, and ATP to 1 mM in 0.1 M Na_2SO_4. Unlike the bare (Figure 31) and TMODA Nafion modified (Figure 32), significant faradaic responses to these chemicals are apparent at cell modified electrodes. These data are similar to those obtained when studying

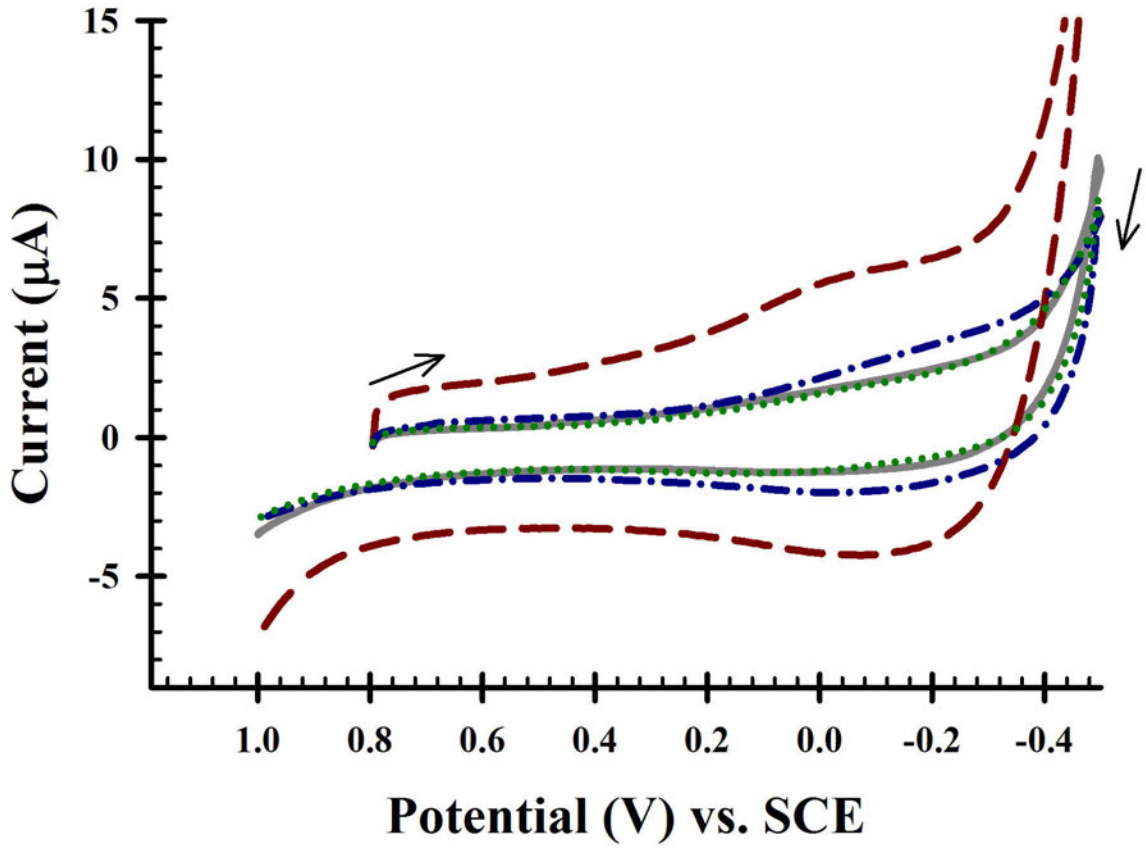

Figure 31. Cyclic voltammetric responses from a bare electrode to compare the effect of mediating/cofactor chemical additions. Cyclic voltammogram overlay of bare electrodes in 0.1 M Na_2SO_4,control (——), 1 mM NADPH (— —), 0.01 mg/mL ferredoxins (— ·), and 1 mM ATP (· · ·). Pt mesh counter electrode, SCE reference electrode, 100 mV/s.

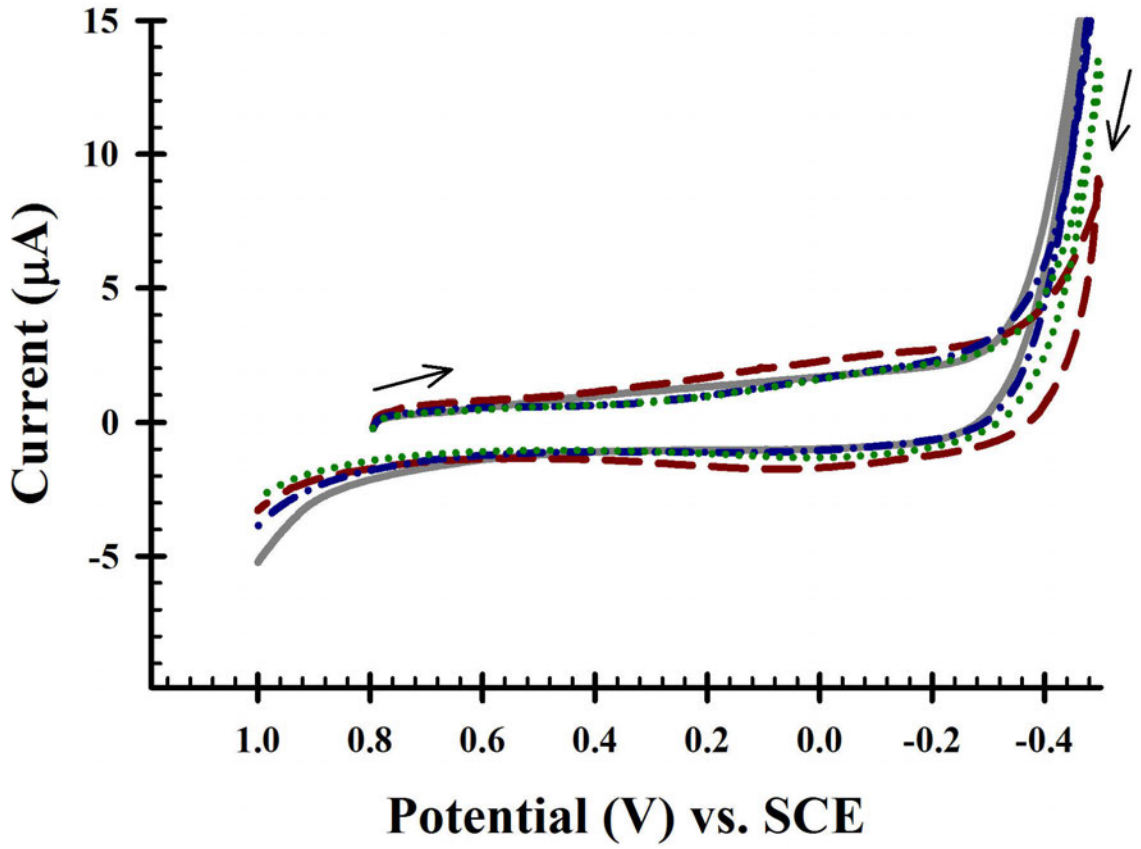

Figure 32. Cyclic voltammetric responses from a TMODA Nafion electrode to compare the effect of separate and independent additions of mediating/cofactor chemical. Cyclic voltammogram overlay of TMODA-Nafion electrodes in 0.1 M Na_2SO_4,control (——), 1 mM NADPH (— —), 0.01 mg/mL ferredoxins (· · ·), and 1 mM ATP (— ·). Pt mesh counter electrode, SCE reference electrode, 100 mV/s.

single chemical additions (Figures 29 and 30). Additionally, NADPH to 1 mM plus ferredoxins to 0.01 mg/mL were added to the background electrolyte simultaneously. Both NADPH and ferredoxins mediate the nitrate/nitrite reductase production of ammonia. NADPH and ferredoxins share a very similar formal potential, thus the combined effect of both species biochemically suggests similar electrochemical reactions. Five significant observations from the overlay are: 1) the faradaic waves at 0.2 V and 0.6 V are largest for NADPH plus ferredoxins, but the ATP did not alter the magnitude of current. The reductive wave at 0.2 V in 0.1 M Na_2SO_4 is shifted to 0.4 V with ATP addition; 2) ferredoxins plus NADPH addition increases the current at 0.2 V; 3) from all additives, forward and reverse waves show higher current and more defined wave character than observed in Na_2SO_4; 4) the current vs. potential background slope increases rather sharply in this experiment. This means the additives cause a higher solution resistance; and 5) when added together, NADPH and ferredoxins cause a significantly higher forward and reverse peak current as compared to the response obtained in only 0.1 M Na_2SO_4. The voltammetric waves for the addition of ferredoxins and ATP appear largely coincident.

Overall, NADPH plus ferredoxins appear to have the greatest electrochemical effect (Figure 33) as compared to a bare or TMODA Nafion electrode where no significant effect is observed (Figures 31 and 32). Table 6 is a summary of [NH_3] and peak current for the experiments at cell modified electrodes. As in Table 6, the reductive current is nearly twice that obtained in the control. When NADPH plus ferredoxins are added to a solution of 0.1 M Na_2SO_4, the currents at the voltammetric waves from cells is significantly enhanced compared to background

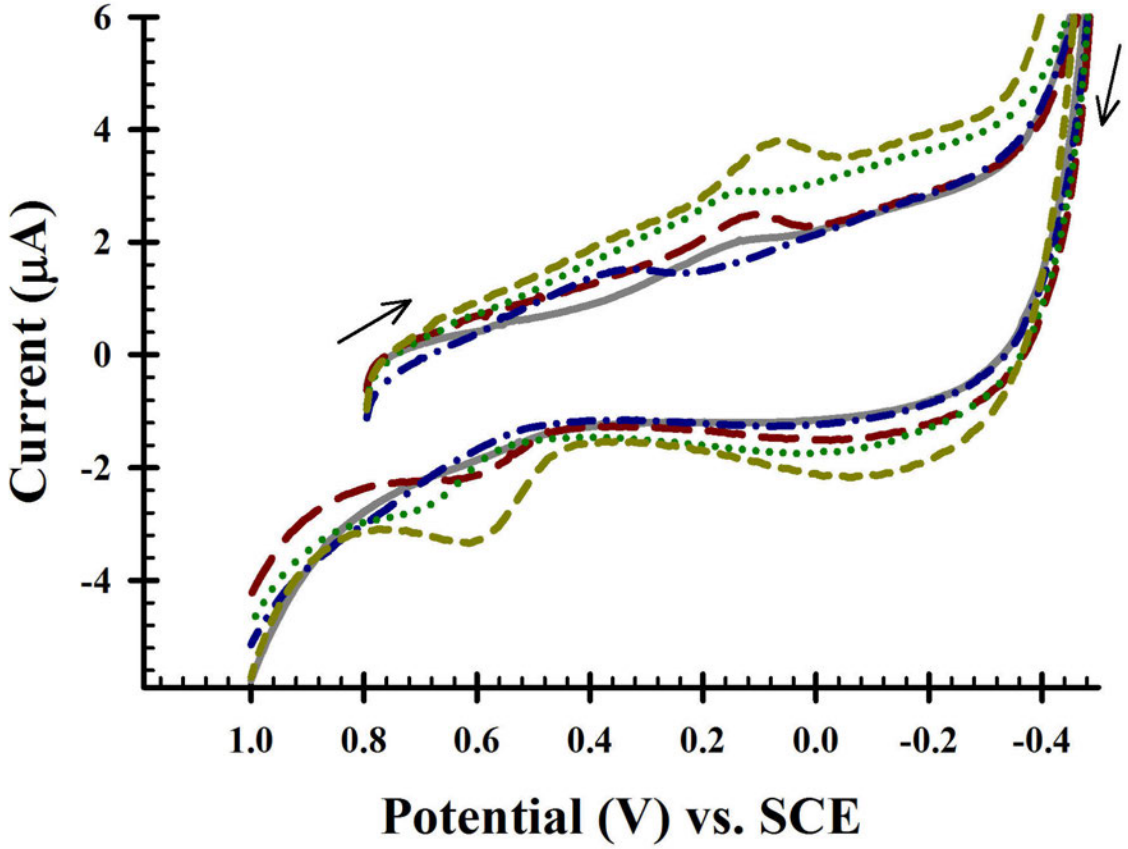

Figure 33. Cyclic voltammetric response overlay for 1:1 (v/v) cells:TMODA Nafion electrodes to compare the effect of individual additions of mediating/cofactor chemicals. Cyclic voltammogram overlay of bare electrodes in 0.1 M Na_2SO_4,control (——), with 1 mM NADPH (— —), 0.01 mg/mL ferredoxins (· · ·),1 mM ATP (— ·), and 1 mM NADPH + 1 mM Ferredoxin (– – –). Pt mesh counter electrode, SCE reference electrode, 100 mV/s.

Table 6. Values of NH_3 concentration, Chl a density, and reductive peak current at 1:1 (v/v) cells:TMODA Nafion modified electrodes after voltammetric perturbation of the system when chemical cofactors are independently added to 0.1 M Na_2SO_4.

Solution	**[NH_3]** (μM)	**[Chl a]** ($\mu g/mL$)	**NH_3 Density** (μmol NH_3/μg Chl a)	**Peak Current** (μA)
0.1 M Na_2SO_4	2.7 ± 0.6	3.9 ± 0.5	1.0 ± 0.2	0.34 ± 0.02
1 mM NADPH	24.7 ± 1.8	4.0 ± 0.3	9.3 ± 0.6	0.79 ± 0.02
0.01 mg/mL Fd	3.0 ± 1.0	4.1 ± 0.5	1.1 ± 0.3	0.39 ± 0.02
1 mM ATP	0	3.2 ± 1.0	0	0.31 ± 0.02
Fd + NAPH	26.1 ± 2.1	3.7 ± 0.4	10.6 ± 1.0	0.82 ± 0.02

Note: Ammonia concentration, measured by ISE, is normalized to chlorophyll a concentration. Total cell volume is 15 mL. Total film casting volume is 10 μL. Chlorophyll a absorbance determined spectrophotometrically after extraction from cell suspension in methanol [80] and reported as $\overline{x} \pm 1\sigma$ for $n = 5$ extraction assays. Peak current is for the forward (reductive) peak (Figure 33) as measured from the leading baseline and is reported as $\overline{x} \pm 1\sigma$ for $n = 4$ electrodes and two 100 mV/s sweeps.

scans and slightly greater than these cells in Na_2SO_4. ATP alone does not alter ammonia concentration of peak current. ATP is a large molecule and not as easily diffused through cell membranes as the smaller NADPH and ferredoxins. ATP function within photosystem I is buried within the cell near the thylakoid membranes and is not likely accessible by the electrode at this time scale. Further, the data for ATP addition are consistent with ATP suppression of ammonia output.

After cyclic voltammetry was completed for each additive the media was collected and NH_3 measured before the addition of a different cofactor chemical These data appear in Table 6. The NH_3 concentration was normalized by known concentration of chlorophyll a, measured prior to cell immobilization. The peak current for the reverse (oxidative) reaction are not reported. The oxidative current signal is difficult to quantify because it often changes response from a diffusional peak to a sigmoidal response. It varies and does not show consistent results as the forward wave does.

A linear relationship between the forward wave and ammonia output is shown in Figure 34. These data suggest that the added NADPH and ferredoxins interact with the cells near the electrode surface. The interaction is measured voltammetrically. This interaction appears to facilitate higher production of NH_3. Certainly, as shown in Figure 1, both NADPH and ferredoxins are essential mediating and cofactor species for nitrogenase and nitrate/nitrite reductase enzyme production of NH_3. These data are not conclusive, but provide initial correlational observations.

3.3.2.5 Successive Additions of Mediating Species NADPH, Ferredoxins, and ATP

In the previous section, mediating and cofactor chemicals NADPH, ferredoxins, and ATP were added individually to the electrolyte and analyzed voltammetrically at cell modified electrodes. When ferredoxins plus NADPH were added to the background electrolyte, a significant increase in both forward and reverse peak currents were observed. Peak currents and ammonia concentration correlate linearly. Here, the cofactor and mediating chemicals are added to the a 0.1 M Na_2SO_4 background successively. After each addition, cyclic voltammetry was performed to study the electrochemical effects of these species and how currents relate to ammonia measured after cyclic voltammetry.. In these experiments, the addition of the mediating species was in the same volume of background electrolyte, so that the final cyclic voltammetric analysis was of a 0.1 M Na_2SO_4 solution containing NADPH, ferredoxins, and ATP.

As observed for individual additions (Figure 31), an overlay of cyclic

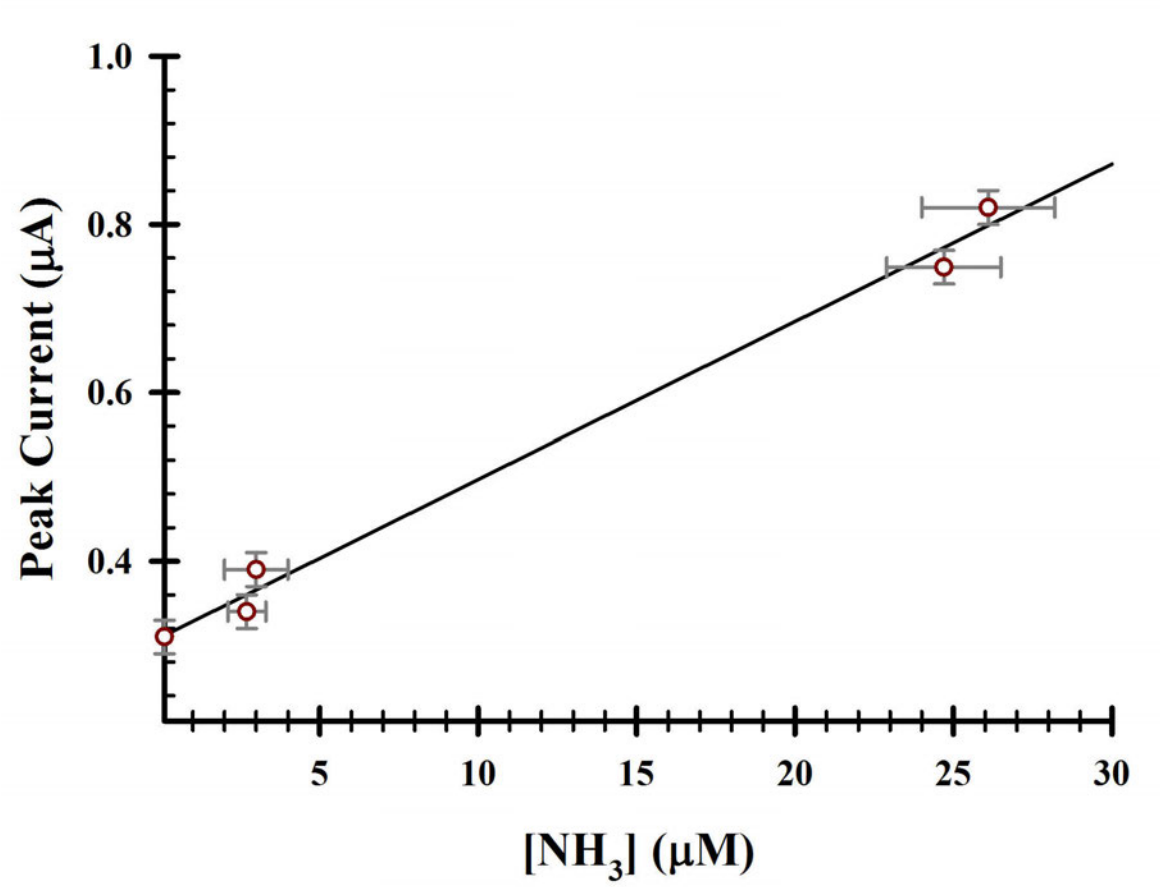

Figure 34. Plot that shows the relationship between forward (reductive) peak current and the measured concentration of NH_3 after independent additions of NADPH, ferredoxins, and ATP after voltammetric pertubation. The data for this plot are from Table 6. The data are presented as $\overline{x} \pm 1\sigma$ for $n = 4$ electrodes in a single experiment. The linear equation is $y = 0.019x + 0.31$, $R^2 = 0.99$.

voltammograms for successive additions of NADPH to 1 mM, then ferredoxins to 0.01 mg/mL, and then ATP to 1 mM are compared in Figure 35. The background cyclic voltammogram in only 0.1 M Na_2SO_4 shows only background charging currents, as expected. After the initial addition of 1 mM NADPH, the wave around 0.1 V observed previously with NADPH addition appears. Addition of 0.01 mg/mL ferredoxins to the NADPH does not alter the current response from that of NADPH alone. 1 mM ATP addition shifts the faradaic waves positive for both the forward and reverse scans. The identity of the species giving rise to a faradaic response is not known. Because direct electrochemical reduction of NADPH has been reported inconsistently, it is likely a solution based chemical species formed that is somewhat electroactive. At electrodes with TMODA Nafion on the surface, these waves are absent. Thus, adsorption of an unknown species to the glassy carbon surface would not complicate the measurements when a polymer is blocking sites for that adsorption.

Figure 36 overlays the responses of the TMODA Nafion modified electrode. The response in 0.1 M Na_2SO_4 is overlaid with the responses following the successive additions of NADPH to 1 mM , then ferredoxins to 0.01 mg/mL, and then ATP to 1 mM. Similarly to the bare electrode response, the cyclic voltammograms reveal only background charging currents. No faradaic current signals are observed. The unexpected broad wave at following NADPH addition at a bare electrode (Figure 35) is absent at TMODA Nafion. From the bare and TMODA Nafion modified electrode responses, the additions of the cofactor and mediating chemicals do not themselves elicit significant responses.

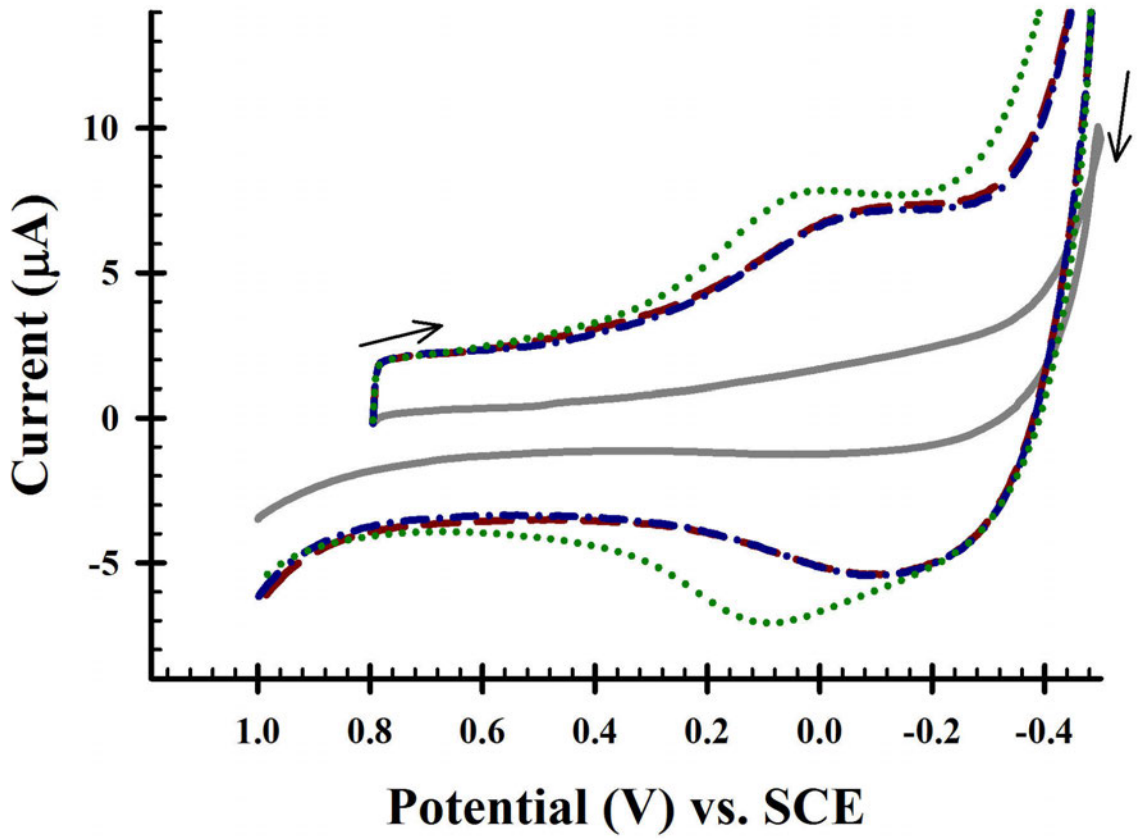

Figure 35. Cyclic voltammogram overlay of a bare glassy carbon working electrode with successive additions of known mediating and cofactor species. Initial CV in 0.1 M Initial CV in 0.1 M Na_2SO_4 (——). Overlayed with CV of same solution and electrode with additions of 1 mM NADPH (— —), followed by 1 mg/mL ferredoxin (— ·), and finally 0.1 mM ATP (· · ·). Pt mesh counter electrode, SCE reference electrode, 100 mV/s.

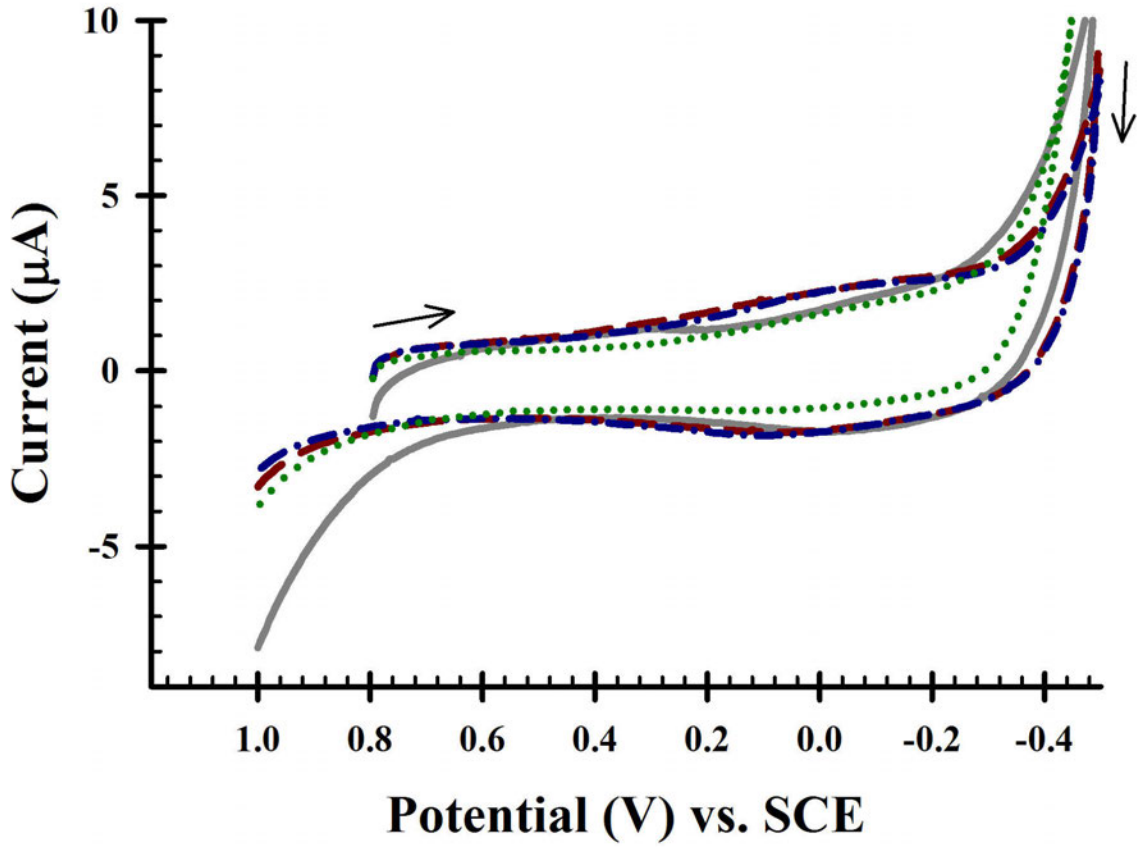

Figure 36. Cyclic voltammogram overlay of a TMODA Nafion glassy carbon working electrode with successive additions of known mediating and cofactor species. Initial CV in 0.1 M Na_2SO_4 (——). Overlayed with CV of same solution and electrode with additions of 1 mM NADPH (— —), followed by 1 mg/mL ferredoxin (— ·), and finally 0.1 mM ATP (· · ·). Pt mesh counter electrode, SCE reference electrode, 100 mV/s.

Figure 37 compares the 1:1 (v/v) cells:TMODA Nafion modified electrode responses to successive additions of NADPH to 1 mM, then ferredoxins to 0.01 mg/mL, and then ATP to 1 mM in 0.1 M Na_2SO_4. Unlike the bare (Figure 35) and TMODA Nafion modified (Figure 36), significant faradaic responses to these chemicals are apparent at cell modified electrodes. These data are similar to those obtained when studying single chemical additions (Figures 29 and 30). As has been shown, ferredoxins and NADPH increase the faradaic current response when cells are present at the electrode surface. Again, addition of 1 mM ATP significantly alters the voltammetric response. It appears ATP suppresses the forward peak and contributes to a higher capacitive current throughout the potential region studied.

Peak current for 1:1 (v/v) cells:TMODA Nafion are reported in Table 7 for each successive addition. The method of this experiment did not allow measurement of NH_3 after each successive addition. Measurement of NH_3 by the ISE renders the media useless after addition sufficient NaOH to convert all dissolved NH_4^+ to NH_3 gas. Thus, only the final NH_3 concentration was measured after all additions and voltammetric scans. The final media contained 24.9 μM NH_3 that compares well to 26.1 ± 2.1 μM measured after the NADPH plus ferredoxins addition previously (Table 6) . The chlorophyll assay extracted 3.5 ± 0.2 $\mu g/mL$ chlorophyll a. The peak current after ATP was not included in Table 7 because the faradaic wave does not overlay with the peak at 0.1 V. Because NH_3 could only be measured following all additions and cyclic voltammograms, these data are not sufficient to build a calibration as in Figure 34. This experiment is closely related, however, and the linear agreement between peak current and NH_3 fits within statistical uncertainty.

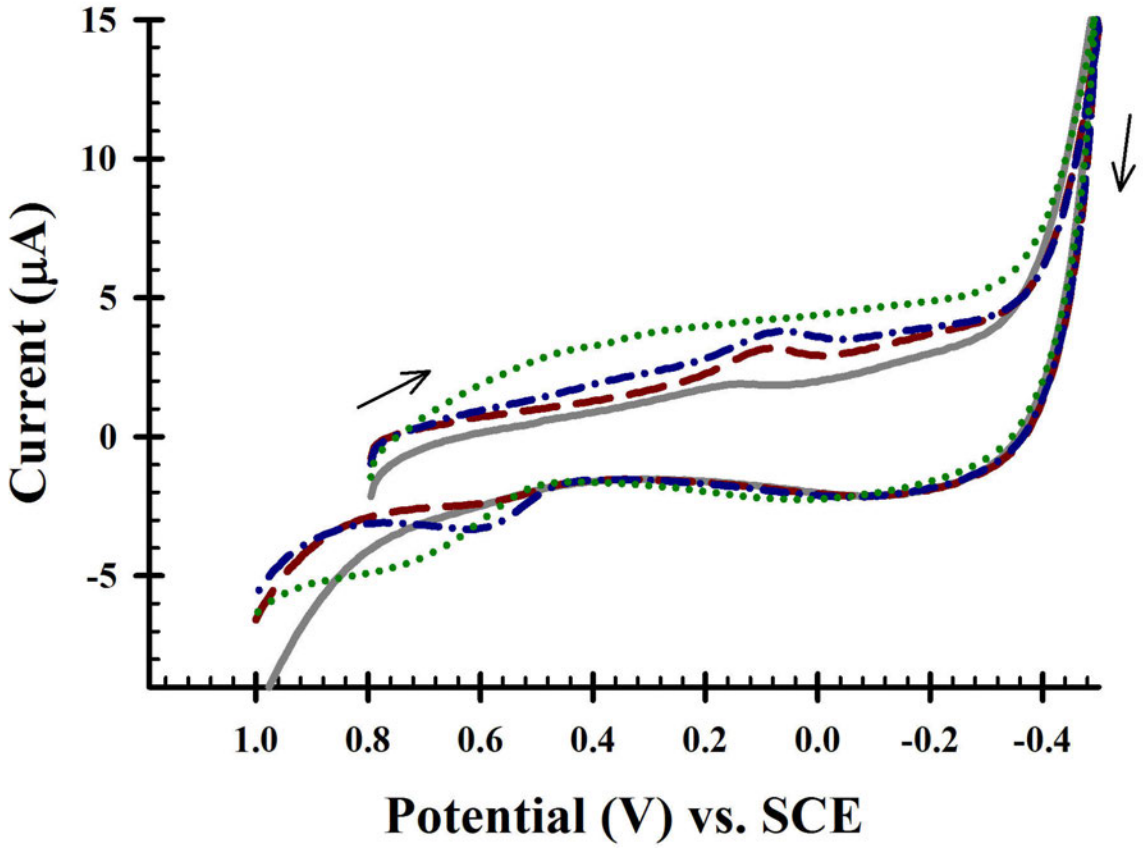

Figure 37. Cyclic voltammogram overlay of a 1:1 (v/v) cells:TMODA-Nafion glassy carbon working electrode with successive additions of known mediating and cofactor species. Initial CV in 0.1 M Na_2SO_4 (——). Overlayed with CV of same solution and electrode with additions of 1 mM NADPH (— —), followed by 1 mg/mL ferredoxin (— ·), and finally 0.1 mM ATP (· · ·). Pt mesh counter electrode, SCE reference electrode, 100 mV/s.

Table 7. Faradaic peak current measurements from 1:1 (v/v) cell:TMODA Nafion modified electrodes after successive additions of chemical cofactors to 0.1 M Na_2SO_4.

Solution	**Peak Current** (μA)	**Current Density** (μA/μg Chl a)
0.1 M Na_2SO_4	0.4 ± 0.1	11.7
1 mM NADPH	0.7 ± 0.1	19.4
0.01 mg/mL Fd	0.9 ± 0.1	34.3
1 mM ATP	0	0

Note: Peak current is for the forward (reductive) peak (Figure 37), as measured from the leading baseline. These currents were measured at 100 mV/s. The peak current is reported as $\overline{x} \pm 1\sigma$ for $n = 4$ electrodes in one experiment. Chlorophyll a absorbance determined spectrophotometrically after extraction from cell suspension in methanol [80].

For the regression of data in Figure 34, a peak current of 0.8 μA is predicted as compared to the 0.9 ± 0.1 μA shown in Table 7. These experiments suggest that mediating and cofactor species NADPH and ferredoxins are important to produce ammonia at polymer modified cell immobilized electrodes. Biochemically, the relationship between NADPH and ferredoxins is known (Figure 1). Further, baseline NH_3 production of *A. var.* is less than between 1 - 3 μM when a subsample of parent culture is analyzed; thus, the increased ammonia production measured after cyclic voltammetry depends on the ten minute voltage perturbation applied.

3.3.3 Cell Disruption Experiments

Anabaena variabilis cell membranes are selective. The membrane contains active pumps (often ATP gated) that allow certain species across the membrane against an energetic gradient. There are also many ion channels that can allow passive diffusion

into and out of the cell. On the 100 mV/s time scale used for most CV experiments, it is a question as to whether reduced or oxidized species can cycle between electrode and active enzyme site. From an electrochemical perspective, resistance prohibits electron transfer to the active site of the enzymes unless the chemical species carrying reductive electrons can enter the cell. The electron hopping distance from the electrode is < 2 nm. The enzyme in the cell is at least 1 μm from the electrode because of the cell membrane thickness. Physically and chemically disrupting this cell membrane barrier exposes the reaction centers. Because the reaction centers are located in the cytosol behind the cell membrane (either in the heterocyst or vegetative cells), trials with ruptured cells were studied. For the purpose of specifically targeting individual enzymes or cellular biochemical pathways, many researchers disrupt the cells and isolate components for precise experimentation [76,77,113–117]. These type of extractions and purifications require instrumentation not available for this research. To address whether the cell membrane inhibits electron transfer between electrode and enzyme, the cell membranes were degraded with sonication and enzymatic breakdown using lysozyme. These partially disrupted cell suspensions were used in place of whole cell suspensions. They were immobilized to an electrode in TMODA Nafion and their electrochemical properties studied.

Five different preparations were made of disrupted cells: sonicated and dried, dried, sonicated and co-cast, lysozyme treated and dried, and lysozyme treated and co-cast preparations. For the preparations where lysozyme was employed, 1.5 mL of a high density cell suspension is treated with 5 mg/mL lysozyme. The suspension is thoroughly mixed by vortexing for 5 minutes. The enzyme reacts with the cells

for 30 minutes at which time the cells and debris are centrifuged from the vial. Solution volume is replaced with 0.1 M Na_2SO_4 to resuspend the disrupted cells and debris. This suspension is then introduced to TMODA Nafion for electrode casting. For the sonication preparations, 10 mL of high density cell culture is exposed to 30 s sonication (40 % duty cycle) by a titanium sonication probe (Biologics, Inc.). These sonicated were cells were then used to make casting suspensions as appropriate. The sonication procedure ruptures most of the vegetative cells, however the thickened outer envelope of the heterocysts do not rupture, but are somewhat damaged near the ends that connect to vegetative cells [53, 76, 77, 114–116, 118]. For the dried preparations, the disrupted cell suspension was pipetted directly onto the electrode surface and allowed to air dry before 10 μL of TMODA Nafion was placed on top to secure the cells to the electrode. For the co-cast suspensions, the disrupted cell suspensions were mixed with TMODA Nafion in a 1:1 (v/v) ratio and cast as a single suspension onto the electrode surface. After the solvents from the films dried, the electrodes were placed into 15 mL of 0.1 M Na_2SO_4.

Data suggest electron flux is higher in the case of disrupted cells (Figure 38). Films are evaluated in 0.1 M Na_2SO_4. As previously, neither bare nor TMODA Nafion electrodes showed any faradaic responses, thus they are not presented here. For both the reductive and oxidative peak currents, disrupting the cells prior to immobilizing to an electrode surface significantly enhanced the current responses. As shown, the peak currents that arise from immobilized whole cells small as compared to those with disrupted cell membranes. The reductive peak current from the disrupted cells, however, is shifted to approximately 0.45 V compared to the

cells that were not disrupted where peak current appears at about 0.1 V. Cells that were sonicated and dried to the electrode surface gave the highest current peak in the forward direction, but a broad, shallow current wave on the reverse scan.

The reductive peak current from the disrupted cells, however, is shifted to approximately 0.45 V compared to the cells that were not disrupted where peak current appears at about 0.1 V. This observation suggests that upon disruption, the cells and release enzymatic contents, such that electron transfer reactions are less inhibited by the cell membrane; however, the identity of the species or processes undergoing reduction/oxidation are not clear. The potential shift to the positive direction may arise from a lower potential necessary to drive catalytic processes, because the reaction centers are more easily accessed and resistance to transport across the cell membrane is eliminated. While there are many possibilities to consider from these data, it is clear disrupting cells increases the faradaic current response. The peak data are reported in Table 8. For each cell preparation technique, four electrodes were prepared in the same manner, thus, the statistics reflect the standard deviation of the peak current over four electrodes.

After a set of cyclic voltammograms at scan rates = 100, 75, 50, and 25 mV/s, the background electrolyte was collected and the NH_3 measured. The results are also reported in Table 8. Each of these experiments were only conducted once, so statistics for the ammonia concentration are not available. Based on the reductive or oxidative currents, correlations were sought between the ammonia measured and the peak current. In Figure 39, the reductive peak current was compared to the total NH_3 concentration. These data show a linear correlation ($R^2 = 0.98$). Previously

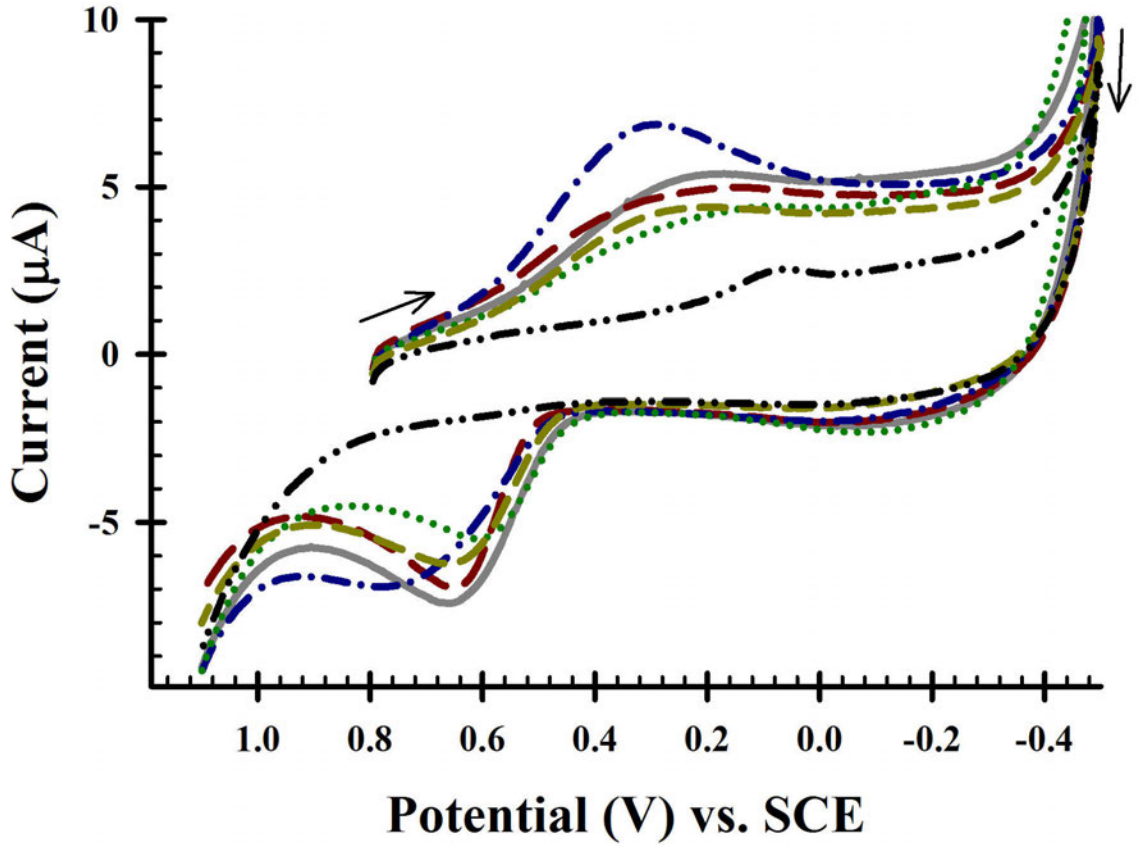

Figure 38. Cyclic voltammogram overlay that shows the effect of different cell preparation techniques. The overlay highlights the differences and similarities in faradaic current responses when cells are present within the immobilization polymer. The data are from whole cells dried to the electrode then covered with TMODA-Nafion (——), sonicated and co-cast with TMODA-Nafion (— —), sonicated and dried to the electrode then covered with TMODA-Nafion (— ·), lysozyme treated and co-cast with TMODA-Nafion (···), and lysozyme treated cells dried to the electrode and covered with TMODA-Nafion (– – –). These cyclic voltammograms are compared to untreated whole cells cast with TMODA-Nafion (— ··). Background electrolyte is 0.1 M Na_2SO_4, Pt mesh counter electrode, SCE reference electrode, 100 mV/s.

Table 8. Faradaic peak current measurements from disrupted cell electrode films.

Technique	**Current**$_{peak,reductive}$ μA	**Current**$_{peak,oxidative}$ μA	[**NH**$_3$] μM
Sonicated & Dried	4.2 ± 1.0	5.1 ± 1.1	11.1
Dried	2.2 ± 0.3	5.5 ± 0.9	6.5
Sonicated & Co cast	1.8 ± 0.2	5.1 ± 1.1	5.9
Lysozyme & Dried	1.8 ± 0.2	4.5 ± 0.8	5.7
Lysozyme & Co cast	1.2 ± 0.2	3.7 ± 0.6	5.3
Untreated	0.7 ± 0.1		3.1

Note: Faradaic wave data measured from cyclic voltammograms with different cell preparation techniques that include sonication for 60 seconds; drying the cell suspension directly to the working electrode surface; and soaking with lysozyme for 30 minutes prior to immobilizing. These data are obtained from the cyclic voltammogram overlay in Figure 38. The reductive and oxidative wave currents are measured as peaks from the leading baseline and reported as $\overline{x} \pm 1\sigma$ for $n = 4$ electrodes. No statistics are available for ammonia production.

correlations between reductive peak current and ammonia output (Figure 34), for different mediating and cofactor chemicals also resulted in a linear agreement. These data further support the existence of a correlated relationship between forward peak current and ammonia production. The significance of the negative intercept is not understood. While peak current can be negative for an oxidative electron transfer reaction, it does not match with observed faradaic repsonses for the reductive (positive) process. The error bars indicate that the faradaic current responses from separate electrodes varied significantly. Because each electrode is cast by hand, there is significant error present in the homogeneity and thickness of the film. These errors result from film casting mixtures that were less dense in both TMODA Nafion and cells than anticipated. The negative intercept is not expected. The slope is also higher than observed previously in studies where the cells were not disrupted. It

is expected that exposing cytosolic components to the electrode surface contributes significantly to electrolysis currents, thus while seeming to be more sensitive, the preparation of cells by disruption allows access to a greater number of electron transfer reactions. We do not report increased sensitivity as the slope may indicate.

Ammonia output is high compared to co-cast whole cell modified electrodes (Table 8). Cyclic voltammetry is sensitive but lacks selectivity. Thus, it is challenging to decouple the increase in peak current and ammonia production to well identified electron transfer reactions. The pathways and reactions shown in Figure 1 represent those targeted in this research, however the diagram is not an exhaustive electrochemical or biochemical model of possible reactions.

3.3.4 Effect of gases and pH

The dissolved gases in the system are important considerations for producing ammonia because the gases may contribute to the reduction sequence or they may displace important reactants, cofactors, and products. These effects can be manifest in voltammetric results and for the electrochemical implications thereof. Both N_2 and Ar are electrochemically inert while O_2, CO_2,and H_2 are electroactive and when in aqueous solution, are often involved in many chemical and electrochemical reactions. For nitrogenase, N_2 is a necessary substrate for the production of NH_3. The nitrogenase enzyme is very susceptible to irreversible deactivation by O_2, because O_2 competitively binds to the same active site as N_2 in nitrogenase. *A. var.* contain hydrogenases that can reduce H_2 when additional H^+ is required by the cells. H_2 is also a byproduct of the nitrogenase reaction, thus, depending on

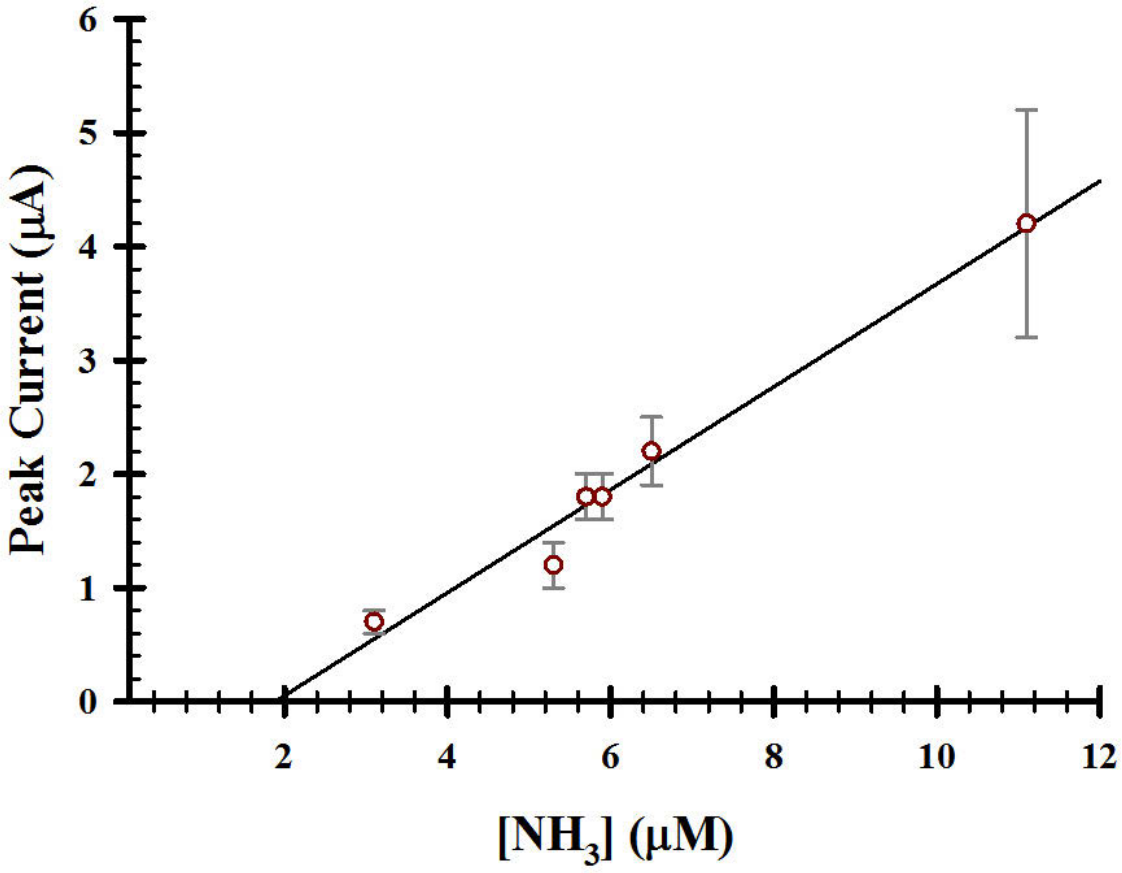

Figure 39. Plot of the relationship between forward (reductive) peak current and the measured concentration of NH_3 following voltammetric pertubation. The data for this plot are from Table 8. The linear equation is $y = 0.45x - 0.85$, $R^2 = 0.98$.

how the cells physiological needs are being met while immobilized on an electrode, it is important to consider the effect of additional H_2 within the system. Absent of complications from hydrogenases, the addition of H_2 as a product of nitrogenase may suppress nitrogen reduction. CO_2 is important for growth of the cells through their photosynthetic respiration route via PSI/II. PSI/II converts CO_2 and H_2O into sugars and protein building blocks with PSII (in vegetative cells only) releasing O_2 as a by product and uses sunlight as an energy source.

The effect of gases on whole cell *A. var.* immobilized to an electrode were studied. Tubing connected to a diffuser is an effective method to sparge solutions. 0.1 M Na_2SO_4 solutions were sparged with the gases listed in Table 9 for 10 minutes at a high pressure. This drives out dissolved gases and concentrates the target gas into solution. After the sparging, prepared electrodes were put into the sparged background electrolyte and the cell covered with ParaFilm to minimize gas dissolution. Cyclic voltammetric analysis of each sparged solution revealed several important observations as summarized in Table 9. The final concentration of NH_3 after the experiments was measured with the ion selective electrode for three replicate electrodes in each gas. Here, we will briefly discuss the most understood results of these experiments.

Increased availability of nitrogenase substrate (N_2) did not increase ammonia production nor did it result in higher currents at the reductive peak. It has been reported that N_2 availability is not the limiting step in nitrogenase action, yet in the system as constructed, finite N_2 is available near the cells and electrode. Increased availability of N_2 would predict increased ammonia production. This suggests that

Table 9. Summary of observations when various gases are introduced to the electrochemical cell.

Species	**Faradaic Wave Effect**	[$\mathbf{NH_3}$] (μM)
Ambient		3.3 ± 0.9
CO_2	Suppressed, no oxidative	3.1 ± 0.7
O_2	Decreased current, no oxidative	2.8 ± 0.5
N_2	Decreased current	2.9 ± 0.8
H_2	Decreased current	3.0 ± 0.4
Ar	Increased current	3.1 ± 0.4

Note: The gases are sparged through solution for 10 minutes. During cyclic voltammetric assessment, the electrochemical cell is covered with parafilm and blanketed with the same analyte gas. Ammonia concentration reported as $\overline{x} \pm 1\sigma$ for $n = 3$ voltammograms at 100 mV/s containing all electrodes in 15 mL 0.1 M Na_2SO_4.

other enzyme pathways capable of producing NH_3 are responsible for increased NH_3 output that has been observed in different experiments.

Both CO_2 and O_2 completely suppressed the oxidative wave. CO_2 suppressed the reductive wave and O_2 decreased the current of the same wave. O_2 is also a substrate for nitrogenase. In whole cells, the heterocyst protects nitrogenase from the undesirable binding of O_2 to the active site. A higher than normal concentration of O_2 would be expected to limit NH_3 output by nitrogenase. We observe that for O_2,the forward peak current and ammonia output are smallest as compared to other gaseous additions.

Ar sparging increased the current for both the reductive and oxidative wave. Presumably, Ar displaced dissolved O_2, leading to higher nitrogenase activity by lowering the competitive binding with N_2 at its active site.

In summary, the experiments with different environmental gases provided some useful insight into the properties of the immobilized cells that contain enzyme.

Overall, the gases had small effects on the faradaic current peak potentials between 0.3 and 0.1 V for the reductive *A. var.* wave and 0.6 to 0.7 V for the oxidative *A. var.* wave. In most cases, the current was decreased. Table 9 reports the significant data and results from different gases introduced into the system.

pH was also considered. *Anabaena variabilis* prefer an environment that is near physiological pH, 7.4. Due to the small density of cells on electrodes (and the relatively small output of measurable chemicals produced therein), global pH changes are not expected as a result of voltammetric analysis. A global pH change may affect certain reaction centers thus, induce changes to the observed voltammetry. The protective microenvironment within TMODA Nafion supports high levels of cellular and enzyme activity [48], but these experiments are not buffered even within this microenvironment. There may be local pH changes.

Because so many pertinent reactions require electrons and H^+ (Figure 1), the concentration of H^+ in the background electrolyte was varied and subsequent CVs were performed to assess the dependencies. Further, CV data collected in previous experiments indicated the presence of a redox reaction at potentials < 0.5 V vs. SCE. Many reactions in the system are thermodynamically accessible at these low potentials (as will be shown in Tables 13, 14, and 15). It is imperative to study the large current at this negative potential to understand its role in the evolving electrochemical model of immobilized *A. var.* Dissolved H_2 or O_2 at sufficient concentrations can give rise to voltammetric peaks at negative potentials.

0.1 M Na_2SO_4 solutions were adjusted to pH = 5, 7, and 9 with dilute HCl and NaOH. In the control experiment the solutions were not sparged (ambient) and in

another each solution was N_2 sparged for 10 minutes prior to use. The cells were immobilized to the glassy carbon electrode after physical and chemical disruption of the cell wall membranes by sonication and lysozyme treatment of cell suspensions. This treated suspension was cast onto the electrode surface and allowed to dry in ambient conditions for 10 minutes. To secure the disrupted cells to the electrode, TMODA Nafion was applied and dried on top of the cell layer.

Figure 40 shows the CVs obtained at various pH and gaseous conditions. Due to O_2 reduction, the forward potential is usually limited to 0.55 V. In the cyclic voltammograms in Figure 40, the potential was swept to 1.1 V. At potentials more negative than 0.5 V, the reduction of oxygen is apparent (Reaction 24).

After sparging with N_2, reduction of O_2 decreases significantly. Further evidence is the peak current for the reduction of O_2 based on the pH. In ambient solutions, the pH sensitivity of Reaction 24 is shown clearly in Figure 40. These observations from the CV overlay in Figure 40 suggest the prominent wave arises due to dissolved O_2

$$O_2 + 4H^+ + 4e \rightleftharpoons 2H_2O \qquad E^{\circ'}_{pH=7} = -1.1 \text{ V vs. SCE} \tag{24}$$

O_2 is well known to have poor electron transfer kinetics. Thus, the significant potential shift for the reduction of O_2 is expected. The reduction of O_2 is an H^+ dependent reaction as well. Thus, changes in measured current can be related to the change in H^+ concentration. Figure 40 shows that as pH increases, the O_2 peak current increases. Kinetics for O_2 reactions are generally faster in base. This same relationship is not observed when the solutions have been purged of most dissolved O_2. These data provide information about the faradaic currents that arise from

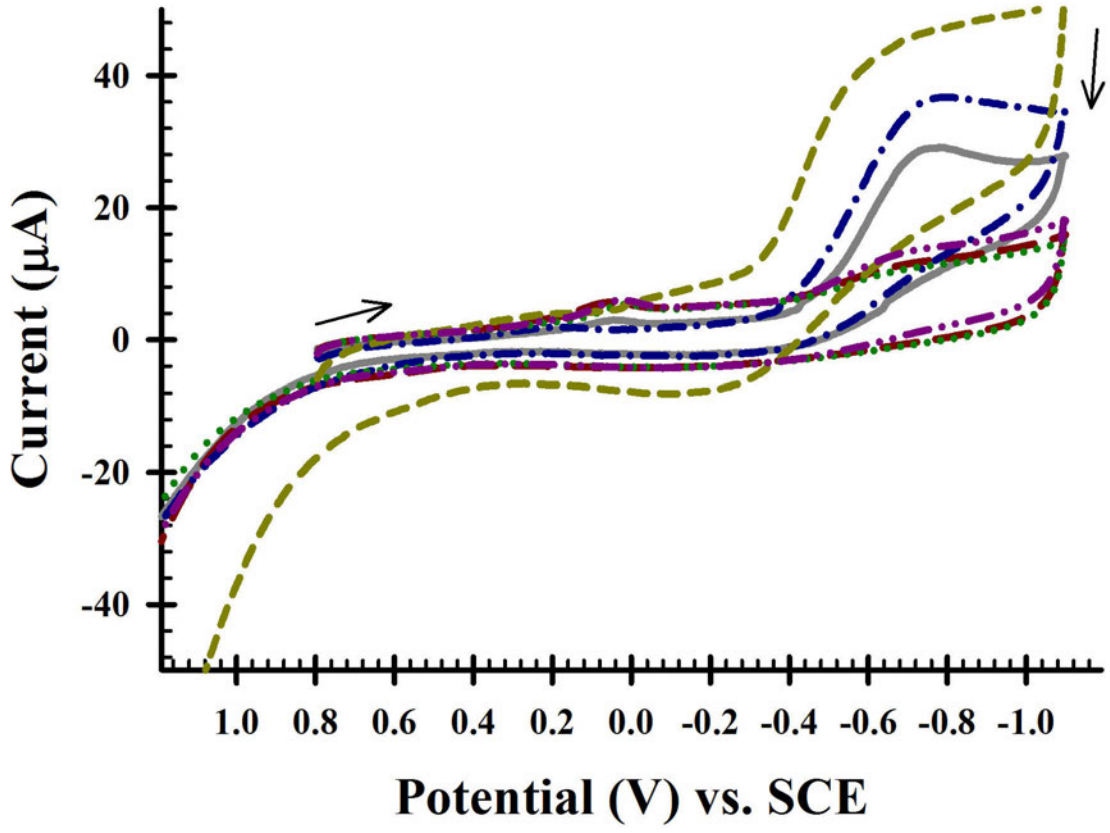

Figure 40. Effect of elevated pH in 0.1 M Na_2SO_4 on sonicated and lysozyme treated cells. Cyclic voltammogram overlay of Sonicated/Lysozyme treated cells dried to an electrode and secured with a layer of TMODA Nafion. The system was either ambient or sparged with N_2 at pH = 5, 7, and 9. Ambient at pH = 5 (——), sparged with N_2 at pH = 5 (— —), Ambient at pH = 7 (— ·), sparged with N_2 at pH = 7 (· · ·), Ambient at pH = 9 (– – –), sparged with N_2 at pH = 9 (—··). Pt mesh counter electrode, SCE reference electrode, 100 mV/s

cells, but the data scale must be adjusted accordingly, as shown in Figure 41

Figure 41 overlays the voltammograms in pH = 5 for the ambient and N_2 sparged cases as in Figure 40, but with current and potential axes expanded to show the affects on the waves at 0.1 and 0.6 V. When solutions are sparged with N_2, the current peak at 0.1 V is prominent at all pH studied. The magnitude of the peak current is not statistically different at pH = 5, 7, or 9. These data show that O_2 can affect the faradaic *A. var.* reductive current. In ambient solutions, pH has a much greater effect, shifting the potential of the reductive wave from 0.1 V at pH = 5 to 0.3 V at pH = 7 and 9 as observed in Figure 41. Further, as pH increases, the current decreases for ambient solutions. The oxidative current is small in this experiment and challenging to quantify, but is present for all N_2 sparged solutions at the same potential, 0.6 V. These data are also consistent with the minimal effect of pH on current as measured at electrode|cell|solution interface. Because the pK_a for NH_3 is 9.3, the higher pH solution affected the NH_3 measurement. Quantification of NH_3 at pH = 5 and pH = 7 then, were not obtained. These experiments conclude that O_2 strongly impacts faradaic current responses and bulk pH does not.

3.3.5 Suppression of Nitrogenase and Nitrate/Nitrite Reductase Specific Analyses

Cells cultured on BG-11_0 medium lacking any source of fixed (reduced) nitrogen results in nitrogen starvation. Nitrogen starvation in *Anabaena variabilis* elicits a genetic response to develop heterocysts and produce ammonia by nitrogenase contained within the heterocysts. Thus, under starvation conditions, nitrogenase

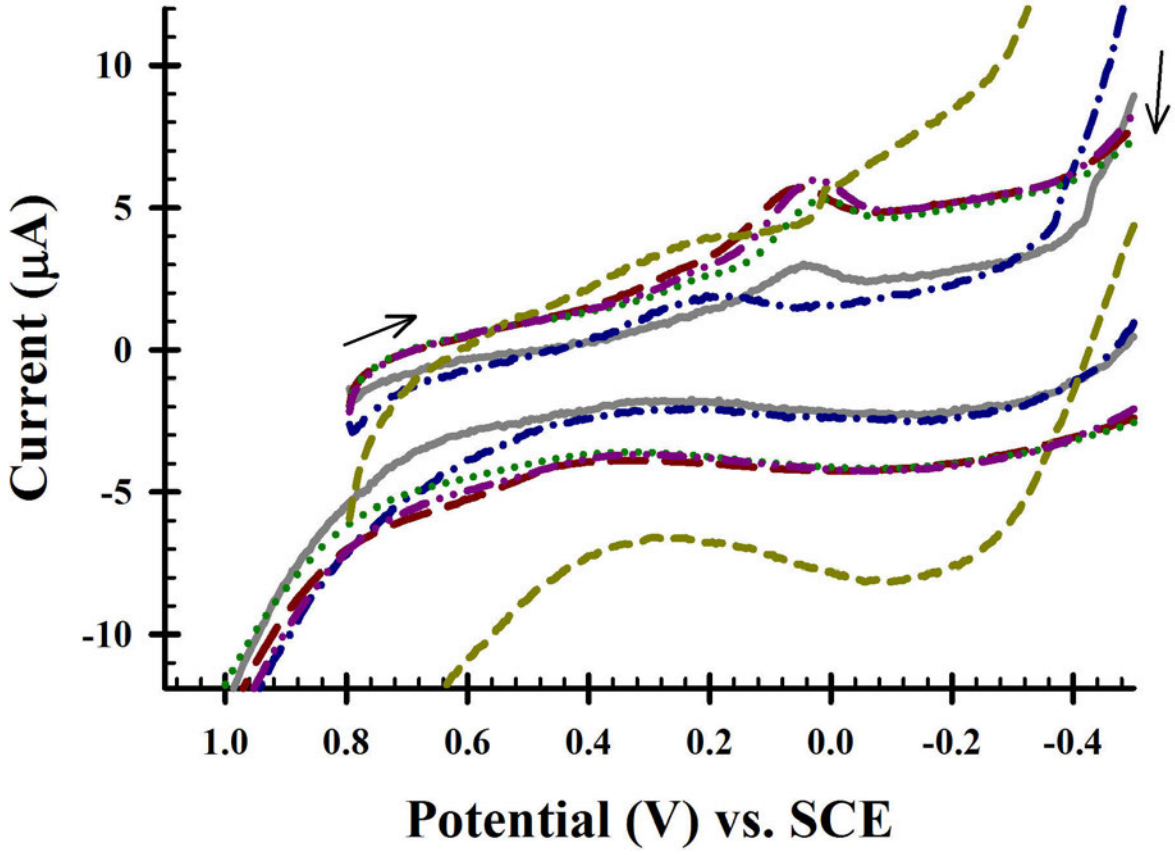

Figure 41. Effect of elevated pH in 0.1 M Na_2SO_4 on sonicated and lysozyme treated cells, with the scale adjusted to highlight the cellular current signals. Cyclic voltammogram overlay of Sonicated/Lysozyme treated cells dried to an electrode and secured with a layer of TMODA Nafion. The system was either ambient or sparged with N_2 at pH = 5, 7, and 9. Ambient at pH = 5 (——), sparged with N_2 at pH = 5 (— —), Ambient at pH = 7 (— ·), sparged with N_2 at pH = 7 (· · ·), Ambient at pH = 9 (– – –), sparged with N_2 at pH = 9 (— ··). Pt mesh counter electrode, SCE reference electrode, 100 mV/s.

nitrogenase becomes extinct and NH_3 is generated by nitrate/nitrite reductase.

To gain correlation between cyclic voltammetric data and nitrogenase processes and related chemical species, cultures of *A. var.* were supplemented with 17 mM $NaNO_3$ and subcultured. With a supply of fixed nitrogen from the nitrate, nitrogenase synthesis and heterocyst formation ceased and the primary route for ammonia synthesis was then nitrate/nitrite reductase enzyme. This was verified with microscopic images of cell cultures. After two weeks of incubation, no visible evidence heterocysts were found in 15 subsamples of several batches of $NaNO_3$ supplemented cells (image *A* in Figure 42). In image *A* of Figure 42 shows a typical filament of *Anabaena variabilis*, however, there are no heterocysts. Image *B* in Figure 42 also shows filaments of *A. var.* with heterocysts marked with an arrow. Thus, fixed nitrogen supplementation in the form of NO_3^- suppresses nitrogenase synthesis and thus heterocyst formation.

Despite the lack of heterocysts and thus, no nitrogenase enzyme, voltammetrically perturbed and electrode immobilized *A. var* continued to produce NH_3. The enzyme responsible for the conversion of nitrate to ammonia is the nitrate/nitrite reductase enzyme. Figure 43 is a drawing of the proposed cell|electrode interface with nitrate supplemented *Anabaena variabilis*. As compared to the drawing in Figure 21, the nitrate/nitrite reductase production of ammonia is less complicated. There are still many levels of biochemical feedback. The drawing in Figure 43 is a schematic to describe the nitrate/nitrite reductase reaction shown previously (Figure 6). Upon cyclic voltammetric analysis, cultures grown on NO_3^- exhibited greater faradaic current for the reductive and oxidative process than from cells grown only

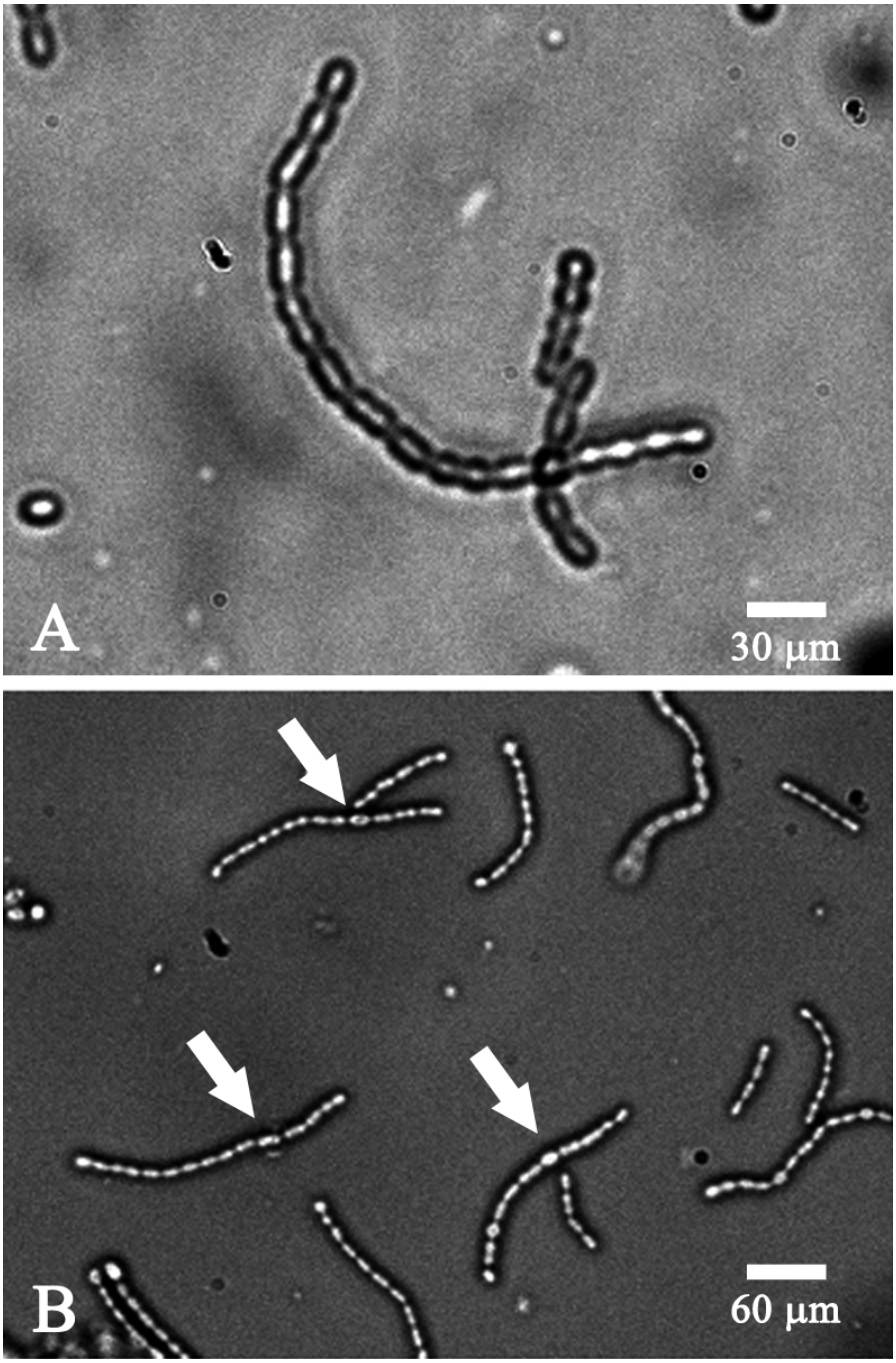

Figure 42. Brightfield microscope images of *Anabaena variabilis* SA-1 that highlight morphological differences dependent upon culture medium at 50× and 100×. *A) A. var.* SA-1 cultured in BG-11_0 with 17 mM $NaNO_3$ added. This image was obtained 3 weeks following initial media change from a nitrogen free BG-11_0. Note the expected filmentous structure but lack of heterocysts. *B)* Image of *A. var.* SA-1 on the same day as in A, but cultured in nitrogen-free BG-11_0. The arrows highlight heterocysts that indicate the presence and continued synthesis of nitrogenase.

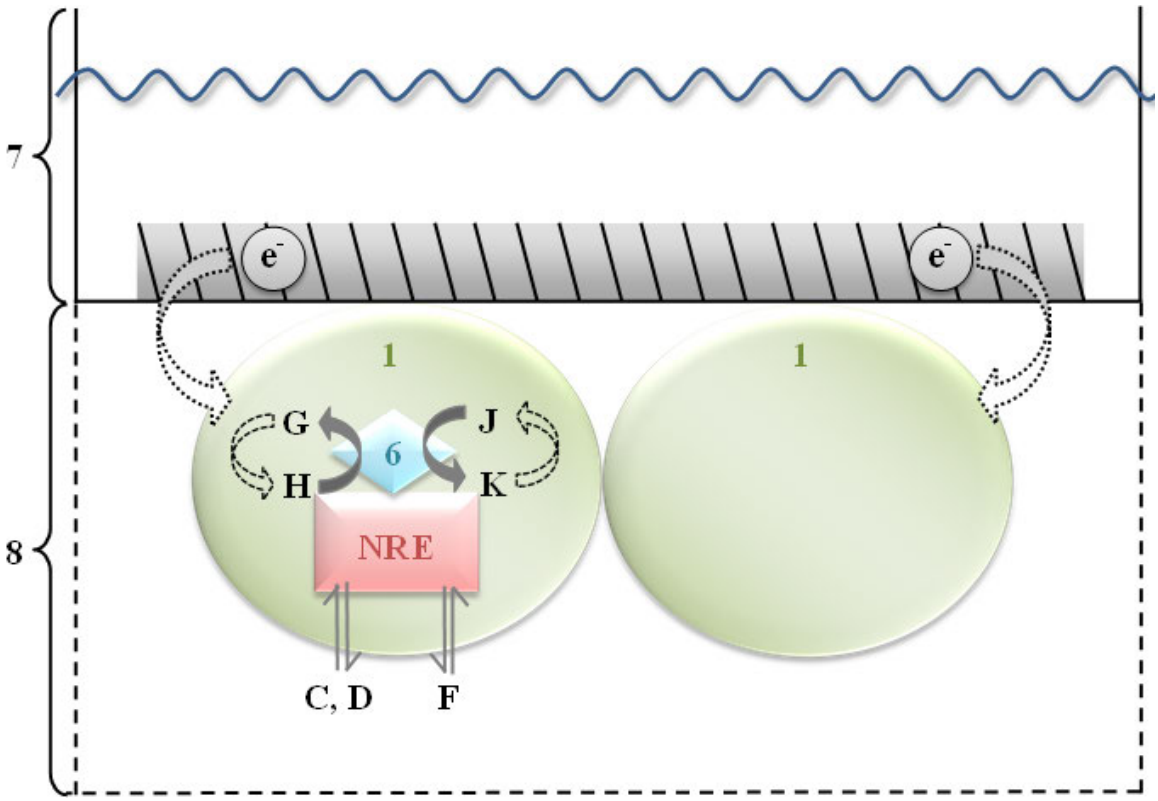

Figure 43. Drawn representation of the species and reaction centers involved in NH_4^+ production by nitrate/nitrite reductase at an electrode. Similar to Figure 21 with the heterocysts and nitrogenase dependent reactions removed. NRE = nitrate/nitrite reductase enzyme. 1) Vegetative cell of *Anabaena variabilis*; 6) NADP–Ferredoxin oxioreductase enzyme catalyzes the redox state of $NADPH/NADP^+$ and $Fe_{reduced}/Fd_{oxidized}$; 7) Glassy carbon working electrode submerged in electrolyte; and 8) 10 μm thick TMODA-Nafion immobilization polymer. Chemicals represented are *C*) NO_3^-; *D*) NO_2^-; *F*) NH_4^+; *G*) reduced Nicotinamide adenine phosphate (NADPH); *H*) Oxidized nicotinamide adenine phosphate ($NADP^+$); *K*) Reduced ferredoxin, Fe(*II*) complex; and *J*) Oxidized ferredoxin, Fe(*III*) complex.

on N_2 and dependent upon nitrogenase produced NH_3 (Figure 44). As compared to bare and TMODA Nafion electrodes where no significant faradaic currents are measured, the cell modified electrodes show faradaic current responses in 0.1 M Na_2SO_4. The current responses for the reductive and oxidative peaks arise at more positive potentials than previously observed, 0.3 V and 0.7 V, respectively. The cell modified electrodes used in Figure 43 contain wild type *Anabaena variabilis*, purchased from ATCC. Recall that most NH_4^+ produced by cyanobacteria never leave the cell and feed into glutamine synthetase; thus, this research employed the SA-1 genetic mutant cell line. *Anabaena variabilis* SA-1 are nitrogenase derepressed and thus release NH_4^+ produced enzymatically within the cell into the external media. From an electrochemical perspective, the SA-1 cells release of NH_4^+ near an electrode surface that can change the ionic strength, pH, and potential gradient at the electrode|solution interface. The potentiostat used in this research does not have iR compensation, thus changes to the resistive environment at the cell surface|solution|electrode interfaces can manifest through cyclic voltammetry as a shift in potential of faradaic current peaks. The pH dependence of redox reactions involved in the nitrate/nitrite reductase enzyme contributes significantly to departure from standard potentials.

If previous correlations between peak current and ammonia production were manifestations of nitrogenase action, then eliminating nitrogenase (by culturing *A. var.* on $NaNO_3$) should eliminate the faradaic currents. This is not observed. As shown in Figure 44, the absence of nitrogenase does not eliminate the faradaic waves near 0.1-0.3 V and 0.6-0.7 V. In fact, NO_2^- supplemented cells exhibit

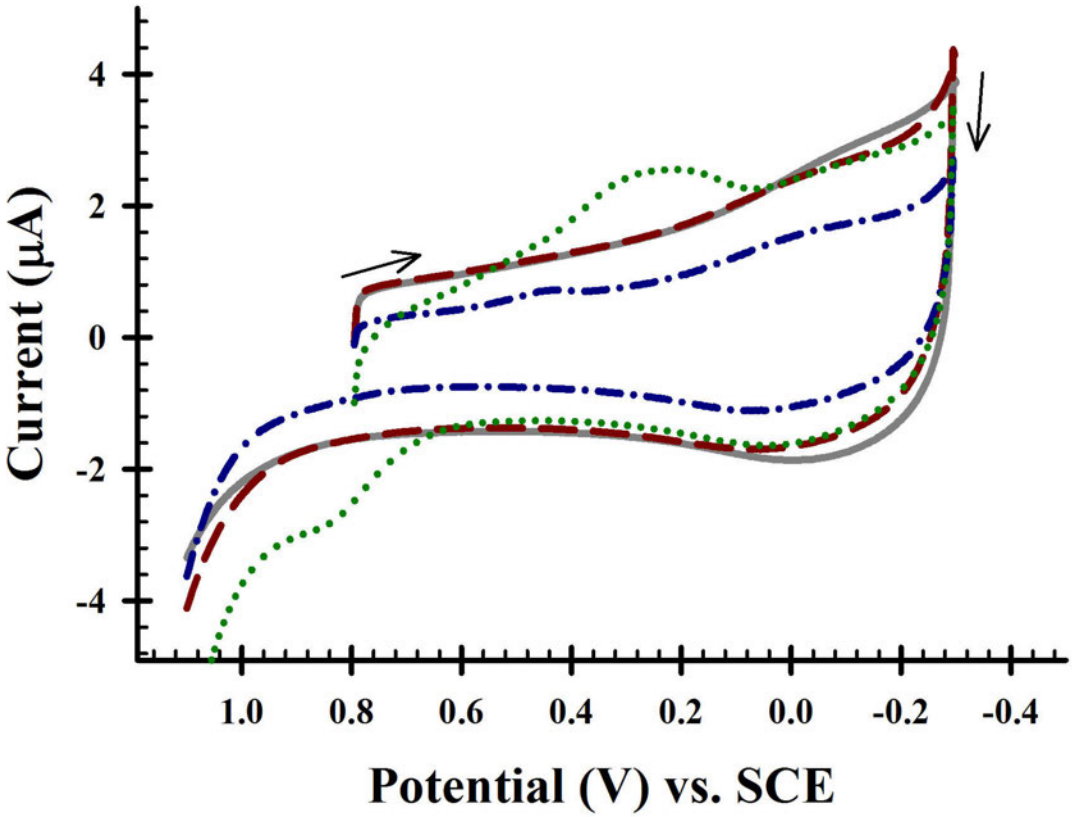

Figure 44. Cyclic voltammetric overlay to compare current responses from 1:1 (v/v) cells:TMODA Nafion films loaded with whole *Anabaena variabilis* filaments, cultured on BG-11_0 and on BG-11 that contains 17 mM $NaNO_2$. Initial CV in 0.1 M Na_2SO_4 of bare (——), 10 μm TMODA Nafion (— —), 1:1 (v/v) cells:TMODA Nafion where cells were grown on BG-11_0 (— ·), and 1:1 cells:TMODA Nafion where cells were grown on BG-11_0 that contained 17 mM $NaNO_2$ (· · ·). Pt mesh counter electrode, SCE reference electrode, 75 mV/s.

higher current and more characteristic voltammetric responses than cells cultured without a fixed source of nitrogen, BG-11_0 media. These data are consistent with voltammetric interaction with enzymes other than nitrogenase. In all cases studied, supplementation of $NaNO_3$ enriched *Anabaena variabilis* with NO_2^- or NO_3^- in the external media resulted in ammonia output concentrations above the basal level of ammonia production (Table 11).

As mentioned, the SA-1 mutant of *A. var.* are nitrogenase derepressed. Nitrogenase derepression means that external concentrations of NH_4^+ do not inhibit nitrogenase synthesis or fixation of N_2 to NH_4^+. Sufficient external NH_4^+ represses nitrogenase synthesis in wild type *A. var.* Thus, *A. var.* SA-1 were selected for use in all experiments described in this research. The cyclic voltammograms in Figure 45 compare the voltammetric current response of both wild type and SA-1 cells. Both the wild type and SA-1 cells have been grown on either BG-11_0 or BG-11 with $NaNO_2$ added to 17 mM. As shown, at cell modified electrodes, both the wild type and SA-1 mutant show a faradaic current response . The reductive peak is significantly higher than background and bare and TMODA Nafion electrodes (not shown for clarity). The oxidative waves have higher current for both cell types, and significant above bare and TMODA Nafion electrode responses.

These observations support electrochemical interactions with the nitrate/nitrite reductase enzyme. In table 10 ammonia output after CV perturbation, reductive peak currents, and a calculated NH_3 density normalized by Chlorophyll a concentration are reported. The voltammetric data coincide with what is expected biochemically.

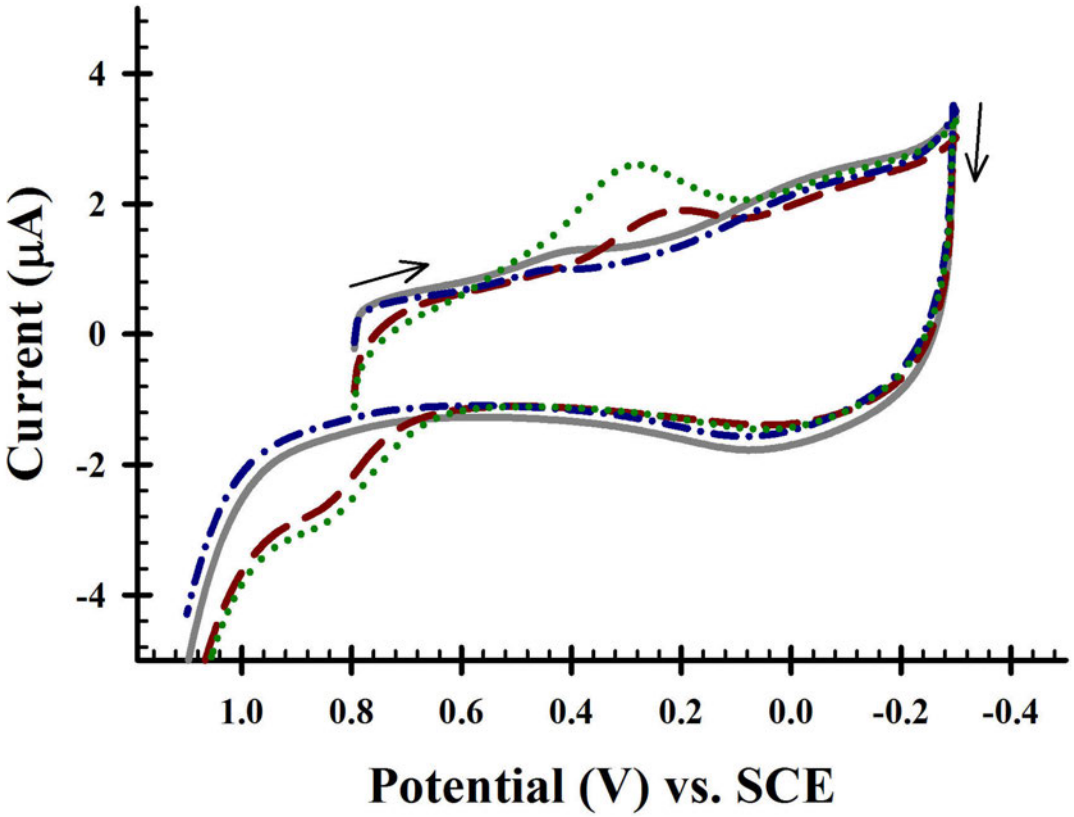

Figure 45. Cyclic voltammetric overlay to compare current responses from wild type *A. var.* and *A. var.* SA-1 cells cultured on BG-11_0 and on BG-11 that contains 17 mM $NaNO_2$. All electrode were 1:1 (v/v) cells:TMODA Nafion modified and analyzed in 0.1 M Na_2SO_4. Wild type cells cultured in BG-11_0 (——), wild type cells cultured in BG-11 and 17 mM $NaNO_2$ (— —), SA-1 type cells cultured in BG-11_0 (— ·), SA-1 type cells cultured in BG-11 and 17 mM $NaNO_2$ (· · ·). Pt mesh counter electrode, SCE reference electrode, 75 mV/s.

Cells grown on BG-11_0 have both nitrogenase and nitrate/nitrite reductase enzymes that produce NH_3 while those grown on BG-11_0 + 17 mM $NaNO_3$ contain only nitrate/nitrite reductase. A plot of reductive peak current versus NH_3 production density shows a linear agreement (Figure 46). Thus, wild type *A. var* cultured on BG-11_0 immobilized to an electrode have the smallest peak current and lowest level of NH_3 production. This strain is limited in its NH_4^+ production because nitrogenase produced NH_4^+ is destined for glutamine synthesis while any NH_4^+ produced by the nitrate/nitrite reductase enzyme feeds back to the cell to limit the synthesis of both nitrogenase and nitrate/nitrite reductase. Addition of NO_3^- to the culture medium results in more than twice the current for the reductive wave and nearly twice the amount of ammonia produced. The *A. var.* SA-1 cells elicit significantly higher reductive peak current and ammonia production. As expected, NH_4^+ is produced in higher densities because enzymatic reduction of N_2 (for nitrogenase, cells cultured on BG-11_0) is genetically altered to not be affected by high levels of NH_4^+. It also follows that the measured peak current for the forward reaction scales linearly with ammonia output Table 10 and Figure 46 ($R^2 = 0.98$). The linear correlation in Figure 46 complements linear correlations observed in previous studies (Figures 24, 25, 34, and 39). While negative current is physically possible, zero current is expected for no ammonia produced. The errors in current measurement result from inherent reproducibility in casting cell:TMODA Nafion films on electrodes.

For the experiments shown in Tables 11 and 12, *A. var.* SA-1 cells, grown on NO_3^- supplemented BG-11_0, were co-cast with TMODA Nafion 1:1 (v/v) onto

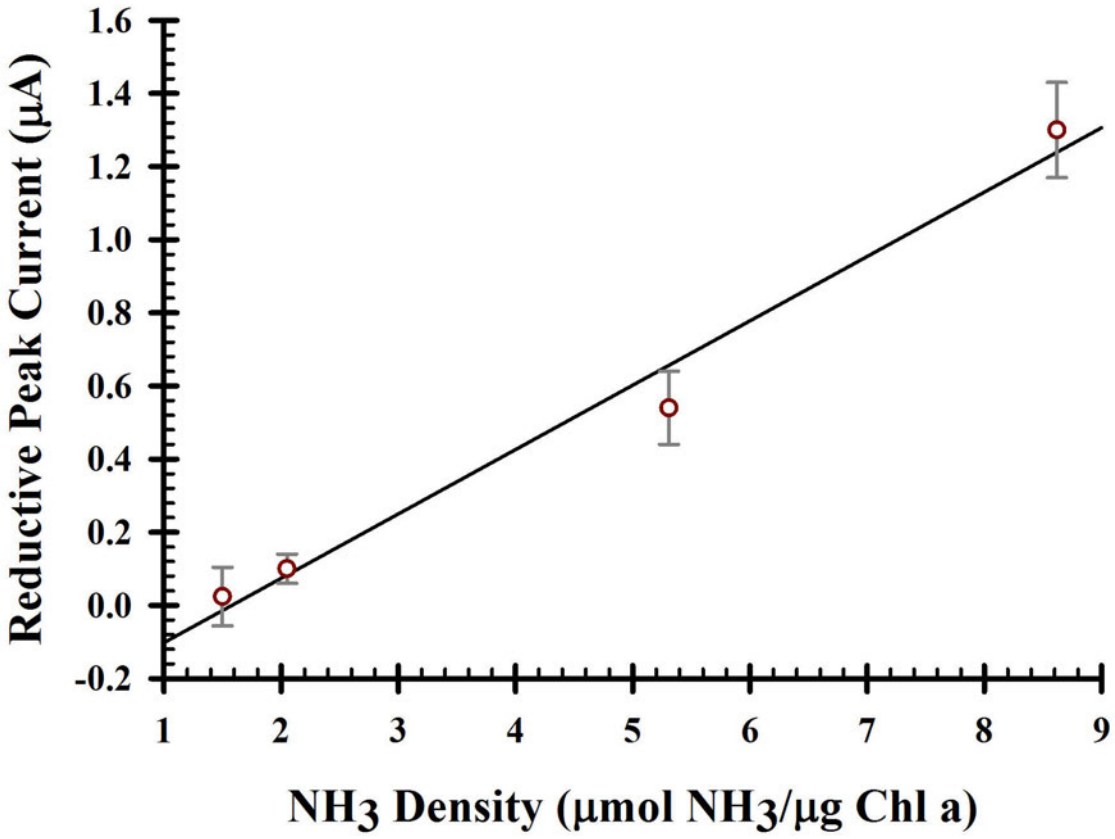

Figure 46. The relationship between forward (oxidative) peak current and NH_3 density following voltammetric pertubation of immobilized *A. var.* (wild type or SA-1 mutant) cultured in either BG-11_0 or BG-11_0 + 17 mM $NaNO_3$. The data for this plot are from Table 10. NH_3 concentration is normalized to chlorophyll a density, by methanolic extraction and subsequent absorbance measurement [80]. Error bars represent the error in peak current measurement for $n = 4$ electrodes. The regression equation is $y = 0.18x - 0.28,\ R^2 = 0.98$.

Table 10. Quantitative values of NH_3 concentration, Chl a density, and reductive peak current with wild type or SA-1 mutant *A. var.* strains used in the preparation of 1:1 (v/v) cells:TMODA Nafion modified electrodes after voltammetric perturbation of the system.

Electrode and Media	**[NH_3]** (μM)	**[Chl a]** ($\mu g/mL$)	**NH_3 Density** (μmol NH_3/μg Chl a)	**Peak Current** (μA)
Wild BG-11_0	2.1	2.1 ± 0.5	1.5	0.02 ± 0.01
Wild BG-11_0 + NO_3^-	5.2	3.8 ± 0.3	2.1	0.1 ± 0.04
SA-1 BG-11_0	8.5	2.4 ± 0.2	5.3	0.5 ± 0.1
SA-1 BG-11_0 + NO_3^-	22.4	3.9 ± 0.2	8.6	1.3 ± 0.1

Note: For each cell type, data are calculated for their culture in BG-11_0 with or without addition of 17 mM $NaNO_3$. Ammonia concentration, measured by ISE, is normalized to chlorophyll a concentration. Total cell volume is 15 mL. Total film casting volume is 10 μL. Chlorophyll a absorbance determined spectrophotometrically after extraction from cell suspension in methanol [80] and reported as $\overline{x} \pm 1\sigma$ for $n = 3$ extraction assays. Peak current is for the forward (reductive) peak (Figure 45) as measured from the leading baseline and is reported as $\overline{x} \pm 1\sigma$ for $n = 4$ electrodes in a single CV experiment.

electrodes. The concentrations of $NaNO_2$, $NaNO_3$, NADPH, and ferredoxins added to the 0.1 M Na_2SO_4 background electrolyte were systematically varied to probe the interaction between nitrate/nitrite reductase and increased availability of substrates and cofactor chemicals. For each experiment (Code in Tables 11 and 12) electrodes were analyzed with cyclic voltammetry at scan rates = 100, 75, 50, 25, 50, and 75 mV/s. Thus total time a potential was dropped across the electrode was ten minutes. After the electrochemical analysis, the total concentration of NH_3 in 15 mL of solution was tested with the NH_3 ion selective electrode. The resultant reductive peak current was measured and current density calculated by normalizing peak current to the chlorophyll a content used in the film casting suspension (Tables 11 and 12). Preparation of spent electrolyte for ammonia quantification is destructive, thus, the ammonia measurements are not reported with error.

In lieu of presenting cyclic voltammograms, the raw data are sufficient to see that ammonia production and current densities are high compared to experiments where *A. var.* SA-1 were starved of nitrogen and dependent primarily upon nitrogenase for ammonia synthesis. In all experiments, the ammonia production density was higher than for the control (Code N in Tables 11 and 12). Further, all experiments in which NADPH was supplemented to the electrolyte, ammonia production was significantly higher than control.

The NH_3 production data from NO_2^- and NO_3^- additions alone, while higher in ammonia production and reductive peak current than control, do not follow a systematic pattern. It is reasonable to assume that increasing substrate concentration and availability to the enzyme would increase its activity, however it must be more complex than that. Possibilities and a kinetic model framework are presented in Chapter 4.

Data from Table 12 were used to estimate the correlation between the forward reduction wave and the ammonia density measured after voltammetric perturbation. In a plot of peak current versus ammonia density, a linear relationship with a near zero intercept resulted (Figure 47). The resultant linear regression is $y = 0.06x + 0.07,\ R^2 = 0.91$. These data continue to support other observations that peak current varies linearly with ammonia production by *A. var.*

Early in this research, flasks of cells were subjected to two chemicals, methionine D,L sulfoximine (MSX), which blocks the reuptake of NH_4^+ and $NaNO_2$. Many researchers measure increased and sustained production of ammonia and hydrogen by cyanobacteria through the use of these chemicals [11, 64, 79, 92, 93, 121]. MSX

Table 11. List of experimental conditions tested to explore ammonia production by nitrate/nitrite reductase after cyclic voltammetric perturbation at 1:1 (v/v) *Anabena variabilis* SA-1:TMODA Nafion electrodes.

Code	**[NO_2^-]** (mM)	**[NO_3^-]** (mM)	**[NADPH]** (mM)	**[ferredoxin]** (mg/mL)	**[NH_3]** (μM)	**NH_3 Density** (μmol NH_3/μg Chl a)
A1	0.1	0	0	0	7.3	3.4
A2	0.3	0	0	0	4.7	2.6
A3	0.5	0	0	0	5.6	3.2
B1	0	0.1	0	0	5.2	2.3
B2	0	0.3	0	0	5.9	3.5
B3	0	0.5	0	0	15.7	6.7
C	0.5	0.5	0	0	13.8	6.3
D	0.5	0.1	0	0	9.3	4.5
E	0.1	0.5	0	0	6.1	2.4
F	0	0	0.01	0	37.8	20.3
G	0	0	0	0.01	3.6	1.7
H	0	0	0.01	0.01	21.5	11.5
I	0.5	0	0.01	0.01	21.6	10.1
J	0	0.5	0.01	0.01	19.1	9.9
K	0.5	0.5	0.01	0.01	13.7	6.4
L	0.5	0	0.01	0	26.3	12.7
M	0	0.5	0	0.01	29.9	12.5
N	0	0	0	0	2.9	1.6

Note: Concentrations of specieis involved with the nitrate/nitrite reductase enzyme include NO_2^-, NO_3^-, NADPH, and ferredoxin added to 0.1 M Na_2SO_4 for final concentrations as listed. A code was assigned to each set of experimental conditions. For each experiment, the conecntrations of NO_2^-, NO_3^-, NADPH, and ferredoxin used appear in the table. Duplicate CVs were obtained at 100, 75, 50, and 25 mV/s. Electrodes were then removed and NH_3 and was measured. NH_3 measurements are vs. a stadard calibration of NH_4Cl. These data are for multiple electrodes in a single solution, thus only one ammonia concentration measurement was made following cyclic voltammetry. TheNH_3 density is normalized to the concentration of chlorophyll a. Chlorophyll a absorbance determined spectrophotometrically after extraction from cell suspension in methanol [80].

Table 12. Values of chlorophyll a concentration, reductive peak current, and current density for each experiment designated in Table 11.

Code	**[Chl a]** (μg/mL)	**Current**$_{\text{peak,reduction}}$ (μM)	**Current Density** (μA/μg Chl a)
A1	3.2 ± 0.1	0.29 ± 0.11	9.1 ± 0.03
A2	2.7 ± 0.2	0.12 ± 0.10	4.4 ± 0.04
A3	2.6 ± 0.2	0.21 ± 0.11	8.1 ± 0.04
B1	3.4 ± 0.2	0.14 ± 0.04	4.1 ± 0.01
B2	2.5 ± 0.4	0.25 ± 0.13	10.0 ± 0.05
B3	3.5 ± 0.1	0.57 ± 0.10	16.3 ± 0.03
C	3.3 ± 0.4	0.55 ± 0.11	16.7 ± 0.04
D	3.1 ± 0.4	0.28 ± 0.14	9.0 ± 0.05
E	2.8 ± 0.1	0.16 ± 0.09	4.7 ± 0.03
F	3.1 ± 0.5	1.07 ± 0.33	39.3 ± 0.12
G	3.1 ± 0.2	0.11 ± 0.07	3.5 ± 0.02
H	2.8 ± 0.4	0.77 ± 0.17	28.2 ± 0.07
I	3.1 ± 0.4	0.56 ± 0.14	18.4 ± 0.05
J	2.9 ± 0.3	0.77 ± 0.10	26.6 ± 0.04
K	3.2 ± 0.7	0.59 ± 0.09	18.4 ± 0.05
L	3.1 ± 0.1	0.81 ± 0.16	26.1 ± 0.05
M	3.6 ± 0.1	0.87 ± 0.13	24.2 ± 0.04
N	2.7 ± 0.3	0.08 ± 0.02	3.0 ± 0.01

Note: Values of chlorophyll a concentration, reductive peak current, and current density for each experiment designated in Table 11. The lettered experiment code corresponds to concentrations of specieis involved with the nitrate/nitrite reductase enzyme that include NO_2^-, NO_3^-, $NADP^+$, and ferredoxins that were added to 0.1 M Na_2SO_4. Chlorophyll a absorbance determined spectrophotometrically after extraction from cell suspension in methanol [80] and is reported as $\overline{x} \pm 1\sigma$ for $n = 2$ extraction assays. For a set of experimental conditions, duplicate CVs were obtained at 100, 75, 50, and 25 mV/s. Four cell modified electrodes are present in each solution, thus the reductive peak current is reported as $\overline{x} \pm 1\sigma$ for $n = 4$ electrodes in one solution. The current density is normalized to the chlorophyll a assay.

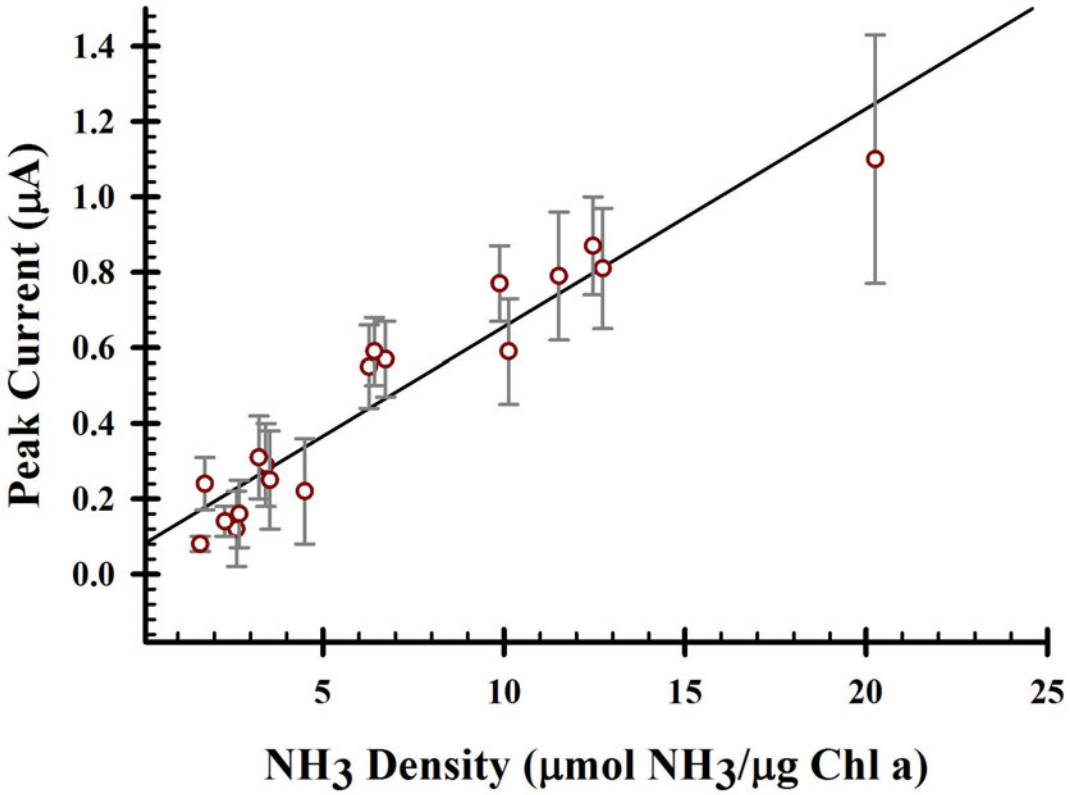

Figure 47. The relationship between forward (oxidative) peak current and NH_3 density following voltammetric pertubation of immobilized *A. var.* SA-1 mutants cultured in BG-11_0 + 17 mM $NaNO_3$ (nitrogenase repressed). The data for this plot are from Table 12. NH_3 concentration is normalized to chlorophyll a density, measured methanolic extract and abosrbance measurement [80]. Error bars represent the standard deviation for current measurements for $n = 4$ electrodes in a single volume and study. The regression equation is $y = 0.06x + 0.07$, $R^2 = 0.91$.

blocks the glutamine synthetase reuptake of NH_4^+ thereby increasing ammonia output. The increased ammonia output can only be sustained for a few days. After sufficient build up of NH_4^+ within the cytosol or external media, nitrogenase will be repressed. Further, MSX causes bleaching of photosynthetic pigments and impacts cell viability after four or more days exposed the chemical. $NaNO_2$ has been used similarly because it supports increased production for extended times. Figure 48 shows the effects of MSX and NO_2^- are as expected for *A. var.* SA-1 . 125 mL of dense cell suspensions were treated with 50 μM MSX, 50 μM MSX and 0.1 mM $NaNO_2$, and 0.1 mM $NaNO_3$ under full illumination and agitation in the incubator. At 24 hour intervals, a 50 mL samples of cell suspension was collected. The cells were centrifuged to a pellet and the spent media decanted. The cell pellet was returned to the parent flask and the void volume replaced with the appropriately modified BG-11_0. The spent media ammonia concentration was quantified with the NH_3 ion selective electrode and plotted versus time. The ammonia concentration was normalized to chlorophyll a content as determined by methanolic extracts [80]. As shown in Figure 48, the combination of an NH_4^+ uptake blocking agent (MSX) and a substrate for the nitrate/nitrite reductase enzyme ($NaNO_2$) resulted in the highest densities of ammonia, followed by $NaNO_2$. MSX alone did not elicit as high a density of ammonia. As compared to untreated basal production of NH_3, the importance of NO_2^- for increased ammonia production by *Anabaena variabilis* is conclusive.

A control system was constructed to evaluate the effect and dependence of voltammetric perturbation on *Anabaena variabilis* produced NH_3. The

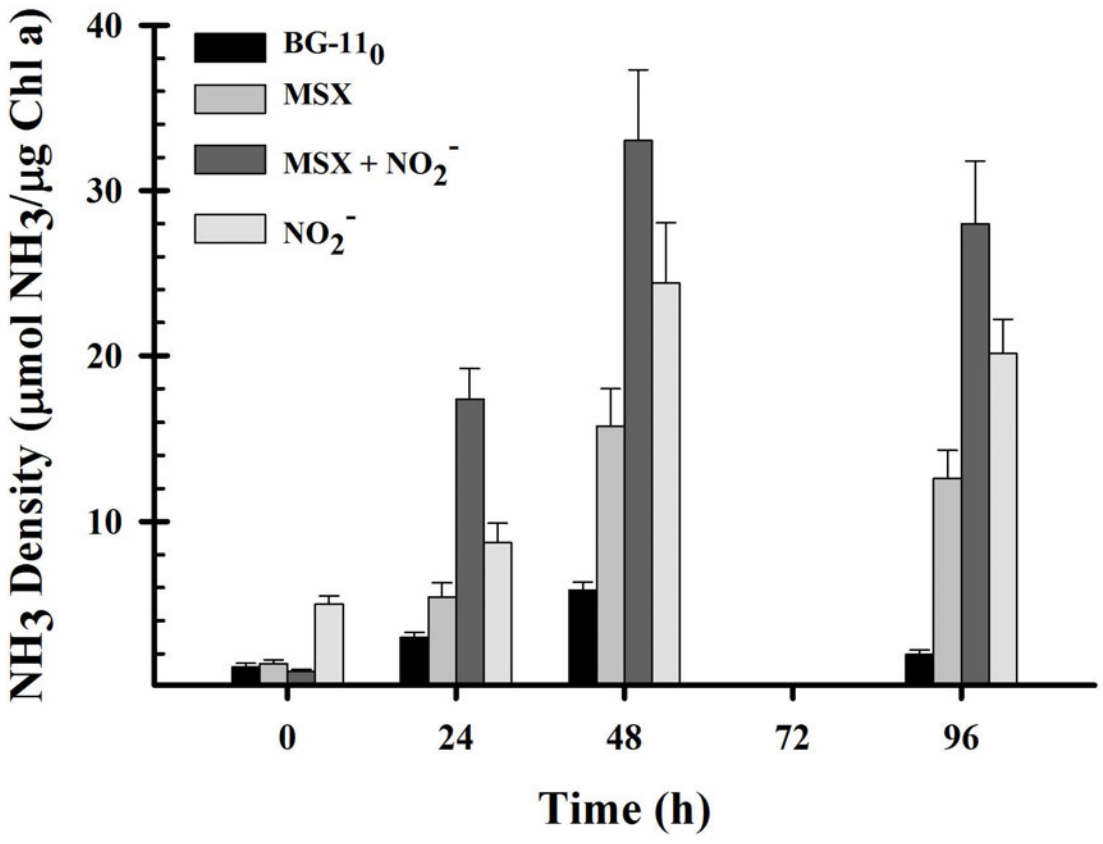

Figure 48. NH_3 output from *A. var.* SA-1 during media supplementation with $NaNO_2$ and methionine D,L-sulfoximine (MSX) over a 4 day period. Ammonia production normalized to chlorophyll a content as determined with a methanolic extraction and absorbance measurement [80]. Control ($BG\text{-}11_0$ media, N-free), methionine D,L-sulfoximine (MSX, inhibits reutpake of NH_4^+), MSX + 1.4 mM $NaNO_2$, 1.4 mM $NaNO_2$ supplemented cultures are compared. Error bars represent the standard error in ammonia measurment vs. the calibration.

electrochemical cell was setup in the same manner described throughout Chapter 3. Eight working electrodes of which two were bare, two were modified with TMODA Nafion, and four were modified with 1:1 (v/v) cells:TMODA Nafion were prepared and equilibrated into 15 mL of 0.1 M Na_2SO_4 to which NADPH was added to 1 mM and ferredoxins were added to 1 mM as in Figure 33 and 37. The cells used in the film were grown on BG-11_0 containing 17 mM $NaNO_3$. After 10 minutes without applying a potential gradient, the electrodes were removed and the concentration of NH_3 measured. Note, 10 minutes is the same amount of time used during cyclic voltammetry and corresponds to the time a potential is applied. 2.5 ± 1 μM NH_3 was measured in the solution. When the same system was subject to cyclic voltammetry, 21.5 μM NH_3 was measured as shown in Table 11. This observation suggests that applied potential is required to produce increased NH_3. Cells that were subjected to cycled potential produced a ten-fold increase in NH_3, all other parameters and conditions equal. Ammonia production by the bioelectrocatalytic device requires an externally applied driving force. Chapter 4 presents a simplified mechanistic model for ammonia production by the nitrate/nitrite reductase enzyme.

3.4 Summary

Upon consideration of all data collected and analyzed, direct electron transfer between electrode and enzyme is not apparent. This is consistent with the nitrogenase buried within the heterocysts of *Anabaena variabilis* where the enzyme is too remote from the electrode surface to allow direct electron transfer. It is approximated that the distance for electron transfer from the electrode to a species

in solution ≤ 1 nm. The cells are several microns and the enzymes are not bound near the cell wall because the cells are prokaryotic, thus enzyme location within the cell is not constant. This suggests that the conversion of dinitrogen to ammonia or other nitrogen containing species will be achieved through either introduction of an appropriate mediator or by disruption of the cell membranes such that the enzymes are able to contact directly the electrode and direct electron transfer is possible. Species explored include known nitrogenase mediating and cofactor species. The results in Table 9 contributed to the body of data that suggested nitrogenase was not being probed directly. Data with nitrogen species like NO_2^-, NO_3^-, and NH_4^+ had significant effects on the voltammetry and ammonia output.

The overarching electrochemical focus has been to determine what is present at cell modified electrodes that is electroactive. Many chemical and environmental variables such as air gases, possible mediating chemical species, and pH were examined in this research. The electrochemical activity has demonstrated dependence upon chemical constituents and environmental variables including species generated by the partially reduced dinitrogen, nitrogen containing species, and the addition of chemicals normally present *in vivo.* There exists linear correlations between electrochemical peak currents from cell modified electrodes and the density of ammonia produced under voltammetric perturbation.

By subjecting the cell immobilized electrode to voltammetric perturbation, significantly more ammonia is produced then is expected physiologically. Low basal levels of ammonia production by batch (125 mL) cultures of *A. var.* have been measured with an ammonia ion selective electrode. This measurement represents

the *in vivo* output of NH_3. This basal output of ammonia from 15 mL samples of well mixed cultures (where cells and debris are removed) is <4 μM Following voltammetric perturbation of the same density of cells immobilized to the electrodes at various scan rates, average ammonia production for select experimental conditions increases, in some cases to over 30 μM.

Alternative enzyme pathways that produce ammonia are present in *Anabaena variabilis* such as the nitrite/nitrate reductase enzyme. The data presented are more consistent with this nitrate/nitrite reductase than nitrogenase based on the following: 1) Both NADPH and ferredoxins share a critical role in electron transfer to and from nitrate/nitrite reductase; 2) Voltammetric currents appear and are increased when nitrogenase synthesis has been repressed; 3) Nitrogenase substrate N_2 and cofactor ATP do not increase ammonia production or increase the electrochemical signals observed; 4) NH_4^+ can inhibit and suppress both nitrogenase and nitrate/nitrite reductase, yet even the SA-1 strain, which also contains nitrate/nitrite reductase, achieves sustained and increased production of NH_3; and 5) The heterocyst offers great protection of the nitrogenase enzyme from oxygen but also severely limits the ability to induce a reductive environment within the cell due to thick cell walls and lack of ion channels and gated pumps. Nitrogenase are buried and protected behind thick heterocyst cell membranes and likely not accessible by small mediators, on the short analyses times, and there is no known mechanism to transfer electrons directly to the cytosol.

An externally applied driving force appears to be necessary to produce NH_3 from immobilized *A. var.* Without cyclic voltammetric perturbation, electrode

immobilized cells did not produce concentrations of ammonia above the basal level.

Nitrogenase and nitrate/nitrite reductase are very different enzymes. They share one feature of interest in this research, production of ammonia at ambient temperature and pressure. From a biochemical perspective, if the electrode can induce a more reductive environment within the cytosol, nitrogenase and nitrate/nitrite reductase efficiency and activity would certainly increase. The data presented in this section highlight that the *A. var.*, void of nitrogenase, still produce significant levels of ammonia. Additional linear relationships between electrochemical peak current and ammonia production that has been normalized to an indirect measure of enzyme density (chlorophyll a assay) support that nitrate/nitrite reductase is accessible in the electrochemical cell as described.

CHAPTER 4

DEVELOPMENT OF MECHANISTIC MODEL FRAMEWORK FOR AMMONIA PRODUCTION

4.1 Model Considerations

The research discussed here describes a system where whole cells of *Anabaena variabilis* are immobilized to an electrode surface. After voltammetric perturbation, ammonia density in the external media is higher than compared to the basal level for parent cells and from the data, a linear relationship between reductive peak current and this ammonia output is found. In cultures grown on 17 mM $NaNO_3$, nitrogenase is no longer synthesized and the primary route for ammonia production is by nitrate uptake and reduction to NH_3. This nitrate update and reduction is catalyzed by the nitrate/nitrite reductase enzymes. Electrochemical data are useful to explain the thermodynamics and kinetics of electron transfer and chemical reactions involved enzyme based ammonia production at an electrode surface on the cyclic voltammetric time scale. The data discussed in Chapter 3 are consistent with a significant role of nitrate/nitrite reductase in producing ammonia from immobilized *Anabaena variabilis*.

Throughout the 1980's, the structure and function parameters of nitrate and nitrite reductase were an area of research focus. During this time, several conflicting reports were made as to the mechanisms of the nitrate/nitrite reductase enzymes [122–125]. In the mid 1990's, a more definitive model proposed of nitrate uptake

and enzymatic reduction to nitrite and ammonia has advanced [126]. Even so, several reviews on the role of nitrate and nitrite in cyanobacteria are not consistent. Some site evidence that some photosynthetic bacteria may synthesize NADPH [122] dependent nitrate reductase and others report that photosynthetic bacteria synthesize only ferredoxin dependent nitrate reductase [127, 128]

Cyclic voltammetry data provide thermodynamic and kinetic data simultaneously. The kinetic and thermodynamic parameters are embedded within the current versus potential curves. These data are not always readily extracted and often require construction of a model before extraction of the values. The complexity of bioelectrochemical reactions, even when specifically targeting those involved in the production of ammonia, require several types of simultaneous kinetic analyses to map pertinent and accessible reactions. Due to the multiple levels of biochemical feedback present within a whole cell system, the simple model here makes initial assumptions. The basic model framework establishes a foundation to incorporate additional redox considerations such as mediators and additional electron transfer reactions. The model presented here is the framework to describe the basic foundation for the electrochemical contribution to the kinetics of ammonia production by the nitrate/nitrite reductase enzyme. It does not consider all contributing reactions. The model described here complements electrochemical, ammonia output, and cell density data obtained in the types of experiments discussed in Chapter 3. The model reflects the union of reported biochemical pathways and experimental electrochemical data. The framework described here is foundational. Until this work, no electrochemical to biochemical correlational data strictly focused on

Anabaena variabilis ammonia production has been published.

4.1.1 Redox Reactions

Much has been reported about the structure and function of cyanobacterial nitrate/nitrite reductase [122, 123, 126–130]. These reports take advantage of enzyme isolation to study the nitrate/nitrite reductase dynamics. Preparation of cell free extracts is time consuming and can often require strict environmental control. Further, the integrity of long term (greater than 1 day) measurements of isolated systems are often compromised due to insufficient nutrients and biochemical mediators present to drive catalysis that requires external supplementation. Instead, whole cell analysis of enzymatic systems, while extremely complex, is advantageous because it studies a functional system without the complications of providing all necessary biochemicals to observe sustained behavior. The goal in this research is to electrochemically support biochemical production of ammonia at ambient temperature and pressure, not to evaluate and determine enzyme kinetics of whole cells. Thus, a brief discussion of the pertinent redox reactions as they relate to this goal are appropriate.

The redox reactions that involve NO_2^- and NO_3^- are pH dependent reactions. The optimal pH for *Anabaena variabilis* is 7.2, yet changes in pH at the electrode|cell interface have significant effect on the potential required to drive a reduction or oxidation. In some cases, a 12 molar excess of H^+ is chemically required to overcome kinetic limitations of involved electron transfer reactions. Also, pH near the electrode can be altered as H^+ produced from redox reactions alter the pH

microenvironment near the electrode, the site of heterogenous electron transfer. Bulk pH measurements do not describe the pH environment at the electrode interface. Tables 13, 14, and 15 list many of the possible redox reactions that are thermodynamic possibilities. The reactions in Table 13 are the nitrate and nitrite reactions at different values of pH. For each reaction, the electrochemical potential is reported at pH = 0, 6, 7, and 8. These pH adjusted electrochemical potentials are calculated by the Nernst equation (Equation 25).

$$E = E^{\circ} + \frac{RT}{nF} \ln \frac{\alpha_O}{\alpha_R} \tag{25}$$

In the Nernst equation, E, the measured electrode potential, can be calculated from a the standard thermodynamic potential of a redox reaction, E° for the general electrochemical reduction, $O + ne \rightleftharpoons R$. Equation 25 is shown for the case where there is one reactant and one product species. When there are multiple chemical species, the expressions under the logarithm are changed. The product of the activities of the oxidized species raised to their stoichiometric coefficient (k), $\prod_{n=1}^{j} \alpha_n^k$ replaces α_O and the product of the activities of the reduced species raised to their stoichiometric coefficients (p), $\prod_{i=1}^{m} \alpha_i^p$, replaces α_R. R is the gas constant (8.31 J mol^{-1}K^{-1}), T is temperature in K, F is Faraday constant (96485 C mol^{-1}), and n is the number of electrons transferred in the overall reaction.

For reactions that are pH dependent, either H^+ or OH^- is a product or reaction. As evident from Equation 25, change in one pH unit is a decade change in $[H^+]$. As a product or reactant, the electrode potential shifts in response to changes in pH. When pH is changed, the number of electrons transferred, n ,also impacts the shift

from E° at standard temperature.. The formal potential, $E^{\circ\prime}$, calculated in Tables 13 and 14 assumes $\alpha = 1$ for all species other than H^+, which changes based on the pH, and the appropriate number of electrons transferred for each reduction reaction. A formal potential is calculated from the standard potential (E°) for conditions other than standard; here, $[H^+] \neq 1$ M. Thus, these electrode potentials show the significant manifestation of the H^+/e ratio for reactions at the electrode|solution|cell interface. It is important to recognize that localized changes in pH impact electrode potentials for reactions. As pH and potential shift, thermodynamically allowed disproportionation reactions may become more or less likely when a species common to two or more reactions is present.

The redox reactions in Table 13 are representative of the nitrate and nitrite reductions, those related to the mechanism and ammonia production capabilities of the nitrate/nitrite reductase enzyme. The electrode potential reported has been calculated thermodynamically and do not consider any kinetic limitations [131]. *Anabaena variabilis* prefer a local external pH of 7.2, but reactions at the electrode surface can deplete local H^+ or generate additional OH^-. Experiments in this work are not conducted in a buffered electrolyte, thus electrochemical turnover of these pH dependent reactions can have a significant effect on the pH at the electrode|cell interface.

The redox reactions in Table 14 are for reductions of nitrogen species. These nitrogen reduction reactions represent possible intermediate steps in the electrocatalytic conversion of nitrate and nitrite to ammonia. N_2 is not involved in the nitrate/nitrite reductase pathway, but is shown in the Table because in

Table 13. Listing of possible NO_2^- and NO_3^- and redox reactions at various pH.

Species	**Redox Reaction**	$\mathbf{E}^\circ_{pH=0}$	$\mathbf{E}^{\circ'}_{pH=6}$	$\mathbf{E}^{\circ'}_{pH=7}$	$\mathbf{E}^{\circ'}_{pH=8}$
			V vs. SCE		
$\mathbf{NO_2^-}$	$2NO_2^- + 8H^+ + 6e \rightleftharpoons N_{2(g)} + 4H_2O$	1.279	0.806	0.727	0.648
	$2NO_2 + 6H^+ + 6e \rightleftharpoons N_2O_{(g)} + 3H_2O$	0.988	0.633	0.574	0.515
	$NO_2^- + 2H^+ + e \rightleftharpoons NO_{(g)} + H_2O$	0.961	0.251	0.133	0.014
	$NO_2 + 2H^+ + 2e \rightleftharpoons NO_{(g)} + H_2O$	0.804	0.449	0.390	0.331
	$NO_2^- + 8H^+ + 6e \rightleftharpoons NH_4^+ + 2H_2O$	0.623	0.150	0.071	-0.008
	$NO_2^- + 7H^+ + 6e \rightleftharpoons NH_{3(aq)} + H_2O$	0.565	0.092	0.013	-0.066
	$NO_2^- + 7H^+ + 6e \rightleftharpoons NH_{3(g)} + 2H_2O$	0.548	0.134	0.065	-0.004
$\mathbf{NO_3^-}$	$2NO_3^- + 12H^+ + 10e \rightleftharpoons N_{2(g)} + 6H_2O$	1.005	0.579	0.508	0.437
	$2NO_3^- + 10H^+ + 8e \rightleftharpoons N_2O_{(g)} + 5H_2O$	0.875	0.431	0.357	0.283
	$NO_3^- + 4H^+ + 3e \rightleftharpoons NO_{(g)} + 2H_2O$	0.716	0.243	0.164	0.085
	$NO_3^- + 3H^+ + 2e \rightleftharpoons HNO_2 + H_2O$	0.699	0.167	0.078	-0.011
	$NO_3^- + 10H^+ + 8e \rightleftharpoons NH_4^+ + 3H_2O$	0.634	0.190	0.116	0.042
	$NO_3^- + 2H^+ + 2e \rightleftharpoons NO_2^- + H_2O$	0.594	0.239	0.180	0.121
	$2NO_3^- + 4H^+ + 2e \rightleftharpoons N_2O_{4(g)} + 2H_2O$	0.562	-0.148	-0.266	-0.385
	$NO_3^- + 2H^+ + e \rightleftharpoons NO_{2(g)} + H_2O$	0.534	-0.176	-0.294	-0.413

Note: These thermodynamic values are calculated at pH = 0, 6, 7, 8 to include the standard potential and potentials relevant at physiological pH. All pH values are reported vs. SCE.

Table 14. Possible redox reactions of intermediate nitrogen containing species that may contribute to ammonia production by nitrate/nitrite reductase at various pH.

Species	Redox Reaction	$E^{\circ}_{pH=0}$	$E^{\circ'}_{pH=6}$	$E^{\circ'}_{pH=7}$	$E^{\circ'}_{pH=8}$
			V vs. SCE		
N_2	$N_2 + 8H^+ + 6e \rightarrow 2NH_4^+$	0.034	-0.439	-0.518	-0.597
	$N_2 + 6H^+ + 6e \rightarrow 2NH_{3(g)}$	-0.298	-0.653	-0.712	-0.771
N_2O	$N_2O_{(g)} + H_2O + 8H^+ + 8e \rightleftharpoons 2NH_{3(aq)}$	0.269	-0.086	-0.145	-0.204
	$N_2O_{(g)} + 10H^+ + 8e \rightleftharpoons 2NH_4^+ + H_2O$	0.406	-0.038	-0.112	-0.186
	$N_2O_{(g)} + 2H^+ + 2e \rightleftharpoons N_{2(g)} + H_2O$	1.77	1.415	1.356	1.297
NO	$NO_{(g)} + 5H^+ + 5e \rightleftharpoons NH_{3(aq)}$	0.486	0.131	0.072	0.013
	$NO_{(g)} + 6H^+ + 5e \rightleftharpoons NH_4^+ + H_2O$	0.595	0.169	0.098	0.027
	$NO_{(g)} + 4H^+ + 4e \rightleftharpoons N_2 + 2H_2O$	1.678	1.323	1.264	1.205
	$NO_{(g)} + 2H^+ + 2e \rightleftharpoons N_2O_{(g)} + H_2O$	1.59	1.235	1.176	1.117
N_2O_4	$N_2O_{4(g)} + 16H^+ + 14e \rightleftharpoons 2NH_4 + 4H_2O$	0.649	0.243	0.176	0.108
	$N_2O_{4(g)} + 8H^+ + 8e \rightleftharpoons N_{2(g)} + 4H_2O$	1.116	0.761	0.702	0.643
	$N_2O_{4(g)} + 4H^+ + 2e \rightleftharpoons 2NO^+ + 2H_2O$	0.529	-0.181	-0.299	-0.418
	$N_2O_{4(g)} + 2H^+ + 2e \rightleftharpoons 2HNO_2$	0.829	0.474	0.415	0.356

Note: These thermodynamic values are calculated at pH = 0, 6, 7, 8 to include the standard potential and potentials relevant at physiological pH. All pH values are reported vs. SCE.

a system not completely void of nitrogenase, ammonia production by nitrogen fixation can still occur. For species such as N_2O, NO, and N_2O_4, these are possible intermediate reduction products on the path from NO_2^- and NO_3^- to NH_4^+. Some have been identified as known mediators for nitrate assimilation and denitrification in cyanobacteria [41]. As for Table 13, the electrode potential reported for the reductions in Table 14 are calculated thermodynamically and do not consider any kinetics [131].

The reduction reactions listed in Table 15 are not specific to the nitrate/nitrite reductase enzyme, but important reactions to consider for NH_3 production by immobilized *A. var.* For example, both N_2H_4 and NH_2OH are reduction

intermediates in the inorganic reduction of N_2 to NH_3. This work explored the effect of adding these species to the background electrolyte during cyclic voltammetric analysis of cells on electrodes, but did not contribute significantly to the correlation between peak current and ammonia production (data not shown). These reductions are reported because the complexity of bioelectrocatalytic system require consideration of the multiple levels of electrochemical feedback present in whole cellular systems. These data were adjusted to a saturated calomel electrode (SCE) reference and adapted from literature [131].

Simultaneous consideration of all reductions shown in Tables 13, 14, and 15 is challenging. Employing whole cells as the source of catalyst requires consideration of numerous possibilities when mapping pertinent kinetic pathways and possibilities The H^+/e ratio further complicates the reaction possibilities. From an electrochemists' view, plotting these reactions on a potential axis aids in visualizing thermodynamic possibilities from which to begin kinetic and mechanistic modeling efforts. The potential axis (Figure 49) is a horizontal axis with oxidative potential (more positive) on the left and reductive potential (more negative) on the right. For each redox reaction under consideration, a vertical line is drawn at the appropriate E. The oxidized species appears on the left of the vertical line and the reduced of the redox couple is written on the right.

A potential axis maps out reaction possibilities. The potentials for the redox couple diagrammed in Figure 49 are calculated thermodynamically. Consider the utility in the potential axis. The reduction reactions for $NADP^+|NADPH$ and $\text{ferredoxin}_{\text{ox}}|\text{ferredoxin}_{\text{red}}$ (represented as $Fd(Fe^{+z})$, $z = 2, 3$) are plotted on a single

Table 15. Listing of intermediate species and cofactor redox reactions considered in this research.

Species	**Redox Reaction**	**$E^{\circ'}$ (V vs. SCE)**[a]
$\mathbf{N_2}$	$N_2 + 2H_2O + 2e \rightleftharpoons 2NH_2OH + 2OH^-$	-3.281[b,c]
	$N_2 + 4H_2O + 4e \rightleftharpoons N_2H_4 + 4OH^-$	-1.401[b,c]
$\mathbf{N_2H_4}$	$N_2H_4 + 4H_2O + 2e \rightleftharpoons NH_{3(aq)} + 2OH^-$	-0.141[b,c]
$\mathbf{NH_2OH}$	$2NH_2OH + 2e \rightleftharpoons N_2H_4 + 2OH^-$	0.489[b,c]
	$NH_2OH + 2H_2O + 2e \rightleftharpoons NH_{3(aq)} + 2OH^-$	0.179[b,c]
$\mathbf{NH_4}$	$2NH_4^+ + 2e \rightleftharpoons 2NH_{3(aq)} + H_2$	-0.791[d]
NAD	$NAD^+ + H^+ + 2e \rightleftharpoons NADH$	-0.561
	$NADP^+ + H^+ + 2e \rightleftharpoons NADPH$	-0.561
$\mathbf{Fd}^{e}_{A.\ var.}$	$Fd\,(Fe^{3+}) + e \rightleftharpoons Fd\,(Fe^{2+})$	-0.596
$\mathbf{H_2}$	$2H^+ + 2e \rightarrow H_2$	-0.241
	$2H_2O + 2e \rightarrow H_2 + 2OH^-$	-1.069
Adenosine[f]	$Ad\,(II) + 2e + 2H^+ \rightarrow Ad\,(I)$	1.458
	$Ad\,(III) + 2e + 2H^+ \rightarrow Ad\,(II)$	0.958

Note: These reactions are not specific to nitrogenase or nitrate/nitrite reductase, but rather general reactions to consider in whole cell analysis of cyanobacteria. [a]Calculated as follows from referenced values: V vs. NHE $-0.241V$ = V vs. SCE. [b]Calculated thermodynamically, may not be kinetically possible at given conditions. [c]For alkaline conditions, E° is reported vs. NHE with $a_{OH^-} = 1$. [d]Pt, NH_4Cl, 25 $^\circ C$. [e]Fd = ferredoxin. The exact redox potential depends upon the structure 2Fe-2S or 4Fe-4S clusters. Here the ferredoxin reaction is treated as a one electron transfer process for the iron center. [f]Ad = adenine.

potential axis vs. SCE at pH = 7 (Figure 49).

$$NADP^+ + H^+ + 2e \rightleftharpoons NADPH \qquad E^{\circ\prime} = 0.561 \text{ V vs. SCE} \qquad (26)$$

$$Fd\left(Fe^{3+}\right) + e \rightleftharpoons Fd\left(Fe^{2+}\right) \qquad E^{\circ\prime} = 0.596 \text{ V vs. SCE} \qquad (27)$$

Subtraction of standard potential for Reaction 27 from Reaction 26 yields the cell potential for the reaction of $NADP^+$ with $Fd(Fe^{3+})$, $E_{cell} = 0.035$ V. After multiplication of Reaction 27 by 2 so that there are the same number of electrons in both reactions, the corresponding net reaction is found by subtraction of Reaction 27 from Reaction 26.

$$NADP^+ + H^+ + 2Fd\left(Fe^{2+}\right) \rightleftharpoons NADPH + 2Fd\left(Fe^{3+}\right) \qquad (28)$$

Gibbs' free energy is related to electrochemical potential as shown in Equation 29, where $\Delta G^{\circ\prime}$ is Gibbs' free energy (in kJ mol^{-1}) under the specified conditions, n is the number of electrons transferred, F is Faraday's constant (96,485 C mol^{-1}), and $E^{\circ\prime}_{cell}$ is the overall cell potential for a given reaction. For a spontaneous reaction, $\Delta G^{\circ} < 0$.

$$\Delta G^{\circ\prime} = nFE^{\circ\prime}_{cell} \qquad (29)$$

For Reaction 28, $\Delta G^{\circ} = 6.75$ kJ mol^{-1}; thus, the reaction is thermodynamically spontaneous as written. When the potential axis is used for Reaction 28, the spontaneous reaction is shown with arrows. In Figure 49, the oxidized form of the $NADP^+|NADPH$ reaction ($NADP^+$) on the left of the vertical line at 0.561 V reacts spontaneously with the reduced form of the $Fd(Fe^{3+})|Fd(Fe^{2+})$ reaction ($Fd(Fe^{2+})$), which appears on the right of the vertical line at 0.596 V. Indeed, as inferred by

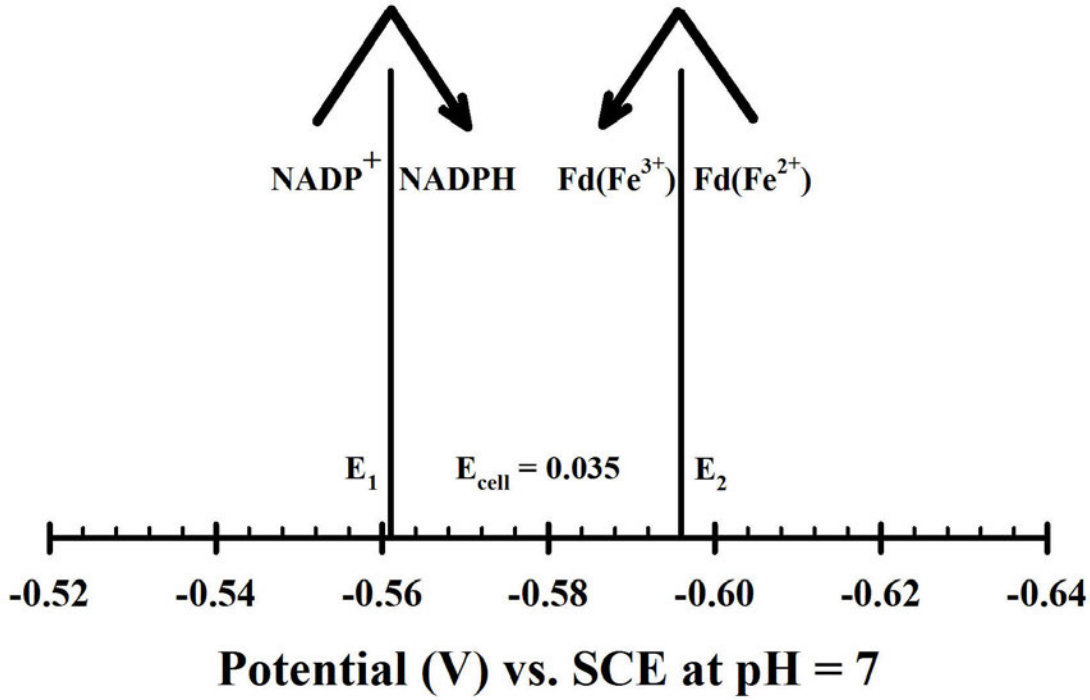

Figure 49. Potential axis for NADPH/$NADP^+$ and ferredoxin (oxidized component LEFT, reduced component RIGHT). The arrows show spontaneous reaction possibilities. E_1 is the redox potential for the $NADP^+$|NADPH couple; E_2 is the redox potential for the $Fd(Fe^{3+})|Fd(Fe^{2+})$ couple, the spontaneous reaction of $NADP^+$ and $Fd(Fe^{2+})$ result in the production of NADPH and $Fd(Fe^{3+})$ at $E_{cell} = 0.035$ V vs. SCE at pH = 7.

Equation 29, the reaction is spontaneous. The discussion of this example highlights the utility of the potential axis. and identify species that can react spontaneously.

The reduction reactions reported in Table 13 have been plotted on the potential axis in Figure 29 at pH = 7. There are additional thermodynamic possibilities at more positive and negative potentials than shown; however, under voltammetric perturbation, the suggested linear correlation between faradaic peak current and ammonia production result from current peaks between 0 and 0.3 V vs SCE for the reductive wave and 0.6 to 0.8 V vs SCE for the oxidative wave. As shown in Figure 29, thermodynamic possibilities are numerous with overlapping redox potentials. Consider some nitrogen species X, Y, and Z that are plotted on the potential axis in Figure 29, for example. Species X is generated at the electrode under voltammetric perturbation, which can then chemically react spontaneously with species Y to produce Z, which itself is electroactive and has a reduction potential near that of X. There are numerous possible events of this type, thus, electrochemical evaluation of nitrate/nitrite reductase system must consider kinetic limitations and requirements to limit the reaction possibilities and determine critical reactions in the process.

4.1.2 Nitrate/Nitrite Reductase Production of Ammonia

Redox reactions given in Tables 13 and 14 and plotted on the potential axis in Figure 29 represent the thermodynamically possible reactions consistent with the reduction of nitrate to nitrite to ammonia. The successive multi proton, multi electron reduction of NO_3^- to NH_4^+ in *Anabaena variabilis* is possible by the

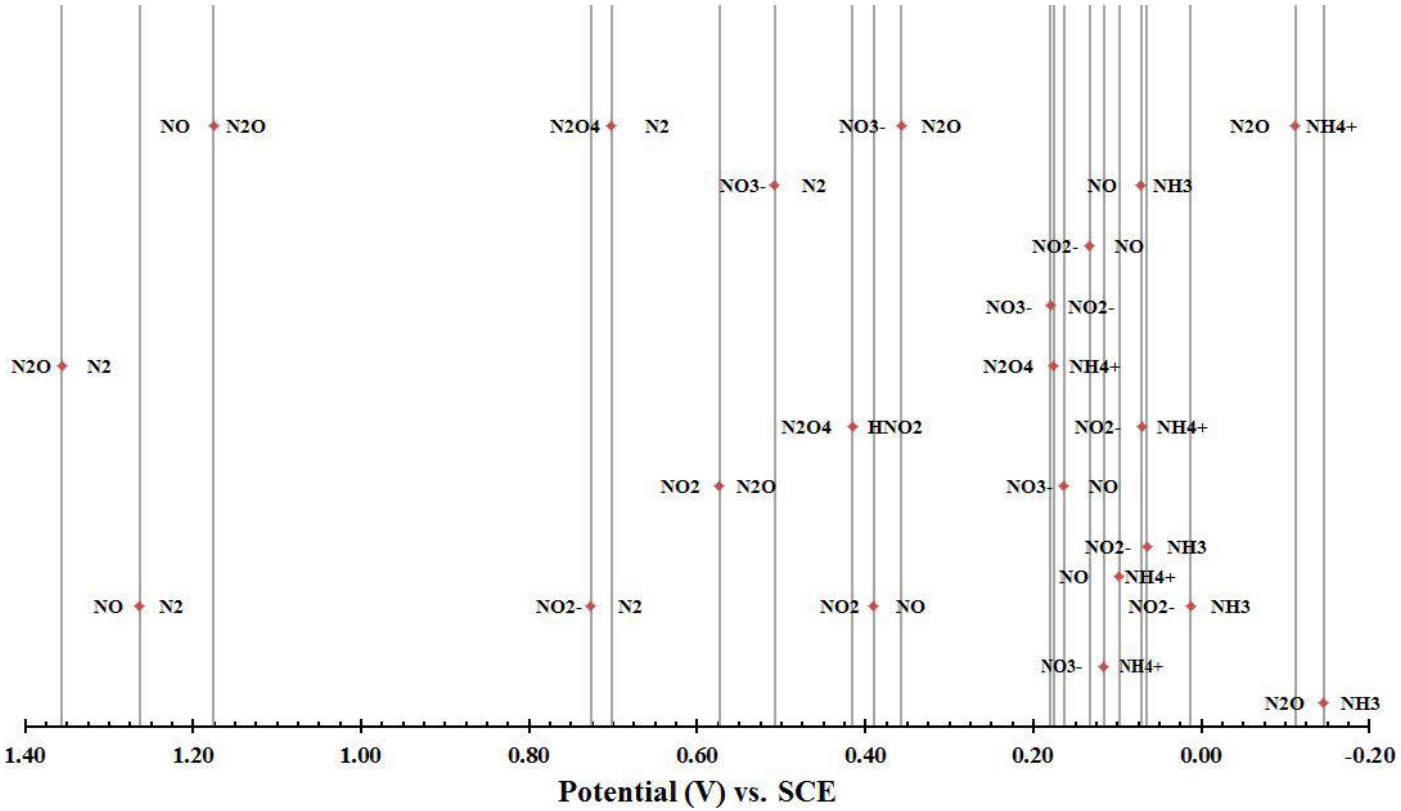

Figure 50. Potential axis of possible NO_3^- and NO_2^- redox reactions at pH = 7. This representation aids in visualizing thermodynamic reaction possibilities. For a given redox couple, the $E^{\circ'}$ is plotted at the appropriate potential. The species left of the vertical line is the more oxidized form of the couple while the species right of the vertical line is the more reduced of the couple.

nitrate/nitrite reductase enzyme. Data presented and discussed in Chapter 3 for *A. var.* are grown on $NaNO_3$ are consistent with the ammonia measured in the external media that result, not from nitrogenase, but nitrate/nitrite reductase. From the data, a linear correlation between forward peak current and ammonia output is found.

Consider the previous example with NADPH and ferredoxins (Reaction 28 and Figure 49). From Chapter 3, the cyclic voltammograms in Figures 29 and 30 show that additions of NADPH and ferredoxins to a background electrolyte solution resulted in higher current forward waves at 0.1 V. Simultaneous additions of NADPH and ferredoxins significantly increase the forward and reverse current at the 0.1 V and 0.6 V peaks (Figure 37) as compared to a solution containing only Na_2SO_4. Before ammonia can be produced by the nitrate/nitrite reductase enzyme, conditions must be satisfactory for the cells to produce the enzyme. While this mechanism, whether by repression, inhibition, or other process, is not clearly understood [123–125, 132, 133], it is generally accepted that NO_3^- is present and NH_4^+, if present, is not uptaken by the *A. var.* SA-1 cells. These two constraints are confirmed in the model for the results outlines in Chapter 3.

In this research, *A. var.* SA-1 are cultured in BG-11_0 + 17 mM $NaNO_3$. Thus, both conditions are satisfied; the addition of $NaNO_3$ provides enzyme substrate, and the SA-1 mutant is nitrogenase derepressed because NH_4^+ is not uptaken into the glutamine synthetase pathway. NO_3^- enters the cell through ATP gated channels. Some NO_3^- is stored within the cell but most is destined for nitrate reductase. Biologically, it has been shown that in photosynthetic nitrogen fixing bacteria,

such as *Anabaena variabilis*, the reductant required by nitrate reductase is reduced ferredoxin. Others have proposed NADPH as an alternative reductant, especially in environments scarce of Fe. The overall two step process by which nitrate/nitrite reductase converts NO_3^- to NH_4^+ is summarized by Reactions 30 and 33. As written, both of these reactions are spontaneous. The potential was calculated from the reported ΔG at pH = 7 [122]. Note, these reactions do not occur absent the nitrate/nitrite reductase catalyst at a bare electrode.

$$NO_3^- + NADPH + H^+ + 2e \rightleftharpoons NO_2^- + NADP^+ + H_2O \tag{30}$$

$$\Delta G^{\circ'}_{pH=7} = 34\ kcal \cdot mol^{-1} = nFE^{\circ'}_{cell} \tag{31}$$

$$E^{\circ'}_{cell} = 0.837\ \text{V} \tag{32}$$

$$NO_2^- + 6Fd_{red} + 8H^+ + 6e \rightleftharpoons NH_4^+ + 6Fd_{ox} + 2H_2O \tag{33}$$

$$\Delta G^{\circ'}_{pH=7} = 103.5\ kcal \cdot mol^{-1} = nFE^{\circ'}_{cell} \tag{34}$$

$$E^{\circ'}_{cell} = 0.748\ \text{V} \tag{35}$$

$E^{\circ'}_{cell}$ for the Reactions 30 and 33 are within the potential limits of cyclic voltammetric analysis of this system. These reactions also represent the biochemical reactions without regard to the influence of an applied potential. The challenge in the construction of the model framework for this system is to determine which of several reaction possibilities arise in the system as constructed. Both Reactions 30 and 33 are pH dependent, thus the influence of the H^+/e ratio complicates several disproportionation reaction possibilities. Figure 51 shows potential axes for the

reduction reactions in Table 13 at pH = 6 (A), pH = 7 (B), and pH = 8 (C) at a potential range appropriate to cover the oxidative backwave observed under previous experimentation (for example, in Figures 29, 30, and 38). The cyclic voltammograms obtained and corresponding data is reported in Table 11 in Chapter 3 are consistent with the observation that when NO_2^- is present in the external media, the oxidative wave near 0.6 V has higher current above the baseline at cell modified electrodes. Consideration of the oxidative back wave observed near +0.6 V in terms of NO_2^- provides a correlation as discussed from the experiments focused on nitrate/nitrite reductase (Figures 44 and 45). There are several redox reactions from Table 13 that involve NO_2^- as a product or reactant near 0.6 V In figure 52, potential axes for the reduction reactions in Table 13 at pH = 6 (A), pH = 7 (B), and pH = 8 (C) all shown at a potential range appropriate to cover the reductive forward peak observed under previous experimentation (for example, in Figures 44 and 45). As the potential axes in Figure 52 show, there are significantly more thermodynamic reactions possibilities to consider. The correlation between forward peak current and ammonia production do not suggest an electrochemical mechanism. The relationship between electrochemical current, ammonia production, and $\left[NO_2^-\right]$ and $\left[NO_3^-\right]$ (Tables 11 and 12, Figure 47) collectively suggest that reactions such as those shown in Figure 52 are responsible for the observed effects. Coupling between various reactions is a strong possibility. Previously, it was shown in Figures 40 and 41 that bulk pH does not appreciably affect the faradaic current response. Further, by the linear correlations between faradaic current and NH_3 production shown previously in Figures 34, 39, 46, and 47, bulk pH is not expected to affect NH_3

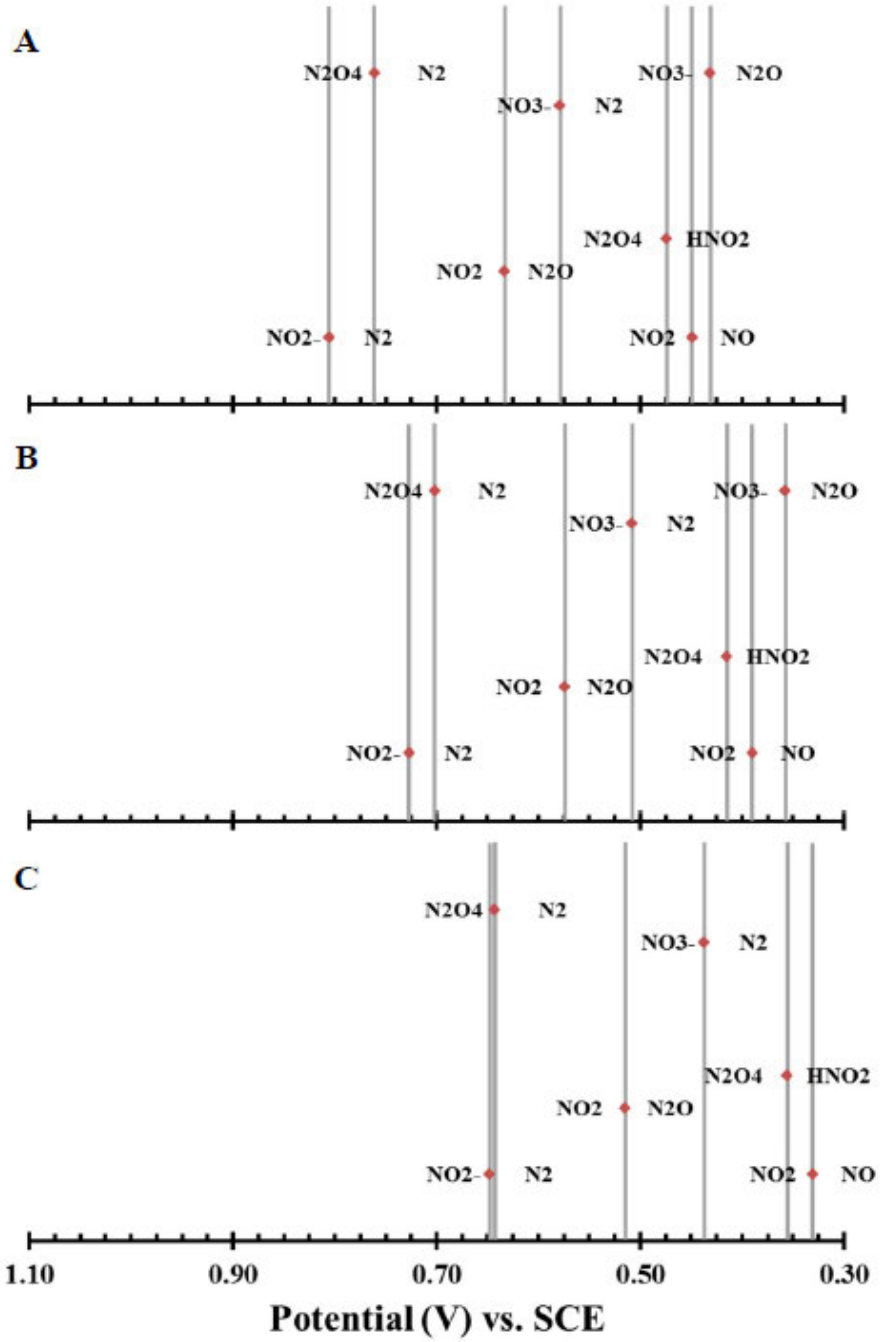

Figure 51. Potential axes of thermodynamically possible nitrate and nitrite reductase reduction reactions between 1.10 and 0.3 V vs. SCE. The potential window, 1.10 to 0.30 V vs. SCE, reflects the species near the $E_{1/2}$ for the oxidative current cyclic voltammogram wave observed at an electrode with immobilized *Anabaena variabilis*. pH = 6 (*A*), pH = 7 (*B*), and pH = 8 (*C*).

production. The research here is mostly concerned with interfacial electron transfer; thus, the local pH at the electrode|cell interface is expected to significantly effect the driving force necessary to achieve electrolysis for the reactions from Tables 13 and 14. The interfacial change in pH changes the formal potentials of these reactions, as shown in Figure 52 for pH = 6 (A), 7 (B), and 8 (C).

There are many reactions from which to choose, each having distinct intermediate products, reduction potentials, and kinetic limitations. NO, for example, is a known free radical mediating species in many organisms. In the human body, for example, NO is a significant neurotransmitter. Several NO_2^- and NO_3^- redox reactions share NO as an intermediate.

The model framework presented here arose from the observations shown in Table 11. The relationship to NH_3 output and substrate input did not suggest an immediate correlation. Thus, the model presented here focuses on nitrate/nitrite reductase substrates NO_2^- and NO_3^- in a simple kinetic model.

4.1.3 Model Simplifications

The model presented here provides a framework to consider the observations presented in Chapter 3. The framework relies upon data consistent with the nitrate/nitrite reductase enzyme production of NH_3 under voltammetric perturbation. The framework has been simplified by not considering side reaction, concomitant reactions, enzyme feedback, or the role of mediators and low potential reductants. Instead, it only considers that reduction of NO_3^- to NO_2^- to NH_3. Others have modeled kinetics of the enzyme system but from a biological viewpoint

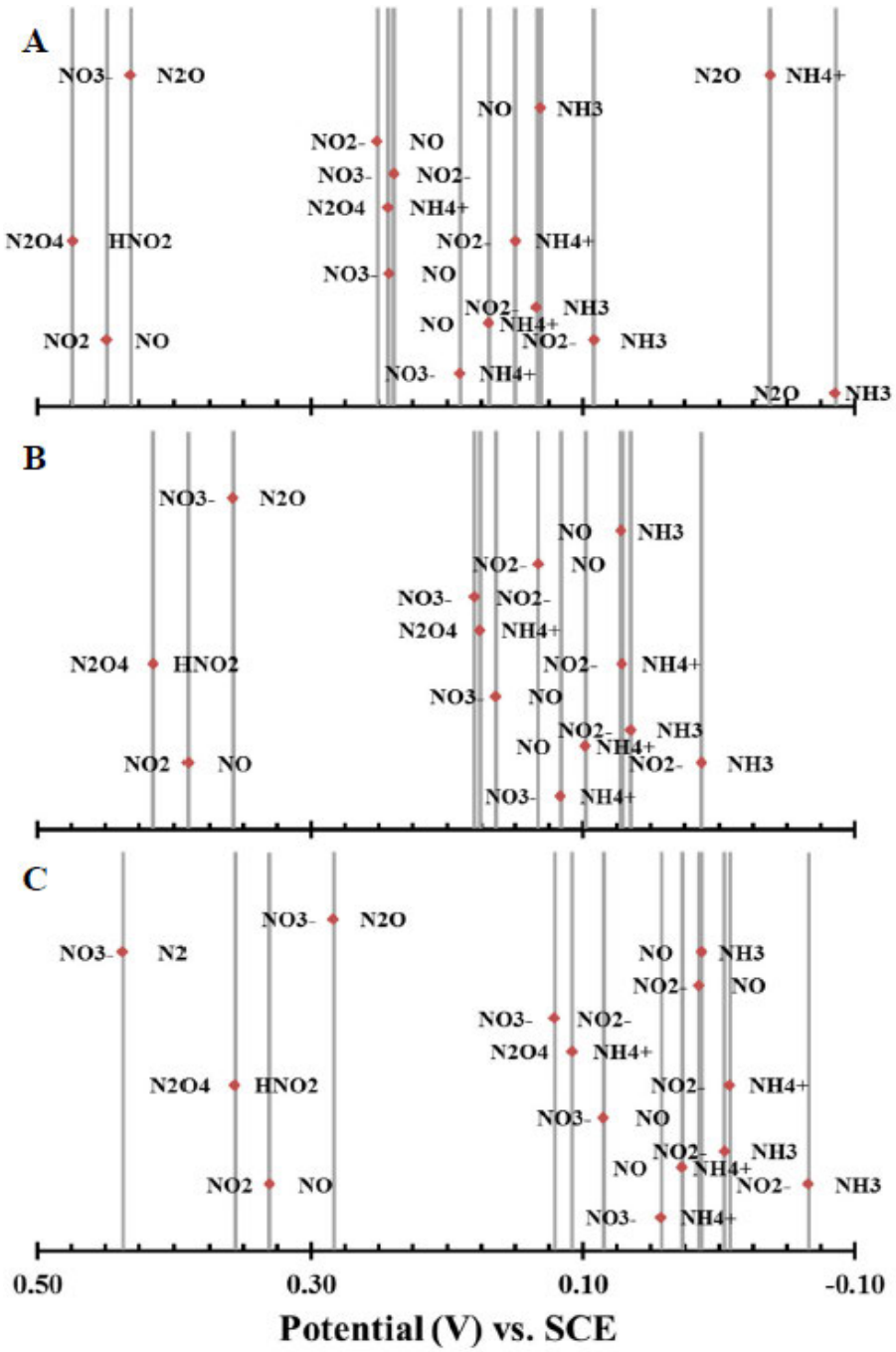

Figure 52. Potential axes of thermodynamically possible nitrate and nitrite reductase reduction reactions between 0.5 and -0.1 V vs. SCE. The potential window, 0.5 to -0.10 V vs. SCE, reflects the species near the $E_{1/2}$ for the reductive current cyclic voltammogram wave observed at an electrode with immobilized *Anabaena variabilis*. pH = 6 (*A*), pH = 7 (*B*), and pH = 8 (*C*).

using Michaelis Menten kinetics [41, 122, 130]. The Michaelis Menten model of reaction and enzyme kinetics is appropriate in many enzyme studies, but does not account well for conditions under voltammetric perturbation.

Figure 53 diagrams the bioelectrochemical system when the cells do not contain nitrogenase. Figure 53 includes two possible indirect electron transfer mechanisms by which the reductive power of the electrode is translated to the cell and eventually the nitrate/nitrite reductase enzyme for the purpose of ammonia production. One mechanism is by indirect electron transfer that uses a mediating chemical species (left in Figure 53). In this mechanism, an electroactive species facilitates electron transfer to the cell, itself recycling at the electrode surface. Because there are no known electron channels in a cell membrane, the mediating species modulates electron transfer between a cell surface species that is membrane permeable. The other possible mechanism is a chemical mediating species that itself enters the cell to mediate electron transfer with the nitrate/nitrite reductase active sites (right in Figure 53). The oxidized form diffuses from the cell to be recycled at the electrode. The model data presented in the following section does not specifically differentiate these possibilities. As the framework transitions to a more robust and complete model, it may allow discrimination of the possibilities shown in Figure 53.

Here, the model assumes: 1) all species react by first order reactions; 2) no intermediate species or partially reduced products are significant; and 3) the reactions are chemically and electrochemically irreversible. Given these assumptions, no feedback processes are considered.

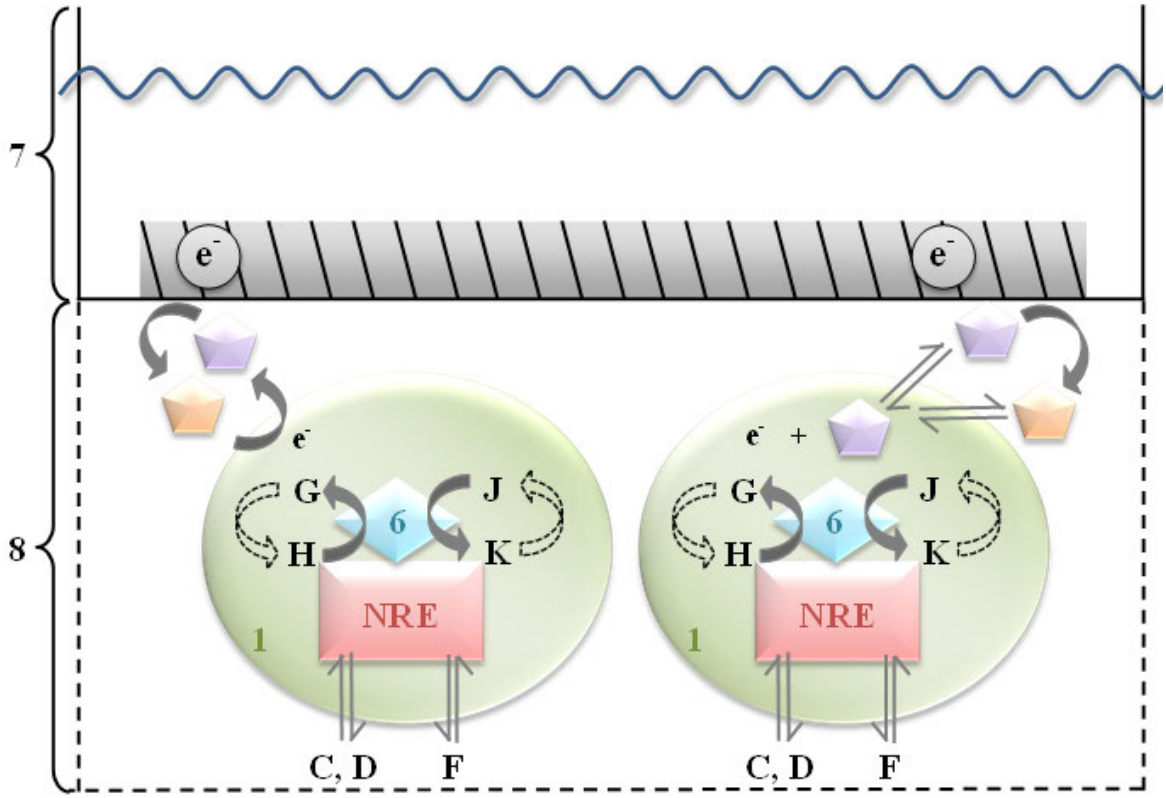

Figure 53. Illustration of the indirect electron transfer possibilities with the nitrate/nitrite reductase enzyme of *A. var.* Vegetative cell on the left shows the chemical mediated process of electron transfer. A redox active species cycles electrons between the electrode and cell, itself undergoing reduction and oxidation as appropriate. The vegetative cell on the right shows the mediated process for a chemical species that undergoes reduction and carries electrons into the cytosol by diffusion (active or passive) across the cell membrane. 6) NADP-Ferredoxin oxioreductase enzyme catalyzes the redox state of NADPH/$NADP^+$ and $Fe_{reduced}/Fd_{oxidized}$; 7) Glassy carbon working electrode submerged in test cell; and 8) $10\mu m$ thick TMODA Nafion immobilization polymer. Chemicals represented are *C*) NO_3^-; *D*) NO_2^-; *F*) NH_4^+; *G*) reduced nicotinamide adenine phosphate (NADPH); *H*) oxidized nicotinamide adenine phosphate ($NADP^+$) *K*) reduced ferredoxin, Fe(*II*) complex; and *J*) oxidized ferredoxin, Fe(*III*) complex.

4.2 Model

This model framework is a kinetic derivation of the NO_3^- to NO_2^- to NH_4^+ catalysis by the nitrate/nitrite reductase enzyme in NO_3^- supplemented *Anabaena variabilis*.

For the general reaction

$$A \underset{k_1}{\longrightarrow} B \underset{k_2}{\longrightarrow} C \tag{36}$$

which is a simplified reaction sequence for the overall nitrate/nitrite reductase reactions

$$NO_2^- \underset{k_1}{\rightarrow} NO_3^- \underset{k_2}{\rightarrow} NH_4^+ \tag{37}$$

Let the concentrations of each species at some time, t, be represented as

$$A(t) = \left[NO_3^-\right] \tag{38}$$

$$B(t) = \left[NO_2^-\right] \tag{39}$$

$$C(t) = \left[NH_4^+\right] \tag{40}$$

Allow initial concentrations A^*, B^*, and C^*, where k_1 and k_2 are conditional rate constants. Thus, in this manner, all other kinetic parameters are constant and all concentrations are either negligible or in excess such that the dependence is pseudo first order. Further, assume all reaction steps are first order. Then the reaction rates are

$$\frac{dA(t)}{dt} = -k_1 A(t) \tag{41}$$

$$\frac{dB(t)}{dt} = k_1 A(t) - k_2 B(t) \tag{42}$$

$$\frac{dC(t)}{dt} = k_2 B(t) \tag{43}$$

The kinetic equations are solved by Laplace transforms (Appendix A). The amount

of ammonia generated, based on starting concentrations A^*, B^*, and C^* is $C(t)$. Define a difference in concentration of ammonia at a specific t, ΔC, where ΔC is the concentration of ammonia generated since the start of measurement. To simplify, define dimensionless rates $k_1 t = X_1$ and $k_2 t = X_2$.

$$\begin{aligned} \Delta C &= C(t) - (C^* + A^* + B^*) && (44) \\ &= \frac{A^*}{\frac{k_1}{k_2} - 1}\left(\exp[-k_1 t] - \frac{k_1}{k_2}\exp[-k_2 t]\right) - B^*\exp[-k_2 t] && (45) \\ &= \frac{A^*}{\frac{X_1}{X_2} - 1}\left(\exp[-X_1] - \frac{X_1}{X_2}\exp[-X_2]\right) - B^*\exp[-X_2] && (46) \end{aligned}$$

4.3 Results

Equation 46 relates initial concentrations of A^* and B^* to $C(t)$ (Reaction 36). These parameters represent NO_2^- and NO_3^- the output of NH_4^+ according to simplified the reaction scheme (Reaction 37). Correlations sought between these parameters are achieved by normalizing the terms in Equation 46 to known experimental quantities. Consider a normalization by A^*.

$$\frac{\Delta C}{A^*} = \frac{1}{\frac{X_1}{X_2} - 1}\left(\exp[-X_1] - \frac{X_1}{X_2}\exp[-X_2]\right) - \frac{B^*}{A^*}\exp[-X_2] \qquad (47)$$

such that a plot of $\frac{\Delta C}{A^*}$ versus. $\frac{B^*}{A^*}$ evaluated at a fixed time should be linear with

$$\begin{aligned} slope_A &= -\exp[X_2] && (48) \\ intercept_A &= \frac{\exp[-X_1] - \frac{X_1}{X_2}\exp[-X_2]}{\frac{X_1}{X_2} - 1} && (49) \\ &= \frac{\frac{X_2}{X_1}\exp[-X_1] - \exp[-X_2]}{1 - \frac{X_2}{X_1}} && (50) \end{aligned}$$

Figure 54 is a plot of $\frac{\Delta C}{A^*}$ versus $\frac{B^*}{A^*}$ at a fixed time, $t = 600\ s$. At the end of

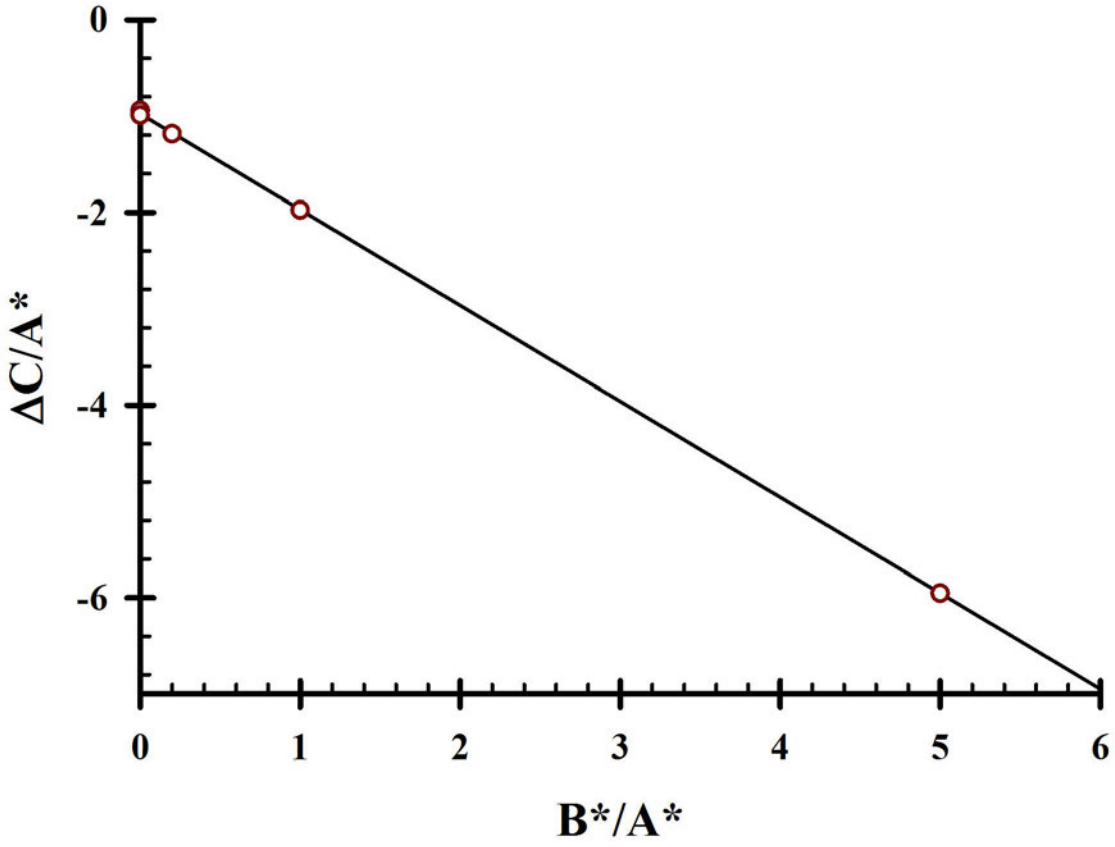

Figure 54. Model output normalized by A^* (NO_3^-) for the nitrate/nitrite reductase enzyme, at a fixed time $t = 600\ s$.

the experiment when NH_3 is measured, A^* and B^* are the initial concentrations of NO_3^- and NO_2^-. C^* is the initial NH_4^+ concentration as determined experimentally (Table 11). As predicted, the agreement is linear $(y = 0.99x - 0.98,\ R^2 = 0.99)$. The linearity of the data in Figure 54 indicate that the ammonia produced, ΔC, normalized by the initial concentration of NO_3^-, A^*, correlate to a $k_2 = 8{\times}10^{-6}\ s^{-1}$.for $t = 600\ s$. By Newton's method, $k_1 = 8 \times 10^{-6}\ s^{-1}$.

If Equation 46 is instead normalized by B^*, nearly the same output results but

the slope and y-intercept are reversed. Normalization of Equation 46 by B^* yields

$$intercept_B = -\exp[X_2] \quad (51)$$

$$slope_B = \frac{\exp[-X_1] - \frac{X_1}{X_2}\exp[-X_2]}{\frac{X_1}{X_2} - 1} \quad (52)$$

Normalization by B^* does not offer any new information.

4.4 Discussion

From the model framework, there are several aspects to discuss. First consider the case of basal production of NH_4^+ by the nitrate/nitrite reductase enzyme. Data in Table 11 report 2.9 μM NH_3 was measured after 10 minutes of cyclic voltammetric perturbation and without the addition of NO_3^- or NO_2^-. Applied to the model, then $A^* = 0$ and $B^* = 0$ and the model relation 44.

$$\begin{aligned} \Delta C &= C(t) - (C^* + A^* + B^*) \\ &= C(t) - (C^*) \\ &= 0 \text{ mol } NH_3 \end{aligned}$$

Therefore, there must be residual nitrate and nitrite in the system that is driving the reaction. It has been reported that *Anabaena variabilis* stores NO_3^- intracellularly [122, 127, 133].

Secondly, if one considers

$$\Delta C = \frac{A^*}{\frac{k_1}{k_2} - 1}\left(\exp[-X_1] - \frac{k_1}{k_2}\exp[-X_2]\right) - B^*\exp[-X_2] \quad (53)$$

when there is no nitrate added, $A^* = 0$ (but we assume the ammonia production observed results solely from the nitrate/nitrite reductase enzyme), $A^* = 0$ and

$C^* = 0$. Then,

$$\Delta C = C(t) - B^* = -B^* \exp[X_2] \quad (54)$$

$$\text{Ammonia Measured} = C(t) = B^*(1 - \exp[-X_2]) \quad (55)$$

Therefore, for $\exp[X_2] < 1$, $C(t)$ scales with B^*. $X_2 = 0.995$ in Figure 54. It would be true then that $C(t)$ scales with B^*. Data from Table 11 do not support this conclusion. A plot of $\left[NO_2^-\right]$ vs. $[NH_3]$ results in a linear equation of $y = 5.3x + 3.0, R^2 = 0.072$. With exclusion of the ammonia output measured after NO_2^- was added to 0.1 mM from Table 11 (considering only $\left[NO_2^-\right] = 0, 0.3$,and 0.5 mM), a plot of $\left[NO_2^-\right]$ vs. $[NH_3]$ results in a linear equation of $y = 5.5x + 2.9,\ R^2 = 0.99$. More experiments with small incremental changes in $\left[NO_2^-\right]$ and $\left[NO_3^-\right]$, with and without added NADPH and ferredoxins will reduce the error of fit between experimental data and the model. Statistically, no confidence is calculated for the NH_3 output from the experiments that collected the data in Table 11. There are several hypotheses about the certainty of NH_3 production data after additions of NO_2^- and NO_3^-.

Thirdly, consider

$$\Delta C = \frac{A^*}{\frac{k_1}{k_2} - 1}\left(\exp[-X_1] - \frac{k_1}{k_2}\exp[-X_2]\right) - B^* \exp[-X_2] \quad (56)$$

when there is no nitrite added. Allow $B^* = 0$ and $C^* = 0$. Then,

$$\Delta C = C(t) - A^* = \frac{A^*}{\frac{k_1}{k_2} - 1}\left(\exp[-X_1] - \frac{k_1}{k_2}\exp[-X_2]\right) \quad (57)$$

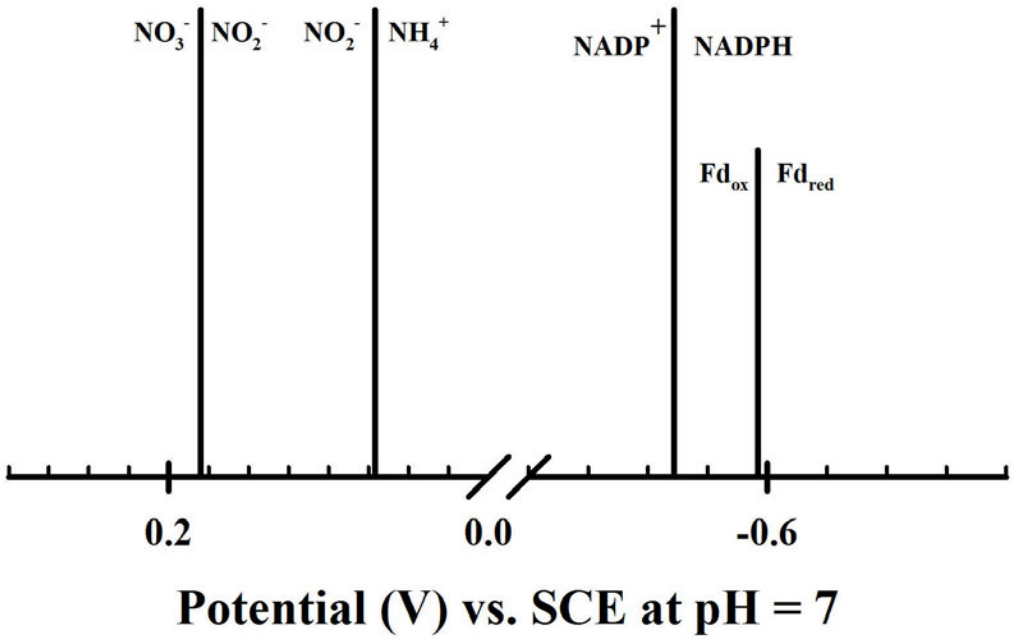

Figure 55. Potential axis with the primary nitrate/nitrite reductase enzyme substrates and cofactors listed.

Ammonia Measured $= C(t) =$

$$= A^* \left(1 + \frac{1}{\frac{X_1}{X_2} - 1} \left(\exp\left[-X_1\right] - \frac{k_1}{k_2} \exp\left[-X_2\right] \right) \right) \tag{58}$$

$$= A^* \left(\frac{\exp\left[-X_1\right] - 1 - \frac{X_1}{X_2} \left(\exp\left[-X_2\right] 1 \right)}{\frac{k_1}{k_2} - 1} \right) \tag{59}$$

Therefore, depending on X_1 and X_2, amount of ammonia generated may increase or decrease with nitrate concentration.

In consideration of the model and $\left[NO_2^-\right]$, $\left[NO_3^-\right]$, [NADPH] ,and [ferredoxins] mediator and substrate additions in Table 11, there are several observations made. The following discussion references Figure 55. The potential axis in Figure 55 is a simplified plot from the reactions listed in Tables 13, 14, and 15. The potential axis aids in visualizing thermodynamic reaction possibilities such as spontaneous reactions. The oxidized form of one redox couple can be electrolyzed by the reduced form of another redox couple further down the axis, as explained with Figure 49.

Several observations make clear that the most likely redox reactions involved in increased production of NH_3 from immobilized *A. var.* under applied driving force are those involved in the nitrate/nitrite reductase enzyme path. The model framework has also been constructed for the same enzyme, thus, qualitative analysis of the data from Table 11 lead to mapping of reaction pathways. The following discussion topics suggest mechanistic routes of ammonia production by nitrate/nitrite reductase at cyanobacteria modified electrodes. The following discussions illustrate how to organize the data and how they contribute to the mechanistic framework. Not all statements in this discussion have been experimentally verified.

A 0.01 mg/mL ferredoxins in 0.1 M Na_2SO_4 background electrolyte. Low ammonia output (3.6 μM) results when NO_3^- and NO_2^- were added. Ferredoxins are not limiting or needed in the cell. The cells have sufficient ferredoxins available to catalyze the reduction of the inherent levels NO_2^- and NO_3^-. Also, spontaneous oxidation of the ferredoxin from the Fe^{2+} to Fe^{3+} would diminish the ability of ferredoxin to effectively donate electrons to nitrate/nitrite reductase. Solutions from which data are correlated were not sparged of dissolved O_2. High ammonia output

(29.9 μM) results when only NO_3^- was added. Ferredoxins are diverted rapidly to the nitrate to nitrite conversion step in the enzyme. Remaining ferredoxins available to reduce NO_2^- to ammonia. The potentials are properly poised if the catalysis is not kinetically limited.

A 1 mM NADPH in 0.1 M Na_2SO_4 background electrolyte. The highest ammonia output (37.8 μM) was measured without NO_2^- or NO_3^- addition. NADPH is a cofactor for nitrate reductase (Figure 6). *A. var.* can store NO_3^- in the cytosol. Provision of reduced NADPH, if limiting intracellularly, increased enzyme turnover of stored NO_3^- to produce a high amount of NO_2^-. Assumes sufficient reduced ferredoxins present in the cytosol provide electrons to nitrite reductase, NO_2^- in excess by high turnover of NO_3^- to NO_2^-. This results in high amount output. High ammonia output (26.3 μM) was measured with NO_2^- or NO_3^- addition. NH_4^+ and NO_3^- can react spontaneously to produce NO_2^-. Increased NO_2^- depends on fixed availability of reduced ferredoxins, no supplied additionally. Thus, NH_3 output not as high as without NO_2^- and NO_3^- due to loss of NH_4^+ and limiting ferredoxins. Until supplies exhausted, high enzyme turnover results in high ammonia output.

Ferredoxins to 0.01 mg/mL plus NADPH to 1 mM in 0.1 M Na_2SO_4 background electrolyte. $NADP^+$|NADPH and $Fd(Fe^{3+})|Fd(Fe^{2+})$ reactions have nearly the same formal potential. When added to solution simultaneously, the fraction of oxidized and reduced forms readily changes based on local pH. Non zero fraction of NO_3^-/NO_2^- additions result in statistically similar ammonia output. High ammonia output (21.5 μM) was measured without NO_2^- or NO_3^- addition. Lower ammonia output than observed when NADPH and $Fd(Fe^{2+})$ were added separately.

Suggests neither NO_2^- nor NO_3^- are limiting. High ammonia output (19.1 μM) was measured with NO_3^- addition. NADPH spontaneous reduction of NO_3^- to a product other than NO_2^- away from nitrate reductase, thus NO_2^- produced. Addition of NO_3^- did not directly increase ammonia production suggest that NO_3^- is not limiting. High ammonia output (21.6 μM) was measured with NO_2^- addition. Similar to 3*b*, addition of NO_2^- did not directly increase ammonia production suggest that NO_2^- is not limiting. Moderate ammonia output (13.7 μM) was measured with NO_3^- and NO_2^- addition. Insufficient cofactor present to catalyze reduction of increased substrates.

There are other types of observations to be made from these data. The framework model presents a foundation for a deeper mechanistic understanding of the *A. var.* production of NH_3.

CHAPTER 5

CONCLUSIONS

The major conclusions of this research are presented here categorically. Overall, the goal of the research was to identify and construct a system to produce ammonia in a renewable manner. This goal was achieved and at ambient temperatures and pressure. A catalyst is still required, as in the commercial Haber Bosch synthesis, however it is sourced from immobilized cyanobacteria. Thus, the system developed in this research produces ammonia from a renewable source with minimal energy input and at ambient temperature and pressure. Overall, the efficiency of the bioelectrocatalytic device as compared to the efficiency of unaltered cyanobacteria in nature has not been calculated or estimated.

5.1 Increased Ammonia Production Depends on Electrode Polarization

As discussed in Chapter 3, without the application of cyclic voltammetry to the cells, ammonia output does not increase above basal output. This suggests that the electrochemical reactions between cells and the electrode respond to an applied potential for the purpose of ammonia production. Cells that were subjected to cycled potential produced a ten-fold increase in NH_3, all other parameters and conditions equal. Ammonia production by the bioelectrocatalytic device requires an externally applied driving force. Therefore, both the electrode and applied potential are key components to ammonia production from immobilized cyanobacteria. In

this research, small potential perturbation is sufficient for NH_3 production by cells immobilized to an electrode surface. Cyclic voltammetry was used to polarize the electrode from 0.8 V to -0.3 V and then potential cycled back to 1.1 V vs SCE. While a specific electrolysis potential was not identified, it must fall within this potential range employed in this research. The free energy barrier (ΔG) to produce ammonia from nitrogenase is -3.3 kJ and from nitrate/nitrite reductase is -17.4 kJ for NO_3^- to NO_2^- and -6.9 kJ for NO_2^- to NH_4^+. Thus, when the electrode is polarized at 1 V, $\Delta G = -96$ kJ for a one electron transfer. Thus, from an thermodynamic treatment, this system is energetically efficient. The energy available to drive the enzyme catalysis is more than sufficient to drive each step in the conversion process. There are kinetic, concentration, and access considerations that alter the thermodynamic efficiency of this system, however they are not yet fully understood so such a calculation is not presented.

5.2 Ammonia Production at Ambient Temperature and Pressure

Low basal levels of ammonia production by batch (125 mL) cultures of *A. var.* have been measured with an ammonia ion selective electrode. This measurement represents the *in vivo* output of NH_3. This basal output of ammonia from 15 mL samples of well mixed cultures (where cells and debris are removed) is 2.8 ± 0.4 μM. After voltammetric perturbation of the same density of cells immobilized to the electrodes at various scan rates, average ammonia production for select experimental conditions increased in the range of 5 to 30 μM, depending on the concentrations of

substrate and cofactor species. Significant energy is required to raise temperature and pressure. Any system that can achieve efficient production, even if not at 100% theoretical efficiency, without the added cost of increasing temperature and pressure and desirable.

5.3 Nitrate/Nitrite Reductase Enzyme Electrochemically Accessible

Alternative enzyme pathways that produce ammonia are present in *Anabaena variabilis* such as the nitrite/nitrate reductase enzyme. The data are more consistent with this enzyme than nitrogenase. Data analyzed do not conflict with known biochemistry of nitrate/nitrite reductase. From the data, a linear relationship exists between the observed faradaic current response from cells immobilized to an electrode and the density of ammonia produced. Electrochemical perturbation is necessary to increase NH_3 produced. Cells immobilized to an electrode and left in the electrochemical cell do not produce increased ammonia unless a potential is applied, as in cyclic voltammetry. After voltammetry is completed, the electrodes that contain cells are more difficult to clean. This suggests that cells are specifically adsorbed to the surface of the electrode during polarization. Mechanistically, this effect is not well defined, but it is believed to be related to alteration of cell membrane permeability. Under polarization, cells interface directly with the electrode, where electron transfer between nitrate/nitrite reductase is enhanced due to a reduction in the physical barrier. There are likely mediating species involved in this system, such as NO, however additions of NO_2^- and NO_3^- have a significant

effects on ammonia production and faradaic current responses (from Chapter 4).

5.4 Mechanistic Framework Model

Initial model output suggest that in a simplified system considering only the reduction of NO_3^- to NO_2^- to NH_3 by the nitrate/nitrite reductase enzyme, the kinetic rate for NO_3^- to NO_2^- is either very fast and not observed at cyclic voltammetric scan rates, or is in fact the same as the kinetic rate of NO_2^- to NH_3. Plotting $\left[NO_2^-\right]$, $\left[NO_3^-\right]$, [NADPH] ,and [ferredoxins] on a single potential axis shows that electrochemically it is difficult to distinguish between NADPH and ferredoxins because they have nearly the same formal potentials. Both NADPH and ferredoxins have been implicated in either step of nitrate/nitrite reductase. Comparison of ammonia output to tested variables suggest several possibilities about limiting reactants and rates for the enzyme under voltametric perturbation. Model output shows linear agreements, yet the kinetic output does not reflect known biochemistry. The model lacks complex levels of feedback and thus, does not accurately reflect known electrochemical or biological steps.

From the data, the mechanism of ammonia production is likely mediated at an electrode surface. From the reaction possibilities plotted in Figures 52 and 51, NO and N_2O are likely candidates for enzyme|electrode mediation. With proper identification of the mediator and any intermediate productions involved in the electrode polarization dependent nitrate/nitrite reductase production of ammonia, the kinetics of the mediator will fold into the framework to offer a more exact description of the observed behavior.

5.5 Possible Impacts and Significance

Here, the feasibility of ammonia produced by the method developed in this research is considered. Ammonia output from the bioelectrocatalytic device was never expected to compete directly with the commercial synthesis. However, there is utility in comparison of the two methods. It is important to note several assumptions and limitations of the bioelectrocatalytic device.

The bioelectrocatalytic device contains living photosynthetic cyanobacteria. With light/dark cycles on earth, high rates of NH_3 production are limited to hours of daylight. This is especially true for a system that obtains its power from a solar device such as a large photovoltaic panel, as suggested in Figure 56. While even photosynthetic organisms have dark reactions that complete respiration cycles in the absence of sunlight, the cells used in this research are illuminated 24 hours a day. After immobilization, cyclic voltammetry with cell modified electrodes is performed in a relatively dark location and in the absence of any applied light. Thus, it is reasonable to conclude there would still be ammonia production by system even during times of darkness. The calculations presented do not include ammonia produced in the dark.

The most efficient use of the produced ammonia by this device would be as a fertilizer. Most notably, the bioelectrocatalytic device has a very small environmental footprint and demonstrates a sound ecological system that consumes wastes to generate fuel. The comparison below does not consider the effort or cost of harvesting aqueous NH_4^+ produced by the cells but could conceivably be applied

physical footprint.

5.6 Comparison to Haber Bosch Commercial Synthesis and Research Significance

The research results described in this dissertation show that common animal wastes, NO_2^- and NO_3^-, are substrates for nitrate/nitrite reductase. Nitrate/nitrite reductase, found in common cyanobacteria, are subjected to a potential gradient by immobilization to an electrode that itself is polarized with minimal energetic input (1 V). Currently, there are no systems reported or commercially available that can achieve ammonia production from animal waste products at ambient temperature and pressure with a minimal dependence on the environment. While the mechanisms and substrate for N_2 reduction to NH_3 by nitrogenase is a distinct manner by which to generate ammonia in cyanobacteria, it is also the most commonly employed commercial synthesis to produce ammonia. Thus, to understand the significant impacts and possible implications of the bioelectrocatalytic device, the ammonia output and energetic input balance for the research here is compared to the commercial Haber Bosch synthesis. It is important to note the distinct differences between the Haber Bosch synthesis of ammonia and the bioelectrocatalytic device production of ammonia. They are not the same process; the Haber Bosch catalytically reduced N_2 to NH_3 at high temperature and pressure, while the bioelectrocatalytic device enzymatically produces ammonia from NO_2^- and NO_3^- at polarized electrodes. Because the world is dependent upon commercially available ammonia, the comparison between Haber Bosch and bioelectrocatalytic ammonia

serves only to illustrate the economic and environmental significance of alternative ammonia production.

In the laboratory, the electrode is connected to a potentiostat. The potentiostat controls the potential drop between the cell immobilized working electrode and the reference electrode. The potentiostat is an electrically powered instrument, but in theory, it could be replaced by simple electronics and powered with a photovoltaic device as shown in Figure 56.

As shown in Table 16, the bioelectrocatalytic device exhibits significant energetic and economic differences as compared to the Haber Bosch synthesis. The data in Table 16 are calculated based on production of 1 ton of NH_3 per day. Several aspects of the scaled up system must be considered. Certainly, a significant portion of land would need to be designated for the device area. The device data presented in Table 16 were extrapolated from small scale laboratory data and at a two dimensional electroactive surface, but as mentioned previously, different electrode materials could be used to construct a three dimensional electrode. Because the production rate is slow compared to commercial syntheses, a large electroactive area with a high density of cells must operate for extended periods. The area required to generate 1 ton NH_3/day could likely be reduced by using a high surface area carbon mesh electrode material. For example, woven carbon fiber, a suitable electrode material, has much higher surface area than the flat non porous surface such as the electrodes used in this research. With appropriate intercalation of larger densities of cells into a higher surface area electrode, the footprint area of the electrode can be reduced proportional to the gain in surface area of the electrode material. Thus, a 31 acre

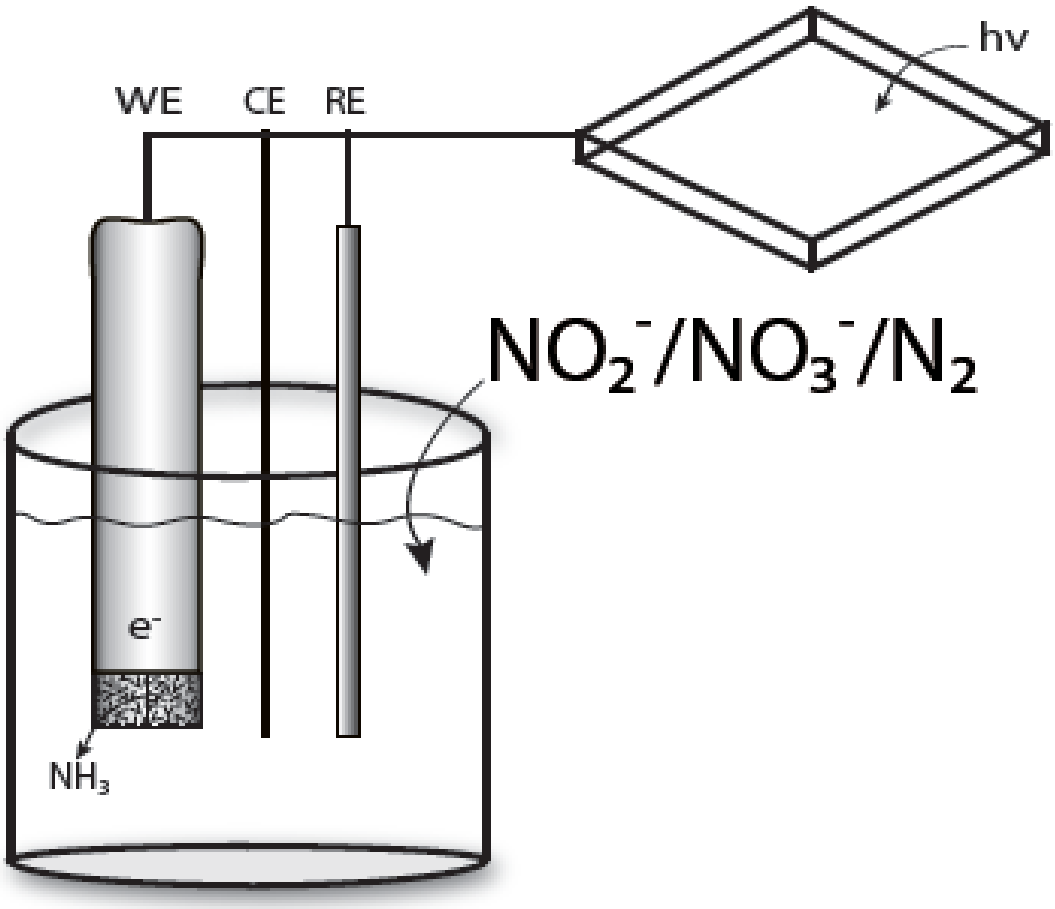

Figure 56. Drawing (not to scale) of the basic bioelectrocatalytic device connected to a solar/PV harvesting system. Cells are immobilzed to a working electrode (WE) with modified-Nafion®. The electrode is polarized by a potential drop between the WE and counter electrode (CE). Measured potentials are compared to the internal redox potential of the reference electrode (RE). A nitrogen source is introduced into the device and is catalyzed to NH_3 by enzymes within the cells. The power necessary to drive the reactions is supplied by an external photovoltaic source.

Table 16. Energy balance calculations comparing the Haber Bosch synthesis and process described by this research.

Factor	**Value**	
	Haber Bosch	*This Research*
Production Cost ($/ton NH_3)	500	10^a
Production Rate (ton NH_3/day)	1800	1^b
Energy Consumption (GJ/ton NH_3)	28	0.04^c
Capital Investment ($/plant)	339,000,000	$100{,}000^d$
Transportation Cost ($/ton NH_3)	172	0
Storage Cost ($/ton NH_3)	500	0

Note: These data are assume 1 ton ammonia is produced in 1 day for subsequent calculations. Data for the Haber Bosch were sourced from [8]. The Production Cost factor includes the cost of any raw chemical materials and the cost of any energetic input in 24 hours. The Energy Consumption factor is the energy consumed per ton of NH_3 produced. The Storage Cost factor represents the cost of high pressure storage. Because anhydrous ammonia is kept liquid at high pressure, a financial and energetic cost is necessary to store as a liquid. [a]Calculated based on photovoltaic power consumption at a rate of $0.097/kwh (NREL PVWatts calculator [134]). Such power is generated at a 75 m^2 solar panel according to the JavaScript Applet calculator [135]. [b]This value is based on a flat and nonporous electrode surface of area = 31 acres (1.24 x $10^5 m^2$). [c]This value is the energy obtained from the solar panel to drive a 0.8 V drop across the 31 acre electrode. [d]This value is estimated and includes the cost of the solar panel and wiring, electrode material, and appropriate aqueous environment (pool/trench) in which the algae to grow and electrode be placed.

bioelectrocatalytic device can be reduced in size significantly.

Energy consumption per ton of NH_3 produced is 0.04 GJ for the bioelectrocatalytic device and converts to 25 kWh. Assuming appropriate typical efficiencies of energy conversion and electrical losses, a single solar panel of 75 m^2 (square of side = 9 m) generates 71 kWh in a single day. Thus, the capital investment per bioelectrocatalytic device is relatively low and mostly to fund the purchase and installation of a per application solar panel. A typical Iowan farmer uses approximately 50 kg of anhydrous ammonia per acre of cropland. This density of

ammonia used is calculated for use on the average farm size in Iowa of 333 acres (2010, USDA National Agricultural Statistics Service), this device could produce enough ammonia as a fertilizer for his farm per year in 18 days. So, the scale of the device footprint is

$$31 \text{ acres} \left(\frac{18 \text{ production days}}{365 \text{ days per year}} \right) = 1.5 \text{ acres} \tag{60}$$

With additional data, the practicality from a financial standpoint is considered. Assume the average Iowa farm is 333 acres and the area of viable farmland a farmer gives up for the bioelectrocatalytic device is 31 acres (as described in Table 16), or as shown in Calculation 60,1.5 acres for production over the course of one year. 31 acres devoted to ammonia production by the bioelectrocatalytic device results in a 9 % loss of potential income due to the physical area needed to construct the ammonia producing device. If the production of 1 ton of NH_3 would be dispersed over 1 year, then a 1 % loss of potential income would arise. Similarly,the average cost of anhydrous ammonia (dependent on the cost of natural gas) is \$850/ton and a farmer applies 0.05 ton/acre, that is a cost of \$47/acre. Based on the USDA National Agricultural Statistics Service *2010 State Agricultural Overview*, corn for grain, Iowa's main agricultural crop generates, \$380/acre. Taking the ratio of the cost of fertilizing with anhydrous ammonia to the profit per area, a farmer loses about 12% income to the cost of fertilizer. Thus, on these financial figures of merit alone, there exists an impetus (1 % $<$ 9 % $<$ 12 %) to use the bioelectrocatalytic device over commercially available NH_3.

Consider that a 333 acre farm generates \$380/acre for a crop of corn. Assume

the farmer spends \$47/acre on Haber Bosch produced NH_3. The crop profitability, profit - cost of ammonia fertilizer, is \$110,889. Compare to a 333 acre farm that produces their own NH_3 by the bioelectrocatalytic device for \$0/acre, but loses 31 acres of land to construct and operate the device. The crop profitability in this case is \$114,760. Thus, the loss of land does not affect the profit of a crop. The savings provided by on site ammonia production by the bioelectrocatalytic device is greater than the lost profit from a smaller crop. There are many types of these calculations that support the financial, energetic, and environmental significance of the research presented here.

Again, it is important to point out that while these calculations offer an impressive future for bioelectrocatalytic produced ammonia from animal wastes NO_3^- and NO_2^-, they have been compared to the Haber Bosch synthesis. The calculations serve only as an impetus to suggest future study in the area of bioelectrocatalytically produced ammonia has the potential to significantly offset world dependence on the environmentally and economically expensive Haber Bosch ammonia.

CHAPTER 6

FUTURE WORK

Overall, the primary goal to generate ammonia at ambient temperature and pressure was achieved. Decoupling the complex network of reactions, feedback, mediators, and analytical correlations has proven complex. The future successes of this research will require division of the project into several smaller research domains. Device construction and testing outside of the laboratory is eventually necessary.

Current cyanobacterial biotechnology research primarily studies hydrogen production and biomass feedstock development. Simultaneously, many study protein and enzyme interactions with electrodes in electroanalytical systems. Yet a third distinct area of cyanobacterial research explores enzyme catalysis in power systems such as fuel cells. The research described here draws from these distinct areas of modern research and establishes an interdisciplinary approach the use of cyanobacteria in a device that produces ammonia at ambient temperature and pressure. While this research describes a system that achieves ammonia production with minimal energy input, the thermodynamics, kinetics, and correlation of the electroanalytical and biological data require additional research and should be the focus of future work.

In all future work, it is imperative to obtain the following data for every experiment: 1) some value of cell density like [chlorophyll a] or [total protein]; 2) ammonia concentration before and after alteration of variables; and 3) bulk and

micro pH quantitation. At minimum, these data must always be collected and available for future correlational mapping.

6.1 Thermodynamic Considerations

The thermodynamics of the bioelectrocatalytic system should be further studied. The influence of electrochemical potential over many simultaneous reduction oxidation reactions should be more closely studied. This research identified several significant reactions of interest, namely those catalyzed by nitrate/nitrite reductase. Calculated electrochemical potentials for the overall nitrate/nitrite reductase reactions

$$NO_3^- + 2H^+ + 2e \rightleftharpoons NO_2^- + H_2O \qquad E^{\circ'}_{ph=7} = 0.594 \text{ V vs. SCE} \quad (61)$$

$$NO_2^- + 8H^+ + 6e \rightleftharpoons NH_4^+ \qquad E^{\circ'}_{pH=7} = 0.623 \text{ V vs. SCE} \quad (62)$$

suggest that under ambient conditions K is favorable for continuous production of NH_4^+. Both reactions are strongly pH dependent, thus further study of the local pH environment should provide equilibrium data that can offer a more specific description of the reactant and product concentration ratios under different potential gradients. The work here employed Na_2SO_4 as the electrolyte. A buffered electrolyte system would better control pH and minimize the impact of the proton/electron ratio common in all nitrate/nitrite reductase reactions. Intermediate products such as NO and N_2O are known for denitrification, the reduction of NO_2^- to N_2. Introduction of NO and N_2O to the system will also aid in the determination of the most probable reactions in the path of NO_2^- to NH_4^+. Further, cyclic voltammetry

was the most used electroanalytical technique. Cycled potentials limit the ability to calculate specific overpotential required to facilitate ideal enzyme optimization and enhanced reaction kinetics. Cyclic voltammetry provides a good spectrum of responses but other voltammetric methods may allow more ready quantification of electroactive materials.

From the reaction possibilities listed in Chapter 4, pH clearly has a significant effect. Nearly all the electrochemical reaction possibilities consume protons. Thus, in addition to the biological significance of bulk vs. micro pH, there are electrochemical interests as well. Tools and methods should be employed to carefully monitor the effect of pH on ammonia production. Micro and nano probes are commercially available to follow pH.

6.2 Further Kinetic Evaluation

Production of NH_4^+ by nitrogenase or nitrate/nitrite reductase are kinetically challenging tasks. The present kinetic framework for the reactions necessary to accomplish efficient enzyme catalysis is overly simplified. It assumes all reactions are first order and does not include redox mediator or cofactor reaction kinetics. As this research has shown, ammonia production by immobilized whole cell filaments of *A. var.* is significantly more complicated than the model framework suggest. While data verified against the model show good agreement, they are not inclusive of known electron donating reactions such as those of ferredoxin and NADPH.

6.3 Biological Considerations

From the data, enzymatic production of NH_4^+ as compared to known biochemistry of *Anabaena variabilis.* Electron transfer across the cell membrane has not been reported, thus the possibility exists the increased ammonia production related to a biophysical interaction between cell or cell product and the electrode. Future work should study cell lysate as has been done for whole cells. A whole cell lysate preparation disrupts cells and removes of all cellular debris. The resultant solution contains cytosolic components such as nitrogenase and nitrate/nitrite reductase. This enzyme containing solution can be equilibrated into an electrode film and studied as this research has. Such research would delineate between cellular and enzymatic processes.

NADPH introduction to the external media has a significant effect on both ammonia production and voltammetry. Some of these effects are likely due to the buffering capacity of NADPH/$NADP^+$. Commercial preparations of reduced NADPH are expensive. For the system described here, studies should be conducted with the redox active moiety of NADPH, nicotinamide. Nicotinamide is inexpensive and can be electrochemically reduced. Nicotinamide could be a electron shuttle for nitrogenase and nitrate/nitrite reductase. Further, the redox state of biological cells is often measured by the ratio between reduced and oxidized forms of $NADP^+$:NADPH. Commercial assay kits are readily available to measure and quantify this ratio. Measurement of the ratio between the oxidized and reduced forms at different stages of voltammetric perturbation can be correlated to ammonia

production. These type of data can be used to expand the model framework to include mediating and cofactor species.

To deconvolute the complex layers of chemical, biological, and electrochemical feedback, biological inhibitors should be employed. For example, as shown in Chapter 3, methionine D,L-sulfoximine (MSX) effectively blocks glutamine sythetase reuptake of NH_4^+. In the future, use of MSX in experiments directly focused on nitrate/nitrite reductase produced ammonia may eliminate several layers of feedback. In measurements from bulk culture, the highest ammonia output was measured from cells that were cultured in BG-11_0 media supplemented with both NO_2^- and MSX.

Another area of future work in the biological realm would be to coordinate with biologists and explore fine level protein control through adequate analytical understanding of the proteins present. Whole cell systems are complicated because there are so many proteins present. It is not clear from the research described here what the most prominent proteins are in the measurement of redox reactions related to the enzymatic production of NH_3. A Western Blot is the separation of proteins through antibody/antigen binding. Higher level identification of the proteins present would limit the redox reaction possibilities and aid in further development of the kinetic model to describe the effect of electrode polarization on ammonia production.

6.4 Experimental Considerations

From an experimental basis, there are several parameters that should be determined and optimized. A significant focus should be placed on localization of the electrochemical reactions that are measured by the electrode. As discussed

in Chapter 4, several prominent reaction possibilities are apparent based on data obtained thus far. Careful construction of experiments with mediators such as NO and N_2O may limit reaction possibilities to only several as compared to thirty or more.

As discussed and shown in Chapters 3 and 4, electrode polarization is necessary to drive the catalytic production of NH_4^+ from NO_2^- and NO_3^-. From the data, it is not yet clear whether a specific potential exists that would efficiently support nitrate/nitrite reductase produced ammonia. Instead of cyclic voltammetry, attention should be given to discreet potentials as in bulk electrolysis. There may be a specific potential necessary to optimally interface between electrode and enzyme. One can envision the bioelectrocatalytic device operation at this specific potential for sustained periods of time where ammonia production may be higher, barring any kinetic of chemical substrate limitations.

APPENDIX A

ANABAENA VARIABILIS CULTURE PROTOCOL AND METHODS

Anabaena variabilis grow natively across the United States in fresh waters. The care and maintenance for the SA-1 genetic mutant are analogous to that of the wild type. A thriving culture must be sustained for regular experimentation, as the cells are the source of the enzyme catalyst for production of ammonia. *Anabaena variabilis* require little maintenance and near ambient conditions for sustained growth. This appendix describes, in detail, the culture protocol and methods employed throughout this research. 125 mL of culture is generally sufficient to resist contamination by ubiquitous species such as *E. coli.*, however care was taken to construct a sterile growth and manipulation environment.

Culture Setup

Anabaena variabilis are a liquid grown culture. With proper environmental and nutrient conditions, they will grow indefinitely. Due to heat produced by the fluorescent bulbs (D in Figure 1) and orbital shaker (B in Figure 1) installed into the incubator (A in Figure 1), the ambient temperature exceeds 32 °C. Thus, it is necessary to modify the incubator and utilize the water jacket to lower the incubator temperature (this model of incubator warms the water jacket but cannot cool). The water jacket inlet port (E in Figure 1) was connected to a water chiller/recirculator (C in Figure 1). Chilled water under pump pressure circulated through the water jacket and exits the incubator through the drain port (F in Figure 1) where it returns

back to the chiller reservoir. Eight 250 mL baffled flasks (G in Figure 1) containing about 150 mL of cell suspension are shaken at 125 RPM 24 hours per day.

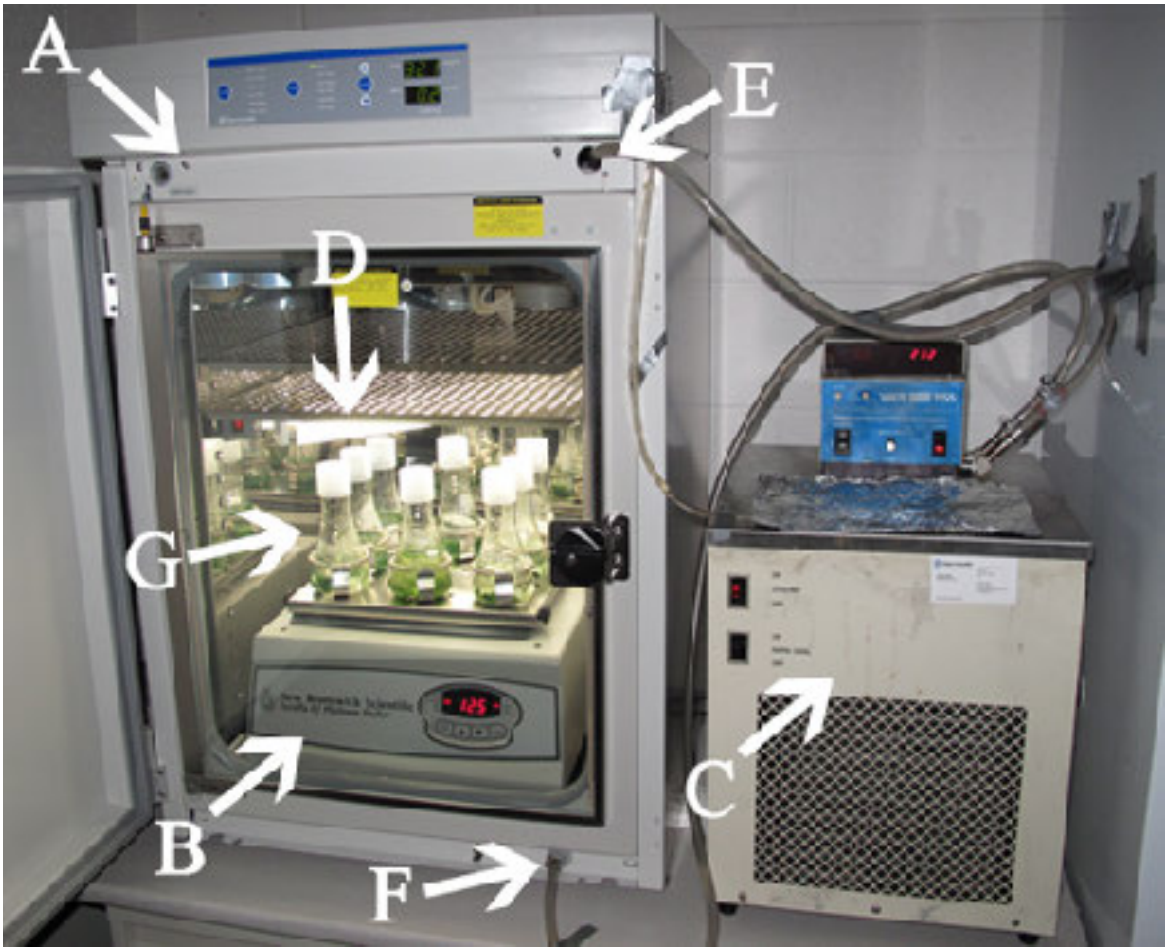

Figure A1. Photograph and description of the culture setup constructed for this research. *A*) Fisher IsoTemp water jacketed incubator; *B*) New Brunswick oscillating shaker; *C*) VWR cold water chiller/recirculator; *D*) Full spectrum fluorescent bulbs; *E*) Water jacket fill port connected to chiller output; and *F*) Water jacket drain port connected to chiller input.

Cell Culture Parameters

The following conditions were employed throughout the continuous culture of Anabaena variabilis: During photosynthesis, *Anabaena variabilis* use energy in the

region of the electromagnetic spectrum from 400 700 nm. The radiation in this range, referred to as Photosynthetically Active Radiation (PAR), is measured as Photosynthetic Photon Flux Density (PPFD), which has units of quanta (photons) per unit time per unit surface area. The units most commonly used are micromoles of quanta per second per square meter. An Einstein (E) is a unit defined as one mole (6.022×10^{23}) of photons.

- Culture volume: 175 mL of cell suspension in 250 mL baffled culture flasks
- Temperature: $32 \pm 2\,^{\circ}\mathrm{C}$
- Illumination: Two 14w Octron (Phillips) 20" full spectrum (400-700 nm) fluorescent lamps installed 20 cm above the top of the culture flasks. These bulbs were illuminated 24 hours a day and provided $31.8 \pm 1.6\ \mu E \cdot m^{-2}s^{-1}$ as measured at the base of the culture flask. The PFFD was measured with a LI 190 Quantum Sensor (Li-Cor).
- Media is changed every two weeks or more frequently as needed.
- The air environment in the incubator has been challenging to determine. Several report the necessity to provide CO_2 for respiration purposes, but this research determined ambient CO_2 levels sufficient. 0.1 % CO_2 has been used for cultures that did not appear to be growing.

Cell Lines

Two strains of *Anabaena variabilis* are cultured simultaneously. In initial inoculate, *Anabaena variabilis* Kutz, was purchased from the American Type Culture Collection (ATCC) in May, 2009. A genetic mutant, the SA-1 strain, was obtained from K.T. Shanmugam of the University of Florida. Samples of each have been frozen for future subculture.

Media Preparation

Anabaena variabilis are grown on BG-11_0, a freshwater algae medium. Media is made in the laboratory as needed. To prepare 1 L of BG-11_0 media:

1. Obtain clean 1 L media bottles (pyrex, orange caps) which have been thoroughly rinsed with DI water and are free of debris.

2. Add the appropriate *Standard Reagents* shown in Table 1 to 1 L DI water and thoroughly mix. Some agitation or light sonication may be necessary to fully dissolve the chemicals.

3. With a 3 point calibrated pH probe, adjust the pH of the solution to 7.1 using HCl and NaOH as necessary.

4. Place the media bottles in the sterilizer with loosely placed caps. Sterilize the media by selecting the liquids cycle (115 °C for 15 minutes).

5. Prepare 1 L of *Trace Metals Mix* by adding the appropriate masses of chemicals shown in Table 2. Store this solution in a refrigerator at 2 °C. It has a shelf life of 2 months providing it is clear of bacterial or fungal contamination.

6. Once sterilized BG-11_0 containing *Standard Reagents* is cooled, add 1 mL of the *Trace Metals Mix* solution to the media and mix well.

7. Store BG-11_0 in the refrigerator at 2 °C for up to two weeks.

Media Change Protocol

Anabaena variabilis media should be changed every two weeks at minimum. If the media contains a fixed source of nitrogen (NO_2^- or NO_3^- for example), the media may have to be changed more frequently due to a higher dependence on fixed nitrogen and a decline in growth following its consumption.

Table A1. Listing of *Standard Reagents* used to prepare BG-11_0 media.

Chemical	**Mass (mg)**	**Final Concentration (μM)**
$NaCl$	25	428
K_2HPO_4	40	230
$MgSO_4 \cdot 7H_2O$	75	304
$CaCl_2 \cdot 2H_2O$	36	245
$C_6H_8O_7$ (Citric Acid)	6.0	31.2
Ferric Ammonium Citrate	6.0	21.4
EDTA	1.0	2.69
Na_2CO_3	20	189

Note: The final concentration is based on 1 L of media.

Table A2. Listing of *Trace Metals Mix* components of which 1 mL is added to 1 L BG-11_0 media.

Chemical	**Mass (g)**	**Stock Concentration (μM)**	**BG-11_0 Concentration (nM)**
H_3BO_3	2.86	46.3	46.3
$MnCl_2 \cdot 4H_2O$	1.81	5.96	5.96
$ZnSO_4 \cdot 7H_2O$	0.22	0.772	0.772
$Na_2MoO_4 \cdot 2H_2O$	0.39	1.61	1.61
$Cu\mathrm{SO}_4 \cdot 5H_2O$	0.08	0.316	0.316
$Co\left(NO_3\right)_2 \cdot 6H_2O$	0.05	0.126	0.126

Note: The stock concentration is for 1 L of Trace Metals Mix while BG-11_0 concentration is the final concentration of the trace metals in 1 L of prepared media.

1. Bring the media to room temperature. In a sterile fashion, transfer the media bottle to the biological safety cabinet and keep capped until ready to use. Do this about 30 minutes before expected use.
2. Obtain a culture flask from the incubator. Shake the contents to break up any cell aggregates.
3. Transfer the entire contents of the flask to the 50 mL conical vials. We culture with about 150 mL of media, so you will likely need three vials.
4. Spin out the cells in the centrifuge at 2.5×1000g for 2.5 minutes.
5. If necessary, obtain a freshly autoclaved flask for the cells.
6. Remove the vials from the centrifuge and decant the media. Keep about 5 10 mL of old media with the cell pellet. Remember if you wish to perform an analysis on the spent media, transfer it to centrifuge vials and label.
7. Transfer the cells to the flask.
8. Add approximately 150 mL of fresh media to the flask.
9. Cap and put back into the incubator.

Spent media, if not being saved for analysis, can be sterilized by the addition of 10% commercial bleach. Following this sterilization, it can be discarded down the drain.

Cell Storage and Freezing Protocol

The protocol described here was adapted from a document entitled *Cryopreservation of Cyanobacteria*, provided by J.J. Brand in the Botany Department at the

University of Texas at Austin. Cells were frozen early in this research to ensure a stock of culture was available had the cultures suffered bacterial contamination. Further, frozen cells allow for temporary suspension of cyanobacteria culture for initiation again at a later date. Samples were obtained from all flasks every 6 months and frozen by the procedure described below.

Cryopreservation refers to the storage of a living organism at ultra low temperature such that it can be revived and restored to the same living state as before it was stored. Cyanobacteria suffer severe osmotic stress and/or ice crystal damage during the freezing and thawing processes. The most effective known ways to minimize these potentially lethal effects are to add a cryoprotective compound to the culture prior to its freezing for storage, and to control the transient cooling and warming rates during preservation.

The steps to preserve *Anabaena variabilis* are as follows:

1. Transfer 3 mL of cyanobacterial liquid culture into a 5 mL cryovial.

2. Pellet the cells by centrifuging the cryovials at 4,400× for 5 minutes. Discard the supernatant after the cells have been pelleted.

3. Add cryoprotective solution containing 1.0 ml of BG-11_0 that contains 8 % DMSO to the pelleted cells (80 μL). Cells are killed by exposure to bright light when in cryoprotective solution. Keep the culture in subdued room light while handling, and in complete darkness at other times.

4. Label all culture vials and note on the master control sheet. Place the cryovials into a cryovial freezer segmented box.

5. Place the box of cells in the -80 °C freezer in the Kohen lab on the second shelf.

Frozen Cell Recovery Protocol

To recover a frozen culture, follow the following steps:

1. Cultures to be revived are removed from storage in the 80 °C freezer and warmed rapidly to room temperature in a heated water bath. Be sure vials are well sealed to prevent bacterial contamination.

2. Pellet the cells at 4,400× for 5 minutes. Discard the supernatant.

3. Add 1 mL of fresh BG-11_0 to resuspend the pellet.

4. Loosen the cryovial lid to allow gas exchange. Keep the contents of the vial in complete darkness for 1 2 days.

5. Transfer the cells to 250 mL baffled flask and add approximately 200 mL BG-11_0 media. After 1 2 days in the illuminated incubator, the cells should begin normal growth.

APPENDIX B

KINETIC MODEL DERIVATION

For the overall reaction scheme

$$A \underset{k_1}{\longrightarrow} B \underset{k_2}{\longrightarrow} C \tag{B.1}$$

which is a simplified reaction sequence for the overall nitrate/nitrite reductase reactions

$$NO_2^- \underset{k_1}{\longrightarrow} NO_3^- \underset{k_2}{\longrightarrow} NH_4^+ \tag{B.2}$$

Let the concentrations of each species at some time, t, be represented as

$$A(t) = \left[NO_3^-\right] \tag{B.3}$$

$$B(t) = \left[NO_2^-\right] \tag{B.4}$$

$$C(t) = \left[NH_4^+\right] \tag{B.5}$$

Allow initial concentrations A^*, B^*, and C^*, where k_1 and k_2 are conditional rate constants. Thus, in this manner, all other kinetic parameters are constant and all concentrations are either negligible or in excess such that the dependence is pseudo first order. Further, assume all reaction steps are first order. Then the reaction rates are

$$\frac{dA(t)}{dt} = -k_1 A(t) \tag{B.6}$$

$$\frac{dB(t)}{dt} = k_1 A(t) - k_2 B(t) \tag{B.7}$$

$$\frac{dC(t)}{dt} = k_2 B(t) \tag{B.8}$$

Assume there are no reaction intermediates, therefore no steady state approximation, and all reactions are first order, the kinetic expressions can be found using Laplace Transforms. Let $\bar{A}(s)$, $\bar{B}(s)$, and $\bar{C}(s)$ be the transformed variables. Upon transform the above become

$$s\bar{A}(s) - A(0) = -k_1 \bar{A}(s) \tag{B.9}$$

$$s\bar{B}(s) - B(0) = k_1 \bar{A}(s) - k_2 \bar{B}(s) \tag{B.10}$$

$$s\bar{C}(s) - C(0) = k_2 \bar{B}(s) \tag{B.11}$$

Allow initial concentrations to be $A(0) = A^*$, $B(0) = B^*$, and $C(0) = C^*$. Then,

$$s\bar{A}(s) - A^* = -k_1 \bar{A}(s) \tag{B.12}$$

$$s\bar{B}(s) - B^* = k_1 \bar{A}(s) - k_2 \bar{B}(s) \tag{B.13}$$

$$s\bar{C}(s) - C^* = k_2 \bar{B}(s) \tag{B.14}$$

Then

$$\bar{A}(s) = \frac{A^*}{s + k_1} \tag{B.15}$$

$$\bar{B}(s) = \frac{B^* + k_1 \bar{A}(s)}{s + k_2} \tag{B.16}$$

$$= \frac{B^*}{s + k_2} + \frac{k_1 A^*}{(s + k_2)(s + k_1)} \tag{B.17}$$

$$\bar{C}(s) = \frac{C^*}{s} + \frac{k_2 \bar{B}(s)}{s} \tag{B.18}$$

$$= \frac{C^*}{s} + \frac{k_2}{s}\left(\frac{B^*}{s+k_2} + \frac{k_1 A^*}{(s+k_2)(s+k_1)}\right) \tag{B.19}$$

$$= \frac{C^*}{s} + \frac{k_2 B^*(s+k_1) + k_1 k_2 A^*}{s(s+k_2)(s+k_1)} \tag{B.20}$$

To find the concentration of ammonium, $C(t)$. the inverse of

$$\frac{k_2 B^*(s+k_1) + k_1 k_2 A^*}{s(s+k_2)(s+k_1)} \tag{B.21}$$

must be found. The inverse solution requires decomposition by partial fractions.

$$\frac{k_2 B^*(s+k_1) + k_1 k_2 A^*}{s(s+k_1)(s+k_2)} = \tag{B.22}$$

$$= \frac{\alpha}{s} + \frac{\beta}{s+k_1} + \frac{\gamma}{s+k_2} \tag{B.23}$$

$$k_2 B^*(s+k_1) + k_1 k_2 A^* = \tag{B.24}$$

$$= \alpha(s+k_1)(s+k_2) + \beta s(s+k_2) \tag{B.25}$$

$$+\gamma s(s+k_1) \tag{B.26}$$

Consider the zero points, $s = \{0, k_1, k_2\}$

$$\lim_{s \longrightarrow 0} k_2 B^*(s+k_1) + k_1 k_2 A^* = k_1 k_2 (A^* + B^*) = k_1 k_2 \alpha \tag{B.27}$$

$$\alpha = A^* + B^* \tag{B.28}$$

$$\lim_{s \longrightarrow k_1} k_2 B^*(s+k_1) + k_1 k_2 A^* = k_1 k_2 A^* = \beta k_1(-k_1 + k_2) \tag{B.29}$$

$$\beta = \frac{k_2 A^*}{k_1 - k_2} \tag{B.30}$$

$$\lim_{s \longrightarrow k_2} k_2 B^*(s+k_1) + k_1 k_2 A^* = k_2 B^*(-k_2 + k_1) + k_1 k_2 A^* = \tag{B.31}$$

$$= -\gamma k_2(-k_2 + k_1) \tag{B.32}$$

$$\gamma = -B^* + \frac{k_1 A^*}{k_2 - k_1} \tag{B.33}$$

Then

$$\frac{k_2 B^* (s+k_1) + k_1 k_2 A^*}{s (s+k_1)(s+k_2)} = \frac{A^* + B^*}{s} + \frac{\frac{k_2 A^*}{k_1 - k_2}}{s+k_1} - \frac{B^* + \frac{k_1 A^*}{k_1 - k_2}}{s+k_2} \tag{B.34}$$

Or

$$\bar{C}(s) = \frac{C^*}{s} + \frac{A^* + B^*}{s} + \frac{\frac{k_2 A^*}{k_1 - k_2}}{s+k_1} - \frac{B^* + \frac{k_1 A^*}{k_1 - k_2}}{s+k_2} \tag{B.35}$$

Upon inverse

$$\begin{aligned} C(t) &= C^* + A^* + B^* + \frac{k_2 A^*}{k_1 - k_2} \exp[-k_1 t] && \text{(B.36)} \\ &\quad - \left(B^* + \frac{k_1 A^*}{k_1 - k_2} \right) \exp[-k_2 t] && \text{(B.37)} \\ &= C^* + A^* + B^* + \frac{k_2 A^*}{k_1 - k_2} \left(\exp[-k_1 t] - \frac{k_1}{k_2} \exp[-k_2 t] \right) && \text{(B.38)} \\ &\quad - B^* \exp[-k_2 t] && \text{(B.39)} \\ &= C^* + A^* + B^* + \frac{A^*}{\frac{k_1}{k_2} - 1} \left(\exp[-k_1 t] - \frac{k_1}{k_2} \exp[-k_2 t] \right) && \text{(B.40)} \\ &\quad - B^* \exp[-k_2 t] && \text{(B.41)} \end{aligned}$$

REFERENCES

[1] Dincer, I. *Renewable and Sustainable Energy Reviews* **2000,** *4,* 157-175.

[2] Bryant, D.; Frigaard, N.-U. *Trends Microbiol.* **2006,** *14,* 488-496.

[3] State of Iowa, State of Iowa Government, Iowa Plan for Energy Independence, Charting Iowa's Course in the New Energy Economy, 2007.

[4] United States Department of Energy, National Energy Information Center, Annual Energy Review 2010, 2010.

[5] Bridgwater, A. V. *Chemical Engineering Journal* **2003,** *91,* 87-102.

[6] Turner, J. A. *Science* **2004,** *305,* 972-974.

[7] Ni, M.; Leung, D. Y. C.; Leung, M. K. H. *Int. J. Hydrogen Energy* **2007,** *32,* 3238-3247.

[8] Pate, M.; Bartels, J. "A feasibility study of implementing an Ammonia Economy", Technical Report 07S-01, Iowa State University, 2008.

[9] Hubbell, D.; Kidder, G. University of Florida Institute of Food and Agricultural Sciences, Biological Nitrogen Fixation (SL16), 2003.

[10] McClintock, J.; Holbrook, J. *National Defense* **2008,** *August 2008,*.

[11] Ramos, J. L.; Guerrero, M. G.; Losada, M. *Appl. and Environ. Microbiol.* **1984,** *48,* 114-118.

[12] Zamfirescu, C.; Dincer, I. *J. Power Sources* **2008,** *185,* 459-465.

[13] Cooper, M.; Botte, G. G. *J. Electrochem. Soc.* **2006,** *153,* A1894.

[14] Vitse, F.; Cooper, M.; Botte, G. G. *J. Power Sources* **2005,** *14,* 18-26.

[15] Schrock, R. R. *Proc. Natl. Acad. Sci.* **2006,** *103,* 17087.

[16] Smil, V. *Enriching the earth: Fritz Haber, Carl Bosch, and the transformation of world food production;* Cambridge: London, 1 ed.; 2004.

[17] United States Geological Survey, Mineral commodity summaries 2011, 2011.

[18] Galvez, H. M.; Steinfeld, A. *Ind. Eng. Chem. Res.* **2007,** *46,* 2042-2046.

[19] Howard, J. B.; Rees, D. C. *Chem. Rev.* **1996,** *96,* 2965-2982.

[20] Ertl, G. *J. Vac. Sci. Technol. A* **1983,** *1,* 1247.

[21] Modak, J. M. *Resonance* **2002,** *7,* 69-77.

[22] Schlogl, R. *Agnew. Chem. Int. Ed.* **2004,** *42,* 2004-2008.

[23] Postgate, J. *The Fundamentals of Nitrogen Fixation;* Cambridge University Press: Cambridge, 1982.

[24] Stewart, W. *Phil. Trans. R. Soc. Lond.* **1976,** *274,* 341-358.

[25] Gallon, J.; Chaplin, A. *An Introduction to Nitrogen Fixation;* Cassell Educational Limited: London, 1987.

[26] Galloway, J. N.; Dentener, F. J.; Capone, D. G.; Boyer, E. W.; Howarth, R. W.; Seitzinger, S. P.; Asner, G. P.; Cleveland, C. C.; Green, P. A.; Holland, E. A.; Karl, D. M.; Michaels, A. F.; Porter, J. H.; Townsend, A. R.; Voosmarty, C. J. *Biogeochem.* **2004,** *70,* 153-226.

[27] Smith, B. E. *Science* **2002,** *297,* 1654-1655.

[28] Schrock, R. *Tech. Rev.* **2006,** .

[29] Swamy, B. E. K.; Venton, B. J. *Anal. Chem.* **2006,** *79,* 744-750.

[30] Allen, P. M.; Bowen, W. R. *Trends in Biotech.* **1985,** *3,* 145-149.

[31] Dixon, R.; Kahn, D. *Nature Rev. Microbiol.* **2004,** *2,* 621-631.

[32] Burgess, B. K.; Lowe, D. J. *Chem. Rev.* **1996,** *96,* 2983-3012.

[33] Haaker, H.; Veeger, C. *Trends in Biochem. Sci.* **1984,** *9,* 188.

[34] Halbelb, C. M.; Ludden, P. W. *J. Nutr.* **2000,** *130,* 1081-1084.

[35] Haaker, H.; Klugkist, J. *FEMS Microbiol.Lett.* **1987,** *46,* 57.

[36] Duyvis, M. G.; Wassink, H.; Haaker, H. *Biochem.* **1998,** *37,* 17345-17354.

[37] Braaksma, A.; Haaker, H.; Grande, H. J.; Veeger, C. *Eur. J. Biochem.* **1982,** *121,* 483-491.

[38] Schrautmeier, B.; Bohme, H.; Boger, P. *Arch. Microbiol.* **1984,** *137,* 14-20.

[39] Crane, B.; Getzoff, E. *Curr. Opin. Struct. Biol.* **1996,** *6,* 744-756.

[40] Dose, M.; Hirasawa, M.; Kleis-SanFrancisco, S.; Lew, E.; Knaff, D. *Plant Physiol.* **1997,** *114,* 1047-1053.

[41] Suzuki, S.; Kataoka, K.; Yamaguchi, K. *Acc. Chem. Res.* **2000,** *33,* 728-735.

[42] Sakurai, T.; Ikeda, O.; Suzuki, S. *Inorg. Chem.* **1990,** *29,* 4715-4718.

[43] Sancho, J.; Peleato, M. L.; Gomez-Moreno, C.; Edmondson, D. E. *Arch. Biochem. Biophys.* **1988,** *260,* 200-207.

[44] Barbara, K. *Enzyme and Microbial Technology* **2004,** *35,* 126-139.

[45] Clark, D. S. *Trends Biotech.* **1994,** *12,* 439-443.

[46] Cosnier, S. *Biosensors and Bioelec.* **1999,** *14,* 443-456.

[47] Mateo, C.; Palomo, J. M.; Fernandez-Lorente, G.; Guisan, J. M.; Fernandez-Lafuente, R. *Enzyme and Microbial Tech.* **2007,** *40,* 1451-1463.

[48] Klotzbach, T. L.; Watt, M.; Ansari, Y.; Minteer, S. D. *J. Membr. Sci.* **2008,** *311,* 81.

[49] Arechederra, R.; Minteer, S. D. *Electrochim. Acta* **2008,** *53,* 6698.

[50] Leger, C.; Elliot, S. J.; Hoke, K. R.; Jeuken, L. J.; Jones, A. K.; Armstrong, F. A. *Biochem.* **2003,** *42,* 8653-8662.

[51] Flexer, V.; Ielmini, M. V.; Calvo, E. J.; Bartlett, P. N. *Bioelectrochemistry* **2008,** *74,* 201-209.

[52] Evans, M.; Albrecht, S. *Biochem. Biophys. Res. Commun.* **1974,** *61,* 1187-1192.

[53] Bohme, H.; Schrautmeier, B. *Biochim. Biophys. Acta* **1987,** *891,* 115-120.

[54] Neuer, G.; Bothe, H. *Arch. Microbiol.* **1985,** *143,* 185-191.

[55] Schultz, F. A.; Gheller, S. F.; Burgess, B. K.; Lough, S.; Newton, W. E. *J. Am. Chem. Soc.* **1985,** *107,* 5364-5368.

[56] Watt, G.; Huang, H.; Reddy, K. *Redox Properties of the Nitrogenase Proteins from Azobacter vinelandii;* Molybdenum Enzyme, Cofactors, and Model Systems American Chemical Saociety: Washington, D.C., 1993.

[57] Smith, R. V.; Noy, R. J.; Evans, M. C. W. *Biochimica et Biophysica Acta* **1971,** *253,* 104-109.

[58] Tel-Or, E.; Stewart, W. D. P. *Biochimica et Biophysica Acta* **1976,** *423,*

189-195.

[59] Deistung, J.; Thorneley, R. N. F. *Biochem. J.* **1986,** *239,* 69-75.

[60] Tsygankov, A. A. *Appl. Biochem. Microbiol.* **2007,** *43,* 250-259.

[61] Fricke, K.; Harnisch, F.; Schroder, U. *Energy Env. Sci.* **2008,** *1,* 144-147.

[62] Yoon, J. H.; Sim, S. J.; Kim, M.-S.; Park, T. H. *Int. J. Hydrogen Energy* **2002,** *27,* 1265.

[63] Spiller, H.; Gunasekaran, M. *Appl. Microbiol. Biotechnol.* **1990,** *33,* 477-480.

[64] Kerby, N. W.; Musgrave, S. C.; Rowell, P.; Shestakov, S. V.; Stewart, W. D. P. *Appl. Microbiol. Biotechnol.* **1986,** *24,* 42.

[65] Jensen, B. B.; Cox, R. P.; Burris, R. H. *Arch. Microbiol.* **1986,** *145,* 241-247.

[66] Kannaiyan, S.; Aruna, S.; Kumari, S. M. P.; Hall, D. *J. Appl. Phyc.* **1997,** *9,* 167-174.

[67] Thiel, T.; Pratte, B. *J. Bacteriol.* **2001,** *183,* 280-286.

[68] Sveshnikov, D.; Sveshnikova, N.; Rao, K.; Hall, D. O. *FEMS Microbiol. Lett.* **1997,** *147,* 197-301.

[69] Borodin, V.; Tsygankov, A.; Rao, K.; Hall, D. O. *Biotechnol. Bioeng.* **2000,** *69,* 478-485.

[70] Spiller, H.; Bookjans, G.; Shanmugam, K. *J. Bacteriol.* **1983,** *155,* 129-137.

[71] Shanmugam, K. T.; Valentine, R. *Proc. Natl. Acad. Sci.* **1975,** *72,* 136-139.

[72] Andersen, K.; Shanmugam, K. *J. Gen. Microbiol.* **1977,** *103,* 107-122.

[73] Latorre, C.; Lee, J. H.; Spiller, H.; Shanmugam, K. T. *Biotecnol. Lett.* **1986,** *8,* 507-512.

[74] Spiller, H.; Latorre, C.; Hasan, M.; Shanmugam, K. T. *Word J. Microbiol. Biotech.* **1994,** *10,* 55-58.

[75] Champe, P. C.; Harvey, R. A.; Ferrier, D. R. *Lippincott's Illustrated Reviews* **2005,** .

[76] Kumar, A.; Tabita, F. R.; Baalen, C. V. *J. Bacteriol.* **1983,** *155,* 493-497.

[77] Kumar, A.; Tabita, F. R.; Baalen, C. V. *Arch. Microbiol.* **1982,** *133,* 103-109.

[78] Musgrave, S. C.; Kerby, N. W.; Codd, G. A.; Stewart, W. D. *Biotechnol. Lett.* **1982,** *4,* 647-652.

[79] Ramos, J. L.; Madueno, F.; Guerrero, M. G. *Arch. Microbiol.* **1985,** *141,* 105.

[80] Mackinney, G. *J. Biol. Chem.* **1941,** *140,* 315-322.

[81] Bradford, M. *Anal. Biochem.* **1976,** *72,* 248-254.

[82] Sedmak, J.; Grossberg, S. *Anal. Biochem.* **1977,** *79,* 544-552.

[83] Atanassov, P.; Apblett, C.; Banta, S.; Brozik, S.; Barton, S. C.; Cooney, M.; Liaw, B. Y.; Mukerjee, S.; Minteer, S. D. *Interface* **2007,** *Summer,* 28-31.

[84] Mauritz, K. A.; Moore, R. B. *Chem. Rev.* **2004,** *104,* 4535-4586.

[85] Moore, C. M.; Akers, N. L.; Hill, A. D.; Johnson, Z. C.; Minteer, S. D. *Biomacromol.* **2004,** *5,* 1241-1247.

[86] Klotzbach, T.; Watt, M.; Ansari, Y.; Minteer, S. D. *J. Membr. Sci.* **2006,** *282,* 276-283.

[87] Akers, N. L.; Moore, C. M.; Minteer, S. D. *Electrochim. Acta* **2005,** *50,* 2521.

[88] Schrenk, M. J.; Villigram, R. E.; Torrence, N. J.; Brancato, S. J.; Minteer, S. D. *J. Membr. Sci.* **2002,** *205,* 3-10.

[89] Moore, C. M.; Hackman, S.; Brennan, T.; Minteer, S. D. *J. Membr. Sci.* **2005,** *255,* 233-238.

[90] Bard, A.; Faulkner, L. *Electrochemical Methods;* John Wiley & Sons, Inc.: New York, Second ed.; 2001.

[91] Solorzano, L. *J. Limnol. Oceanogr.* **1969,** *14,* 799-801.

[92] Reich, S.; Almon, H.; Boger, P. *FEMS Microbiol. Lett.* **1986,** *34,* 53-56.

[93] Jeanfils, J.; Loudeche, R. *Biotechnol. Lett.* **1986,** *8,* 265.

[94] Matsunaga, T.; Namba, Y. *Anal. Chem.* **1984,** *56,* 798-801.

[95] Salamon, Z.; Tollin, G. *Arch. Biochem. Biophys.* **1992,** *294,* 382-387.

[96] Salamon, Z.; Tollin, G. *J. Electroanal. Chem.* **1992,** *342,* 381-391.

[97] McLeod, D. D. N.; Freeman, H. C.; Harvey, I.; Lay, P. A.; Bond, A. M. *Inorg. Chem.* **1996,** *35,* 7156-7165.

[98] Verhagen, M. F. J. M.; Link, T. A.; Hagen, W. R. *FEBS Lett.* **1995,** *361,* 75-78.

[99] Guilbault, G. G. *Analytical uses of immobilized enzymes;* Modern Monographs in Analytical Chemistry Marcek Dekker, Inc.: New York, 1984.

[100] Kim, J.; Jia, H.; Wang, P. *Biotech. Adv.* **2006,** *24,* 296.

[101] Serebryakova, L.; Medina, M.; Zorin, N. A.; Gogotov, I. N.; Cammack, R. *FEBS Lett.* **1996,** *383,* 79-82.

[102] Madoz, J.; Rernandez-Recio, J.; Gomez-Moreno, C.; Fernandez, V. M. *Bioelectrochem. Bioenerg.* **1998,** *47,* 179-183.

[103] Armstrong, F. A.; Hill, H. A. O.; Walton, N. J. *Acc. Chem. Res.* **1988,** *21,* 407-413.

[104] Aliverti, A.; Hagen, W. R.; Zanetti, G. *FEBS Lett.* **1995,** *368,* 220-224.

[105] Haystead, A.; Stewart, W. D. P. *Arch. Microbiol.* **1972,** *82,* 325.

[106] Bohme, H.; Schrautmeier, B. *Biochim. Biophys. Acta* **1987,** *891,* 1-7.

[107] Schrautmeier, B.; BÃűhme, H. *FEBS Lett.* **1985,** *184,* 304-308.

[108] Tagawa, K.; Arnon, D. I. *Nature* **1962,** *195,* 537-543.

[109] Im, S.-C.; Kohzuma, T.; McFarlane, W.; Gaillard, J.; Sykes, A. G. *Inorg. Chem.* **1997,** *36,* 1388-1396.

[110] Landrum, H. L.; Salmon, R. T.; Hawkridge, F. M. *J. Am. Chem. Soc.* **1977,** *99,* 3154-3158.

[111] Greiner, L.; Schroder, I.; Muller, D. H.; Liese, A. *Green Chem.* **2003,** *5,* 697-700.

[112] de Lacey, A. L.; Bes, M. T.; Gomez-Moreno, C.; Fernandez, V. M. *J. Electroanal. Chem.* **1995,** *390,* 69-76.

[113] Zhou, R.; Wolk, C. P. *J. Bacteriol.* **2002,** *184,* 2529-2532.

[114] Peterson, R. B.; Wolk, C. P. *Proc. Natl. Acad. Sci.* **1978,** *75,* 6271-6275.

[115] Fay, P.; San, P. A. 73 Heterocyst isolation, in *Methods in Enzymology*, Vol. 69; Academic Press: New York, 1980 pages 801–812.

[116] Peterson, R.; Burris, R. *Arch. Microbiol.* **1976,** *108,* 35-40.

[117] Lynn, M.; Ownby, J. *Arch. Microbiol.* **1987,** *148,* 115-120.

[118] Peterson, R.; Burris, R. *Arch. Microbiol.* **1978,** *116,* 125-132.

[119] Fay, P.; Stewart, W.; Walsby, A.; Fogg, G. *Nature* **1968,** *220,* 810-812.

[120] Haselkorn, R. *Ann. Rev. Plant Physiol.* **1978,** *29,* 319-344.

[121] Stewart, W. D.; Rowell, P. *Biochem. Biophys. Res. Commun.* **1975,** *65,* 846-856.

[122] Guerrero, M. G.; Vega, J. M.; Losada, M. *Ann. Rev. Plant Physiol.* **1981,** *32,* 169-204.

[123] Herrero, A.; Flores, E.; Guerrero, M. G. *J. Bacteriol.* **1981,** *145,* 175-180.

[124] Herrero, A.; Flores, E.; Guerrero, M. G. *FEMS Microbiol. Lett.* **1985,** *26,* 21-25.

[125] Herrero, A.; Guerrero, M. G. *J. Gen. Microbiol.* **1986,** *132,* 2463-2468.

[126] Frias, J. E.; Flores, E.; Herrero, A. *J. Bacteriol.* **1997,** *179,* 477-486.

[127] Ohashi, Y.; Shi, W.; Takatani, N.; Aichi, M.; ichi Maeda, S.; Watanabe, S.; Yoshikawa, H.; Omata, T. *J. Exp. Bot.* **2011,** *62,* 1411-1424.

[128] Flores, E.; Frias, J. E.; Rubio, L. M.; Herrero, A. *Photosyn. Res.* **2005,** *83,* 117-133.

[129] Ramos, J. L.; Guerrero, M. G. *Arch. Microbiol.* **1983,** *136,* 81-83.

[130] Salome, J. P.; Amutha, R.; Jagannathan, P.; Josiah, J. J. M.; Berchmans, S.; Yegnaraman, V. *Biosensors and Bioelec.* **2009,** *24,* 3487-3491.

[131] Maloy, J. Nitrogen, Phosphorous, Arsenic, Antimony, and Bismuth, in *Standard Potentials in Aqueous Solutions*; Bard, A. J.; Parsons, R.; Jordan, J., Eds.; CRC Press: New York, 1985 pages 127–139.

[132] Martin-Nieto, J.; Flores, E.; Herrero, A. *Plant Physiol.* **1992,** *100,* 157-163.

[133] MartÃŋn-Nieto, J.; Herrero, A.; Flores, E. *Arch. Microbiol.* **1989,** *151,* 475-478.

[134] National Renewable Energy Laboratories, U.S. Department of Energy, NREL PVWatts Calculator, http://www.nrel.gov/rredc/pvwatts, 2012.

[135] Cronk, S. Solar and Wind Estimator, http://www.solar-estimate.org, 2012.